Table of Contents

From the Editors of the CNS Journal

Five years ago, a group of enterprising students conceived the idea to showcase a selection of theses that represented the best of the research master programme in cognitive neuroscience at the Radboud University of Nijmegen. That idea was the genesis of the Proceedings of the Cognitive Neuroscience Master of the Radboud University. Today, this tradition continues in the spirit in which it began and serves to immerse the students of the programme in the important aspects of academia, namely the communication of research findings. The student journal does so by affording students the opportunity to participate in the mutual exchange of ideas and criticisms via peer reviews. This process simultaneously emphasizes the importance of good writing which is an essential skill for a successful career in the sciences. In other words, the student journal is an important platform on which our fellow students begin their journey into the world of research. Proof of the journal's accomplishment is evinced by theses that have subsequently been accepted into international scientific journals.

The contents of this student journal highlight the interdisciplinary character of the master programme. The theses are a sample of research conducted by students from each specialization: Psycholinguistics; Action, Perception, & Consciousness; and Neurocognition. The diversity of topics reflects the wide-ranging interests of our fellow students who come from a variety of academic backgrounds – from psychology to biology to physics – and who also come from all across the globe to come together in Nijmegen. This diversity is further enriched through the cooperation of various faculties and research institutes that all share in the common goal of scientific progress.

The year 2010 marks an important milestone for the cognitive neuroscience programme with the introduction of a new specialization: Brain Networks and Neuronal Communication. Moreover, in February 2010, we welcomed the first group of students to begin their studies in a second entry date of the academic year. This is evidence that the programme is growing in number and in demand. We trust that more exciting and promising things are yet to come!

All submitted theses undergo a strict review process to ensure the highest standards of the student journal. Every thesis is assigned to a senior reviewer and a student reviewer. Based on these evaluations, the journal committee makes an informed decision to either accept the thesis for publication, or not. The best theses are then published in the printed edition while the remaining theses are made available to the public at the journal website [www.ru.nl/master/cns/journal].

In this issue, we are proud to present experimental and computational neuroscientific studies that address topics ranging from memory to expectations in perception, language and more generally, interneural communication. We are confident that you will gain valuable insight from the works presented in this issue, and we sincerely invite you to share in our pride of the achievements of our fellow students.

On behalf of the committee, we thank you for your interest in the journal.

Marius Zimmermann & Kevin Lam
Editors-in-Chief

From the Director of the Max Planck Institute for Psycholinguistics

Nijmegen CNS, the Proceedings of the Cognitive Neuroscience Research Master's degree at the Radboud University Nijmegen, has now reached Volume 5. Just as in Volumes 1-4, there are in the present volume results from a variety of perspectives, reflecting the interdisciplinary nature of the CNS program and the many opportunities open to our students. This year is the first intake in which the CNS courses are also taken by students of the International Max Planck Research School in the Language Sciences, a further testimony to the interdisciplinary strength of this program.

The existence of Nijmegen CNS suggests that we, the associated faculty members, set considerable store by the publication of research results. Indeed we do. Publication is an essential part of the research process, and so training in publication ought to be an integral part of the training in research that constitutes any research master's degree.

Writing in the real world of science needs to be learned, because it is so different from the writing in which we have previously been trained. All the reports we wrote at school or as undergraduates were read by teachers who were grading us, and how well we had learned the material or performed the required task. In the real world of science reporting, however, the only thing that matters is our results. There is a metaphor that recurs in writings about careers in science: "building the wall of science". Research results, viewed as bricks in the wall of science, should obviously be solid so that others can build on them securely. But they must also be clearly visible and presented in a way that makes their contribution obvious – so that others will build on them. This not only means understandable writing; it sometimes means recounting experiments in a different order than that in which they were actually done, or dropping conditions or experiments that turn out not to have anything to add to the final story – things we do not do when writing for teachers. In the real world of science the author is the facilitator of the research findings. Communication of the findings is essential if they are to have their deserved impact. It is really worth getting this step right!

Prof. dr. Anne Cutler
Director, Max Planck Institute for Psycholinguistics

Nijmegen CNS
Proceedings of the Cognitive Neuroscience Master of the Radboud University

Contact information:
Journal CNS
Radboud University
P.O. Box 9104
6500 HE Nijmegen
The Netherlands
nijmegencns@gmail.com

Tactile expectation modulates pre-stimulus β-band oscillations in human primary somatosensory cortex

Freek van Ede[1]
Supervisors: Ole Jensen[1], Eric Maris[1]

[1]*Donders Institute for Brain, Cognition and Behaviour, Radboud University, Nijmegen, The Netherlands*

Neuronal oscillations are postulated to play a fundamental role in top-down processes of expectation. We used magnetoencephalography (MEG) to investigate whether expectation of a tactile event involves a pre-stimulus modulation of neuronal oscillations in human somatosensory cortex. In a bimodal attention paradigm, participants were presented with a predictable spatio-temporal pattern of lateralized tactile stimulations and simultaneously occurring non-lateralized auditory stimuli. Before the onset of a series of such combined audio-tactile stimuli, a cue was presented that indicated the sensory stream that had to be attended. By investigating lateralized patterns of oscillatory activity, we were able to study both attentive (when the tactile stream was attended) and non-attentive (when the auditory stream was attended) tactile expectation. For both attention conditions, we observed a lateralized modulation of the amplitude of beta band oscillations prior to a predictable – and accordingly lateralized – tactile stimulus. As such, we show that anticipatory modulation of ongoing oscillatory activity is not restricted to attended sensory events. Attention did enlarge the size of this modulation. We argue that this modulation constitutes a suppression of beta oscillations that originate at least partly from primary somatosensory cortex (S1) contralateral to the expected stimulation. We discuss our results in the light of the hypothesis that ongoing beta oscillations over sensorimotor cortex reflect a brain state in which neuronal processing efficacy is low. Pre-stimulus suppression of these oscillations then prepares the system for future processing. This shows that perception is an active process that starts even prior to sensation.

Keywords: expectation, anticipation, attention, neuronal oscillations, pre-stimulus, event-related desynchronization (ERD), beta, primary somatosensory cortex (S1), Magnetoencephalography (MEG)

Corresponding author: Freek van Ede, Donders Centre for Cognition, Montessorilaan 3, PO Box 9104 6525 HR Nijmegen, The Netherlands, Email: f.vanede@donders.ru.nl

1. Introduction

Perception is not mere registration of sensory input. Rather, it is an active process in which top-down mechanisms play important roles. Expectation constitutes one such top-down mechanism. Specifically, expectations about upcoming sensory events can be utilized to prepare sensory cortices by instantiating a neural context that allows for enhanced processing of the forthcoming event (Engel et al., 2001). Neuronal oscillations might define such a context, as they have been hypothesized to be involved in gating neuronal activity (Engel et al., 2001; Fries, 2005; Fries et al., 2001; Pfurtscheller and Lopes da Silva, 1999; Salinas and Sejnowski, 2001). In particular, because neuronal oscillations reflect rhythmic shifts of excitability they influence spike timing and synchronicity (Lampl and Yarom, 1993; Volgushev et al., 1998). Accordingly, pre-stimulus modulations of oscillatory activity may affect cortical information transfer of initial afferent input and is therefore considered a mechanism by which expectation can guide perception. Here we investigated whether expectation of a tactile event involves a pre-stimulus modulation of neuronal oscillations in human somatosensory cortex.

Because neuronal oscillations can be sustained in the absence of identifiable sensory input or motor output, they are likely to be involved in the neurophysiological mechanisms behind top-down influences such as expectation. These sustained neuronal oscillations can be identified because they are region and frequency specific (Hari and Salmelin, 1997). For instance, over posterior sites of the brain, alpha oscillations (8-12 Hz) are observed. This rhythm is affected by information processing, because its amplitude is modulated by visual input, as was already shown by Hans Berger (1929). Importantly, the alpha rhythm is also affected by top-down influences, as is demonstrated by the fact that its amplitude is modulated in anticipation of a visual stimulus (Foxe et al., 1998; Kelly et al., 2006; Rihs et al., 2007; Sauseng et al., 2005; Thut et al., 2006; Worden et al., 2000; Wyart and Tallon-Baudry, 2008). Similarly, over sensorimotor cortex, so-called mu (8-12 Hz) and beta (15-35 Hz) rhythms are observed, whose amplitudes are reduced over the contralateral hemisphere not only during, but also prior to voluntary movement (Jasper and Penfield, 1949; Nagamine et al., 1996; Pfurtscheller and Lopes da Silva, 1999; Taniguchi et al., 2000; Zhang et al., 2008a). It has further been shown that the sensorimotor mu rhythm is reduced in anticipation of nociceptive stimuli (Babiloni et al., 2003). The present paper provides evidence for another type of pre-stimulus modulation of an ongoing oscillation. Specifically, we show that the amplitude of beta oscillations over sensorimotor cortex is modulated by expectation of a tactile stimulus.

Because sensory afferents enter the cortex in the primary sensory cortices, this is the first neocortical terminal in which information can be gated. In studies measuring the BOLD-signal, expectation-related increases in regional blood flow have been observed in V1 (Kastner et al., 1999; McMains et al., 2007; Ress et al., 2000), S1 (Carlsson et al., 2000), early auditory cortices (Voisin et al., 2006) and even the LGN (O'Connor et al., 2002). Precise localizations on the basis of extra-cranial recordings of human electromagnetic brain activity are generally more problematic. Consequently, studies that implicate primary sensory cortices in anticipatory modulations of neuronal oscillations are rare. The human somatosensory system provides a unique system for investigating the role of primary sensory cortices in relation to expectation-induced modulation of neuronal activity. This is because, in the somatosensory system, only the primary sensory cortex (S1) receives (thalamic) input unilaterally (Burton, 1976; Hari et al., 1993). We made use of this fact by having participants expect either a left or right hand stimulation. Importantly, left and right hand stimulations are processed by the same S2 cortices, but different S1 cortices. By contrasting expected events with a different lateralization we could thus deduce the neuronal origin without the need for assumption-dependent source localization methods. As such, the present paper provides evidence for the involvement of S1 in oscillatory dynamics during expectation.

Empirically, effects of expectation have often been conflated with those of attention (Summerfield and Egner, 2009). For example, in the Posner cueing paradigm (a paradigm used in many of the abovementioned studies) expectation constitutes the primary source for the endogenously directed focus of attention. Anticipatory processes of expectation are, however, not necessarily confined to attended events. In the present study, we therefore examined whether the expectation-induced modulation of pre-stimulus oscillatory activity was restricted to task-relevant stimuli. For this, expectation was manipulated by a predictable spatio-temporal pattern of tactile stimulations. Because stimulus patterns are predictable regardless of their task-relevance, they allow for a dissociation between effects of attentive and non-attentive expectation. Interestingly, we provide evidence that the pre-stimulus modulation

of beta oscillations is not restricted to task-relevant and therefore attended events.

2. Materials and Methods

2.1 Participants

A total of 22 healthy subjects voluntarily participated in the experiment (12 male, mean age: 24y, range: 20-33y). Four participants were excluded from the analysis due to excessive artifacts. Two participants returned for a follow-up session, about two months after their first session. All participants provided written consent and were paid in accordance with guidelines of the local ethics committee (CMO Committee on Research Involving Humans subjects, region Arnhem-Nijmegen, the Netherlands). The experiment was in compliance with national legislation as well as the code of ethical principles (declaration of Helsinki).

2.2 Apparatus

Both tactile and auditory stimuli were presented. For tactile stimulation, piezoelectric Braille cells (Metec, Stuttgart, Germany) were used. A single Braille cell consists of eight pins, aligned in two series of four, that can be raised and lowered. Five such cells, together with a response button, were built in to a graspable device (see Figure 1A), one for each hand. Tactile stimuli were produced by transiently raising the pins of all Braille cells overlying the five fingertips of a single hand. 20 ms after being raised, the pins would be lowered into the cells again – rendering the subjective experience of a tactile stimulus as a 'hit' to the fingers. Auditory stimuli consisted of brief (80 ms) noise bursts that were presented binaurally via MEG compatible air-tubes. The complete experiment was programmed and run using the software package Presentation (http://nbs.neurobs.com).

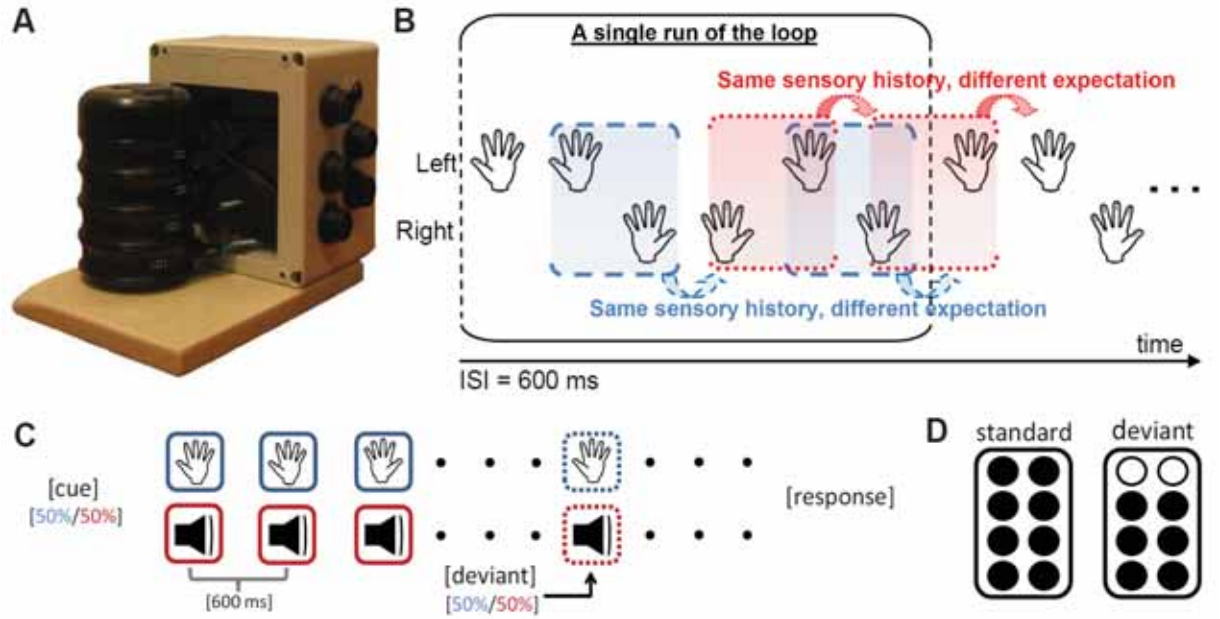

Figure 1. Stimulation apparatus, the spatio-temporal pattern used to manipulate tactile expectation, the trial structure and the tactile deviants. **A.** Stimulation apparatus. Built-in are five Braille cells (four on the side, one on the top) and a response button (also on the top). Individual Braille cell positions are adjustable. When grasped, all five fingertips overlie a Braille cell. **B.** Spatio-temporal pattern of tactile stimulation. First the left hand is stimulated twice, then the right hand is stimulated twice, then the left hand is stimulated once and finally the right hand is stimulated once. This series of six stimulations is then looped. Note the presence of identical tactile stimulation segments (i.e. histories) with different forthcoming predictable tactile events. That is: after the sensory history Left-Right (LR, blue boxes) once the right hand and once the left hand is stimulated. Likewise for the sensory history Right-Left (RL, red boxes). It is here, prior to these predictable events, where windows of analysis are situated. **C.** Schematic representation of a single trial. At the beginning of each trial a cue is presented that indicates the sensory stream in which a deviant stimulus has to be detected. Cues to the auditory and tactile stream have an equal probability of occurrence. A deviant stimulus can occur in either modality (hence can be either a target or a distracter), comes between the fifth and forty-fifth stimulus position and replaces a standard. After a deviant, the trial is continued for up to four to seven stimulations, allowing the subject to respond. Note that each depicted tactile event denotes the stimulations of a single hand. Six such events make up the pattern depicted in B. **D.** Schematic representation of a standard and a deviant tactile stimulus. While a standard tactile stimulation consist of a transient raise of all eight pins of each of the five Braille cells stimulating a single hand, a deviant is characterized by only six pins being transiently raised for each of those cells. In the auditory stream, a deviant was of lower dB than a standard.

2.3 MEG recording

The MEG system (CTF MEG TM Systems Inc., Port Coquitlam, Canada) contained 275 axial gradiometers and was housed in a magnetically shielded room. Additionally, a bipolar surface-ECG was recorded using two Ag/AgCl electrodes. All data were low-pass filtered by an analogue filter (300 Hz cutoff), digitized at 1200 Hz, and stored for offline analysis. No EOG data were recorded because subjects were instructed to close their eyes during the experiment.

2.4 Experimental design and paradigm

The factors expectation and attention were experimentally manipulated in a crossed two-factorial design. Expectation was manipulated by presenting a recurrent, and thus predictable, spatio-temporal pattern of tactile stimulations (see Figure 1B). In this pattern, participants could at any time predict whether the right or the left hand would be stimulated and when this would happen. The prediction of the forthcoming stimulus within such a pattern is based on its tactile history. To control for the sensory effects of the tactile history, a pattern was used that contains left and right hand stimulations that are each preceded by identical segments of tactile stimulations. This is shown in Figure 1B by the blue (red) boxes, which contain the same segment of tactile stimulations, but once followed by a stimulation of the left and once by a stimulation of the right hand. The presence of identical tactile stimulation histories (boxes of the same color), with different forthcoming and predictable events thus allows for an investigation of expectation while controlling for tactile history.

On top of the stream of tactile stimulations, we presented a binaural auditory stream consisting of brief noise-bursts (see Figure 1C). Sensory events occurred simultaneously in the tactile and the auditory modality. Attention was manipulated by instructing participants to attend to either modality. Specifically, before the onset of a series of simultaneously occurring tactile and auditory stimuli, a cue was presented signaling the sensory modality in which deviant stimuli had to be detected and responded to by means of a button-press. It must be noted that the auditory stream was only included for the purpose of experimental control. Our data analyses (see further) focused on lateralized expectation-related activity, and since only tactile stimulations occurred lateralized, only tactile expectation was investigated. Thus, tactile expectation was investigated once when the tactile stream was attended and once when it was not.

Attention was manipulated by instructing subjects to detect deviant stimulations in one of the two sensory modalities. In both modalities, deviant stimulations were defined by their strength. An auditory deviant was characterized by a lower amplitude (individually adjusted; on average 4.1 dB, SD = 1.1). A tactile deviant was characterized by the fact that six instead of eight pins were raised in each of the Braille cells stimulating a single hand (see Figure 1D) – subjectively appearing as a 'hit' to the fingers of lower intensity.

Figure 1C schematically depicts the structure of a trial. A single trial consisted of a cue followed by a sequence of up to 50 combined audio-tactile stimulations with an ISI of 600 ms – ISI referring to the interval between the onsets of the combined audio-tactile stimulation. The cue was a one second repetitive stimulus presented in either the tactile or the auditory modality. With regard to the tactile stream, the pattern of tactile stimulations would start randomly at one of the six stimulations of which the pattern consist. Each trial contained a single deviant that could either be a target (presented in the cued modality) or a distracter (presented in the non-cued modality). The uncued stream always had to be ignored. As such, the cued stream would be maximally attended. As a drawback we were not able to quantify the strength of attention orienting on the basis of detection performance (as no behavioral responses were required to unattended stimuli). The deviant stimulus was randomly presented between the fifth and forty-fifth stimulus-position and replaced the standard. The trial ended either after the participant had pressed the response button, or within four to seven stimulations after a deviant (giving enough time to respond in case a target was detected). Thereafter, a new cue was presented starting the next trial. Each cue was chosen randomly resulting in both attention conditions being randomly intermixed. After nine trials, there was a rest period that the participant could terminate by pressing the response button. In total, the experiment consisted of seven such blocks containing nine trials and lasted about 1 hour.

2.5 Experimental procedure

Before data acquisition, participants were familiarized with the pattern of tactile stimulations as well as the deviant stimuli. Thereafter, ECG-electrodes were placed and the participant was positioned into the MEG that was put into supine position. After instruction of the task, lights were

turned off and the recording and experimental session started. Afterwards, participants were debriefed on the aims of the experiment.

2.6 Data analysis

Data were analyzed using Matlab (Mathworks, http://www.mathworks.com). We made extensive use of FieldTrip (http://www.ru.nl/neuroimaging/fieldtrip), an open source Matlab toolbox developed at the Donders Institute for Brain, Cognition and Behaviour (Nijmegen, the Netherlands).

Both pre- and post-stimulus activity was analyzed. Data of pre- and post-stimulus segments were cut out and processed separately to avoid bleeding in of post-stimulus activity into pre-stimulus segments (e.g. as a result of digital filtering). For the analysis of the post-stimulus activity, we used all left and all right hand stimulations, irrespective of the experimental condition. Around 1000 trials were obtained for each hand. For the analysis of pre-stimulus activity, only a sub-set of pre-stimulus segments were of interest, namely those with a different expectation while controlling for tactile history. This resulted in four distinct pre-stimulus segments ([1] LR->R, [2] LR->L, [3] RL->R and [4] RL->L, see Figure 1B) per attention condition. The segments following the deviants were not analyzed. Around 80 trials were obtained for each of the four segments.

To clean up the data, we first removed ECG-components. An automatic routine that was implemented in FieldTrip detected QRS peaks in the ECG channel. Segments from 200 ms before until 400 ms after the QRS peak were selected and an independent component analysis was performed on the MEG data in this window. Components whose virtual time-courses were highly coherent with the ECG were then removed from the data. Next, segments were visually inspected and those contaminated by artifacts were removed. We also removed channels that were excessively noisy. Line noise was removed by calculating the Discrete Fourier Transform (DFT) of the epochs at 50, 100 and 150 Hz and then subtracting the sine waves that were constructed from the DFT-estimated amplitudes and phases. Finally, we removed the DC-component of the signals (which includes the offset of the SQUIDs) by subtracting the mean of each segment.

We calculated power spectra for all MEG channels. This produces two-dimensional arrays with a spatial (the MEG channels) and a spectral (the frequencies) dimension. However, these spatio-spectral arrays were reduced to a single value that was subsequently contrasted between the two experimental conditions: left and right hand expectation. Specifically, participant-specific post-stimulus induced modulations of oscillatory activity were used to zoom in on pre-stimulus oscillatory activity. The rationale behind this approach is double: (1) we want to increase sensitivity by reducing the influence of inter-individual variability in the spatial and spectral domain, and (2) we want to reduce the number of statistical comparisons in subsequent analysis over subjects.

The steps involved in this reduction are the following:

1. Determination of every individual's temporo-spectral locus of the oscillatory activity that is modulated by tactile stimulation.
2. Determination of every individual's spatial locus of the modulated oscillatory activity, which involves a selection of channels above left and right S.
3. Estimation of pre-stimulus power in the selected frequency band and visualization of effects of expectation.
4. Calculation of a pre-stimulus lateralization index of the power in the specified frequency band by contrasting channels above left and right S1.

In the following, we elaborate on each of the above steps. We describe these steps for oscillatory activity in the beta band. However, the exact same analysis was done for mu and gamma band activity. Several steps in this analysis are graphically depicted in Figure 2.

Step 1. For both left and right hand stimulation segments, trials were baseline corrected (with a baseline-window of 50 milliseconds pre-stimulus) and averaged. Topographies of these averages showed a clear dipolar pattern over the contralateral hemisphere between 40 and 60 ms post-stimulus, which will be denoted as the M50 (see Figure 2A). To extract the one-dimensional topography of this dipolar pattern, we applied singular value decomposition (SVD) to the spatiotemporal array of evoked responses between 40 and 60 ms. The first singular vector was then taken as the topography of the M50 source. We subsequently projected the single-trial data on this singular vector and in this way obtained an S1 virtual channel. We did this separately for left and right hand stimulations, and thus obtained two S1 virtual channels, one for the right and one for the left hemisphere, respectively. Oscillatory power of both virtual S1 channels was then estimated with a short-time Fourier analysis (5-100 Hz), involving 200 ms sliding time-windows, 5 ms steps, and a Hanning taper. This resulted in a time-frequency representation (TFR) of the

data. Per virtual channel we then contrasted the oscillatory power for contralateral and ipsilateral stimulations and normalized this difference (contra minus ipsi) by dividing it by the summed power over both conditions (contra plus ipsi). This was done per time-frequency sample. Subsequently, we averaged the normalized TFRs of both virtual channels. For every participant, a time-frequency window was selected that captured the contralateral suppression of the power in the beta band. This was done on the basis of visual inspection of the TFR (see Figure 2B). On average, beta ranged from 16 to 33 Hz and was suppressed between 100 and 350 ms post-stimulus.

Step 2. Power in the participant-specific beta-range was estimated for all MEG channels over the participant-specific time-window. We estimated the power using the multitaper method (Percival and Walden, 1993). Herein, squared Fourier coefficients of differently tapered data (all Slepian tapers) are averaged to estimate the power in a frequency interval. On average, 5 tapers were used. Besides these power estimates for the original axial gradiometer data, we also calculated power estimates for synthetic planar gradiometer data. The synthetic gradiometer data for a given channel consists of two components, of which one measures the spatial derivative along the anterior-posterior axis of the MEG-helmet, and the other along the left-right axis. These synthetic planar gradiometer data for a given channel were calculated as linear combinations of the axial gradiometer data for this channel plus all neighboring channels.

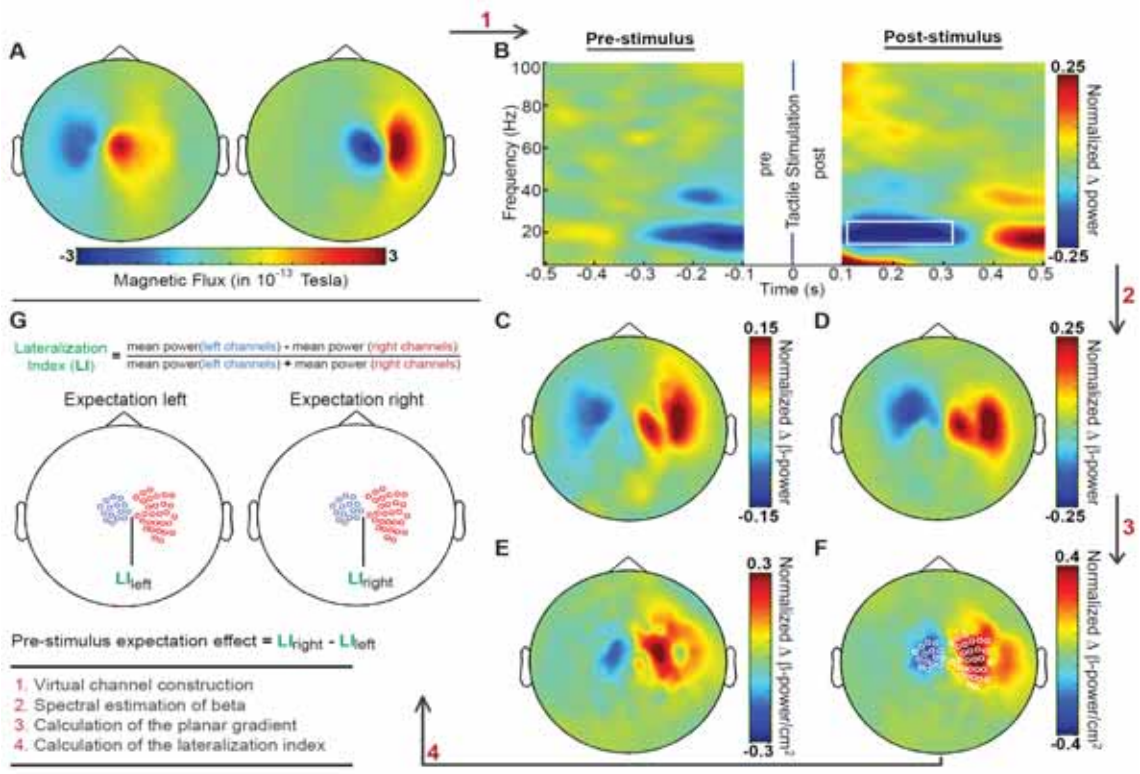

Figure 2. Illustration of analysis procedure and main result for a single representative subject. **A.** Topographies of the ERF between 40 and 60 ms after right and left hand stimulation, respectively. Two virtual S1 channels were constructed on the basis of these data (step 1 in the Figure). **B.** Pre- and post-stimulus representations of the time-resolved power difference between contralateral and ipsilateral virtual S1 channels. The gap in the middle is due to the sliding-window being 200 ms for both pre- and post-stimulus data segments that were cut-out separately. The white box in the post-stimulus TFR represents the selected beta band for this participant. Power in the selected band was then estimated (Step 2 in the Figure). **C.** Topography of the beta modulation during attentive-expectation of a lateralized tactile stimulus. Beta power was estimated over a window 350 ms to stimulus onset. Color coded is the normalized difference in beta power between conditions of right and left hand expectation (i.e. [right minus left] / [right plus left]). The modulation topography was calculated on the axial gradiometer data. **D.** Topography of the beta modulation following a lateralized tactile stimulus (represented by the white box in B). Same conventions as for C. **E., F.** Identical to C and D, except topographies were calculated on the synthetic planar gradient data (step 3 in the Figure). White circles superimposed on the post-stimulus modulation topography denote selected channels above left and right S1. Channels were selected on the basis of the same contrast, for which also t-values were calculated (not shown). **G.** Illustration of the lateralization index in relation to the expectation effect. After having selected both the individual's spectral (B) and spatial (F) loci of beta, a lateralization index was calculated (step 4 in the Figure). This was done separately for both expectation conditions (left and right). Importantly, the pre-stimulus expectation effect is obtained by contrasting our lateralization index between conditions of right and left hand expectation.

Every synthetic planar gradiometer pair defines a plane, and we linearly combined (rotated) the two components of the synthetic planar gradiometer using coefficients that maximized the power of this linear combination. In this way, the two-component synthetic planar gradiometer data were mapped onto a single-component measure of oscillatory power. For every channel, we then calculated an independent samples t-statistic in which we contrasted the trials with a right and a left hand stimulation (right minus left). Channels to be used for pre-stimulus analysis were selected on the basis of these results. The selection was based on the following criteria: (1) channels must have a t-value higher (lower) than 1.96 (-1.96) and (2) they must be within 8 cm from the right (left) virtual S1 channel (see Figure 2F for an example of selected channels). The position of this virtual channel was calculated as a linear combination of all channel coordinates, with the elements of the defining singular vector (see Step 1) being the coefficients of this linear combination.

Step 3. After identifying the participant's spatial and spectral locus of the post-stimulus beta modulation, pre-stimulus oscillatory activity in the selected participant-specific frequency interval was analyzed. The pre-stimulus window was chosen to be the interval [-350, 0] ms, with 0 ms being stimulus onset. Two separate analyses were then performed, one focusing on the visualization of the pre-stimulus expectation and the post-stimulus stimulation effect (Step 3), and one focusing on the quantification of the pre-stimulus expectation effect as a single number (Step 4). For visualization, we calculated channel-specific quantifications of the expectation and the stimulation effect in the following way. For each channel, mean power during left hand expectation/stimulation was subtracted from mean power during right hand expectation/stimulation. This was then divided by the summed mean power in the two experimental conditions, resulting in a normalized topography of the beta modulation. Normalized topographies were then averaged across subjects, yielding a grand average topography. These calculations were performed on the power estimates obtained from the synthetic planar gradiometer data. For the participant showing the strongest effect, we additionally performed the same calculations on the power estimates obtained from the axial gradiometer data. For the same participant, we also performed a time-resolved frequency analysis on the virtual S1 channels for the pre-stimulus segment. For this, we used the short-time Fourier analysis described in Step 1.

Step 4. In this step, we combine the pre-stimulus oscillatory activity that is observed over the selected channels (see Step 2) and quantify the extent to which it is modulated by expectation. For every trial, we estimated the power in the selected frequency interval and averaged it over the selected channels above left and right S1. The average power over right S1 was then subtracted from the average power over left S1, and we normalized this difference by the trial-specific summed power over both channel subsets:

$$LI^{1} = \frac{\text{mean power (LC)}^{1} - \text{mean power (RC)}^{1}}{\text{mean power(LC) + mean power (RC)}}$$

This is a lateralization index, similar to Thut et al. (2006) that is positive when the channels above left S1 have a higher power, and that is negative when the channels above right S1 have a higher power. Because selection of the frequency range and the channels was done on the basis of post-stimulus activity, our lateralization index is an unbiased measure. And because this selection is participant-specific, it is likely to be sensitive to a pre-stimulus modulation of neuronal activity in the same areas that produce this post-stimulus activity. This lateralization index was averaged separately over the left and the right hand expectation trials. If expectation of a lateralized tactile stimulus results in a lateralization of pre-stimulus oscillatory activity, then expectation of left and right hand tactile stimuli should produce different values of our index.

2. 7 Statistical evaluation

In all statistical evaluations, lateralized events were contrasted. That is, for the pre-stimulus period, left and right hand expectation were compared, and for the post-stimulus period, left and right hand stimulation were compared. Since binaural auditory events were identical during left and right hand stimulation, our statistical comparisons will not be affected by auditory-related activity.

For the selection of the participant-specific channel subsets (Step 2), independent samples t-tests were performed within participants (treating the trials as statistical replications). All statistical evaluations of the expectation effect were performed across participants (treating the participants as statistical replications). The dependent variable for this statistical evaluation was the trial-averaged lateralization index, calculated separately for the left

[1] LI = Lateralization Index, LC = left channel, RC = right channel

and the right hand expectations. The expectation effect was statistically tested by means of a paired-samples t-test. This statistical test was performed for both attention conditions (tactile and auditory) separately. Additionally, a repeated-measures ANOVA was performed on the factors expectation (left and right) and attention (tactile and auditory).

2.8 Follow-up session

Two participants, whose MEG data showed the strongest expectation effect, returned for a follow-up session in which also EMG activity was recorded. In all trials, these participants were cued to attend to the tactile modality. Two new blocks were added in which participants were asked to contract their left and right hand either strongly or weakly. We indicated which hand the participants had to contract by means of a transient tactile stimulation of their thumb. Bipolar surface-EMG was measured from both arms using two Ag/AgCl electrodes. The electrodes were placed over the flexors of the forearm, with one electrode placed near the wrist and the other near the elbow in order to map digit a-specific contractions. For analysis, EMG traces were high-pass filtered (40 Hz cutoff) and rectified. For every EMG channel, we calculated the difference between two experimental conditions, each corresponding to one of the two hands. In the contraction blocks, every experimental condition corresponds to one contracted hand, and in the tactile stimulation block, it corresponds to one hand that was expected to be stimulated. We normalized every difference by dividing it by the summed power over the conditions. Finally, we averaged the normalized difference time-courses of both EMG-channels in the following way: we averaged the difference [left-right] contraction/stimulation for the left hand EMG with the difference [right-left] contraction/stimulation for the right hand EMG. Thus, we averaged the differences [ipsi-contra] of the two EMG channels.

3. Results

3.1 Behavioral performance

Average detection rates, expressed as the percentage of targets detected, were 69.7 (SD = 27.7) for tactile targets and 75.1 (SD = 24.3) for auditory targets. Few participants detected all targets in either sensory stream. All participants reported the task to be difficult and attention-demanding, consistent with the detection rate.

3.2 Pre-stimulus β-activity reflects tactile expectation (a representative participant)

Figure 3 shows our main result for this single participant: an expectation-induced pre-stimulus modulation of oscillatory activity in the beta band. In Figure 3A, a representation of the time-resolved power difference between contralateral and ipsilateral virtual S1 channels is shown. Following a tactile stimulus (right TFR), there is a contralateral suppression of beta power, as indicated by the white box. This is in accordance with previous studies that applied tactile stimulation to the human hand region (Bauer et al., 2006; Cheyne et al., 2003; Gaetz and Cheyne, 2006). Interestingly, in anticipation of a lateralized tactile stimulus (left TFR), a similar modulation of beta power is observed. Starting from around 300 ms prior to the expected stim¬¬ulation, lower power in the beta band is observed over contralateral relative to ipsilateral sensorimotor cortex. This effect increases over time and is therefore

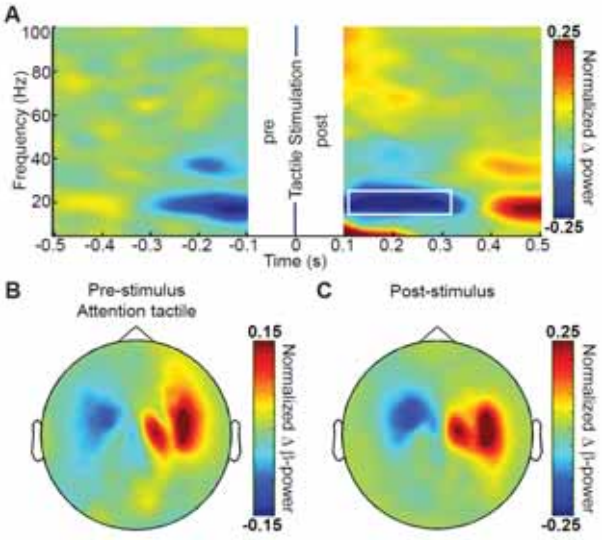

Figure 3. Expectation and stimulation induced modulations of beta, for a representative participant. **A.** Pre- and post-stimulus representations of the time-resolved power difference between contralateral and ipsilateral virtual S1 channels (contralateral minus ipsilateral). The gap in the middle is due to the sliding-window being 200 ms for both pre- and post-stimulus data segments that were cut-out separately. The white box in the post-stimulus TFR represents the selected beta band for this participant. **B.** Topography of the beta modulation during attentive-expectation of a lateralized tactile stimulus. Beta power was estimated over a window 350 ms to stimulus onset. Color coded is the normalized difference in beta power between conditions of right and left hand expectation (i.e. [right minus left] / [right plus left]). The modulation topography was calculated on the axial gradiometer data. **C.** Topography of the beta modulation following a lateralized tactile stimulus. Same conventions as for B, except now beta was estimated for the post-stimulus window that is indicated in the white box in A.

consistent with a role in sensory preparation.

We selected the spectral-temporal window in which beta power was suppressed after a tactile stimulus (as indicated by the white box in Figure 3A) and estimated power within this window for all channels. We then contrasted conditions of right and left hand stimulation (right minus left). Figure 3C shows the topography of this contrast. Evidently, over left sensorimotor cortex beta power is lower after stimulation of the right hand (negative values), whereas over right sensorimotor cortex beta power is lower after stimulation of left hand (positive values). Figure 3B shows a similar contrast topography that was now calculated for the selected beta-range over a window of 350 ms to stimulus onset, thus during tactile expectation. Importantly, the topography of the pre-stimulus modulation of beta power strongly resembles the post-stimulus modulation. Thus, whereas Figure 3A shows spectral correspondence between the stimulation- and expectation-induced modulation of beta, Figure 3B and 3C show that the pre-stimulus effect resembles the post-stimulus effect also in terms of spatial topography. Strikingly, both modulation topographies show dipolar patterns that are similar between pre- and post-stimulus modulations of beta. This is suggestive of a common neuronal generator of the beta oscillation that is suppressed not only by stimulation but also by expectation. These dipolar topographies furthermore resembled the dipolar topographies of the M50 components of the ERF (see Figure 2A). Note that pre- and post-stimulus data segments were cut-out and processed separately, excluding the possibility of post-stimulus effects bleeding into pre-stimulus windows.

3.3 Grand average β-modulation during tactile expectation

In Figure 4, we show the grand average topographies of the stimulation- and the expectation-induced beta modulation. Beta power was calculated on the synthetic planar gradient data (see Materials and Methods), which is robust against inter-individual differences in source orientation because its greatest activity lies directly above the source (Hämäläinen et al., 1993). Figure 4A shows the stimulus-induced modulation of beta power. This serves as a reference for evaluating the topographies of the two expectation-induced modulations of pre-stimulus beta power. Figure 4B shows the topography of the expectation-induced modulation of pre-stimulus beta power that is observed during states of attentive expectation (i.e. when the tactile stream is behaviorally relevant). It is very clear that this topography is highly similar to the topography of the stimulus-induced modulation of beta power. Figure 4C shows the topography of the expectation-induced modulation of pre-stimulus beta power that is observed during states of non-attentive expectation (i.e. when the non-lateralized auditory stream is behaviorally relevant). Over left sensorimotor cortex, we again observe an expectation-induced modulation of pre-stimulus beta power, i.e. beta-power over left sensorimotor cortex differentiates between conditions of left and right hand expectation. This modulation is, however, not clear over the right sensorimotor cortex, at least not in the grand average topography.

Because participants take different positions in the MEG-helmet and have a different head-shape

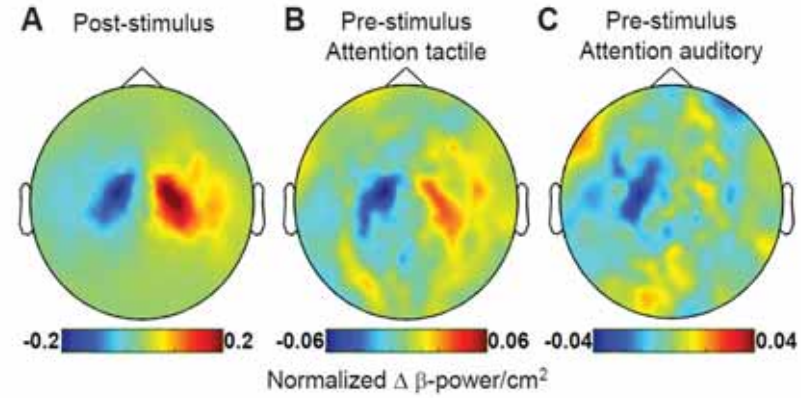

Figure 4. Grand average beta modulation topographies of post- and both pre-stimulus attention conditions. **A.** Topography of the post-stimulus induced modulation of beta. Color coded is the normalized difference in beta power between conditions of left and right hand stimulation (i.e. [right minus left] / [right plus left]). Depicted are grand average values of this contrast. Note that these differences were calculated on the synthetic planar gradient data. **B.** Topography of the modulation of pre-stimulus beta power during states of attentive expectation (i.e. when the tactile stream is behaviorally relevant). Same conventions as for A (i.e. right minus left). **C.** Topography of the modulation of pre-stimulus beta power during states of non-attentive expectation (i.e. when the non-lateralized auditory stream is behaviorally relevant). Same conventions as for A.

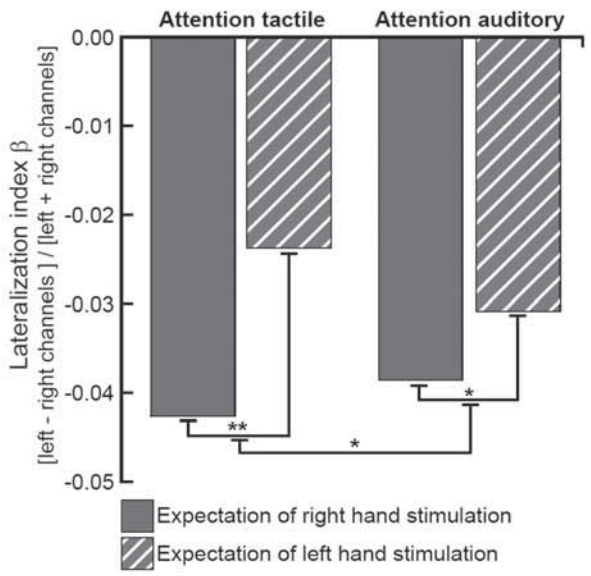

Figure 5. Grand average lateralization index values during left and right hand expectation for both attention conditions. For all four experimental conditions we calculated a lateralization index over the pre-stimulus interval of 350 ms to stimulus onset. This was done with respect to power in the post-stimulus selected beta band, using post-stimulus selected (synthetic planar gradient) channels above left and right sensorimotor cortex. Depicted are grand average values of this index. For both attention conditions a significant difference in the values of the lateralization index is observed between conditions of left and right hand expectation. Furthermore, this difference is significantly greater during the tactile attention condition, thus during states of attentive-expectation. The direction of the differences shows that for both attention conditions beta power is lower over contralateral compared to ipsilateral channels, relative to the upcoming tactile event. * = $p < 0.05$; ** = $p < 0.001$.

and cortical folding, topographies calculated over subjects (as in Figure 4) are not optimally sensitive. We therefore devised a measure that is robust against inter-individual variability in both the spectral and the spatial domain, the participant-specific lateralization index (see Materials and Methods, and Figure 2G). Figure 5 shows the mean lateralization indices for the four conditions of our experimental design. The negative values in all conditions indicate a general hemispheric asymmetry in beta power (which is on average higher over the right than over the left channels) and is not of further interest. We are mainly interested in differences between the conditions with respect to the lateralization index. For both attention conditions, the lateralization index is significantly more negative during expectation of right as compared to left hand stimulation ($t(17) = -4.43$, $p < 0.001$, for the tactile attention condition; $t(17) = -2.54$, $p < 0.05$, for the auditory attention condition). This implies that beta power is significantly lower over channels contralateral as compared to channels ipsilateral to the forthcoming tactile stimulus. Thus, tactile expectation modulates the (lateralization of) beta power while attending as well as while not attending the tactile input stream. Analysis of variance further showed a significant main effect of expectation ($F(1,17) = 20.15$, $p < 0.001$) and a significant interaction between expectation and attention ($F(1,17) = 6.19$, $p < 0.05$). The latter shows that there is a stronger expectation-induced modulation of beta power for attended as compared to unattended upcoming tactile events.

Similar analyses for mu and gamma power yielded no significant results. It must be noted that, for the mu and gamma band, we could not select participant-specific frequency bands on the basis of the stimulus-induced effect. This is because post-stimulus modulations in mu and gamma band oscillations were less strong and not detectable in all subjects. Therefore, we did our analyses with predefined frequency-bands: 8-12 Hz for mu and 60-90 Hz for gamma.

3.4 Refutation of a motor confound

A major concern relates to the involvement of primary motor cortex (M1) in our task. This is because M1 and S1 both process information in a lateralized fashion and lie next to each other on the cortical surface. As a result, M1 and S1 have a large common projection to the SQUIDs.

A motor confound would be picked up by our analysis if (and only if) motor activity follows the pattern of tactile stimulations. This is the case when participants actively contract along with the forthcoming stimulation. To rule out this interpretation of our results, EMG was recorded in a follow-up session with the two participants that showed the strongest expectation effect. In separate blocks, these participants were instructed to either strongly or weakly contract one of their hands. Figure 6A and 6B show that during strong (A) and weak (B) contractions, a reliable increase in the EMG difference signal (ipsi-contra) (see Materials and Methods) could be detected. In Figure 6C, we show the EMG difference signals for the pre-stimulus period in which the participants expected a tactile stimulus. As is clear from Figure 6C, there is no expectation-induced modulation of the EMG difference signal. Thus, expectation of a lateralized tactile stimulus is not accompanied by a contraction of the hand on which the tactile stimulation is expected to occur. During these follow up sessions also MEG data were collected and the expectation-induced modulation of beta was again observed.

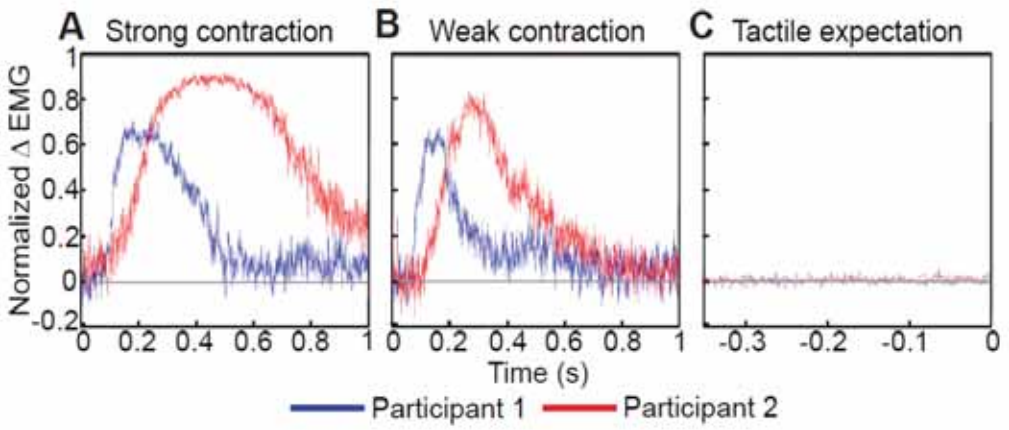

Figure 6. EMG activity during contraction and expectation. **A.** EMG difference signal (i.e. ipsi minus contra) during explicitly instructed strong contraction of the whole hand. Shown are data from two participants that were recorded in a follow-up session. As expected, contraction of the hand results in a significant increase in muscular activity over the contracted hand. **B.** EMG difference signal during explicitly instructed weak contraction of the whole hand. Contraction can still reliably be detected. **C.** EMG difference signal during tactile expectation, shown for the time-window in which the cortical effect is observed. Evidently, expectation of a lateralized tactile stimulus is not accompanied by a contraction of the hand on which the tactile stimulation is expected to occur.

Another potential confound is pre-stimulus response preparation. However, this potential confound is refuted because of the following simple fact: participants had a preferred response hand with which they responded, irrespective of location of the target.

4. Discussion

We set out to investigate whether expectation of an upcoming tactile event involves a pre-stimulus modulation of neuronal oscillatory activity in human somatosensory cortex, and primarily S1. Additionally, we set out to test whether such a modulation would be restricted to attended events. During expectation of a lateralized tactile event, we observed an accordingly lateralized modulation of neuronal oscillatory activity in the beta band. This modulation resembled the modulation observed post-stimulus, both in terms of spectral content as in spatial topography. The effect was specific to the beta band and could not be explained by motor planning or behavior. Although we observed a stronger modulation during states of attentive expectation, we observed a qualitatively similar effect during states of non-attentive expectation. Thus, the anticipatory modulation of oscillatory activity was not restricted to attended events. These observations are well in line with previous studies – primarily in the visual and motor domain – that implicate a modulation of ongoing oscillatory activity in anticipation of neuronal processing. Our observations complement this literature by showing such a modulation (1) in the tactile domain, and (2) during states of both attentive and non-attentive expectation. In the following we speculate about the neural origin of the observed lateralized modulation, discuss our result against the background of the hypothesis that ongoing oscillations reflect a brain state in which neuronal processing efficacy is low and elaborate on attention in relation to expectation.

4.1 The neural origin of the expectation-induced modulation of beta oscillations

The most straightforward interpretation of the observed lateralized modulation of beta band oscillatory activity is a modulation within contralateral S1. In fact, this is the first neocortical area where the forthcoming information will be processed. However, there is increasing evidence that areas not receiving the expected thalamocortical input also show anticipatory modulation of oscillatory activity. For example, during anticipation of a visual stimulus, alpha activity does not only decrease over areas receiving input from the attended visual field (Sauseng et al., 2005; Thut et al., 2006; Wyart and Tallon-Baudry, 2008), but also increases over areas receiving input from the unattended visual field (Kelly et al., 2006; Rihs et al., 2007; Worden et al., 2000). In the absence of a neutral baseline, we contrasted conditions of left and right hand expectation directly. Accordingly, we were not able to dissociate an ipsilateral increase from a contralateral decrease. We nevertheless believe that our observed modulation at least partially involves a contralateral suppression. First, we observed a qualitatively similar modulation in both attention conditions. If beta were

involved in active inhibition of non-relevant stimuli (i.e. disengagement of the cortical areas that process these non-relevant stimuli), as was suggested for alpha on the basis of aforementioned findings, then this is not expected. Rather, with attention directed to the auditory modality, one would expect to find either no lateralization (in case of general disengagement of both S1 cortices) or even a reversed lateralization (in case of a selective disengagement of that S1 that will receive the distracting input). Second, it has been hypothesized that the observed increases in alpha power in aforementioned studies relate to distracter suppression (Kelly et al., 2006; Worden et al., 2000). In the present study, no distracters were presented on the non-expected hand. Third, we observed a highly similar spatial topography and spectral signature in the pre- and the post-stimulus modulation of beta. This is suggestive of a common neuronal generator of the beta oscillation that is affected both by stimulation and expectation. Despite above arguments, new experiments are required to address this issue properly.

We also argue that the observed pre-stimulus modulation of beta originates at least partly from the post-central gyrus and therefore indexes anticipation of somatosensory processing. The main argument for this claim is that this pre-stimulus modulation could not be related to motor planning or behavior. We further argue that this pre-stimulus modulation originates from primary somatosensory cortex. This follows from the fact that a lateralized pre-stimulus modulation most likely originates from the primary sensorimotor cortex, as only here information is processed in a lateralized fashion. That is, left and right hand stimuli are processed by different S1 cortices but the same S2 cortices. Therefore, the observed difference between left and right hand expectation most likely originates from primary rather than secondary somatosensory cortex. Thus, we have evidence for the involvement of S1 in expectation-induced modulations of oscillatory brain activity. This implies that S1 is subject to top-down influences and that expectations are effective from the initial cortical processing stages on. This complements the existing literature on sensory expectation by showing that a primary sensory cortex is involved in anticipatory modulations of oscillatory activity.

Regarding the rolandic rhythms, traditionally mu is considered to be primarily a post-central rhythm whereas beta is considered to be primarily a pre-central rhythm (Salmelin and Hari, 1994). Accordingly, beta is attributed to the motor and mu to the somatosensory system. This notion is in conflict with our interpretation that the observed beta modulation indexes somatosensory anticipation. However, recent evidence suggests that this traditional view is probably an oversimplification. First, tactile stimulation induces changes in beta power (present study; Bauer et al., 2006; Cheyne et al., 2003; Gaetz and Cheyne, 2006). Second, intracranial electrophysiological measurements, directly on the post-central gyrus, have shown beta oscillations that originated from S1 (Brovelli et al., 2004; Crone et al., 1998). Witham and Baker (2007) even recorded stronger beta oscillations in S1 than in M1. Finally, pre- and post-stimulus beta oscillations are related to conscious detectability of tactile stimuli (Linkenkaer-Hansen et al., 2004; Palva et al., 2005). All three sets of observations, together with our observation, show that beta oscillations play a role in somatosensation.

4.2 Ongoing oscillations reflect a non-efficacious mode of processing and are susceptible to top-down influences of expectation

Oscillations impact upon neuronal excitability and therefore produce a neural context that affects the processing of sensory input and motor output. There is ample evidence that oscillations that can be sustained in the absence of sensory input and motor output are inversely related to processing efficacy. For instance, pre-stimulus alpha power has been shown to be negatively correlated with visual discrimination performance (van Dijk et al., 2008), detection performance (Ergenoglu et al., 2004; Hanslmayr et al., 2007), speed of visuomotor processing (Thut et al., 2006; Zhang et al., 2008b) and cortical excitability (Romei et al., 2008). Also sensorimotor alpha and beta oscillations have been associated with reduced cortical excitability (Chen et al., 1998; Tamura et al., 2005; Sauseng et al., 2009), at least in the motor domain. Applying transcranial alternating-current stimulation (tACS) at 20 Hz to the contralateral motor cortex, Pogosyan and colleagues (2009) were even able to slow down movement. Pre-stimulus sensorimotor mu and beta oscillations have furthermore been related to conscious detectability of tactile stimuli (Linkenkaer-Hansen et al., 2004). Taken together, there is ample evidence that ongoing oscillations produce a brain state in which neuronal (e.g. sensory) processing efficacy is low. It follows that the neuronal processing efficacy can be enhanced by altering these oscillations prior to an expected sensory event. In particular, suppressing these oscillations (beta) in regions where the

upcoming event will be processed (contralateral S1), may affect cortical transfer of initial afferent input. (Note that an increase of beta in ipsilateral S1 might also be beneficial, as a disengagement of ipsilateral S1 may suppress competing input.) We provide evidence for such a mechanism by showing an amplitude modulation of beta in anticipation of a tactile stimulus. This observation is in line with similar observations in the visual modality, involving an amplitude modulation of the posterior alpha oscillations in anticipation of a visual stimulus (Foxe et al., 1998; Kelly et al., 2006; Rihs et al., 2007; Sauseng et al., 2005; Thut et al., 2006; Worden et al., 2000; Wyart and Tallon-Baudry, 2008). The observation of a similar phenomenon in a different sensory modality speaks to a general neuronal mechanism of anticipation.

Surprisingly, it has been reported that pre-stimulus beta oscillations in prefrontal cortex are positively correlated with states of anticipation, with higher beta power and coherence being associated with faster reactions times and higher amplitudes of visual-evoked potentials in a visuomotor task (Liang et al., 2002; Zhang et al., 2008b). Likewise, pre-stimulus beta oscillations from parietal cortex have shown to be positively correlated with tactile detection performance (Linkenkaer-Hansen et al., 2004). Thus, brain oscillations in the same frequency band may have a different function dependent on their origin (i.e. prefrontal/parietal versus sensorimotor beta).

Tactile stimuli not only generate a post-stimulus beta suppression; they also generate a beta rebound. In our experiment, this rebound emerges within the time window between two successive tactile stimuli (see Figure 3A). This is consistent with the timing of the beta rebound, as has been reported in several studies (Bauer et al., 2006; Cheyne et al., 2003; Gaetz and Cheyne, 2006). This means that our analysis windows (from 250 ms after the previous stimulus until the next stimulus) also contain the beta rebound in response to the previous stimulus. This implies that the lateralized beta modulation may also be caused by an expectation-induced reduction of the amplitude of the beta rebound. (This would then only apply to those time segments where the upcoming event is on the same hand as the previous stimulation.) Although this clearly is an expectation-induced modulation of beta, it may suggest a different mechanism. From the perspective of metabolic efficiency, in anticipation of an upcoming stimulus that will produce a post-stimulus beta-suppression, it is not desirable to have a rebound. Thus, an account in terms of metabolic rather than sensory efficacy is conceivable. However, two observations go against this interpretation. First, we did not observe a relationship across participants between characteristics of their beta-rebound (i.e. strength, starting-point) and the size of their expectation effect. Second, attention led to a stronger modulation of beta. The latter is clearly predicted from our first account, but not from the metabolic one.

4.3 Expectations are effective outside the realm of attention

Remarkably, we observed that the involvement of neuronal oscillations in sensory expectation is not restricted to attended sensory events. Thus, even when participants were attending the non-lateralized auditory stream, a lateralized modulation of beta oscillations was observed. This implies that participants not only make predictions about unattended events, but also that these predictions are effective in modulating ongoing oscillatory activity in the sensorimotor cortex. In line with the vast literature on implicit learning (Reber, 1993. for an overview), we postulate that the human brain can operate effectively in the absence of deliberate engagement. A similar phenomenon was also observed by Nakano and colleagues (2008) who showed anticipatory modulations in regional blood flow in infants that were asleep.

The validity of the above claim depends on whether the tactile stream was truly unattended when participants were detecting auditory deviants. We deliberately presented tactile and auditory events simultaneously and our task explicitly required participants to selectively attend only to a single sensory stream. Furthermore, targets were hard to detect, as is clear from the detection rates. Thus, in order to do the task properly, maximum attention to the cued modality was required. We conclude that expectation modulates beta oscillations both when upcoming tactile events are behaviorally relevant (i.e., attended) and when they are not (i.e., unattended). Additionally, we showed that attention, as operationalized by behavioral relevance, enlarged the size of the expectation-induced modulation.

5. Conclusion

In the present paper we provided evidence that expectation of a tactile stimulation involves a pre-stimulus modulation of neuronal oscillatory activity in sensorimotor cortex. This modulation occurred in the beta band and most likely is produced by a

contralateral suppression, originating at least partly from S1. We furthermore provided evidence that such an expectation-induced modulation is not restricted to attended events. We argue that the suppression of beta oscillations over the contralateral S1 prepares the system for processing the forthcoming event. Accordingly, the active process of perception starts already prior to sensation.

Acknowledgements

I would first and foremost like to thank Eric Maris for the support, helpful comments and suggestions and interesting discussions we had in the course of the project. Additionally I would like to thank Ole Jensen for his input; Norbert Hermesdorf and Bram Daams for technical supply and assistance; and all the teachers and fellow students in the master CNS who enabled, inspired and encouraged me to do cognitive neuroscience.

References

Babiloni, C., Brancucci, A., Babiloni, F., Capotosto, P., Carducci, F., Cincotti, F., Arendt-Nielsen, L., Chen, A.C., Rossini, P.M., (2003). Anticipatory cortical responses during the expectancy of a predictable painful stimulation. A high-resolution electroencephalography study. Eur J Neurosci 18, 1692-1700.

Bauer, M., Oostenveld, R., Peeters, M., Fries, P., (2006). Tactile spatial attention enhances gamma-band activity in somatosensory cortex and reduces low-frequency activity in parieto-occipital areas. J Neurosci 26, 490-501.

Berger, H., (1929). Über das Elektroenkephalogramm des Menschen. Archiv für Psychiatrie und Nervenkrankheiten 87, 527-570.

Brovelli, A., Ding, M., Ledberg, A., Chen, Y., Nakamura, R., Bressler, S.L., (2004). Beta oscillations in a large-scale sensorimotor cortical network: directional influences revealed by Granger causality. Proc Natl Acad Sci U S A 101, 9849-9854.

Burton, H., (1976). Second somatosensory cortex and related areas. In: Jones, E.G., Peters, A. (Eds.), Cerebral cortex, Vol 5 Sensory-motor areas and aspects of cortical connectivity. Plenum Press, New York, pp. 31-98.

Carlsson, K., Petrovic, P., Skare, S., Petersson, K.M., Ingvar, M., (2000). Tickling expectations: neural processing in anticipation of a sensory stimulus. J Cogn Neurosci 12, 691-703.

Chen, R., Yaseen, Z., Cohen, L.G., Hallett, M., (1998). Time course of corticospinal excitability in reaction time and self-paced movements. Ann Neurol 44, 317-325.

Cheyne, D., Gaetz, W., Garnero, L., Lachaux, J.P., Ducorps, A., Schwartz, D., Varela, F.J., (2003). Neuromagnetic imaging of cortical oscillations accompanying tactile stimulation. Brain Res Cogn Brain Res 17, 599-611.

Crone, N.E., Miglioretti, D.L., Gordon, B., Sieracki, J.M., Wilson, M.T., Uematsu, S., Lesser, R.P., (1998). Functional mapping of human sensorimotor cortex with electrocorticographic spectral analysis. I. Alpha and beta event-related desynchronization. Brain 121 (Pt 12), 2271-2299.

Engel, A.K., Fries, P., Singer, W., (2001). Dynamic predictions: oscillations and synchrony in top-down processing. Nat Rev Neurosci 2, 704-716.

Ergenoglu, T., Demiralp, T., Bayraktaroglu, Z., Ergen, M., Beydagi, H., Uresin, Y., (2004). Alpha rhythm of the EEG modulates visual detection performance in humans. Brain Res Cogn Brain Res 20, 376-383.

Foxe, J.J., Simpson, G.V., Ahlfors, S.P., (1998). Parieto-occipital approximately 10 Hz activity reflects anticipatory state of visual attention mechanisms. Neuroreport 9, 3929-3933.

Fries, P., (2005). A mechanism for cognitive dynamics: neuronal communication through neuronal coherence. Trends Cogn Sci 9, 474-480.

Fries, P., Reynolds, J.H., Rorie, A.E., Desimone, R., (2001). Modulation of oscillatory neuronal synchronization by selective visual attention. Science 291, 1560-1563.

Gaetz, W., Cheyne, D., (2006). Localization of sensorimotor cortical rhythms induced by tactile stimulation using spatially filtered MEG. Neuroimage 30, 899-908.

Hämäläinen, M., Hari, R., Ilmoniemi, R.J., Knuutila, J., Lounasmaa, O.V., (1993). Magnetoencephalography—theory, instrumentation, and applications to noninvasive studies of the working human brain. Reviews of Modern Physics 65, 413-497.

Hanslmayr, S., Aslan, A., Staudigl, T., Klimesch, W., Herrmann, C.S., Bauml, K.H., (2007). Prestimulus oscillations predict visual perception performance between and within subjects. Neuroimage 37, 1465-1473.

Hari, R., Karhu, J., Hamalainen, M., Knuutila, J., Salonen, O., Sams, M., Vilkman, V., (1993). Functional organization of the human first and second somatosensory cortices: a neuromagnetic study. Eur J Neurosci 5, 724-734.

Hari, R., Salmelin, R., (1997). Human cortical oscillations: a neuromagnetic view through the skull. Trends Neurosci 20, 44-49.

Jasper, H., Penfield, W., (1949). Electrocorticograms in man: Effect of voluntary movement upon the electrical activity of the precentral gyrus. Archiv Für Psychiatrie und Zeitschrift Neurologie 183, 163-174.

Kastner, S., Pinsk, M.A., De Weerd, P., Desimone, R., Ungerleider, L.G., (1999). Increased activity in human visual cortex during directed attention in the absence of visual stimulation. Neuron 22, 751-761.

Kelly, S.P., Lalor, E.C., Reilly, R.B., Foxe, J.J., (2006). Increases in alpha oscillatory power reflect an active retinotopic mechanism for distracter suppression during sustained visuospatial attention. J Neurophysiol 95, 3844-3851.

Lampl, I., Yarom, Y., (1993). Subthreshold oscillations of the membrane potential: a functional synchronizing and timing device. J Neurophysiol 70, 2181-2186.

Liang, H., Bressler, S.L., Ding, M., Truccolo, W.A., Nakamura, R., (2002). Synchronized activity in prefrontal cortex during anticipation of visuomotor processing. Neuroreport 13, 2011-2015.

Linkenkaer-Hansen, K., Nikulin, V.V., Palva, S., Ilmoniemi, R.J., Palva, J.M., (2004). Prestimulus oscillations enhance psychophysical performance in humans. J Neurosci 24, 10186-10190.

McMains, S.A., Fehd, H.M., Emmanouil, T.A., Kastner, S., (2007). Mechanisms of feature- and space-based attention: response modulation and baseline increases. J Neurophysiol 98, 2110-2121.

Nagamine, T., Kajola, M., Salmelin, R., Shibasaki, H., Hari, R., (1996). Movement-related slow cortical magnetic fields and changes of spontaneous MEG- and EEG-brain rhythms. Electroencephalogr Clin Neurophysiol 99, 274-286.

Nakano, T., Homae, F., Watanabe, H., Taga, G., (2008). Anticipatory cortical activation precedes auditory events in sleeping infants. PLoS One 3, e3912.

O'Connor, D.H., Fukui, M.M., Pinsk, M.A., Kastner, S., (2002). Attention modulates responses in the human lateral geniculate nucleus. Nat Neurosci 5, 1203-1209.

Palva, S., Linkenkaer-Hansen, K., Naatanen, R., Palva, J.M., (2005). Early neural correlates of conscious somatosensory perception. J Neurosci 25, 5248-5258.

Percival, D.B., Walden, A.T., (1993). Spectral Analysis for Physical Applications: Multitaper and Conventional Univariate Techniques. Cambridge University Press, Cambridge.

Pfurtscheller, G., Lopes da Silva, F.H., (1999). Event-related EEG/MEG synchronization and desynchronization: basic principles. Clin Neurophysiol 110, 1842-1857.

Pogosyan, A., Gaynor, L.D., Eusebio, A., Brown, P., (2009). Boosting cortical activity at Beta-band frequencies slows movement in humans. Curr Biol 19, 1637-1641.

Reber, S., (1993). Implicit Learning and Tacit Knowledge: An Essay on the Cognitive Unconscious. Oxford University Press, Oxford.

Ress, D., Backus, B.T., Heeger, D.J., (2000). Activity in primary visual cortex predicts performance in a visual detection task. Nat Neurosci 3, 940-945.

Rihs, T.A., Michel, C.M., Thut, G., (2007). Mechanisms of selective inhibition in visual spatial attention are indexed by alpha-band EEG synchronization. Eur J Neurosci 25, 603-610.

Romei, V., Brodbeck, V., Michel, C., Amedi, A., Pascual-Leone, A., Thut, G., (2008). Spontaneous fluctuations in posterior alpha-band EEG activity reflect variability in excitability of human visual areas. Cereb Cortex 18, 2010-2018.

Salinas, E., Sejnowski, T.J., (2001). Correlated neuronal activity and the flow of neural information. Nat Rev Neurosci 2, 539-550.

Salmelin, R., Hari, R., (1994). Spatiotemporal characteristics of sensorimotor neuromagnetic rhythms related to thumb movement. Neuroscience 60, 537-550.

Sauseng, P., Klimesch, W., Gerloff, C., Hummel, F.C., (2009). Spontaneous locally restrictedm EEG alpha activity determines cortical excitability in the motor cortex. Neuropsychologia 47, 284-288.

Sauseng, P., Klimesch, W., Stadler, W., Schabus, M., Doppelmayr, M., Hanslmayr, S., Gruber, W.R., Birbaumer, N., (2005). A shift of visual spatial attention is selectively associated with human EEG alpha activity. Eur J Neurosci 22, 2917-2926.

Summerfield, C., Egner, T., (2009). Expectation (and attention) in visual cognition. Trends Cogn Sci 13, 403-409.

Tamura, Y., Hoshiyama, M., Nakata, H., Hiroe, N., Inui, K., Kaneoke, Y., Inoue, K., Kakigi, R., (2005). Functional relationship between human rolandic oscillations and motor cortical excitability: an MEG study. Eur J Neurosci 21, 2555-2562.

Taniguchi, M., Kato, A., Fujita, N., Hirata, M., Tanaka, H., Kihara, T., Ninomiya, H., Hirabuki, N., Nakamura, H., Robinson, S.E., Cheyne, D., Yoshimine, T., (2000). Movement-related desynchronization of the cerebral cortex studied with spatially filtered magnetoencephalography. Neuroimage 12, 298-306.

Thut, G., Nietzel, A., Brandt, S.A., Pascual-Leone, A., (2006). Alpha-band electroencephalographic activity over occipital cortex indexes visuospatial attention bias and predicts visual target detection. J Neurosci 26, 9494-9502.

van Dijk, H., Schoffelen, J.M., Oostenveld, R., Jensen, O., (2008). Prestimulus oscillatory activity in the alpha band predicts visual discrimination ability. J Neurosci 28, 1816-1823.

Voisin, J., Bidet-Caulet, A., Bertrand, O., Fonlupt, P., (2006). Listening in silence activates auditory areas: a functional magnetic resonance imaging study. J Neurosci 26, 273-278.

Volgushev, M., Chistiakova, M., Singer, W., (1998). Modification of discharge patterns of neocortical neurons by induced oscillations of the membrane potential. Neuroscience 83, 15-25.

Witham, C.L., Baker, S.N., (2007). Network oscillations and intrinsic spiking rhythmicity do not covary in monkey sensorimotor areas. J Physiol 580, 801-814.

Worden, M.S., Foxe, J.J., Wang, N., Simpson, G.V., (2000). Anticipatory Biasing of Visuospatial Attention Indexed by Retinotopically Specific α-Band Electroencephalography Increases over Occipital Cortex. J Neurosci 20:RC63, 1-6.

Wyart, V., Tallon-Baudry, C., (2008). Neural dissociation between visual awareness and spatial attention. J Neurosci 28, 2667-2679.

Zhang, Y., Chen, Y., Bressler, S.L., Ding, M., (2008a). Response preparation and inhibition: the role of the cortical sensorimotor beta rhythm. Neuroscience 156, 238-246.

Zhang, Y., Wang, X., Bressler, S.L., Chen, Y., Ding, M., (2008b). Prestimulus cortical activity is correlated with speed of visuomotor processing. J Cogn Neurosci 20, 1915-1925.

Effects of DHA-, uridine- and choline- containing diets on synapse number and size, brain metabolism and behaviour in APP/PS1 Alzheimer mice

Anna-Lena Janssen[1,2]
Supervisors: D Jansen[1,2], V Zerbi[1,2], A Hafkemeijer[1,2], M Mutsaers[1,2],
CEEM van der Zee[3], PJ Dederen[1,2], LM Broersen[4], A Heerschap[5], AJ Kiliaan[1,2]

[1]*Department of Anatomy, Radboud University Nijmegen Medical Centre, Nijmegen, The Netherlands*
[2]*Donders Institute for Brain, Cognition and Behaviour, Radboud University Nijmegen, Nijmegen, The Netherlands*
[3]*Department of Cell Biology, NCMLS, Radboud University Nijmegen Medical Centre, Nijmegen, The Netherlands*
[4]*Danone Research Wageningen, The Netherlands*
[5]*Department of Radiology, Radboud University Nijmegen Medical Centre, Nijmegen, The Netherlands*

The search for alternative therapies for Alzheimer's disease (AD) is of high interest as medication and immunization therapies are not optimal yet. Intake of the fish oil component docosahexaenoic acid (DHA) seems a promising treatment for AD as it reduces many features of AD and the risk of developing AD. In the first part of this study, we investigated effects of a DHA-enriched diet on hippocampal synapse size and number by quantifying synaptophysin immunoreactive presynaptic boutons (SIPBs) in 8- and 15-month-old APP/PS1 and wild-type mice (wt). SIPB size and number increased with age and AD progression (Size: APP/PS1 $p < 0.005$, wt $p > 0.1$; Number: APP/PS1 $p < 0.01$, wt $p > 0.5$), whereas DHA supplementation significantly reduced age- and AD-related changes in SIPB size in one region of the hippocampus ($p < 0.05$). This finding supports the suggested use of DHA as a treatment for AD. In the second part of the study, the phospholipid precursors uridine-monophosphate (U) and choline (C), and other components like anti-oxidants and B-vitamins (+) were added to the DHA diets, as recent studies suggest that these components enhance the beneficial effects of DHA. We investigated effects of DHA/U diets and DHA/UC+ diets on behaviour using the open field test, and on hippocampal brain metabolites using proton magnetic resonance spectroscopy (1H-MRS). The diets could neither ameliorate behavioural symptoms nor increase levels of the brain metabolite N-acetylaspartate. However, in comparison to mice on standard diets, DHA/UC+ fed mice showed significantly higher ratios of choline-containing compounds (Cho; $p < 0.05$). Increased Cho levels might enhance regrowth of neuronal membranes and memory processes and thereby reduce cognitive symptoms of AD. Our findings emphasize the importance of the combination of poly-unsaturated fatty acids and membrane precursors as treatment for Alzheimer's disease.

Keywords: DHA, choline, uridine, Alzheimer's disease, synaptophysin, behaviour, MRS.

Corresponding author: Anna-Lena Janssen, e-mail: j.anna.lena@gmail.com

1. Introduction

Alzheimer's disease (AD) is a neurodegenerative disease and the most common cause of dementia. In the progression of the disease, patients' abilities of learning and memory decline and personality changes like increased anxiety and restlessness manifest.

The cause of neurodegeneration in AD is not clear and the disease is still not curable. The less-prevalent early-onset form of AD is caused by mutations in genes involved in the production of amyloid beta (Aβ). Consequently, this peptide was also attributed a central role in the pathogenesis of late-onset or sporadic AD. Aβ accumulates in the parenchyma of the brain in the form of plaques and in the walls of cerebral blood vessels as cerebral amyloid angiopathy (CAA). Researchers are trying to develop immunization therapies against Aβ, but these are not safe in humans yet. In multiple transgenic mouse models, active and passive immunization lowered brain amyloid levels and improved cognition. However, when active immunization advanced to clinical trials, a subset of patients developed meningo-encephalitis (Wilcock and Colton, 2008). Moreover, Aβ immunization results in solubilization of plaque Aβ which is, in part, cleared from the brain via the perivascular pathway. This, however, can cause a transient increase in the severity of CAA (Boche et al., 2008). Additionally, soluble Aβ oligomers, rather than Aβ plaques, seem to be responsible for the most deleterious effects of Aβ (Klein et al., 2001). Hence, before vaccines against the Aβ peptide can be used by AD patients to lower their symptoms, refinement of the method is required. Alternative therapies therefore are of great interest, also because it is still unclear whether Aβ is the initiator of AD.

Instead of one sole mechanism it might rather be the case that a combination of diet, lifestyle, vascular, genetic, and amyloid related factors is the cause of the disease. Lately a lot of research has therefore focused on diets and dietary supplements as therapy. The importance of a dietary influence on the pathogenesis of AD is reflected by the finding that high serum cholesterol levels (Kivipelto et al., 2002), obesity (Kivipelto et al., 2005) and diabetes (Biessels and Kappelle, 2005) are risk factors for developing AD.

1.1 Multiple ways in which DHA might slow down AD progression

A promising dietary treatment against AD is intake of the fish oil component docosahexaenoic acid (DHA) (Freund-Levi et al., 2006). This omega-3 long chain poly-unsaturated fatty acid is a constituent of cell membranes and particularly important in the maintenance of brain mechanisms underlying cognitive functions (Eilander et al., 2007). Epidemiological studies show that sufficient DHA intake reduces the risk of developing AD (Kalmijn et al., 1997; Barberger-Gateau et al., 2002; Morris et al., 2003). In support of this notion, studies in APP transgenic mice showed decreased brain Aβ levels after dietary DHA supplementation (Lim et al., 2005; Oksman et al., 2006; Hooijmans et al., 2007, 2009). Moreover, DHA can reduce cognitive decline in AD patients (Freund-Levi et al., 2006; Kotani et al., 2006; van Gelder et al., 2007). DHA might influence the development of AD via a combination of multiple mechanisms.

First, DHA protects against oxidative stress (Yavin et al., 2002; Wu et al., 2004; Bazan, 2005). In AD patients, oxidative stress is increased, leading to an increased production of Aβ (Misonou et al., 2000), which in turn causes oxidative stress and thereby promotes its own production and AD pathogenesis. DHA can be transformed to "neuroprotectin D1", which suppresses Aβ neurotoxicity (Lukiw et al., 2005) and might thereby slow down AD pathogenesis.

Second, DHA has a positive effect on vascular health (de Wilde et al., 2002, 2003; Breslow, 2006). It is suggested that cerebrovascular dysfunction is an early pathogenic event in AD (Iadecola, 2004; Kalaria, 2009). Hypoperfusion of the brain may lead to lowered energy metabolism, increased oxidative stress and increased Aβ production (Bennett et al., 2000; Farkas and Luiten, 2001; de la Torre, 2000, 2002) and can thereby finally lead to neuronal cell death (Farkas and Luiten, 2001; Velliquette et al., 2005; Zlokovic, 2005). Indeed, patients with AD show cerebrovascular abnormalities and decreased cerebral perfusion (Farkas and Luiten, 2001; Ruitenberg et al., 2005; Schreiber et al., 2005). The finding that hypertension (Heijer et al., 2003) and atherosclerosis (van Oijen et al., 2007) are risk factors for developing AD further strengthens the hypothesis that cerebrovascular pathology is the primary trigger in the development of sporadic AD (de la Torre, 2000, 2004). As DHA improves vascular health, it could be hypothesized that DHA slows down AD progression by improving cerebral perfusion.

Third, DHA can increase membrane fluidity (Hashimoto et al., 1999) and might thereby lead to reduced Aβ production. The peptide is generated via cleavage of the amyloid precursor protein (APP) by

β- and γ-secretase. If APP is cleaved by the non-amyloidogenic α-secretase then Aβ production is prohibited. According to the membrane fluidity hypothesis (Wolozin, 2001), cleavage by the amyloidogenic β- and γ-secretases is increased in cholesterol-rich, and therefore rigid, lipid domains within the membrane (Fassbender et al., 2001; Wahrle et al., 2002). In contrast, in fluid phosphatidylcholine domains, APP is better accessible for cleavage by α-secretase which results in reduced production of Aβ (Wolozin, 2001, 2004). DHA increases the production of phosphatidylcholine (Wurtman et al., 2006) – and hence increases membrane fluidity – as it is an essential precursor in the synthesis of phosphatidylcholine (Figure 1). DHA might thereby promote the non-amyloidogenic pathway.

Finally, as phosphatidylcholine is the major constituent of neuronal membranes, DHA might stimulate regrowth of these by increasing the availability of phosphatidylcholine. Indeed, it could be shown that DHA promotes the synthesis of synaptic membranes (Wurtman et al., 2006) and increases the number of dendritic spines (Sakamoto et al., 2007).

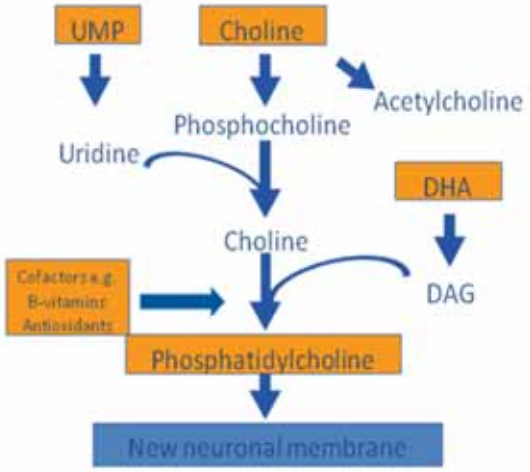

Figure 1. Kennedy Cycle production of phosphatidylcholine.

1.2 Uridine and choline might enhance beneficial effects of DHA

Recent studies report that the addition of the nucleotide uridine to DHA diets enhances the positive effects of DHA on membrane quality and cognition. Uridine is, like DHA, a precursor of phosphatidylcholine and is found e. g. in tomatoes, brewer's yeast or breast milk. Co-administration of uridine (in the form of uridine-mono-phosphate, UMP) and DHA increases brain levels of phosphatidylcholine in rats (Holguin et al., 2008a) and enhances dendritic spine levels and cognitive functions (Wurtman et al., 2009). A dietary supplement containing DHA and UMP hence seems to be more effective than a diet containing only DHA.

However, the addition of choline, another phosphatidylcholine precursor, might further enhance the effects of the DHA-UMP-mix. Sources of choline are e.g. mother's milk, soy and lecithin. The combination of DHA, UMP and choline increases the quantities of phosphatidylcholine and specific synaptic proteins and the number of dendritic spines (Holguin et al., 2008b). Moreover, it enhances the production of acetylcholine, the key neurotransmitter in memory processes (Lee et al., 2001). DHA, UMP and choline are all phosphatidylcholine precursors and are all individually able to limit the overall rate of phosphatidylcholine synthesis. A combination of DHA, UMP and choline might therefore be a better treatment than a mix only containing DHA and UMP.

The synthesis of phosphatidylcholine can additionally be enhanced by the addition of co-factors of this cycle. These include B-vitamins and anti-oxidants. As brain tissue in AD patients is exposed to oxidative stress (e.g., protein oxidation, lipid oxidation, and glycoxidation) (Markesbery, 1997), anti-oxidants may be beneficial for reducing damage caused by free radicals. In support of this notion, epidemiological studies in humans show positive effects of the use of anti-oxidant supplements on the risk of developing Alzheimer disease (Head, 2009).

In summary, all three compounds – DHA, UMP and choline – might individually ameliorate some of the manifestations of Alzheimer's disease. A combination of all three plus B-vitamins and anti-oxidants might be the most effective treatment.

1.3 Experimental paradigm and predictions

A well established mouse model for studying treatment effects in AD is the double transgenic APPswe/PS1ΔE9 mouse (Borchelt et al, 1997; Spires and Hyman, 2005). This mouse model exhibits progressive increase in brain Aβ levels as well as disease-related cognitive and behavioural changes. First plaques occur in hippocampus and cortex at the age of 6-months. We therefore use 6 - 9-months-old mice and concentrate our analysis of synaptic and

metabolic changes on the hippocampus, as this brain structure plays a major role in learning and memory (Knowles et al., 1992; Alvarez et al., 1995).

In the present study, we test the hypotheses that DHA can ameliorate behavioural symptoms and reduce synaptic alterations in AD, and that the addition of UMP, or UMP plus choline plus components like anti-oxidants and B-vitamins can enhance the beneficial effects of DHA.

To test the hypothesis that DHA can slow down AD-related synaptic alterations, we measure the effects of a DHA diet on synapse number and size in different regions of the hippocampus in 8- and 15-months-old mice. The analysis of synaptophysin immunoreactive presynaptic boutons (SIPBs) is a well established method to study size and number of synapses (Rutten et al., 2005). We expect AD-related synaptic changes to be lower in mice fed DHA compared to mice fed a standard diet (STD).

To test the hypothesis that UMP or choline can enhance the beneficial effects of DHA, we study the effects of a diet enriched with DHA and UMP (DHA/U), and a diet enriched with DHA, UMP, choline and other components (DHA/UC+) on open field behaviour. APP/PS1 mice typically show hyperactivity and increased anxiety behaviour. In a former study in 8-months-old APP/PS1 mice, behavioural symptoms could not be reduced by a diet only enriched with DHA (Hooijmans et al., 2009). Here we investigate whether DHA diets with additional enrichments are able to decrease hyperactivity and anxiety in 6-months-old mice.

Additionally, we investigate effects of genotype and of DHA/U and DHA/UC+ diets on levels of N-acetylaspartate (NAA) and choline-containing compounds (Cho). These brain metabolites are markers for neuronal density and cell membrane turnover, respectively, and can be measured non-invasively using proton magnetic resonance spectroscopy (1H-MRS). We use single-voxel 1H-MRS which allows investigation of chemicals in a defined brain region of interest, in this case the hippocampus.

In summary, we test whether a DHA-enriched diet can ameliorate AD-related synaptic changes measured by quantifying SIPBs, and whether diets enriched with DHA plus UMP or DHA plus UMP, choline, antioxidants and b vitamins, can be more effective in reducing behavioural changes than a diet with DHA alone. Additionally, we investigate brain metabolite profiles and test whether the combinatorial diets can reduce metabolic alterations in APP/PS1 mice.

2. Animals and Methods

2.1 Animals and diets

The APPswe/PS1dE9 founder mice were obtained from John Hopkins University, Baltimore, USA (D. Borchelt and J. Jankowsky, Department of Pathology) and a colony was established at the Radboud University, Nijmegen, the Netherlands. Mice were created by co-injection of chimeric mouse/human APPswe (mouse APP695 harbouring a human Aβ domain and mutations K595N and M596L linked to Swedish familial AD pedigrees) and human PS1-dE9 (deletion of exon 9) vectors controlled by independent mouse prion protein promoter elements. The two transfected genes co-integrate and co-segregate as a single locus (Jankowsky et al., 2001). The breeder mice were backcrossed to C57BL6/J for 9 generations to obtain mice for the current study.

Throughout the experiments, the animals were housed in a controlled environment, with room temperature at 21°C, and an artificial 12:12h light:dark cycle (lights on at 7 a.m.). Mice used for immunohistochemistry were housed individually; mice used for open field and 1H-MRS were housed in groups of 2 - 3 animals per cage. Water was available ad libitum. A defined number (= 3.5g/mouse) of food pellets were given per cage and day. The experiments were performed according to Dutch federal regulations for animal protection and were approved by the Veterinary Authority of the Radboud University Nijmegen Medical Center.

Male APP/PS1 transgenic mice and their wild type littermates were assigned to five different diet groups, which varied with respect to the composition of the 5% fat in the diets and with respect to the amount of additional supplements. Standard control diet 1 (STD1) and 2 (STD2) contained intermediate amounts of saturated fatty acids (SFA) and long chain poly-unsaturated fatty acids (lc-PUFAs) and an intermediate n-6/n-3 lc-PUFA ratio. The DHA-enriched diets contained a low percentage SFA, a high percentage lc-PUFAs and a low n-6/n-3 lc-PUFA ratio. The DHA diet contained 0.35% DHA. The DHA/U diet contained 0.70% DHA and 1g uridine-mono-phosphate (UMP) replacing 1g corn starch. In the DHA/UC+ diet an additional 1.45g corn starch was replaced by nutrients like choline, B-vitamins and anti-oxidants. A complete overview of the contents of fatty acids and additional supplements in the experimental diets is available in Table 1. Feeding with the diets started at the age of 2 months and was

Table 1. Sources of fatty acids and amounts of additional supplements in the experimental diets in g/100g. Diets STD1 and DHA were used for immunohistochemistry; diets STD2, DHA/U and DHA/UC+ were used for open field test and 1H MR spectroscopy. FAs = fatty acids.

	Dietary groups				
	STD1	DHA	STD2	DHA/U	DHA/UC+
Source of FAs					
Soy oil	2.87	3.25	1.9	-	-
Coconut oil	1.57	0.05	0.9	0.1	0.1
Corn oil	-	-	2.2	1.87	1.87
Fish oil	-	1.45	-	3.03	3.03
DHA	-	0.35	-	0.70	0.70
EPA	-	0.08	-	0.16	0.16
Sunflower oil	0.26	-	-	-	-
Linseed oil	0.30	0.25	-	-	-
Total amount	5.00	5.00	5.0	5.0	5.0
Additional supplements					
Pyridoxine-HCL	-	-	-	-	0.00328
Folic acid	-	-	-	-	0.00067
Cyanocobalamin	-	-	-	-	0.0035
Ascorbic acid	-	-	-	-	0.16
dl-α-tocopheryl acetate	-	-	-	-	0.465
UMP disodium	-	-	-	1.0	1.0
Choline chloride	-	-	-	-	0.402
Soy lecithine	-	-	-	-	0.412
Sodium selenite	-	-	-	-	0.00023
Total amount	0.0	0.0	0.0	1.0	2.45

maintained for the whole experimental period.

Diets STD1 and DHA were used for determination of synaptophysin immunoreactivity in 8- and in 15-months-old mice. The diets were isocaloric and diet groups were balanced for weight. The brain weights of the mice were determined before decapitation. For an overview of the number of mice used in each experimental group, see Table 2. STD2, DHA/U and DHA/UC+ were used for behavioural testing and 1H-MR spectroscopy. Again, the diets were isocaloric and diet groups were balanced for weight. The DHA/U diet was given to wild-type mice only as the purpose was to compare the efficacy of this diet with the DHA/UC+ diet within the APP/PS1 group. Mice were behaviourally tested during the light phase at the age of 6 - 7 months (mean = 6.3 months), in four cohorts of 15 mice, balanced by genotype and diet. Subsequently, at the age of 8 - 10 months (mean = 9.1 months), mice were used for 1H-MRS. They were tested during the light phase in an order balanced by genotype and diet. Body weights of the mice were determined one day before the start of the open field test and on the day of MRS measurements. For an overview of the number of mice used in each experimental group, see Table 2.

2.2 Synaptophysin immunohistochemistry

To assess synaptic integrity, we measured size and number of synaptophysin immunoreactive presynaptic boutons (SIPBs). Mice were transcardially perfused starting with a 0.1M phosphate buffered saline (PBS) followed by Somogyi's fixative (4% paraformaldehyde, 0.05% glutaraldehyde and 0.2% picric acid in 0.1M phosphate buffer, PB, pH=7.2). Following transcardial perfusion fixation, mice were decapitated and brains were removed from the skull. The entire brain, without the spinal cord, was post-fixed for 15h at 4°C in Somogyi's fixative and subsequently stored in PB at 4°C.

Before sectioning, the brain tissue was cryoprotected by overnight immersion in 30% sucrose in PB at 4°C. Series of 40µm coronal sections were cut through the brain using a sliding microtome (Microm HM 440, Walldorf, Germany) equipped with an object table for freeze sectioning at −60°C. Immunohistochemistry was

Table 2. Number of mice used in each experimental group. IHC = immunohisto-chemistry, 1H-MRS = proton magnetic resonance spectroscopy, wt = wild-type, tg = APP/PS1

			IHC
		8	15
Groups		months	months
STD1(wt)		7	7
STD1(tg)		7	6
DHA(wt)		5	7
DHA(tg)		7	7
		Open field	1H-MRS
		6	9
Groups	total	months	months
STD2(wt)	12	12	5
STD2(tg)	13	13	7
DHA/U(tg)	10	10	4
DHA/UC+(wt)	13	13	4
DHA/UC+(tg)	11	11	4

performed using standard free-floating labeling procedures (Hooijmans et al., 2007). Synaptophysin immunoreactivity was visualized using monoclonal mouse anti-synaptophysin antibody (1:6000). M.O.M biotinylated anti-mouse IgG (1:2500) was used as a secondary antibody.

Synaptophysin immunoreactivity was determined in the parenchyma of stratum lucidum (SL), stratum radiatum (SR) and outer (OML) and inner molecular layer (IML) of dentate gyrus of the hippocampus (Figure 2). The hippocampus was chosen because it demonstrates neurodegeneration and Aβ deposition in early stages of AD and because of its relevance for cognitive and emotional tasks. Appropriate sections were digitalized and photomicrographed using the Neurolucida System (Stereo Investigator), equipped with a 100× oil immersion objective and a 10× projection lens. Per region of interest, two photos were taken in the intended brain areas. All measurements were performed double blind by two investigators, resulting in a total of four photos per brain region.

Quantitative analyses were done by image analysis using AnalySIS-pro software (Soft Imaging System, Münster, Germany). All settings were kept identical for all analyses and background levels were equalized using a threshold. For every photomicrograph, the region of interest (ROI) was defined. Shading correction was performed before measurement to correct for irregularities in illumination in the microscopic field. A differential contrast enhancement (DCE) filter was applied to selectively enhance weak differences in contrast. To eliminate noise signal and to differentiate between possible artifacts and specific SIPBs, particles were classified based on size. Particles ranging between 0.1 and 4.5μm² were considered as normal SIPBs (Mulder et al., 2007). For every photomicrograph, the region of interest (ROI) was defined. The average number of SIPBs per photo was calculated as total number of SIPBs in the ROI divided by the area of the ROI. The average number of SIPBs per brain region was then calculated as average of the total four photos per region. Values for total hippocampus (HC) were calculated as mean of the values for OML, IML, SL and SR. The same principle was used for calculating the mean size of the SIPBs.

2.3 Open field test

To analyze explorative behaviour, an open field test as described by Streijger et al. (2005) was used. Mice were placed in an open field box of 50x50x50cm

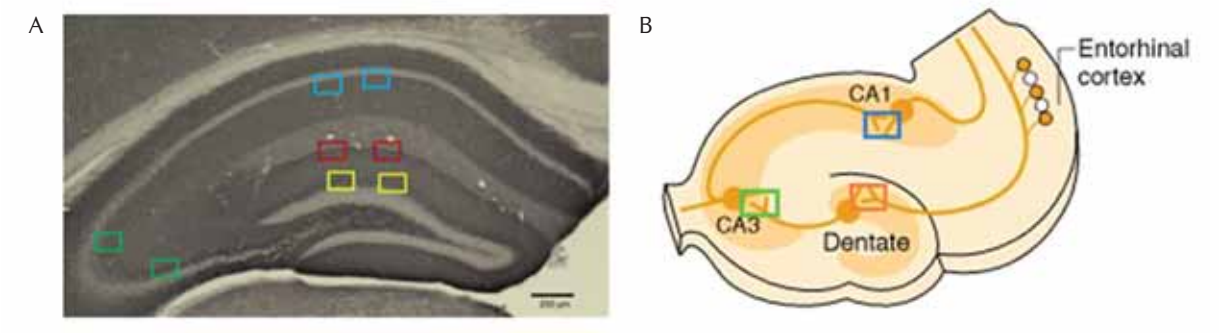

Figure 2. A. Representative photomicrograph of frontal section through the hippocampus of a 15-month-old APP/PS1 mouse. The colored squares represent the areas where the high-power photomicrographs for quantitative SIPB analysis were taken within OML (red), IML (yellow), SL (green) and SR (blue). **B.** Diagram of the hippocampal network showing which synapses were analysed. In IML and OML (orange square) synaptic contacts are formed between neurons of the entorhinal cortex and granule cells of the dentate gyrus, synapses connecting granule cells and CA3 pyramidal cells lie in SL, and CA3-CA1 synapses are found in the SR. Modified picture from Agranoff, Cotman, and Uhler.

for 30min. Durations (s) of walking, wall leaning, rearing, sitting and grooming were scored and afterwards analyzed in three blocks of 10min. In addition, moving latency, i. e. the time before starting to move after being placed in the open field, and the total number of feces were recorded.

The open field activities were DVD-recorded and analyzed using Noldus Ethovision 3.1 software (Noldus Information Technology, Inc., Leesburg, VA). Measures of total walking distance, mobility and peripheral and central locomotion were obtained.

The center of the box was defined as a square measuring 20x20cm, the periphery was defined as the outer 15cm wide zone and corners measured 10x10cm. Mobility parameters were set as follows: immobility threshold (5%), mobile threshold (20 - 60%), strong mobile threshold (95%). A threshold set to 5.0%, for example, means that there is no more than 5.0% change in the pixels of a detected object between current sample and previous sample (see section 12.3.3 of EthoVision 3.1 Reference Manual).

2.4 1H-MRS

Following the open field test, metabolite concentrations in the hippocampus were determined using 1H-MRS with single voxel technique. Before starting with the MR measurements, the mice were weighed. During the MR experiments, mice were anesthetized with 1.5% - 2.0% isoflurane (Nicholas Piramal (I) Limited, London, United Kingdom) in a mixture of oxygen and N2O (2:1) through a nose cone. The body temperature was maintained at 35.2 ± 1.2°C using a heated air ventilator and monitored with a rectal fiber-optic temperature probe. Mice were completely covered with a paper tissue to avoid skin irritations from hot air. Respiratory rate was monitored continuously using Mode 1025 Small Animal Monitoring & Gating System (SA Instrument, Inc. Stony Brook, NY 11790, USA).

MRI was performed using a 7.0 T magnet with a horizontal bore (BIOSPEC BC70/30USR Bruker, Karlsruhe, Germany) equipped with a 21cm inner diameter self-shielded gradient system. An elliptical shaped surface coil (Clinscan SUC 300 1H RATBR, Bruker, Karlsruhe, Germany) was used for signal transmission and reception. The spectroscopic volume of interest (VOI) of 1.0×1.0×1.6mm was positioned in the left frontal hippocampus (Figure 3). Anatomic magnetic resonance scans were used for image-guided positioning of the voxel. Water-suppressed 1H-MRS spectra were acquired with STEAM (Stimulated Echo Acquisition Mode) sequence with repetition time (TR) = 1500ms and TE = 13ms with 1024 signal averages. Water suppression was performed with variable pulse power and optimized relaxation delays (VAPOR) with repetition time (TR) = 1500ms and TE = 13ms with 32 signal averages. Automatic and manual 3D shimming of the VOI was performed before every scan.

The JAVA version of the MRUI software package (jMRUI) was used for handling the data. The phase of each metabolite spectrum was corrected with its water reference spectrum and the water peak was suppressed with HLSVD algorithm in JMRUI. Using an appropriate dataset of prior knowledge, all the metabolite peaks were identified. To suppress the baseline of the signal, the first points of the time-domain signal, the FID, are multiplied with a quarter-sine wave. For the same reasons, the first three points of the FID were truncated. The quantification of the peak areas was performed using the AMARES (advanced method for accurate,

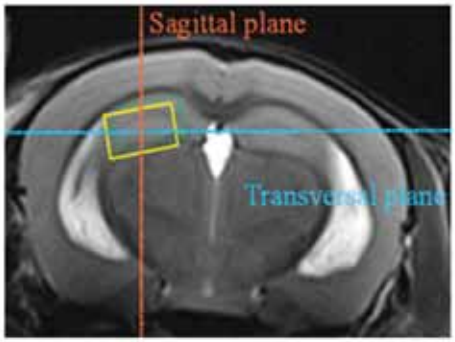

Figure 3. Representative image of positioning the volume of interest into a mouse brain.

robust, and efficient spectral fitting) algorithm of the JMRUI software package. AMARES is an interactive method for accurate and efficient parameter estimation of MRS signals with use of prior knowledge (Vanhamme et al., 1997). Metabolite concentrations are given relative to total creatine (Cr) as applied by others (Frederick et al., 2004; Ackl et al., 2005; Godbolt et al., 2006).

2.5 Statistical analyses

Data are expressed as mean ± SEM and were analyzed with SPSS for windows 16.0 software (SPSS Inc., Chicago, IL, USA). The repeated measures ANOVA was used for the open field parameters (with the ANOVA's were conducted to analyze possible differences between the two genotypes and the diet groups in the open field parameters and the

MR spectra. MANOVA's were also applied to body weights. The between group factors were Genotype and Diet. If interactions between genotype and diet (between-group-factors) were present, the data were split for the concerning factor and thereafter analyzed with the MANOVA. To evaluate regional differences in synaptophysin immunohistochemistry, a one-way ANOVA was used. If no interactions between the genotype and diet were present and overall analysis revealed a significant difference, the separate groups were analyzed post hoc by using Tukey's HSD test. Statistical significance was set at $p \leq 0.05$.

3. Results

3.1 Synaptophysin immunohistochemistry

3.1.1 Brain weight

Relative brain weight was not affected by genotype or diet in both 8- and 15-months-old mice. Overall mean brain weight was 1.60 ± 0.03% of total body weight in the 8-months-old mice and 1.17 ± 0.03% in the 15-months-old group. Absolute brain weights did not differ either.

3.1.2 Size of SIPBs

Genotype effects were observed in 8-months-old mice only. At this age, transgenic mice had smaller SIPBs in SL ($p<0.05$), SR ($p=0.052$) and total HC ($p<0.05$) in comparison with wild-type mice (wt; Figure 4A). At the age of 15-months, differences between genotype groups were not observed any longer (Figure 4B). The reason for that is that SIPB size increased with age and that SIPB size increased more significantly in APP/PS1 mice (SL, SR and HC: $p<0.005$) than in wild-type mice (SL, SR and HC: $p>0.1$). Age-related increases in SIPB size were also observed in IML (APP/PS1: $p<0.01$; wt: $p<0.05$) and OML (APP/PS1: $p<0.005$; wt: $p<0.05$). Diet effects were observed in the SL in both age groups. Mice fed DHA had smaller SIPBs in SL (8-months: $p<0.01$; 15-months: $p<0.05$; Figure 4C-D) than STD1 fed mice. Genotype*diet interactions were not observed.

3.1.3 Number of SIPBs

Genotype effects were observed in 15-months-old mice only. At this age, transgenic mice had more SIPBs in OML ($p<0.05$), SR ($p=0.078$) and HC ($p=0.058$) than wild-type mice (Figure 4D). Like SIPB size, SIPB number increased with age more significantly in APP/PS1 mice (IML, OML, HC: $p<0.01$) than in wild-type mice (IML: $p>0.01$; OML, SR and HC: $p>0.5$). Diet effects or genotype*diet interactions were not observed in any group.

3.2 Open field test

3.2.1 Body weight

All mice were weighed one day before starting the open field test. Body weight was not affected by genotype or diet. Mean body weight was 28.7 ± 1.9 g.

3.2.2 Types of activities

The behaviour of the mice changed with time. During the 30 min of observation, in all mice the time spent walking ($p<0.001$) and wall leaning ($p<0.001$) decreased, whereas the time spent sitting ($p<0.001$) and grooming ($p<0.001$) increased. The time spent rearing did not change significantly. APP/PS1 mice were more anxious than wild-type mice: They spent less time grooming than wild-type mice ($p=0.066$). Genotype*diet interactions were observed in the time spent sitting and in the amount of urine. In the DHA/UC+ group, transgenic mice increased the time spent sitting more pronouncedly than wild-type mice ($p<0.05$). DHA/UC+ fed wild-type mice urinated the most in comparison with the other groups ($p<0.05$). There were no differences in types of activities between APP/PS1 mice on STD2, DHA/U and DHA/UC+ diets.

3.2.3 Preferred zones and mobility

APP/PS1 mice were more active in the open field than wild type mice. They walked a longer distance (Figure 5A; $p<0.05$) and showed strong mobility more frequently ($p=0.068$) than wild-type mice. APP/PS1 mice also behaved more anxiously than wild-type mice. They entered corners (Figure 5B; $p<0.01$) and periphery ($p<0.05$) of the open field arena more frequently than wild-type mice. There were no diet effects between wild-type and APP/PS1 mice on STD2 and DHA/UC+ diets or between APP/PS1 mice on STD2, DHA/U and DHA/UC+ diets.

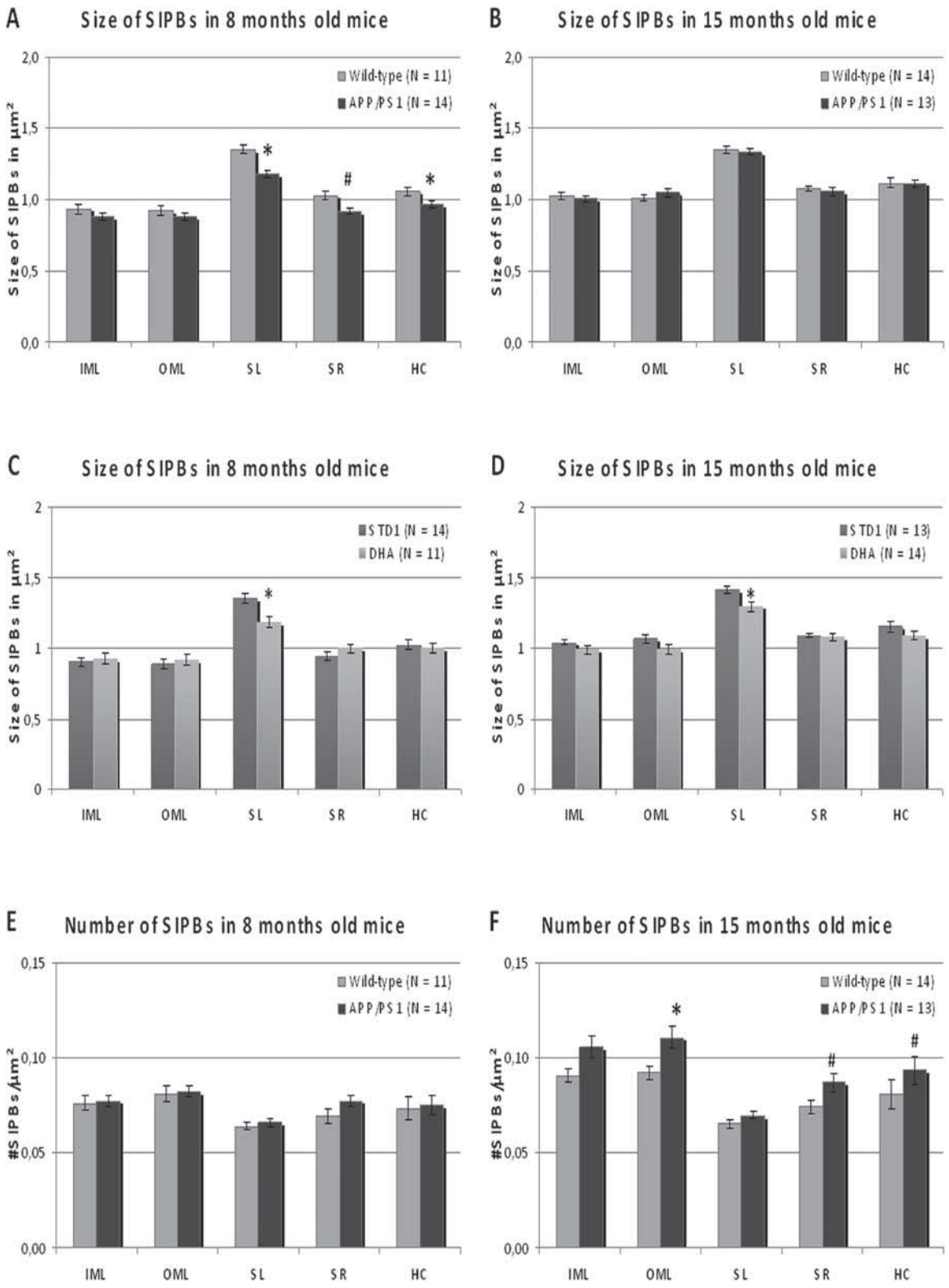

Figure 4. Number and size of SIPBs in hippocampal regions of 8 and 15 months old APP/PS1 and wild-type mice. **A.** 8 months old APP/PS1 mice have smaller SIPBs in SL, SR and total HC. **B.** Genotype differences in SIPB size are not observed in 15 months old mice. The reason for that is that SIPB size increases with age more significantly in APP/PS1 mice (HC: $p < 0.001$) than in wild-type mice (HC: $p > 0.1$). **C.** 8 months old and **D.** 15 months old mice on DHA diet have smaller SIPBs in SL compared to mice on STD1 diet. **E.** Number of SIPBs in 8 months old mice does not differ between APP/PS1 and wild-type mice. **F.** 15 months old APP/PS1 mice have more SIPBs in OML, SR and total HC. Mean number and sizes ± SEM are shown. * $p < 0.05$, # $p < 0.1$.

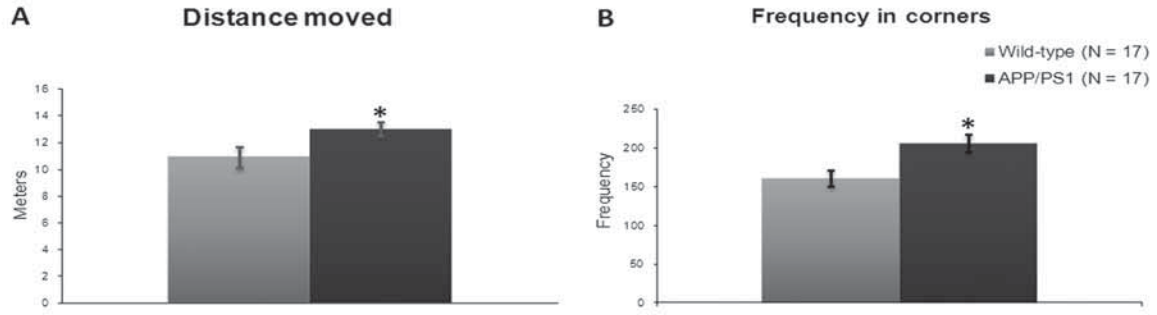

Figure 5. Open field behavior in 6 - 7 month old APP/PS1 and wild-type mice. Different open field parameters were measured within a 30 min period. **A.** Total distance moved. **B.** Frequency entering in corners. APP/PS1 mice moved a greater distance ($p < 0.05$) and more frequently entered the corners of the open field arena ($p < 0.01$) than wild-type mice. Mean values ± SEM are shown. * $p < 0.05$; # $p < 0.1$.

3.3 Proton magnetic resonance spectroscopy

3.3.1 Body weight

All mice were weighed on the day of the MR experiments. Body weight was not affected by genotype or diet. Overall mean body weight was 29.9 ± 2.43 g.

3.3.2 NAA ratio

Wild-type mice had higher ratios of NAA than APP/PS1 mice (Figure 6A; $p<0.1$). There were no diet effects (Figure 6B) or genotype*diet interactions. Diet effects were neither observed when comparing only transgenic mice on diets.

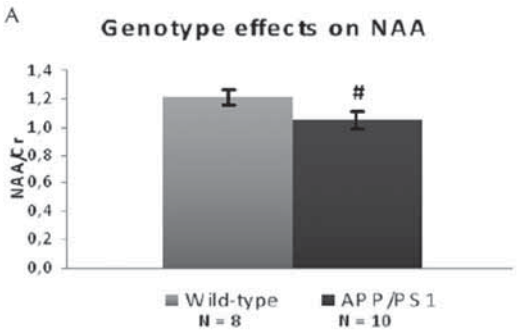

Figure 6. Effect of genotype and diet on hippocampal metabolite ratios. **A.** APP/PS1 mice have lower NAA/Cr ratios ($p < 0.1$) **B.** DHA/UC+ fed mice have higher levels of Cho+Tau than mice on STD2 diet ($p < 0.05$). **C.** Levels of Cho+Tau do not differ significantly between APP/PS1 mice fed STD2, DHA/U or DHA/UC+ diets. Mean ratios ± SEM are shown. Tg = APP/PS1 mice.

3.3.3 Cho+Tau ratio

Mice on DHA/UC+ diet had significantly higher Cho+Tau/Cr ratios than mice on STD2 diet (Figure 6C; $p<0.05$). There were no significant differences between genotypes and no genotype*diet interactions. When comparing only transgenic mice on diets, there were no significant diet effects ($p = 0.108$).

3.3.3 Tau ratio

There were no significant differences in Tau/Cr ratio between genotypes or diet groups and no genotype*diet interactions. Also when comparing only transgenic mice on diets, diet effects were not observed.

One methodological problem of the present

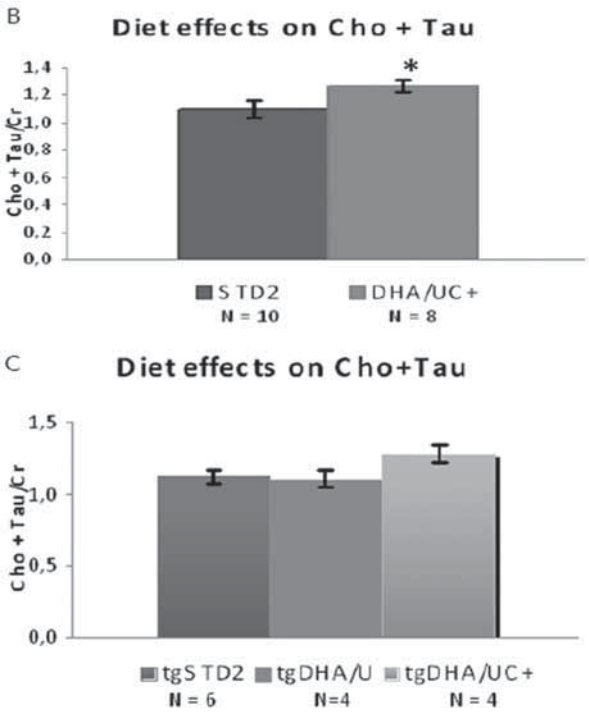

study was that the signals of choline-containing compounds overlapped with the signal of taurine and that the resulting Cho+Tau peak could not be differentiated into two individual Cho and Tau peaks (Figure 7). However, the contribution of taurine to the Cho+Tau peak might be rather small, as the frequency of the analyzed peak was set at the frequency of Cho. The contribution of taurine levels to possible changes in the Cho+Tau ratio can also be estimated as taurine is reflected twice in a MRS spectrum. Genotype or diet effects on Tau can hence be estimated in the individual Tau peak. For example, if the Cho+Tau ratio would change in one condition while the Tau peak would remain stable, one may suppose that changes in the Cho+Tau peak depend mainly on changes in Cho levels. In our study, taurine ratios did not differ between genotype groups. This is in line with a study of Marjanska et al. (2005) in which taurine levels did not differ between APP/PS1 mice and wild-type mice. The Cho+Tau ratio in our study hence seems to rely mainly on the contribution of choline components.

4. Discussion

4.1 Synaptophysin immunohistochemistry

Synaptic loss is a pathological hallmark of AD and a decrease in synaptic density is a consistent finding in the hippocampus of AD patients (Masliah et al., 1996; Scheff and Price, 1998) and AD mouse models (Mucke et al., 2000; Rutten et al., 2005; Dong et al., 2007). However, recent studies suggest that synapse loss might not be an early event in the progression of AD, as a decrease in synapses is only seen in later stages of the disease, where pathology is more widespread (Boncristiano et al., 2005; Mukaetova-Ladinska et al., 2000, Masliah et al., 1994).

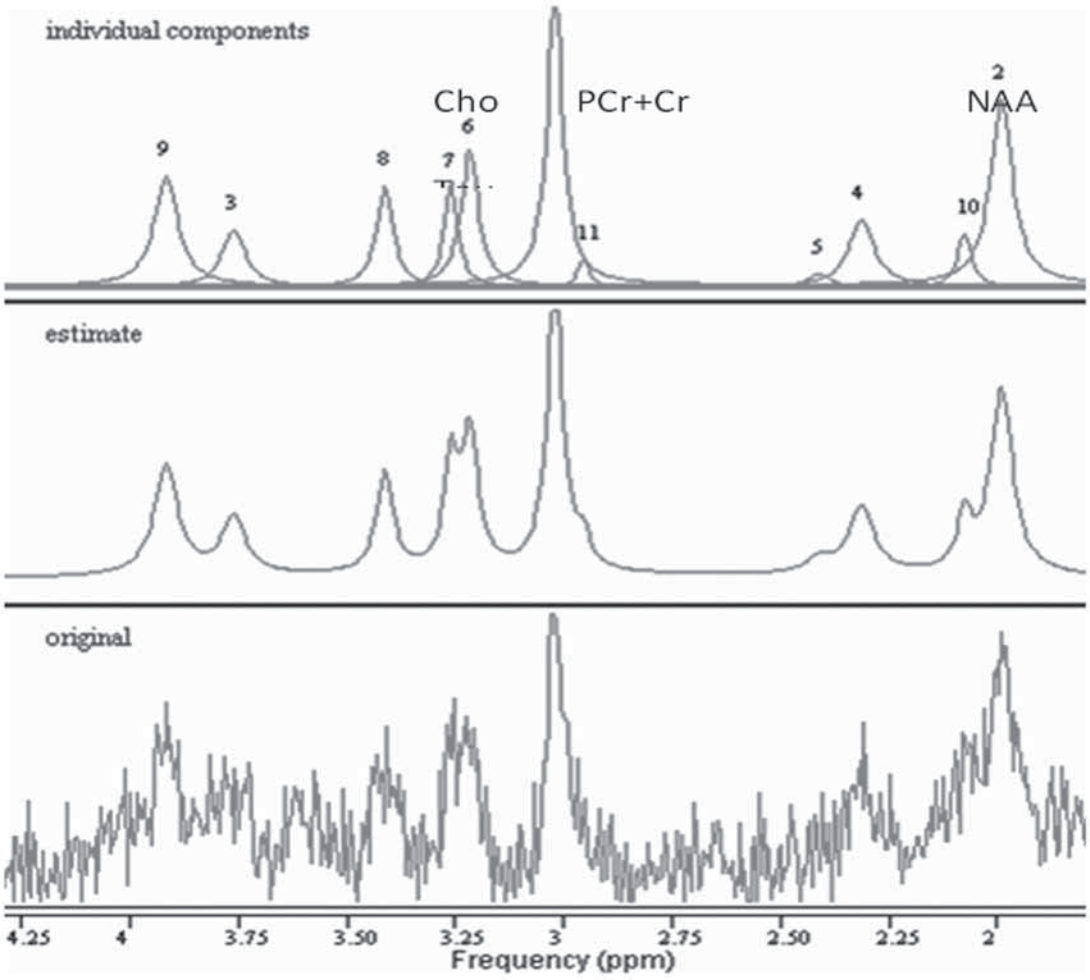

Figure 7. Representative MRS spectrum of mouse hippocampus and metabolite quantification with jMRUI. Bottom: original spectrum. Middle: estimate of spectrum after filtering. Top: Estimate of individual components contributing to the estimated spectrum.

4.1.1 Genotype effects

In the present study, 15-months-old APP/PS1 mice showed higher SIPB numbers in outer molecular layer, stratum radiatum and total hippocampus in comparison to wild-type mice. In line with our findings, King and Arendash (2002) reported significantly higher synaptophysin immunoreactivity in the OML of 19- months-old APP mice compared to age-matched wild-type mice. They and other groups suggest a compensatory mechanism for early stages of the disease, meaning that neurons try to compensate for degenerating synapses by forming new synapses or by increasing the size of remaining synapses (Boncristiano et al., 2005; Scheff and Price, 2003; King and Arendash, 2002; Bronfman et al., 2000). Paraterminal sprouting or enlargement of existing synaptic terminals has also been reported in patients in early stages of AD (Mukaetova-Ladinska et al., 2000).

The increase in SIPB number might alternatively be explained by a higher package of synapses per μm^2 due to shrinkage of the measured brain regions. Shrinkage was observed in the OML of our 15-months-old mice. However, results of other experiments in the same mice showed a cholesterol induced increase in SIPB number without measurable shrinkage of the brain region was observed (unpublished data of our group). Hence, increased SIPB number is not necessarily the result of increased package density.

SIPB sizes were smaller in 8-months-old transgenic mice. At the age of 15-months, differences in SIPB size were not present any longer. The reason for that is that SIPB size increased with age, possibly reflecting a compensatory response to age-related synapse degeneration, and that SIPB size increased even more significantly in APP/PS1 mice compared to wild-type mice, possibly reflecting the suggested compensatory response to AD-related synapse degeneration.

To resolve the question whether increased SIPB size and number reflect a true increase in synapse size and number, careful stereological analysis of synaptic numbers and determinations of bouton size is needed. However, electron microscopy is costly and labour intensive and despite of these limitations, quantification of SIPBs makes it possible to compare an estimate of synaptic boutons between experimental groups. Another question is whether SIPBs in APP/PS1 mice represent functional synapses. It might therefore be interesting to investigate number and size of postsynaptic spines, combined with measuring the expression of autophosphorylated Ca(2+)/ calmodulin-dependent protein kinase II at threonine 286, a key post-synaptic protein. This approach has been used to study density and functionality of synapses (Long et al., 2009).

4.1.2 Diet effects

We expected that alterations in synapse number or size would be lower in mice fed DHA compared to mice on STD1 diets. As age and AD increased number and size of SIPBs in our mice, this would have meant that DHA should have decreased these values. Indeed, in 8- and 15-months-old mice fed DHA we found smaller SIPBs in the SL compared to STD1 fed mice. Hence, at least in the SL, DHA diets seem to have had a positive effect on synapse morphology.

4.2 Open field test

The analyzed open field parameters can be used to estimate the grade of anxiety and agitation in the mouse. Increased activity is a specific characteristic of many APP transgenic mice (Lalonde et al., 2005; Puolivali et al., 2002) and may reflect elevated anxiety levels (Pugh et al., 2007; Puolivali et al., 2002). Restlessness and anxiety are also increased in AD patients (Grossberg, 2003; Patterson et al., 1990).

4.2.1 Genotype effects

In this study, at the age of 6 months, APP/PS1 mice showed increased activity compared to their wild type littermates as they walked a longer distance ($p<0.05$) and more frequently showed strong mobility ($p=0.068$) than wild-type mice. APP/PS1 mice also showed increased levels of anxiety as they spent less time grooming than wild-type mice ($p=0.066$) and entered corners ($p<0.01$) and periphery ($p<0.05$) of the open field arena more frequently than wild-type mice. However, at this age we did not observe differences between APP/PS1 and wild-type mice in parameters like walking, sitting, leaning and rearing. Differences in these parameters were present in a former study of our group using 8-months-old mice (Hooijmans et al., 2009). Hence, behavioural symptoms seem not to be fully manifested in 6-months-old APP/PS1 mice.

4.2.2 Diet effects

In the same study of Hooijmans and colleagues (2009), a diet containing DHA but no UMP or choline could not ameliorate behavioural signs in the 8-months-old mice. Using a mix of DHA, UMP and choline in the present study, we expected to find positive effects of these diets on hyperactivity and anxiety levels. However, these effects were not observed. It is possible that benefits of DHA-mix diets take a longer supplementation time to establish their effects, than the 4 months used in this study. We will therefore repeat the investigations in the same mice when they are 12-months-old.

4.3 Proton magnetic resonance spectroscopy

Because of its non-invasive and repeatable nature, 1H-MRS is attractive to use for monitoring progression of AD and efficacy of treatments. Here we investigated how levels of NAA and Cho differ between APP/PS1 mice and wild-type mice and how DHA/U and DHA/UC+ diets influence metabolic ratios.

4.3.1 NAA

The amino acid N-acetylaspartate (NAA) is used as a marker for neuronal density and/or function (Rudkin and Arnold, 1999), as it is primarily present in mature neurons and neuronal processes. Numerous 1H-MRS studies have provided consistent evidence for a reduction of NAA in patients with AD (Valenzuela and Sachdev, 2001; Ackl et al., 2005; Jessen et al., 2009), reflecting a decreased number of functional neurons. Because of the high consistency of NAA reduction in patients with AD in numerous studies, Jessen et al. (2009) propose NAA measures as an additional biomarker candidate for AD. APP/PS1 mice exhibit NAA profiles analogous to that present in human AD patients: levels of NAA are significantly lower in APP/PS1 mice than in wildtype mice (Marjanska et al., 2005; Oberg et al., 2008).

In line with these findings, our 8 - 10-months-old APP/PS1 mice showed significantly lower NAA ratios in comparison to age-matched control mice. This finding is striking as the number of mice per group was very low. Diet effects were not observed: DHA/U or DHA/UC+ diets did not change NAA ratios. To see whether time is a limiting factor here, we will investigate the influence of these diets in the same mice again when they are 12 months old.

4.3.2 Cho + Tau

Choline is a product of membranial phosphatidylcholine breakdown (Firbank et al., 2002) and is therefore used as a marker for cell membrane turnover and degradation (Soares et al., 2009). Choline-containing compounds are also required precursors for synthesis of acetylcholine, the key neurotransmitter in memory processes. The substances that mainly contribute to the choline peak in a MRS spectrum are free choline, glycerophosphocholine and phosphocholine (den Heijer et al., 2006). Findings concerning Cho ratios in AD are inconsistent. 1H-MRS studies comparing patients with AD and healthy control subjects show either increases (Kantarci, 2000; Griffith et al., 2008), decreases (Chantal et al., 2002) or no differences (Wang et al., 2009) in Cho ratios. In mice, hippocampal Cho levels do not differ between APP/PS1 and wild-type mice (Oberg et al., 2008, Westman et al., 2009).

Our study in 8 - 10-months-old mice reflects the findings of Wang et al. as they show comparable Cho+Tau ratios in both genotypes. However, we cannot exclude that this finding resulted from the low number of mice used. The significantly higher Cho+Tau/Cr ratios in mice on DHA/UC+ ($p<0.05$) reveal a dietary influence on levels of Cho+Tau. As explained in the results section, the change in Cho+Tau ratios is mainly dependent on changes in Cho levels, as ratios of the individual taurine peak did not differ between diet groups. Dietary choline intake hence resulted in higher availability of choline-containing compounds in the brain. Higher Cho ratios are also reported in AD patients receiving cholinesterase inhibitors compared with AD patients without cholinesterase inhibitors (Griffith et al., 2008). Hence, higher Cho levels seem beneficial as they can be used for production of phospholipid and acetylcholine. In a recent study, it is even suggested that the Cho signal intensity observed by 1H-MRS may be used as an indicator of acetylcholine level (Wang et al., 2008). Higher levels of Cho in DHA/UC+ fed animals could consequently also reflect higher levels of acetylcholine. The question remains whether higher availability of Cho results in increased phospholipid production and thereby increasees membrane quality. Future studies could address this question using phosphorus-MRS (31P-MRS). This method can provide important information about neuronal membranes, such as levels of phosphomonoesters that reflect the building blocks of neuronal membranes and phosphodiesters that reflect breakdown products. 31P-MRS can also

provide information about bioenergetics (Reddy and Keshavan, 2003).

There were two limitations concerning the MRS measurements in this study. First, the number of mice was low (n=4-6). Second, the method that we used for metabolite quantification is not the best one. A commonly used method for metabolite quantification is LCModel. This method was not established in our lab but will be used for the following measurements. However, these data provide a first glance on how AD and diets might influence metabolite ratios. In a follow-up study, we will investigate effects of genotype and diet in the same mice at the age of 12 months using LCModel for metabolite quantification.

Conclusions

In summary, we observed an age-related increase in number and size of SIPBs, which was larger in APP/PS1 mice, probably reflecting increased need for compensation of degenerated or dysfunctional synapses. A DHA-enriched diet seems to have positive effects on synapse morphology as it induced a decrease in SIPB size. AD-related alterations in open field behaviour could not be ameliorated by a DHA diet in 8-months-old mice in a former study, neither by diets containing DHA, choline and/or uridine in 6-months-old mice in the recent study. However, because of the age differences, we do not conclude that the mix-diets are as ineffective in reducing behavioural symptoms as the DHA diet. 1H-MRS measurements in the hippocampus showed that levels of NAA were reduced in APP/PS1 mice, but were not increased by diets containing DHA, choline and/or uridine. However, a diet enriched with DHA, uridine, choline and additional components could induce an increase in the levels of choline-containing compounds. These can be used for synthesis of phosphatidylcholine and might thereby stimulate regrowth of neuronal membranes, and can be used for acetylcholine production, and might thereby improve memory processes.

These findings have significant implications for public health as they show that synapse morphology can be improved by intake of fish oil, and that membrane quality and acetylcholine ratios might be increased by diets containing DHA + uridine + choline + components like B-vitamins and anti-oxidants. As the experimental diets also had higher ratios of poly-unsaturated fatty acids than the standard diets, positive effects might in part result from the higher content of 'good fats'. Hence, our results emphasize the importance of fatty acids and membrane precursors in the pathogenesis of and as treatment for Alzheimer's disease.

Acknowledgements

I want to thank Amanda Kiliaan and Diane Jansen for their great support and trust, Valerio Zerbi for helping me with MRS data analysis, Jos Dederen, Anne Hafkemeijer and Maartje Mutsaers for helping with IHC, Henk Arnts for taking care of the mice and helping with animal preparations, Jocelien Olivier, Laurens Nonkens and Judith Homberg for supporting me with EthoVision, and Andor Veltien for helping with MRS measurements, Arend Heerschap for MRS equipment, Laus Broersen for the diets, Ineke van der Zee for open field equipment and my reviewers for their helpful comments. This project has received funding from the European Community's Seventh Framework Programme (FP7/2007-2013) under grant agreement no 202167.

References

Ackl N., Ising M., Schreiber Y.A., Atiya M., Sonntag A., & Auer D.P. (2005). Hippocampal metabolic abnormalities in mild cognitive impairment and Alzheimer's disease. Neurosci Lett, 384(1–2), 23-28.

Alvarez P., Zola-Morgan S., & Squire L.R. (1995). Damage limited to the hippocampal region produces long-lasting memory impairment in monkeys. J Neurosci, 15, 3796–3807.

Bazan N.G. (2005). Neuroprotectin D1 (NPD1): a DHA-derived mediator that protects brain and retina against cell injury-induced oxidative stress. Brain Pathol, 15, 159–166.

Barberger-Gateau P., Letenneur L., Deschamps V., Peres K., Dartigues J.F., & Renaud S. (2002). Fish, meat, and risk of dementia: cohort study. BMJ, 325, 932–933.

Bennett S.A., Pappas B.A., Stevens W.D., Davidson C.M., Fortin T., & Chen J. (2000). Cleavage of amyloid precursor protein elicited by chronic cerebral hypoperfusion. Neurobiol Aging, 21, 207–214.

Biessels G.J., & Kappelle L.J. (2005). Increased risk of Alzheimer's disease in Type II diabetes: insulin resistance of the brain or insulin-induced amyloid pathology? Biochem Soc Trans, 33(5), 1041-1044.

Boche D., Zotova E., Weller R.O., Love S., Neal J.W., Pickering R.M., Wilkinson D., Holmes C., & Nicoll J.A. (2008). Consequence of Abeta immunezation on the vasculature of human Alzheimer's disease brain. Brain, 131, 3299-3310.

Boncristiano S., Calhoun M.E., Howard V., Bondolfi L., Kaeser S.A., Wiederhold K.H., Staufenbield M., & Jucker M. (2005). Neocortical synaptic bouton number is maintained despite robust amyloid deposition in APP23 transgenic mice. Neurobiol Aging, 26, 607-613.

Borchelt D.R., Ratovitsky T., van Lare J., Lee M.K., Gonzales V., Jenkins N.A., Copeland N.G., Price D.L., & Sisodia S.S. (1997). Accelerated amyloid deposition in the brains of transgenic mice co-expressing mutant presenilin 1 and

amyloid precursor proteins. Neuron, 19, 939–945.
Breslow J.L. (2006). N-3 Fatty acids and cardiovascular disease. Am J Clin Nutr, 83, 1477S–1482S.
Bronfman F., Moechars D., & Van Leuven F. (2000). Acetylcholinesterase-positive fiber deafferentation and cell shrinkage in the septohippocampal pathway of aged amyloid precursor protein london mutant transgenic mice. Neurobiol Disease, 7, 152–168.
Chantal S., Labelle M., Bouchard R.W., Braun C.M., Boulanger Y. (2002). Correlation of regional proton magnetic resonance spectroscopic metabolic changes with cognitive deficits in mild Alzheimer disease. Arch Neurol, 59, 955-962.
De la Torre J.C. (2000). Critically attained threshold of cerebral hypoperfusion: the CATCH hypothesis of Alzheimer's pathogenesis. Neurobiol Aging, 21, 331–342.
De la Torre J.C. (2002). Vascular basis of Alzheimer's pathogenesis. Ann NY Acad Sci, 977, 196–215.
De la Torre J.C. (2004). Is Alzheimer's disease a neurodegenerative or a vascular disorder? Data, dogma, and dialectics. Lancet Neurol, 3, 184-190.
Den Heijer T., Sijens P.E., Prins N.D., Hofman A., Koudstaal P.J., Oudkerk M., & Breteler M.M. (2006). MR spectroscopy of brain white matter in the prediction of dementia. Neurology, 66(4), 540-544.
De Wilde M.C., Farkas E., Gerrits M., Kiliaan A.J., & Luiten P.G. (2002). The effect of n-3 poly-unsaturated fatty acid-rich diets on cognitive and cerebrovascular parameters in chronic cerebral hypoperfusion. Brain Res, 947, 166–173.
De Wilde M.C., Hogyes E., Kiliaan A.J., Farkas T., Luiten P.G., & Farkas E. (2003). Dietary fatty acids alter blood pressure, behaviour and brain membrane composition of hypertensive rats. Brain Res, 988, 9–19.
Dong H., Martin M.V., Chambers S., & Csernanskyet J.G. (2007). Spatial Relationship Between Synapse Loss and β-Amyloid Deposition in Tg2576 Mice, J Comp Neurol, 500(2), 311–321.
Eilander A., Hundscheid D.C., Osendarp S.J., Transler C., & Zock P.L. (2007). Effects of n-3 long chain polyunsaturated fatty acid supplementation on visual and cognitive development throughout childhood: a review of human studies. Prostaglandins Leukot Essent Fat Acids, 76, 189-203.
Farkas E., & Luiten P.G. (2001). Cerebral microvascular pathology in aging and Alzheimer's disease, Prog Neurobiol, 64, 575–611.
Fassbender K., Simons M., Bergmann C., Stroick M., Lutjohann D., Keller P., Runz H., Kuhl S., Bertsch T., von Bergmann K., Hennerici M., Beyreuther K., & Hartmann T. (2001). Simvastatin strongly reduces levels of Alzheimer's disease beta-amyloid peptides abeta 42 and abeta 40 in vitro and in vivo. Proc. Natl Acad Sci USA, 98, 5856–5861.
Firbank M.J., Harrison R.M., & O'Brien J.T. (2002). A comprehensive review of proton magnetic resonance spectroscopy studies in dementia and Parkinson's disease. Dement Geriatr Cogn Disord, 14(2), 64-76.
Frederick B.D., Lyoo I.K., Satlin A., Ahn K.H., Kim M.J., Yurgelun-Todd D.A., Cohen B.M., & Renshaw P.F. (2004). In vivo proton magnetic resonance spectroscopy of the temporal lobe in Alzheimer's disease. Prog Neuropsychopharmacol Biol Psychiatry, 28, 1313–1322.
Freund-Levi Y., Eriksdotter-Jönhagen M., Cederholm T., Basun H., Faxén-Irving G., Garlind A., Vedin I., Vessby B., Wahlund L.O., & Palmblad J. (2006). Omega-3 fatty acid treatment in 174 patients with mild to moderate Alzheimer disease: OmegAD study: a randomized double-blind trial. Arch Neurol, 63, 1402–1408.
Godbolt A.K., Waldman A.D., MacManus D.G., Schott J.M., Frost C., Cipolotti L., Fox N.C., & Rossor M.N. MRS shows abnormalities before symptoms in familial Alzheimer disease. Neurology, 66(5), 718–722.
Griffith H.R., den Hollander J.A., Okonkwo O.C., O'Brien T., Watts R.L., & Marson D.C. (2008). Brain metabolism differs in Alzheimer's disease and Parkinson's disease dementia. Alzheimers Dement, 4(6), 421-427.
Grossberg G.T. (2003). Diagnosis and treatment of Alzheimer's disease. J Clin Psychiatry, 64(S9), 3–6.
Hashimoto M., Hossain S., Yamasaki H., Yazawa K., & Masumura S. (1999). Effects of eicosapentaenoic acid and docosahexaenoic acid on plasma membrane fluidity of aortic endothelial cells. Lipids, 34(12), 1297-304.
Head E. (2009). Oxidative Damage and Cognitive Dysfunction: Antioxidant Treatments to Promote Healthy Brain Aging. Neurochem Res, 34, 670-678.
Heijer T., Skoog I., Oudkerk M., de Leeuw F.E., de Groot J.C., Hofman A., & Breteler M.M. (2003). Association between blood pressure levels over time and brain atrophy in the elderly. Neurobiol Aging, 24(2), 307-313.
Hooijmans C.R., Rutters F., Dederen P.J., Gambarota G., Veltien A., van Groen T., Broersen L.M., Lütjohann D., Heerschap A., Tanila H., & Kiliaan A.J. (2007). Changes in cerebral blood volume and amyloid pathology in aged Alzheimer APP/PS1 mice on a docosahexaenoic acid (DHA) diet or cholesterol enriched Typical Western Diet (TWD). Neurobiol Dis, 28(1), 16–29.
Hooijmans C.R., Van der Zee C.E., Dederen P.J., Brouwer K.M., Reijmer Y.D., van Groen T., Broersen L.M., Lütjohann D., Heerschap A., & Kiliaan A.J. (2009). DHA and cholesterol containing diets influence Alzheimer-like pathology, cognition and cerebral vasculature in APPswe/PS1dE9 mice. Neurobiol Dis, 33(3), 482–498.
Holguin S., Huang Y., Liu J., & Wurtman R. (2008). Chronic administration of DHA and UMP improves the impaired memory of environmentally impoverished rats. Behav Brain Res, 191(1), 11–16
Holguin S., Martinez J., Chow C., & Wurtman R. (2008). Dietary uridine enhances the improvement in learning and memory produced by administering DHA plus choline to gerbils. FASEB J, 22(11), 3938-3946.
Iadecola C. (2004). Neurovascular regulation in the normal brain and in Alzheimer's disease. Nat Rev Neurosci, 5, 347-360.
Jankowsky J.L., Slunt H.H., Ratovitski T., Jenkins N.A., Copeland N.G., & Borchelt D.R. (2001). Co-expression of multiple transgenes in mouse CNS: a comparison of strategies. Biomol Eng, 17(6), 157-165.
Jessen F., Gür O., Block W., Ende G., Frölich L., Hammen T., Wiltfang J., Kucinski T., Jahn H., Heun R., Maier W., Kölsch H., Kornhuber J., & Träber. (2009). A multicenter 1H-MRS study of the medial temporal lobe in AD and MCI. Neurology, 72, 1735-1740.
Kalaria R.N. (2009). Linking cerebrovascular defense mechanisms in brain ageing and Alzheimer's disease. Neurobiol Aging, 30(9), 1512-1514.
Kalmijn S., Launer L.J., Ott A., Witteman J.C., Hofman A., & Breteler M.M. (1997). Dietary fat intake and the risk of incident dementia in the Rotterdam Study. Ann Neurol, 42(5), 776–782.
Kantarci K., Jack C.R. Jr, Xu Y.C., Campeau N.G., O'Brien P.C., Smith G.E., et al. (2000). Regional metabolic patterns in

mild cognitive impairment and Alzheimer's disease: a 1H-MRS study. Neurology, 55, 210–217.

King D.L., & Arendash G.W. (2002). Maintained synaptophysin immunoreactivity in Tg2576 transgenic mice during aging: correlations with cognitive impairment. Brain Res, 926, 58–68.

Kivipelto M., Helkala E.L., Laakso M.P., Hänninen T., Hallikainen M., Alhainen K., Iivonen S., Mannermaa A., Tuomilehto J., Nissinen A., & Soininen H. (2002). Apolipoprotein E epsilon4 allele, elevated midlife total cholesterol level, and high midlife systolic blood pressure are independent risk factors for late-life Alzheimer disease. Ann Intern Med, 137(3), 149–155.

Kivipelto M., Ngandu T., Fratiglioni L., Viitanen M., Kåreholt I., Winblad B., Helkala E.L., Tuomilehto J., Soininen H., & Nissinen A. (2005). Obesity and vascular risk factors at midlife and the risk of dementia and Alzheimer disease. Arch Neurol, 62(10), 1556-1560.

Klein W.L, Krafft G.A., & Finch C.E. (2001). Targeting small Aβ oligomers: the solution to an Alzheimer's disease conundrum? Trends Neurosci, 24(4), 219–224.

Knowles W.D. (1992). Normal anatomy and neurophysiology of the hippocampal formation. J Clin Neurophysiol, 9, 252–263.

Kotani S., Sakaguchi E., Warashina S., Matsukawa N., Ishikura Y., Kiso Y., Sakakibara M., Yoshimoto T., Guo J., & Yamashima T. (2006). Dietary supplementation of arachidonic and docosahexaenoic acids improves cognitive dysfunction. Neurosci Res, 56(2), 159–164.

Lalonde R., Kim H.D., Maxwell J.A., & Fukuchi K. (2005). Exploratory activity and spatial learning in 12-month-old APP(695) SWE/co+PS1/DeltaE9 mice with amyloid plaques. Neurosci Lett, 390(2), 87-92.

Lee T.F., Shiao Y.J., Chen C.F., & Wang L.C. (2001). Effect of ginseng saponins on beta-amyloid-suppressed acetylcholine release from rat hippocampal slices. Planta Med, 67(7), 634-7.

Lim G.P., Calon F., Morihara T., Yang F., Teter B., Ubeda O., Salem N. Jr, Frautschy S.A., & Cole G.M. (2005). A diet enriched with the omega-3 fatty acid docosahexaenoic acid reduces amyloid burden in an aged Alzheimer mouse model, J Neurosci, 25(12), 3032–3040.

Long L.H., Liu R.L., Wang F., Liu J., Hu Z.L., Xie N., Jin Y., Fu H., & Chen J.G. (2009). Age-related synaptic changes in the CA1 stratum radiatum and spatial learning impairment in rats. Clin Exp Pharmacol Physiol, 36(7), 675-681.

Lukiw W.J., Cui J.G., Marcheselli V.L., Bodker M., Botkjaer A., Gotlinger K., Serhan C.N., & Bazan N.G. (2005). A role for docosahexaenoic acid-derived neuroprotectin D1 in neural cell survival and Alzheimer disease. J Clin Invest, 115(10), 2774–2783.

Marjanska M., Curran G.L., Wengenack T.M., Henry P.G., Bliss R.L., Poduslo J.F., Jack C.R. Jr, Ugurbil K., & Garwood M. (2005). Monitoring disease progression in transgenic mouse models of Alzheimer's disease with proton magnetic resonance spectroscopy. Proc Natl Acad Sci USA, 102(33), 11906-11910.

Markesbery W.R. (1997). Oxidative stress hypothesis in Alzheimer's disease. Free Radic Biol Med, 23, 134-147.

Masliah E., Mallory M., Hansen L., DeTeresa R., Alford M., & Terry R. (1994). Synaptic and neuritic alterations during the progression of Alzheimer's disease. Neurosci Lett, 174, 67–72.

Masliah E., Sisk A., Mallory M., Mucke L., Schenk D., & Games D. Comparison of neurodegenerative pathology in transgenic mice overexpressing V717F beta-amyloid precursor protein and Alzheimer's disease. J. Neurosci, 16, 5795–5811.

Misonou H., Morishima-Kawashima M., & Ihara Y. (2000). Oxidative stress induces intracellular accumulation of amyloid β-protein (Aβ) in human neuroblastoma cells. Biochemistry, 39(23), 6951-9659.

Morris M.C., Evans D.A., Bienias J.L., Tangney C.C., Bennett D.A., Wilson R.S., Aggarwal N., & Schneider J. (2003). Consumption of fish and n-3 fatty acids and risk of incident Alzheimer disease Arch Neurol, 60(7), 940-946.

Mucke L., Masliah E., Yu G.Q., Mallory M., Rockenstein E.M., Tatsuno G., Hu K., Kholodenko D., Johnson-Wood K., & McConlogue L. (2000). High-level neuronal expression of abeta 1-42 in wild-type human amyloid protein precursor transgenic mice: synaptotoxicity without plaque formation, J Neurosci, 20(11), 4050–4058.

Mukaetova-Ladinska E.B., Garcia-Siera F., Hurt J., Gertz H.J., Xuereb J.H., Hills R., Brayne C., Huppert F.A., Paykel E.S., McGee M., Jakes R., Honer W.G., Harrington C.R., & Wischik C.M. (2000). Staging of cytoskeletal and beta-amyloid changes in human isocortex reveals biphasic synaptic protein response during progression of Alzheimer's disease, Am J Pathol, 157(2), 623–636.

Mulder M., Koopmans G., Wassink G., Al Mansouri G., Simard M.L., Havekes L.M., Prickaerts J., & Blokland A. (2007). LDL receptor deficiency results in decreased cell proliferation and presynaptic bouton density in the murine hippocampus. Neurosci Res, 59(3), 251-256.

Oberg J., Spenger C., Wang F.H., Andersson A., Westman E., Skoglund P., Sunnemark D., Norinder U., Klason T., Wahlund L.O., & Lindberg M. (2008). Age related changes in brain metabolites observed by 1H-MRS in APP/PS1 mice. Neurobiol Aging, 29, 1423–1433.

Oksman M., Iivonen H., Hogyes E., Amtul Z., Penke B., Leenders I., Broersen L., Lütjohann D., Hartmann T., & Tanila H. (2006). Impact of different saturated fatty acid, polyunsaturated fatty acid and cholesterol containing diets on beta-amyloid accumulation in APP/PS1 transgenic mice, Neurobiol Dis, 23, 563–572.

Patterson M.B., Schnell A.H., Martin R.J., Mendez M.F., Smyth K.A., & Whitehouse P.J. (1990). Assessment of behavioral and affective symptoms in Alzheimer's disease. J Geriatr Psychiatry Neurol, 3, 21–30.

Pugh P.L., Richardson J.C., Bate S.T., Upton N., & Sunter D. (2007). Non-cognitive behaviours in an APP/PS1 transgenic model of Alzheimer's disease. Behav Brain Res, 178(1), 18-28.

Puolivali J., Wang J., Heikkinen T., Heikkila M., Tapiola T., van Groen T., et al. (2002). Hippocampal A beta 42 levels correlate with spatial memory deficit in APP and PS1 double transgenic mice. Neurobiol Dis, 9(3), 339-347.

Reddy R., & Keshavan M.S. (2003). Phosphorus magnetic resonance spectroscopy: Its utility in examining the membrane hypothesis of schizophrenia. Prostaglandins Leukot Essent Fatty Acids, 69(6), 401-405.

Rudkin T.M., & Arnold D.L. (1999). Proton magnetic resonance spectroscopy for the diagnosis and management of cerebral disorders. Arch Neurol, 56, 919–926.

Ruitenberg A., den Heijer T., Bakker S.L., van Swieten J.C., Koudstaal P.J., Hofman A., & Breteler M.M. (2005). Cerebral hypoperfusion and clinical onset of dementia: the Rotterdam Study. Ann Neurol, 57(6), 789-794.

Rutten B.P., Van der Kolk N.M., Schafer S., van Zandvoort M.A.,

Bayer T.A., Steinbusch H.W., & Schmitz C. (2005). Age-related loss of synaptophysin immunoreactive presynaptic boutons within the hippocampus of APP751SL, PS1M146L, and APP751SL/ PS1M146L transgenic mice. Am J Pathol, 167(1), 161–173.

Sakamoto T., Cansev M., & Wurtman R.J. (2007). Oral supplementation with docosahexaenoic acid and uridine 5'-monophosphate increases dendritic spine density in adult gerbil hippocampus. Brain Res, 1182, 50-9.

Scheff S.W., & Price D.A. (1998). Synaptic density in the inner molecular layer of the hippocampal dentate gyrus in Alzheimer disease. J Neuropathol Exp Neurol, 57, 1146–1153.

Scheff S.W., & Price D.A. (2003). Synaptic pathology in Alzheimer's disease: a review of ultrastructural studies. Neurobiol Aging, 24, 1029–1046.

Schreiber S.J., Doepp F., Spruth E., Kopp U.A., & Valdueza J.M. (2005). Ultrasonographic measurement of cerebral blood flow, cerebral circulation time and cerebral blood volume in vascular and Alzheimer's dementia. J Neurol, 252(10), 1171-1177.

Soares D.P., & Law M. (2009). Magnetic resonance spectroscopy of the brain: review of metabolites and clinical applications. Clin Radiol, 64(1), 12-21.

Spires T.L., & Hyman B.T. (2005). Transgenic models of Alzheimer's disease: learning from animals. NeuroRx, 2(3), 423-437.

Streijger F., Oerlemans F., Ellenbroek B.A., Jost C.R., Wieringa B., & Van der Zee C.E. (2005). Structural and behavioural consequences of double deficiency for creatine kinases BCK and UbCKmit. Behav Brain Res, 157, 219–234.

Van Gelder B.M., Tijhuis M., Kalmijn S., Kromhout D. (2007). Fish consumption, n-3 fatty acids, and subsequent 5-y cognitive decline in elderly men: the Zutphen Elderly Study. Am J Clin Nutr, 85(4), 1142-7.

Valenzuela M.J., & Sachdev P. (2001). Magnetic resonance spectroscopy in AD. Neurology, 56, 592–598.

Vanhamme L., van den Boogaart A., van Huffel S. (1997). Improved method for accurate and efficient quantification of MRS data with use of prior knowledge. J Magn Reson, 129, 35–43.

Van Oijen M., de Jong F.J., Witteman J.C., Hofman A., Koudstaal P.J., & Breteler M.M. (2007). Atherosclerosis and risk for dementia. Ann Neurol, 61(5), 403-410.

Velliquette R.A., O'Connor T., & Vassar R. (2005). Energy inhibition elevates beta-secretase levels and activity and is potentially amyloidogenic in APP transgenic mice: possible early events in Alzheimer's disease pathogenesis. J Neurosci, 25(47), 10874-10883.

Wahrle S., Das P., Nyborg A.C., McLendon C., Shoji M., Kawarabayashi T., Younkin L.H., Younkin S.G., & Golde T.E. (2002). Cholesterol-dependent gamma-secretase activity in buoyant cholesterol-rich membrane microdomains. Neurobiol Dis, 9, 11–23.

Wang X.C., Du X.X., Tian Q., & Wang J.Z. (2008). Correlation between choline signal intensity and acetylcholine level in different brain regions of rat. Neurochem Res, 33(5), 814-819.

Wang Z., Zhao C., Yu L., Zhou W., & Li K. (2009). Regional metabolic changes in the hippocampus and posterior cingulate area detected with 3-Tesla magnetic resonance spectroscopy in patients with mild cognitive impairment and Alzheimer disease. Acta Radiol, 50(3), 312-319.

Westman E., Spenger C., Öberg J., Reyer H., Pahnke J., & Wahlund L.O. (2009). In vivo 1H-magnetic resonance spectroscopy can detect metabolic changes in APP/PS1 mice after donepezil treatment. BMC Neuroscience, 10, 33

Wilcock D.M., & Colton C.A. (2008). Anti-amyloid-beta immunotherapy in Alzheimer's disease: relevance of transgenic mouse studies to clinical trials. J Alzheimers Dis, 15, 555-569.

Wolozin B. (2001). A fluid connection: cholesterol and Abeta. Proc Natl Acad Sci USA, 98, 5371–5373.

Wolozin B. (2004). Cholesterol and the biology of Alzheimer's disease. Neuron. 41, 7–10.

Wu A., Ying Z., & Gomez-Pinilla F. (2004). Dietary omega-3 fatty acids normalize BDNF levels, reduce oxidative damage, and counteract learning disability after traumatic brain injury in rats. J Neurotrauma, 21, 1457–1467.

Wurtman R.J., Ulus I.H., Cansev M., Watkins C.J., Wang L., & Marzloff G. (2006). Synaptic proteins and phospholipids are increased in gerbil brain by administering uridine plus docosahexaenoic acid orally. Brain Res, 1088, 83–92.

Wurtman R.J., Cansev M., & Ulus I.H. (2009). Synapse Formation Is Enhanced by Oral Administration of Uridine and DHA, the Circulating Precursors of Brain Phosphatides. J Nutrition, Health & Aging, 3, 189-197.

Yavin E., Brand A., & Green P. (2002). Docosahexaenoic acid abundance in the brain: a biodevice to combat oxidative stress. Nutr Neurosci, 5, 149-157.

Zlokovic B.V. (2005). Neurovascular mechanisms of Alzheimer's neurodegeneration. Trends Neurosci, 28(4), 202-208.

Rhinal and hippocampal gamma power during retrieval decreases when encoding occurs before and after sleep

Roemer van der Meij[1]
Supervisors: Ingrid L.C. Nieuwenhuis[1], Ole Jensen[1]
Data contribution: Nikolai Axmacher[2,3]

[1]*Donders Institute for Brain, Cognition and Behaviour, Centre for Cognitive Neuroimaging, Radboud University Nijmegen, Nijmegen, The Netherlands*
[2]*Department of Epileptology, University of Bonn, Bonn, Germany*
[3]*Life and Brain Center of Academic Research, Bonn, Germany*

Memory consolidation gradually transfers memory traces from hippocampus and other medial-temporal lobe structures to neocortex. This process is thought to mainly occur during sleep. Surprisingly few studies have reported electrophysiological evidence of memory consolidation in humans during sleep on medial-temporal lobe activity. Using intracranial recordings from hippocampus and rhinal cortex we investigated the effects of sleep before and after encoding on subsequent retrieval. Subjects were presented with pictures before (remote) and after (recent) a 60 min nap or a sleepless rest period on different days. Retrieval occurred after the recent session on each day. Power spectra and time-frequency representations of power were calculated over the retrieval period and compared using a memory related contrast representing successful recall. The data revealed a clear difference in memory related gamma power in hippocampus and rhinal cortex between the nap and no-nap days. In both structures memory related gamma power (70-90 Hz) for remote items was lower on the nap day compared to the no-nap day and lasted from 0 to 0.7 s post-stimulus. Additionally, a similar trend was observed for recent items. We propose that the decrease of memory related gamma power for remote items on the nap day represents an effect of consolidation and thereby a decreased rhinal and hippocampal contribution to the memory trace. We suggest the trend for recent items reflects an enhanced coding phase on the nap day.

Keywords: declarative memory, consolidation, hippocampus, rhinal cortex, intracranial EEG, sleep, gamma, oscillations

Corresponding author: Roemer van der Meij, Donders Institute for Brain, Cognition and Behaviour: Centre for Cognitive Neuroimaging, P.O. Box 9101, NL-6500 HB Nijmegen, The Netherlands, email: roemer.vandermeij@donders.ru.nl.

1. Introduction

Consolidation is the process of strengthening newly formed declarative memories, reinforcing our memories for events and facts. This process can be described at the synaptic level and at the systems level (Dudai, 2004). While synaptic consolidation refers to the stabilizing, growing and restructuring of synaptic connections, systems level consolidation refers to the reorganization of brain regions supporting memories. It has been shown from lesion studies in the past that newly formed memories initially depend on the integrity of the hippocampus and other medial-temporal-lobe (MTL) structures (Eichenbaum, 2000; Squire, Stark, & Clark, 2004), but that this reliance dissipates with time (Squire & Bayley, 2007). According to the standard consolidation model (Alvarez & Squire, 1994; Frankland & Bontempi, 2005), this can be explained as the hippocampus serving as a linking node which binds together the neocortical networks that represent the memory. As memories become more consolidated their cortico-cortical connections strengthen and they become less dependent on MTL structures for retrieval. This gradual reorganization of brain regions supporting memory can start within hours after encoding and can continue for up to several decades (Dudai, 2004).

Declarative memory consolidation has been shown to occur during sleep (Born, Rasch, & Gais, 2006; Marshall & Born, 2007; Talamini, Nieuwenhuis, Takashima, & Jensen, 2008). Declarative memory performance increases after periods of sleep and a lack of such improvements after sleep-deprivation have been found in many paradigms (e.g.: Idzikowski, 1984; Lahl, Wispel, Willigens, & Pietrowsky, 2008; Plihal & Born, 1999; Tucker et al., 2006, for reviews see Born et al., 2006; Stickgold, 2005). One of the primary ways by which consolidation during sleep is thought to occur is by reactivation of newly formed memories. Evidence of replay during sleep has been found in rats, where temporal sequences of neural activity measured from cells in hippocampus have been found to be spontaneously replayed during sleep (Ji & Wilson, 2007; Louie & Wilson, 2001; Peyrache, Khamassi, Benchenane, Wiener, & Battaglia, 2009; Wilson & McNaughton, 1994). This replay is thought to allow a gradual strengthening of new memory traces while integrating them with other neocortical memory networks, preserving previously formed memory traces (McClelland, McNaughton, & O'Reilly, 1995). The standard consolidation model predicts that when neocortical connections strengthen, hippocampal connections weaken. Consolidation during sleep should therefore lead to less activation of the hippocampus during retrieval of memories encoded before sleep compared to memories encoded after sleep. Takashima et al. (2006) report such an effect using functional magnetic resonance imaging (fMRI). By comparing hippocampal blood oxygenation level dependent (BOLD) activity during retrieval of pictures encoded before or after a 90 minute nap they found a substantial decrease in BOLD activity for memories that were encoded before sleep. To our knowledge, the study of Takashima et al. (2006) is the only study using newly formed experimentally controlled memories to directly test the effects of sleep on the neural systems underlying memory retrieval.

Another way to look into effects of consolidation on hippocampal involvement in humans is through electrophysiological methods. Oscillatory synchronization in the gamma band (>30 Hz) has been proposed to reflect active neural processing. When neurons are firing in synchrony in the gamma band the short time-window in which their spikes arrive allows for summation of the excitatory postsynaptic potentials, resulting in successful communication between neurons (Fries, 2005; Jensen, Kaiser, & Lachaux, 2007). Increases in gamma synchronization have been shown to be highly correlated to increases in neuronal activity (for a review see Fries, Nikolic, & Singer, 2007). Gamma synchronization can also occur between networks, resulting in a strong excitatory drive from one network to another that can be used to propagate information. This allows for neuronal networks to be linked together in a fast and transient manner (for a review see Singer, 1999) and can lead to synaptic strengthening (Axmacher, Mormann, Fernandez, Elger, & Fell, 2006; Bikbaev & Manahan-Vaughan, 2008). As memories are thought to be stored in the synaptic weights of hippocampal-cortico-cortical networks it is expected that increased gamma synchronization in memory relevant regions would predict successful declarative memory encoding. This is exactly what has been found by intra-cranial measurements in human hippocampus during encoding (Fell, Fernandez, Klaver et al., 2006; Fell et al., 2003; Fell et al., 2001; Mormann et al., 2005, but also see Fell, Ludowig, Rosburg, Axmacher, & Elger, 2008) and in rat hippocampus (Montgomery & Buzsaki, 2007). During retrieval of declarative memories, an increase in gamma synchronization is also expected, as this would lead to a reactivation of the memory trace. This has also been reported using intra-cranial measurements in human hippocampus

(Ekstrom et al., 2007; Sederberg et al., 2007) and in whole-brain studies using electro- and magneto-encephalography (EEG; MEG; Gruber, Tsivilis, Montaldi, & Muller, 2004; Nieuwenhuis, Takashima, Oostenveld, Fernandez, & Jensen, 2008; Osipova et al., 2006). Rhinal cortex, one of the main input structures to the hippocampus, shows similar patterns of activity as hippocampus during memory encoding (Bauer, Paz, & Pare, 2007; Fell, Fernandez, Klaver et al., 2006; Fell et al., 2003; Fell et al., 2001; Mormann et al., 2005), with increases in gamma synchronization predicting successful memory formation. During retrieval, rhinal cortex shows similar patterns of activity as hippocampus as well (Ekstrom et al., 2007), where increases in gamma synchronization correlate with successful retrieval.

Newly formed memory traces can be consolidated to varying degrees, and are thus dependent on the hippocampus and other MTL structures in varying degrees as well. As consolidation primarily occurs during sleep, it is to be expected that newly formed memories encoded before a period of sleep are more consolidated than memories encoded before a sleepless rest period. When memories become more consolidated they need less involvement of the hippocampus and other MTL structures during retrieval compared to less consolidated memories, which should be reflected by less gamma synchronization. Such findings however, have not been previously reported. In order to investigate the consolidation modulated dependency of memories on hippocampus and other MTL-structures during retrieval we reanalyzed a dataset from Axmacher, Haupt, Fernandez, Elger, and Fell, 2008 containing human intracranial EEG recordings from hippocampus and rhinal cortex during a pictorial memory consolidation paradigm. Subjects were presented with pictures of buildings and landscapes before (remote) and after (recent) a 60 min nap on one day and a sleepless rest period on another day. Retrieval of these pictures occurred after the last encoding session on both days. We investigated oscillatory activity during the retrieval period and contrasted items between both days. As items presented before the nap should have underwent more consolidation than items presented before the rest period, retrieval of these items should involve hippocampus and rhinal cortex to a lesser degree. We therefore expected to see less gamma synchronization in these structures during retrieval of items encoded before the nap compared to items encoded before the rest period.

2. Methods

2.1 Subjects

Six out of eleven patients with unilateral pharmaco-resistant temporal lobe epilepsy (3 women; age 39 (7.6) years (mean (standard deviation (SD))) were selected from the previous study (Axmacher et al., 2008). Only subjects with a hit rate and correct rejection rate higher than 0.20 were analyzed to ensure an evenly distributed task performance for old and new items. Recordings were carried out at the Department of Epileptology, University of Bonn, Germany from 2005 to 2006. During presurgical evaluation all patients were implanted with bilateral MTL depth electrodes along the longitudinal axis of the hippocampus using a computed tomography-based stereotactic insertion technique (Van Roost, Solymosi, Schramm, van Oosterwyck, & Elger, 1998). Locations of electrode contacts were ascertained by MRI and classified as rhinal, hippocampal or otherwise. On average, patients had 2.5 (1.2) rhinal and 5.5 (1.1) hippocampal contacts (mean (SD)). The study was approved by the local medical ethics committee (Bonn, Germany) and all patients gave written informed consent.

2.2 Experimental paradigm

An overview of the experimental paradigm is presented in figure 1. During each of the encoding sessions (remote and recent) subjects were shown pictures of unknown buildings and landscapes. The first encoding session (remote) was performed at 12:00 after lunch. Afterwards subjects had either a sleepless rest-period on the no-nap day or nap period. Five out of six subjects slept for 46.4 (13.3) min. on the nap day (mean (SD)), sleep stages for the sixth subject had not been analyzed at the time of writing. The day with the nap was counterbalanced between the first and second day of the study, two subjects had the nap on the first day and four subjects had the nap on the second day. The subject with an unknown amount of sleep belonged to the latter category. On the nap day subjects lay in an electrically shielded, sound and light attenuated room for 60 min. Polysomnographic recordings consisting of surface EEG, horizontal and vertical eye movements, electrocardiograms and facial electromyograms were obtained during this period. On the no-nap day subjects received no specific instructions but were asked not to sleep. A medical technical assistant assessed whether subjects were

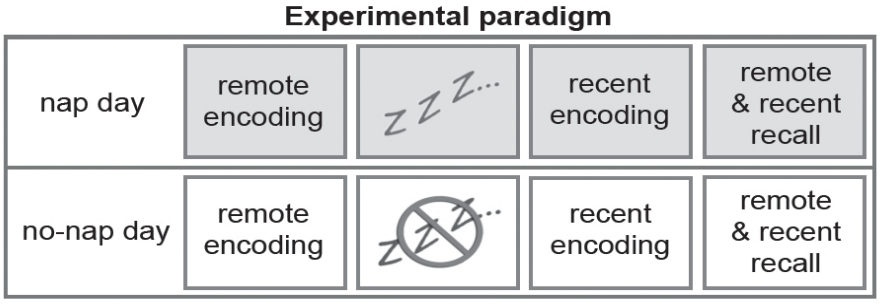

Figure 1. Experimental paradigm. Subjects were shown pictures during 2 encoding sessions (remote and recent) on 2 subsequent days. After the first encoding session (remote) subjects had a period of sleep on the nap day and a similar period of rest without sleep on the no-nap day. After the second encoding session (recent) a recall session took place in which with pictures from both encoding sessions of the same day were presented mixed with new pictures. The order of the nap and no-nap days was counterbalanced over subjects.

awake via video monitoring and inquiry. Fifteen minutes after the nap or no-nap period the second encoding session (recent) was performed. This was followed by a fifteen minute rest period in which the subjects were engaged in conversation with the experimenter to avoid rehearsal of items from the last encoding session. Afterwards, the recall session started, in which subjects were presented with the items from both encoding sessions and a new set of items. In each of the sessions pictures were presented for 1.2 s with an interval of 1.8 ± 0.2 s. During each of the encoding sessions subjects were shown 80 pictures and were instructed to distinguish buildings from landscapes by a button press. In the recall sessions, subjects were shown the 160 pictures from both encoding sessions of the same day interleaved with 80 new pictures, and had to indicate by button press whether they had seen the pictures before or not. Hits were defined as labeling a remote or recent item as 'seen before', misses were defined as labeling the same items as 'not seen before'. Correct rejections were defined as labeling a new item as 'not seen before', false alarms as labeling the same items as 'seen before'. Intracranial EEG was recorded continuously during recall.

2.3 Recordings and preprocessing

Intracranial EEG was referenced to linked mastoids, recorded at a sampling rate of 1000 Hz and band-pass filtered from 0.01 (6 dB/octave) to 300 Hz (12 dB/octave). Trials contaminated with epileptiform activity and other artifacts were identified by visual inspection and discarded. Only data from the hemisphere contralateral to the epileptic focus was used. Preprocessing and subsequent data-analysis was performed using the FieldTrip open source Matlab toolbox developed at the Donders Institute: Centre for Cognitive Neuroimaging (http://www.ru.nl/neuroimaging/fieldtrip). In order to remove power line noise, the data was band pass filtered with a 1 Hz window around 50 and 100 Hz.

Only one rhinal and one hippocampal electrode contact were selected per subject for data analysis. In order to select the contact showing the highest activity during the task we selected those with the highest sum of power in a 1-30 Hz frequency band in its category (rhinal or hippocampal), averaged over a 1 s time-window after stimulus presentation during retrieval. We specifically chose this frequency range as an estimate of general activity of electrode contacts because it is unbiased towards our later statistical analysis in the higher frequencies and because there is a well founded functional relationship between the lower frequencies and memory processes in MTL (e.g. see(Ekstrom et al., 2007, Fell et al., 2001 and Fell et al., 2003). Power was calculated by multiplying the data with a hanning taper and applying Fourier transforms to get a power estimate per frequency bin, averaging across frequency bins and trials. In order to remove a large portion of 1/f noise we used an autoregressive approach. By taking the derivative of the raw data, the first autoregressive component (the component that mainly models 1/f noise) is removed, pre-whitening the data. All artifact-free trials in both recall sessions were used (hits, misses, false alarms, correct rejections) to obtain a non-biased estimate of activity.

2.4 Spectral analysis

Power spectra were calculated for 30-100 Hz for each trial during recall by using a multi-taper approach (Mitra & Pesaran, 1999). The data of each trial (time window: 0 to 1 s post-stimulus) was multiplied with

a set of orthogonal tapers taken from the Discrete Prolate Spheroidal Sequences (DPSS). A frequency smoothing of Δf = 8 Hz was used, which resulted in 15 tapers being applied to the data. Power values were obtained by averaging the Fourier transforms of each of the tapered time windows. Time-frequency representations (TFRs) of power were calculated by using a sliding time window of ΔT = 0.5s (trials defined from -1.2 to 1.2 s post-stimulus) and a frequency smoothing (using the above multi-taper approach) of Δf = 8 Hz, resulting in 3 tapers being applied to the data-segments (similar settings were used in Nieuwenhuis et al., 2008 and Jokisch & Jensen, 2007). Power spectra and TFRs of power were also calculated for the lower frequencies (1-30 Hz) by multiplying the data with a hanning taper and applying Fourier transforms to get a power estimate per frequency bin (time window: 0 to 1 s post-stimulus). These analyses are not reported below as they did not reveal any significant differences between conditions.

Average TFRs of power and power spectra were calculated for remote and recent hits and misses. Memory related contrasts expressing power during successful recall as a ratio of power during unsuccessful recall were computed for each condition and stimulus category separately by subtracting the average for misses from hits before dividing by misses ((hits – misses) / misses). As these contrasts only reflect that part of the power response that distinguishes successful from unsuccessful memory recall it is an ideal measure for investigating differences in power signatures of successful memory recall between conditions. Significance of the differences between conditions was tested using a non-parametric cluster-based permutation procedure as described in Maris and Oostenveld (2007). This test controls the Type-1 error rate in situations with multiple comparisons. First, all frequency-points (for power spectra) or time-frequency-points (for TFRs of power) are identified for which the t-value for the contrast between conditions exceeds a threshold (higher than 2.57 or lower than -2.57). Contiguous frequency- or time-frequency-points exceeding the threshold are grouped in clusters and the sum of t-values of each point in the cluster is calculated, being the cluster-statistic. The largest of these cluster-statistics is used to obtain a permutation distribution assuming exchangeability of the data between conditions, normally calculated by randomly swapping the conditions in subjects 1000 times and calculating the maximum cluster-statistic (sampling the true permutation distribution). A Monte-Carlo estimate of the p-value is then obtained for each cluster by comparing the cluster-statistic to this distribution. In our case however, we could calculate the true permutation distribution as the number of permutations was only $2^6 = 64$. We therefore report exact p-values obtained from the true permutation distribution in contrast to the normally calculated Monte-Carlo p-values. Both types of p-values are limited by the number of unique permutations, in our situation the lowest possible p-value was $1/26 \approx 0.016$.

3. Results

Remote items on the nap day were encoded before a brief period of sleep whereas remote items on the no-nap day were encoded before a sleepless rest period. Recent items were encoded after the same sleep or rest period. During the retrieval sessions only items encoded on the same day needed to be retrieved. Intra-cranial EEG measurements were obtained from rhinal cortex and hippocampus during the whole retrieval period. To investigate the effects of sleep after encoding on retrieval we contrasted remote items between days. Recent items were contrasted between days as well to investigate the effects of sleep before encoding on subsequent retrieval.

3.1 Behavioral performance did not differ between days

In the retrieval session subjects had to indicate whether they had seen an item before or not. Behavioral performance ratings for this task are displayed in table 1 for remote, recent and

Table 1. Means and SEMS of behavioral performance. Remote and recent items were presented during encoding and recall, new pictures were only presented during recall. SEM = standard error of the mean; CR = correct rejection; FA = false alarm.

Condition	Remote			Recent			New	
	Hit	Miss	*d`*	Hit	Miss	*d`*	CR	FA
Nap day	.55 (.05)	.46 (.05)	.33 (.08)	.59 (.03)	.41 (.03)	.43 (.17)	.58 (.06)	.42 (.06)
No-nap day	.56 (.04)	.44 (.04)	.41 (.12)	.57 (.05)	.44 (.05)	.43 (.22)	.60 (.05)	.40 (.05)

new items. Only trials without epileptic artifacts were included in the calculations, as normal cognitive functioning cannot be assumed during epileptic spikes in hippocampus and rhinal cortex. Recognition performance for remote items was not affected by the nap. Hit rates on the no-nap day (0.56 (0.04)) and on the nap day (0.55 (0.05)) (mean (standard error of the mean (SEM))), did not differ significantly (paired sample t-test, $t(5) = 0.20$, $p > .8$). Recognition accuracy assessed by d' values was not affected by the nap as well. Calculating d' values by subtracting the z-transformed false alarm rate from the z-transformed hit rate resulted in d' = .41 (.12) on the no-nap day and d' = .33 (.08) on the nap day (mean (SEM)). D' values did not differ significantly between both days (paired sample t-test, $t(5) = 0.80$, $p > .4$). Recognition performance nor recognition accuracy for recent items differed between days (paired sample t-test, $t(5) = -0.70$, $p > .5$; paired sample t-test, $t(5) = -0.07$, $p > .9$).

3.2 Relative gamma power decreases during retrieval of remote items encoded before the nap

Power spectra and TFRs of power for remote items were calculated over the retrieval period. A memory related contrast was computed representing successful recall by expressing power of remote hits as a ratio of power of remote misses (see methods section). This relative measure of gamma power during successful recall was contrasted between remote items on the no-nap versus remote items on the nap day to investigate the effects of consolidation during sleep on retrieval.

Power spectra revealed that memory related gamma power (70-90 Hz) differed between both days (figure 2). During successful memory recall relative gamma power was higher on the no-nap day than on the nap day, both in rhinal cortex (figure 2A) and hippocampus (figure 2C). In both structures relative gamma power on the nap day was less than

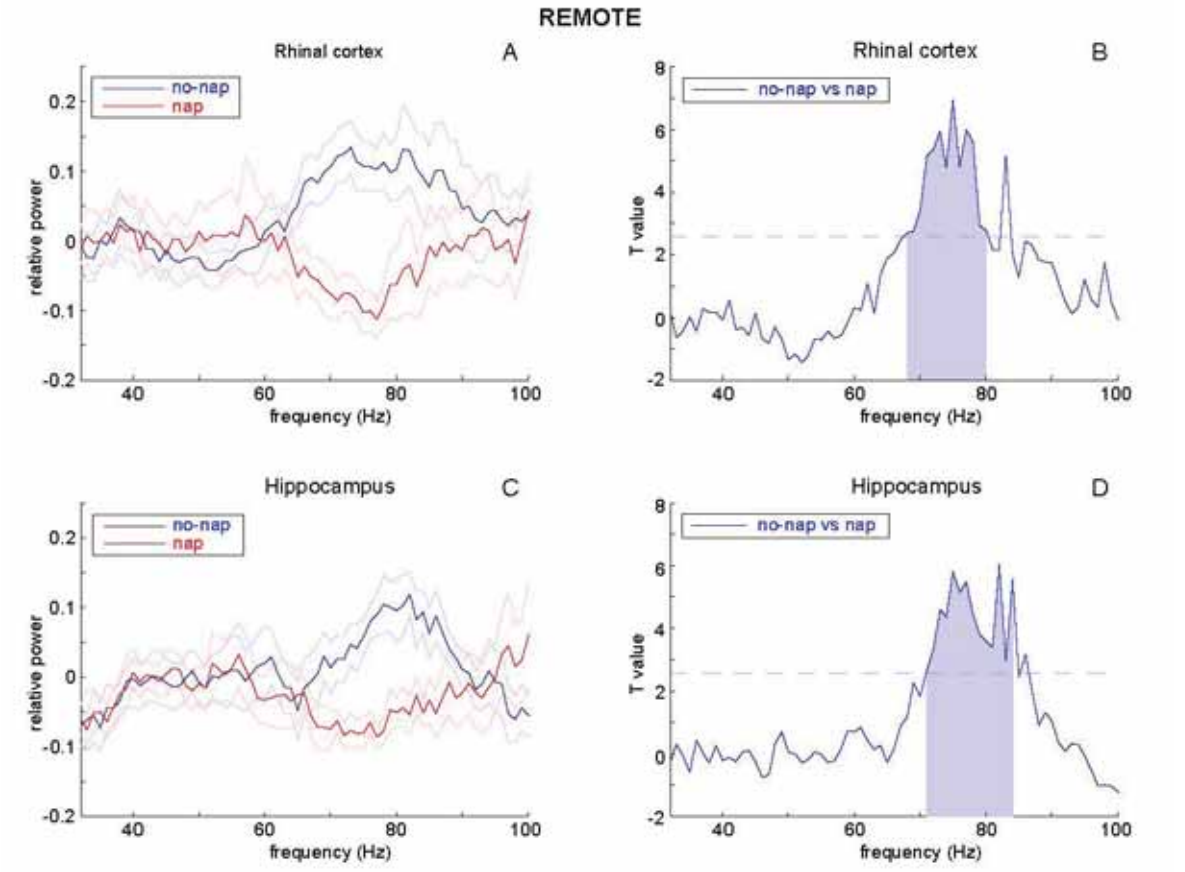

Figure 2. Power spectra during retrieval of remote items. **A,C.** Power spectra of memory related contrast (see methods section) representing successful recall for rhinal cortex and hippocampus. Blue lines represent remote items encoded on the no-nap day, red lines represent remote items encoded on the nap day. Respective SEMs are represented by the shaded blue and red lines. **B,D.** T-values for the difference between the no-nap and nap condition for rhinal cortex and hippocampus. Blue shaded areas denote significant frequency clusters based on the cluster-based permutation procedure (see methods section; one-sided $p \approx 0.016$ (B); one-sided $p \approx 0.031$ (D)). Dashed lines represent threshold for clustering frequency points ($t = 2.57$). SEM = standard error of the mean.

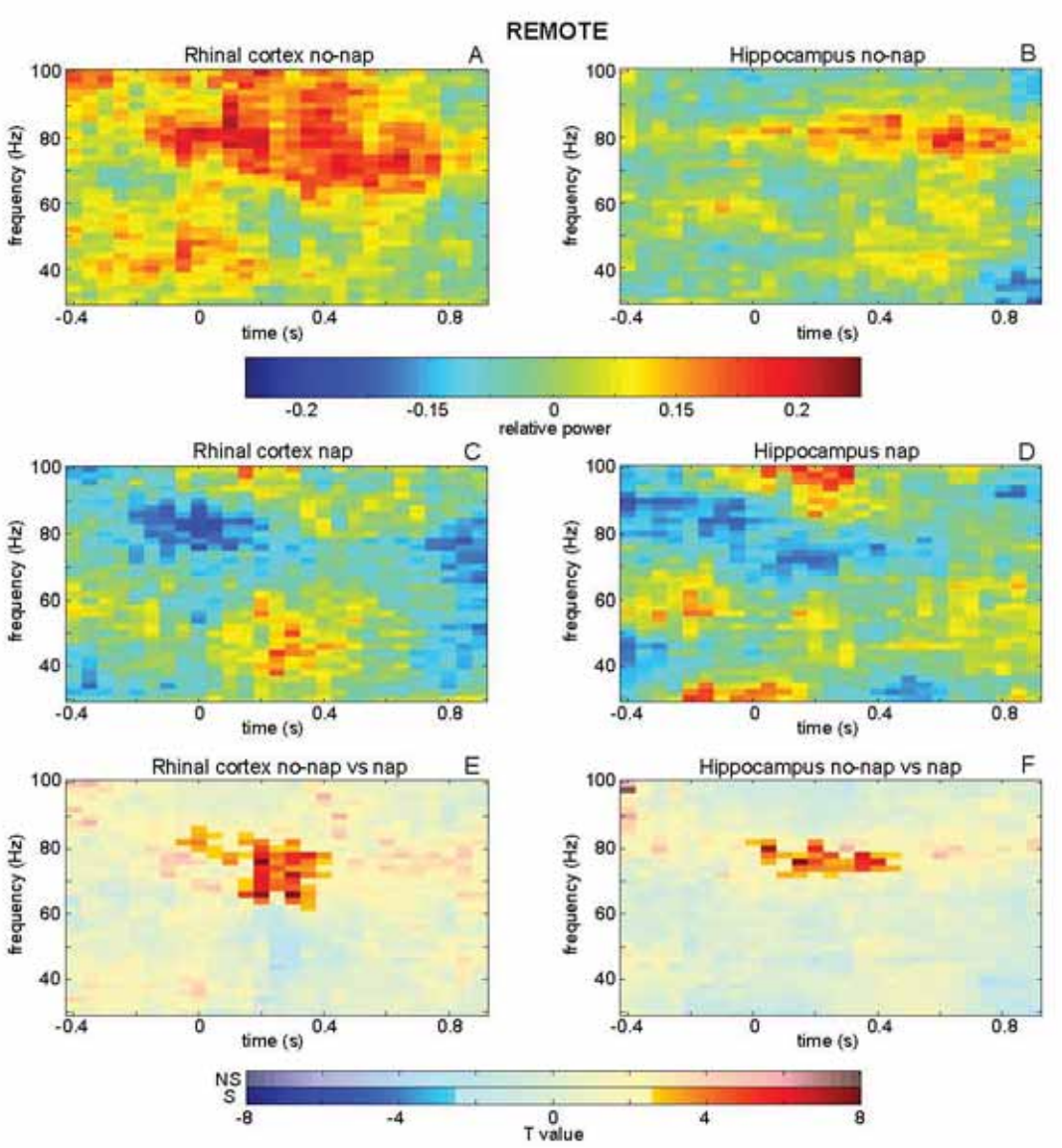

Figure 3. TFRs of power during retrieval of remote items. **A,C.** TFRs of power of memory related contrast (see methods section) representing successful recall for rhinal cortex on the no-nap and nap days. **B, D.** Same as A,B but for hippocampus. **E,F.** TFR of t-values for the difference between the no-nap and nap condition. Significant time-frequency clusters for rhinal cortex (E; one-sided $p \approx 0.047$) and hippocampus (F; one-sided $p \approx 0.047$) based on the cluster-based permutation procedure (see methods section) are opacity masked. Accompanying color bar shows two color axes, one for time-frequency points belonging to the significant (S) cluster and one for non-significant (NS) time-frequency points. Opacity threshold in lower part (S) represents threshold for clustering time-frequency points ($t = 2.57$). TFR = time frequency representation.

zero for ~60-90 Hz, indicating remote hits had less gamma power than remote misses on the nap day. Statistical testing identified a frequency cluster of ~70-80 Hz for which relative gamma power differed significantly between both days for remote items in rhinal cortex (figure 2B, one-sided $p \approx 0.016$) and in hippocampus (figure 2D, one-sided $p \approx 0.031$).

TFRs of power showed differences in memory related gamma power between both days as well, lasting from stimulus onset up to 0.7 s (figure 3). During successful memory recall of remote items on the no-nap day (figure 3A) relative gamma power (65-90 Hz) was higher during -0.1 to 0.7 s in rhinal cortex than on the nap day (figure 3C). The initial relative gamma power difference started at -0.1 s at ~70-85 Hz but extended to a broader frequency range after 0.2 s. Relative gamma power (65-90 Hz) on the nap day was less than zero during -0.1 to 0.7 s, indicating remote hits had less gamma power than remote misses on the nap day. Statistical testing identified a time-frequency cluster with a 60-85 Hz frequency range and a -0.05 to 0.4 s time range (figure 3E; one-sided $p \approx 0.047$) for which relative power differed significantly between both days. Power differences

between -0.1 and 0 s are most likely an artifact caused by the size of the sliding time-window (0.5 ms) used for power calculations. In hippocampus a similar effect was found. During successful memory recall of remote items on the no-nap day (figure 3B) relative gamma power (70-90 Hz) was higher than on the nap day (figure 3D). Relative gamma power (65-90 Hz) on the nap day was less than zero during -0.1 to 0.7 s, indicating remote hits had less gamma power than remote misses on the nap day in hippocampus as well. Statistical testing in this case resulted in a time-frequency cluster with a 70-80 Hz frequency range and a 0 to 0.45 s time range (figure 3F; one-sided $p \approx 0.047$) for which relative power showed a significant difference between both days.

3.3 Trend for relative gamma power decrease during retrieval of recent items encoded after the nap

We also contrasted power spectra for the successful recall of recent items on the no-nap day to recent items on the nap day, to investigate whether sleep before encoding has an effect on power during retrieval. The same memory related contrast representing successful memory recall was used as above.

Power spectra for retrieval of recent items are reported in figure 4. Power spectra revealed that memory related slow gamma power (35-45 Hz) differed between both days for recent items (figure 4). During successful memory recall slow relative gamma power was higher on the no-nap day than on the nap day in rhinal cortex (figure 4A), though a small trend is observable in hippocampus (figure 4C). Statistical testing identified a frequency cluster of ~35-45 Hz for which relative gamma power differed significantly in rhinal cortex (figure 4B, one-sided $p \approx 0.016$), but did not for hippocampus (figure 4D). Relative gamma power on the nap day was less than zero for ~30-50 Hz and ~60-90 Hz in rhinal cortex and for ~60-90 Hz in hippocampus, indicating recent hits had less gamma power than recent misses on the nap day. There appeared to be no differences in rhinal cortex (figure 4A) and hippocampus (figure 4C) in the frequency range reported for remote items (60-90 Hz), though a trend is observable in the direction of the effect for remote items reported above. When comparing the difference for remote items to the difference for recent items, statistical testing revealed no significant differences.

4. Discussion

Oscillatory activity in rhinal cortex and hippocampus was investigated during retrieval of pictures that have been encoded before (remote) and after (recent) a short nap on the nap day or a sleepless rest period on the no-nap day. Retrieval of remote items on the nap day showed a significant decrease of memory related gamma power (70-90 Hz) in both structures compared to retrieval on the no-nap day. A trend was found as well for recent items. Retrieval of recent items on the nap day showed a trend for a decrease of memory related gamma power (70-90 Hz) in both structures compared to retrieval on the no-nap day. The remote and recent effects did not differ significantly.

4.1 Rhinal and hippocampal activity decreases for remote items possibly reflect consolidation

What are the implications of decreased memory related gamma power during retrieval of items encoded before the nap versus items encoded before the rest period? It has been firmly established by previous studies that increases in neuronal activity highly correlated with increases in gamma power. For example, it has been shown in cat visual cortex that spiking neurons activated by sensory stimulation display increased gamma power (Gray, Konig, Engel, & Singer, 1989). In macaque visual cortex it has been shown as well that spiking neurons activated by attention show increased gamma power (Fries, Reynolds, Rorie, & Desimone, 2001) and in macaque parietal cortex that spiking neurons activated during working memory maintenance also display increased gamma power (Pesaran, Pezaris, Sahani, Mitra, & Andersen, 2002). For similar findings see Fries et al. (2007). Moreover, Logothetis, Pauls, Augath, Trinath, and Oeltermann (2001) have shown that there is a strong correlation between fMRI BOLD activity and gamma power, further strengthening the link between gamma power and neuronal activity. As such, we propose that the decrease of relative gamma power in rhinal cortex and hippocampus we report reflects a decrease of rhinal and hippocampal activity. We suggest that this reflects an effect of consolidation, which would be in line with previous research showing a decrease in MTL activity and reduced MTL requirement during retrieval when consolidation has occurred. For example, Takashima et al. (2006) have reported decreased human hippocampal BOLD activity during retrieval of

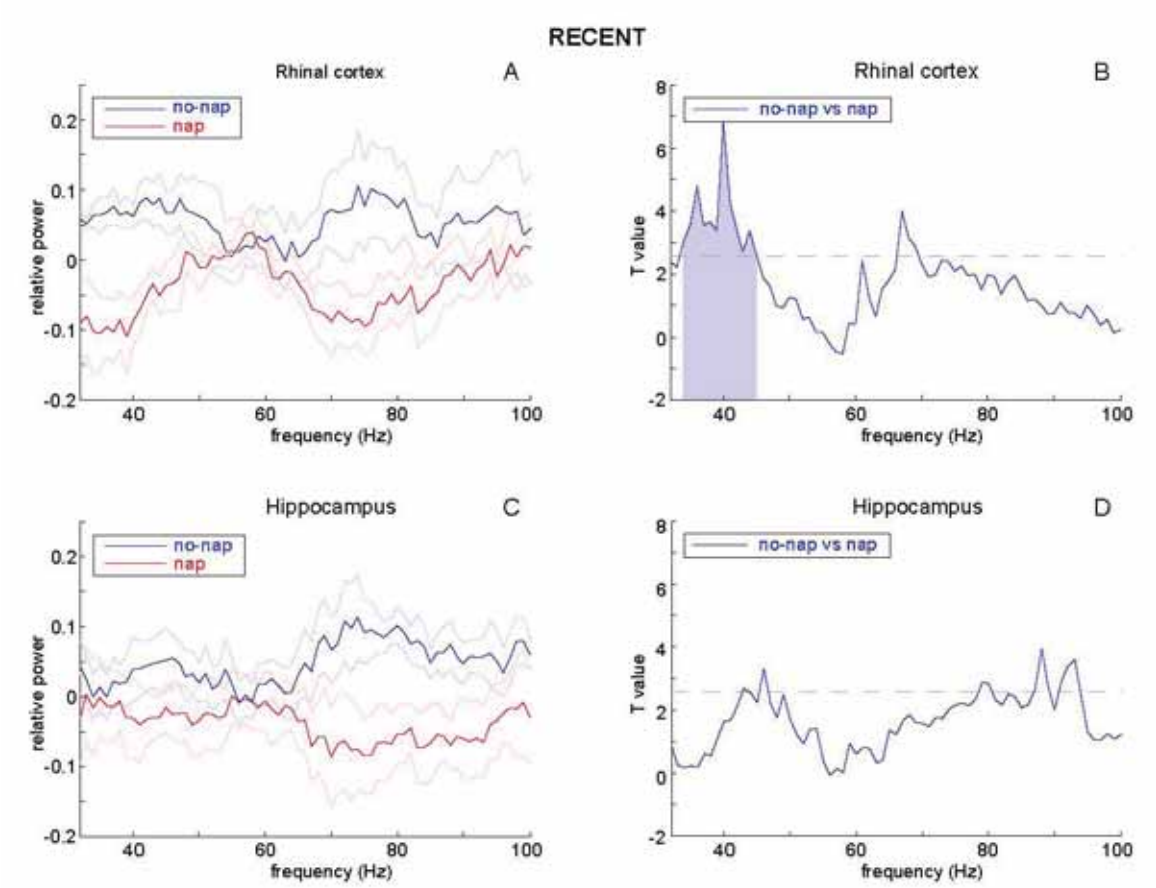

Figure 4. Power spectra during retrieval of recent items. **A,C.** Power spectra of memory related contrast (see methods section) representing successful recall for rhinal cortex and hippocampus. Blue lines represent recent items encoded on the no-nap day, red lines represent recent items encoded on the nap day. Respective SEMs are represented by the shaded blue and red lines. **B,D.** T-values for the difference between the no-nap and nap condition for rhinal cortex and hippocampus. Blue shaded area denotes significant frequency cluster based on the cluster-based permutation procedure (see methods section; one-sided $p \approx 0.016$ (B)). Dashed lines represent threshold for clustering frequency points ($t = 2.57$). SEM = standard error of the mean.

items that were consolidated during a 90 minute nap versus items that were unconsolidated. Furthermore, Gorfine, Yeshurun, and Zisapel (2007) also report decreased MTL activity after a 2 hour nap during retrieval of word-pair associations and Maguire and Frith (2003) have reported decreased hippocampal fMRI BOLD activity when retrieving remote versus recent autobiographical memories. Lesion studies in humans have demonstrated that hippocampal lesions lead to loss of recent (unconsolidated) autobiographical memories but leave remote (consolidated) memories intact (e.g.: Penfield & Milner, 1958; Rempel-Clower, Zola, Squire, & Amaral, 1996; Scoville & Milner, 1957). Additionally, it has been shown that lesioning the hippocampus in rats leads to a loss of recent but not remote contextual fear memories (Kim & Fanselow, 1992), and in nonhuman primates the same effect has been found for object memory (Zola-Morgan & Squire, 1990). Considering the above, we suggest that, if an effect of consolidation occurred in our study, the contribution of rhinal cortex and hippocampus to the memory trace has most likely been decreased, as they would no longer be needed to the same degree for retrieval.

Our study shows a decrease of MTL activity during retrieval already after a 60 min nap with a retention interval of only several hours. When considering this decrease as an effect of consolidation, then the short nap time and retention interval are in line with previous research showing benefits to memory of short amounts of sleep. For example, Mednick, Cai, Kanady, and Drummond (2008) have shown that 60-90 min of sleep improved verbal memory retrieval performance on the same day as encoding and Lahl et al. (2008) have even reported benefits of as little as 30 min and even 6 min of sleep on a similar verbal memory task with a retention interval

of only 60 min. Most importantly, Takashima et al. (2006) and Gorfine et al. (2007) have found decreases in MTL activity after a 90 and 120 min nap respectively with a retention interval of several hours, using a paradigm very similar to ours. It is unlikely that the reorganization of brain systems supporting declarative memory retrieval can already occur after a short nap, as rodent studies typically suggest a time-frame of several days for system level consolidation to occur (for a review see Frankland & Bontempi, 2005). Since Takashima et al. (2006) and Gorfine et al. (2007) have shown a decrease in MTL activity with consolidation on a much shorter time-scale, it is tempting to suggest MTL could have been suppressed during retrieval, as suggested by Frankland and Bontempi (2005).

Although we and others (Gorfine et al., 2007; Takashima et al., 2006) report a decrease in MTL activity during retrieval of memories that are thought to be more consolidated, others have not found the same. For example, Maguire, Henson, Mummery, and Frith (2001) and Ryan et al. (2001) found no relationship of hippocampal fMRI BOLD activity during retrieval and the age of autobiographical memories. Barr, Goldberg, Wasserstein, and Novelly (1990) and Warrington and Duchen (1992) investigated patients with MTL lesions but found no temporal gradient in loss of autobiographical memories (for a more complete view see reviews: Moscovitch et al., 2005; Nadel, Samsonovich, Ryan, & Moscovitch, 2000). We propose that the disagreement between both series of findings lie in which subtype of declarative memory was investigated. Nadel and Moscovitch (1997) proposed that only semantic, and not episodic memory, can become less dependent on MTL. Whereas episodic memory is considered contextual by nature, semantic memory is not. In this context, MTL memory traces primarily provide contextual information, whereas neocortical memory traces do not. This suggests that when episodic memories become more consolidated in neocortex they also become more semantic. This can reconcile the conflicting findings on MTL activity reported above. We propose that in the current study the memories that are thought to be more consolidated became more semantic than episodic while becoming less dependent on MTL. Unfortunately, we were unable to test whether the material retrieved by the participants contained any contextual information, but future studies should be designed to control for this.

4.2 Trend for rhinal and hippocampal activity decreases for recent items possibly reflects enhanced encoding

When comparing successful recall of recent items between conditions a trend can be observed for a decrease around 80 Hz suggesting recent items on the nap day had less relative gamma power than recent items on the no-nap day. This casts doubt on our main interpretation that the relative gamma activity decrease for remote items is an effect of consolidation. However, we believe a different phenomenon is responsible for the trend for recent items. Several recent studies point out that sleep before encoding is beneficial for learning. For example, Yoo, Hu, Gujar, Jolesz, and Walker (2007) reported decreased hippocampal activity during encoding and worse performance after a night of sleep deprivation using a visual memory task. Additionally, Van Der Werf et al. (2009) reported that when subjects experienced more shallow sleep versus deep sleep hippocampal activity during encoding was decreased and performance was lower during verbal memory retrieval. One possible reason for why less sleep leads to worse encoding is that sleep restores synaptic plasticity. Supporting this line of reasoning is that Moser and Moser (1999) have shown that spatial learning can lead to saturation of long-term potentiation in rat hippocampus, which is decreased again with time by NMDA-receptor regulation (Villarreal, Do, Haddad, & Derrick, 2002). Sleep has been hypothesized to facilitate this process (Tononi & Cirelli, 2006). Thus, if encoding would occur immediately after sleep it would benefit from a restored synaptic plasticity in neocortex. This would allow for memory traces to be stored in neocortex already during encoding and MTL structures would be needed less for these memories during retrieval. We propose that the trend of an 80 Hz gamma power decrease for recent items on the nap day is caused by enhanced encoding. This would result in a power difference during retrieval similar to what we report for remote items. Most importantly, this does not exclude an effect of consolidation on remote items.

However, there is another explanation that could account for a decrease of gamma power in both remote and recent items on the nap day. Tononi and Cirelli (2006) have suggested that restoration of synaptic plasticity during sleep occurs by global synaptic downscaling. By lowering the strengths of synapses while retaining the relative difference between them, sleep would lead to more energetically and spatially

efficient cortical networks. The implication of this is that decreased synaptic strengths would lead to smaller excitatory post-synaptic potentials, which would lower gamma power as measured in local field potentials by our intra-cranial electrodes. This would be true across the whole retrieval session on the nap day irrespective of what is retrieved and could account for both the remote effect and the recent trend. Though we do not disagree with the synaptic homeostasis hypothesis put forward by Tononi and Cirelli (2006) per se, we argue that this does not account for the relative power differences we report. We base this on two arguments. Firstly, if there would be a measurable decrease of gamma power caused by synaptic downscaling, then misses on the nap day should have lower raw gamma power than misses on the no-nap day. When looking at supplementary figure 1 (see website, www.ru.nl/master/cns/journal/) however, this is not the case. When averaging over remote and recent items, there are no apparent power differences between misses. As misses are qualitatively equal on both days, any difference caused by synaptic downscaling leading to our main results should have been observable. Secondly, if there would have been a global decrease of gamma power because of synaptic downscaling, our relative power measure should cancel this out. As we express power of hits as a ratio of power of misses any global decrease of power for hits and misses should disappear. Considering both arguments, we are confident that even if there was a global measurable decrease of power due to synaptic downscaling, it would not have affected our analyses.

It still remains an important observation that the remote and recent items show similar patterns during retrieval. Though the data are not entirely conclusive, we believe that our interpretations are the most probable ones. Further control experiments should be conducted to investigate the effects of sleep on MTL power measurements and focus on how long any effect, if present, lasts. Based on an estimated timescale from such experiments a new nap paradigm can be constructed to investigate the effects of consolidation during sleep and the effects of sleep before encoding on retrieval in a manner which would control for the above.

4.3 Relative gamma power decrease and increase centered around 80 Hz

The effects of sleep on gamma power revealed by our data was centered around 80 Hz. This is in line with Montgomery and Buzsaki (2007) and Sederberg et al. (2007) who have also reported memory effects in MTL above 40 Hz. Many others have reported effects centered around 40 Hz (Axmacher et al., 2007; Fell, Fernandez, Klaver et al., 2006; Fell, Fernandez, Lutz et al., 2006; Fell et al., 2003; Fell et al., 2001; Fell et al., 2008; Mormann et al., 2005; Sederberg et al., 2007). One possible reason for so little reports of memory effects around 80 Hz could be caused by a low signal-to-noise ratio when spectral smoothing is not applied. Multi-tapering for example (Mitra & Pesaran, 1999) improves the signal to noise ratio for power at higher frequencies (Nalatore, Ding, & Rangarajan, 2009). While we did report an effect centered around 40 Hz for recent items in rhinal cortex only, it remains an interesting question why our other effects occurred at a higher frequency in rhinal cortex and hippocampus. What role these different frequencies play has recently received attention by Colgin et al. (2009), who report frequency specific (~40 and ~80 Hz) synchronization between parts of the hippocampus and rhinal cortex in freely moving rats. One possible function for this frequency specific synchronization put forward by the authors is the routing and temporal segmentation of information from different sources. It would be interesting if specific memory functions can selectively modulate 40 and 80 Hz synchronization, as both have been reported in intra-cranial studies on memory. Further studies should look into this.

Another point of interest is the similarity between our reported frequency ranges of effect in rhinal cortex and hippocampus. As they are closely overlapping it could indicate a possible frequency coupling between both structures during retrieval. This would be in line with previous research (Fell, Fernandez, Klaver et al., 2006; Fell, Fernandez, Lutz et al., 2006; Fell et al., 2003; Fell, Klaver, Elger, & Fernandez, 2002; Fell et al., 2001) and is made possible by the anatomical organization of MTL (Lavenex & Amaral, 2000; Squire et al., 2004). This is also implicitly expected from the standard consolidation model, as information transfer between MTL and neocortex can only occur when communication is occurring within MTL. Though it is too early to provide preliminary connectivity results, we hope to show reliable sleep modulated phase synchronization and power-power correlations between rhinal cortex and hippocampus during successful memory recall in further analyses.

4.4 Sleep modulates successful memory recall

Behavioral performance was approximately equal on both testing days. This eliminates one important confound that is common in studies on consolidation, the influence of memory strength. When subjects study material before and after a sleep period, behavioral performance differences are common, as subjects usually remember more items from the more recent session than from the more remote session. Any effects in hippocampal activity could therefore potentially be explained by differences in memory strength, as memory traces that have decayed over time would evoke less hippocampal activity and would lead to a performance decrement. As there are no differences in performance on both testing days in our experiment, memory strength can be assumed to be equal for both sets of remote items. Memory trace decay can therefore not explain the difference in activity we find in rhinal cortex and hippocampus.

Our results show an effect of sleep on power during successful memory recall, relative to power during unsuccessful memory recall. Our relative power measure expresses power in remote hits as a ratio of power in remote misses. We chose this contrast because it has a normalizing effect on power, reducing arbitrary variance between subjects and thereby increasing the signal-to-noise ratio. Though it has a similar effect as traditional baselining, this contrast also increases the sensitivity to memory related effects on power. Though one could argue that our reported difference between conditions could have been caused by a difference in misses instead of hits, we do not believe this is the case. Raw power during remote misses appears approximately equal on both days, and appears both higher than raw power during remote hits on the nap day and lower than raw power during remote hits on the no-nap day (supplementary figure 2, see website, www.ru.nl/master/cns/journal/). Though these statements only reflect trends, as inter-subject variation is relatively large, it does indicate that it is unlikely that our effects in relative power stem from differences in power during remote misses, instead of hits.

4.5 Differences with previous analyses

The current study reanalyzed a dataset from Axmacher et al. (2008). The previous analyses showed that recent items had a significantly higher gamma response (60-90 Hz) in hippocampus during retrieval on the no-nap day than on the nap day. The authors concluded that information transfer from hippocampus to neocortex occurred immediately after encoding of recent items on the nap day, suggesting that sleep facilitates consolidation during post-sleep waking state. Our results differ in that we only find a trend for recent items but also a significant difference for remote items between days in the same frequency range. Furthermore, we find the above effects in both hippocampus and rhinal cortex. The difference between our results and the previous study could be explained by several key differences between the analyses. Firstly, we computed a memory related contrast before analyzing power differences between conditions, whereas the previous study used no such contrast. Secondly, we analyzed 6 out of 10 subjects with selection based on stricter performance criteria, whereas the previous analyses were done on all 10 subjects. Thirdly, we based the selection of electrode contacts to be analyzed on the total sum of power in 1-30 Hz, while the previous analyses used selection criteria based on event-related potentials. This resulted in a different selection of contacts. Lastly, we used a multi-taper approach for analyzing power and applying spectral smoothing and cluster-based permutation tests for statistical evaluation, whereas the previous study used a continuous wavelet transformation and an analysis of variance procedure. See methods section for more details.

4.6 Conclusion

In conclusion, we demonstrated that 60 min of sleep after encoding remote items reduces relative gamma power during retrieval in rhinal cortex and hippocampus. We propose that this is an effect of consolidation and thereby reflects a decreased rhinal and hippocampal contribution to the memory trace. We also reported a trend for sleep before encoding recent items decreasing relative gamma power during retrieval. We propose that this reflects enhanced encoding occurring shortly after sleep. The remote and recent effects did not differ significantly.

Acknowledgements

I would like to thank both my supervisors, Ingrid Nieuwenhuis and Ole Jensen, for their excellent theoretical and practical support during the course of this project. I am very thankful to our colleague from Bonn, Nikolai Axmacher, for providing me

with the opportunity to work on intracranially recorded data. Furthermore, I would like to thank the participants of the DCCN MEG-meeting for their suggestions on data-analyses and Eric Maris for our fruitful discussions on statistics.

References

Alvarez, P., & Squire, L. R. (1994). Memory consolidation and the medial temporal lobe: a simple network model. Proc Natl Acad Sci U S A, 91(15), 7041-7045.

Axmacher, N., Haupt, S., Fernandez, G., Elger, C. E., & Fell, J. (2008). The role of sleep in declarative memory consolidation--direct evidence by intracranial EEG. Cereb Cortex, 18(3), 500-507.

Axmacher, N., Mormann, F., Fernandez, G., Cohen, M. X., Elger, C. E., & Fell, J. (2007). Sustained neural activity patterns during working memory in the human medial temporal lobe. J Neurosci, 27(29), 7807-7816.

Axmacher, N., Mormann, F., Fernandez, G., Elger, C. E., & Fell, J. (2006). Memory formation by neuronal synchronization. Brain Res Rev, 52(1), 170-182.

Barr, W. B., Goldberg, E., Wasserstein, J., & Novelly, R. A. (1990). Retrograde amnesia following unilateral temporal lobectomy. Neuropsychologia, 28(3), 243-255.

Bauer, E. P., Paz, R., & Pare, D. (2007). Gamma oscillations coordinate amygdalo-rhinal interactions during learning. J Neurosci, 27(35), 9369-9379.

Bikbaev, A., & Manahan-Vaughan, D. (2008). Relationship of hippocampal theta and gamma oscillations to potentiation of synaptic transmission. Front Neurosci, 2(1), 56-63.

Born, J., Rasch, B., & Gais, S. (2006). Sleep to remember. Neuroscientist, 12(5), 410-424.

Colgin, L. L., Denninger, T., Fyhn, M., Hafting, T., Bonnevie, T., Jensen, O., et al. (2009). Frequency of gamma oscillations directs information flow in the hippocampus.Unpublished manuscript.

Dudai, Y. (2004). The neurobiology of consolidations, or, how stable is the engram? Annu Rev Psychol, 55, 51-86.

Eichenbaum, H. (2000). A cortical-hippocampal system for declarative memory. Nat Rev Neurosci, 1(1), 41-50.

Ekstrom, A., Viskontas, I., Kahana, M., Jacobs, J., Upchurch, K., Bookheimer, S., et al. (2007). Contrasting roles of neural firing rate and local field potentials in human memory. Hippocampus, 17(8), 606-617.

Fell, J., Fernandez, G., Klaver, P., Axmacher, N., Mormann, F., Haupt, S., et al. (2006). Rhinal-hippocampal coupling during declarative memory formation: dependence on item characteristics. Neurosci Lett, 407(1), 37-41.

Fell, J., Fernandez, G., Lutz, M. T., Kockelmann, E., Burr, W., Schaller, C., et al. (2006). Rhinal-hippocampal connectivity determines memory formation during sleep. Brain, 129(Pt 1), 108-114.

Fell, J., Klaver, P., Elfadil, H., Schaller, C., Elger, C. E., & Fernandez, G. (2003). Rhinal-hippocampal theta coherence during declarative memory formation: interaction with gamma synchronization? Eur J Neurosci, 17(5), 1082-1088.

Fell, J., Klaver, P., Elger, C. E., & Fernandez, G. (2002). The interaction of rhinal cortex and hippocampus in human declarative memory formation. Rev Neurosci, 13(4), 299-312.

Fell, J., Klaver, P., Lehnertz, K., Grunwald, T., Schaller, C., Elger, C. E., et al. (2001). Human memory formation is accompanied by rhinal-hippocampal coupling and decoupling. Nat Neurosci, 4(12), 1259-1264.

Fell, J., Ludowig, E., Rosburg, T., Axmacher, N., & Elger, C. E. (2008). Phase-locking within human mediotemporal lobe predicts memory formation. Neuroimage, 43(2), 410-419.

Frankland, P. W., & Bontempi, B. (2005). The organization of recent and remote memories. Nat Rev Neurosci, 6(2), 119-130.

Fries, P. (2005). A mechanism for cognitive dynamics: neuronal communication through neuronal coherence. Trends Cogn Sci, 9(10), 474-480.

Fries, P., Nikolic, D., & Singer, W. (2007). The gamma cycle. Trends Neurosci, 30(7), 309-316.

Fries, P., Reynolds, J. H., Rorie, A. E., & Desimone, R. (2001). Modulation of oscillatory neuronal synchronization by selective visual attention. Science, 291(5508), 1560-1563.

Gorfine, T., Yeshurun, Y., & Zisapel, N. (2007). Nap and melatonin-induced changes in hippocampal activation and their role in verbal memory consolidation. J Pineal Res, 43(4), 336-342.

Gray, C. M., Konig, P., Engel, A. K., & Singer, W. (1989). Oscillatory responses in cat visual cortex exhibit inter-columnar synchronization which reflects global stimulus properties. Nature, 338(6213), 334-337.

Gruber, T., Tsivilis, D., Montaldi, D., & Muller, M. M. (2004). Induced gamma band responses: an early marker of memory encoding and retrieval. Neuroreport, 15(11), 1837-1841.

Idzikowski, C. (1984). Sleep and memory. Br J Psychol, 75 (Pt 4), 439-449.

Jensen, O., Kaiser, J., & Lachaux, J. P. (2007). Human gamma-frequency oscillations associated with attention and memory. Trends Neurosci, 30(7), 317-324.

Ji, D., & Wilson, M. A. (2007). Coordinated memory replay in the visual cortex and hippocampus during sleep. Nat Neurosci, 10(1), 100-107.

Jokisch, D., & Jensen, O. (2007). Modulation of gamma and alpha activity during a working memory task engaging the dorsal or ventral stream. J Neurosci, 27(12), 3244-3251.

Kim, J. J., & Fanselow, M. S. (1992). Modality-specific retrograde amnesia of fear. Science, 256(5057), 675-677.

Lahl, O., Wispel, C., Willigens, B., & Pietrowsky, R. (2008). An ultra short episode of sleep is sufficient to promote declarative memory performance. J Sleep Res, 17(1), 3-10.

Lavenex, P., & Amaral, D. G. (2000). Hippocampal-neocortical interaction: a hierarchy of associativity. Hippocampus, 10(4), 420-430.

Logothetis, N. K., Pauls, J., Augath, M., Trinath, T., & Oeltermann, A. (2001). Neurophysiological investigation of the basis of the fMRI signal. Nature, 412(6843), 150-157.

Louie, K., & Wilson, M. A. (2001). Temporally structured replay of awake hippocampal ensemble activity during rapid eye movement sleep. Neuron, 29(1), 145-156.

Maguire, E. A., & Frith, C. D. (2003). Lateral asymmetry in the hippocampal response to the remoteness of autobiographical memories. J Neurosci, 23(12), 5302-5307.

Maguire, E. A., Henson, R. N., Mummery, C. J., & Frith, C. D. (2001). Activity in prefrontal cortex, not hippocampus, varies parametrically with the increasing remoteness of memories. Neuroreport, 12(3), 441-444.

Maris, E., & Oostenveld, R. (2007). Nonparametric statistical testing of EEG- and MEG-data. J Neurosci Methods, 164(1), 177-190.

Marshall, L., & Born, J. (2007). The contribution of sleep to hippocampus-dependent memory consolidation. Trends

Cogn Sci, 11(10), 442-450.
McClelland, J. L., McNaughton, B. L., & O'Reilly, R. C. (1995). Why there are complementary learning systems in the hippocampus and neocortex: insights from the successes and failures of connectionist models of learning and memory. Psychol Rev, 102(3), 419-457.
Mednick, S. C., Cai, D. J., Kanady, J., & Drummond, S. P. (2008). Comparing the benefits of caffeine, naps and placebo on verbal, motor and perceptual memory. Behav Brain Res, 193(1), 79-86.
Mitra, P. P., & Pesaran, B. (1999). Analysis of dynamic brain imaging data. Biophys J, 76(2), 691-708.
Montgomery, S. M., & Buzsaki, G. (2007). Gamma oscillations dynamically couple hippocampal CA3 and CA1 regions during memory task performance. Proc Natl Acad Sci U S A, 104(36), 14495-14500.
Mormann, F., Fell, J., Axmacher, N., Weber, B., Lehnertz, K., Elger, C. E., et al. (2005). Phase/amplitude reset and theta-gamma interaction in the human medial temporal lobe during a continuous word recognition memory task. Hippocampus, 15(7), 890-900.
Moscovitch, M., Rosenbaum, R. S., Gilboa, A., Addis, D. R., Westmacott, R., Grady, C., et al. (2005). Functional neuroanatomy of remote episodic, semantic and spatial memory: a unified account based on multiple trace theory. J Anat, 207(1), 35-66.
Moser, E. I., & Moser, M. B. (1999). Is learning blocked by saturation of synaptic weights in the hippocampus? Neurosci Biobehav Rev, 23(5), 661-672.
Nadel, L., & Moscovitch, M. (1997). Memory consolidation, retrograde amnesia and the hippocampal complex. Curr Opin Neurobiol, 7(2), 217-227.
Nadel, L., Samsonovich, A., Ryan, L., & Moscovitch, M. (2000). Multiple trace theory of human memory: computational, neuroimaging, and neuropsychological results. Hippocampus, 10(4), 352-368.
Nalatore, H., Ding, M., & Rangarajan, G. (2009). Denoising neural data with state-space smoothing: method and application. J Neurosci Methods, 179(1), 131-141.
Nieuwenhuis, I. L., Takashima, A., Oostenveld, R., Fernandez, G., & Jensen, O. (2008). Visual areas become less engaged in associative recall following memory stabilization. Neuroimage, 40(3), 1319-1327.
Osipova, D., Takashima, A., Oostenveld, R., Fernandez, G., Maris, E., & Jensen, O. (2006). Theta and gamma oscillations predict encoding and retrieval of declarative memory. J Neurosci, 26(28), 7523-7531.
Penfield, W., & Milner, B. (1958). Memory deficit produced by bilateral lesions in the hippocampal zone. AMA Arch Neurol Psychiatry, 79(5), 475-497.
Pesaran, B., Pezaris, J. S., Sahani, M., Mitra, P. P., & Andersen, R. A. (2002). Temporal structure in neuronal activity during working memory in macaque parietal cortex. Nat Neurosci, 5(8), 805-811.
Peyrache, A., Khamassi, M., Benchenane, K., Wiener, S. I., & Battaglia, F. P. (2009). Replay of rule-learning related neural patterns in the prefrontal cortex during sleep. Nat Neurosci.
Plihal, W., & Born, J. (1999). Effects of early and late nocturnal sleep on priming and spatial memory. Psychophysiology, 36(5), 571-582.
Rempel-Clower, N. L., Zola, S. M., Squire, L. R., & Amaral, D. G. (1996). Three cases of enduring memory impairment after bilateral damage limited to the hippocampal formation. J Neurosci, 16(16), 5233-5255.
Ryan, L., Nadel, L., Keil, K., Putnam, K., Schnyer, D., Trouard, T., et al. (2001). Hippocampal complex and retrieval of recent and very remote autobiographical memories: evidence from functional magnetic resonance imaging in neurologically intact people. Hippocampus, 11(6), 707-714.
Scoville, W. B., & Milner, B. (1957). Loss of recent memory after bilateral hippocampal lesions. J Neurol Neurosurg Psychiatry, 20(1), 11-21.
Sederberg, P. B., Schulze-Bonhage, A., Madsen, J. R., Bromfield, E. B., Litt, B., Brandt, A., et al. (2007). Gamma oscillations distinguish true from false memories. Psychol Sci, 18(11), 927-932.
Singer, W. (1999). Neuronal synchrony: a versatile code for the definition of relations? Neuron, 24(1), 49-65, 111-125.
Squire, L. R., & Bayley, P. J. (2007). The neuroscience of remote memory. Curr Opin Neurobiol, 17(2), 185-196.
Squire, L. R., Stark, C. E., & Clark, R. E. (2004). The medial temporal lobe. Annu Rev Neurosci, 27, 279-306.
Stickgold, R. (2005). Sleep-dependent memory consolidation. Nature, 437(7063), 1272-1278.
Takashima, A., Petersson, K. M., Rutters, F., Tendolkar, I., Jensen, O., Zwarts, M. J., et al. (2006). Declarative memory consolidation in humans: a prospective functional magnetic resonance imaging study. Proc Natl Acad Sci U S A, 103(3), 756-761.
Talamini, L. M., Nieuwenhuis, I. L., Takashima, A., & Jensen, O. (2008). Sleep directly following learning benefits consolidation of spatial associative memory. Learn Mem, 15(4), 233-237.
Tononi, G., & Cirelli, C. (2006). Sleep function and synaptic homeostasis. Sleep Med Rev, 10(1), 49-62.
Tucker, M. A., Hirota, Y., Wamsley, E. J., Lau, H., Chaklader, A., & Fishbein, W. (2006). A daytime nap containing solely non-REM sleep enhances declarative but not procedural memory. Neurobiol Learn Mem, 86(2), 241-247.
Van Der Werf, Y. D., Altena, E., Schoonheim, M. M., Sanz-Arigita, E. J., Vis, J. C., De Rijke, W., et al. (2009). Sleep benefits subsequent hippocampal functioning. Nat Neurosci, 12(2), 122-123.
Van Roost, D., Solymosi, L., Schramm, J., van Oosterwyck, B., & Elger, C. E. (1998). Depth electrode implantation in the length axis of the hippocampus for the presurgical evaluation of medial temporal lobe epilepsy: a computed tomography-based stereotactic insertion technique and its accuracy. Neurosurgery, 43(4), 819-826; discussion 826-817.
Villarreal, D. M., Do, V., Haddad, E., & Derrick, B. E. (2002). NMDA receptor antagonists sustain LTP and spatial memory: active processes mediate LTP decay. Nat Neurosci, 5(1), 48-52.
Warrington, E. K., & Duchen, L. W. (1992). A re-appraisal of a case of persistent global amnesia following right temporal lobectomy: a clinico-pathological study. Neuropsychologia, 30(5), 437-450.
Wilson, M. A., & McNaughton, B. L. (1994). Reactivation of hippocampal ensemble memories during sleep. Science, 265(5172), 676-679.
Yoo, S. S., Hu, P. T., Gujar, N., Jolesz, F. A., & Walker, M. P. (2007). A deficit in the ability to form new human memories without sleep. Nat Neurosci, 10(3), 385-392.
Zola-Morgan, S. M., & Squire, L. R. (1990). The primate hippocampal formation: evidence for a time-limited role in memory storage. Science, 250(4978), 288-290.

Semantic expectancy in the comprehension of idiomatic expressions: an ERP study

Joost Rommers[1]
Supervisors: Marcel C.M. Bastiaansen[1,2], Ton Dijkstra[2]

[1] Max Planck Institute for Psycholinguistics, Nijmegen, The Netherlands
[2] Donders Institute for Brain, Cognition and Behavior, Nijmegen, The Netherlands

Evidence from literal sentence comprehension suggests that sufficiently constraining sentence contexts can lead to semantically specified expectations for upcoming words: specific meanings that are likely to come up are expected. It is unknown whether this "semantic expectancy" extends to the case of predictable words in opaque idiomatic expressions, of which the literal word meanings are unrelated to the figurative meaning of the expression as a whole and the predictability must stem from idiom knowledge. We investigated this issue in an event-related potential experiment. Participants were presented with literal and idiomatic sentence contexts in which the critical word was (1) a correct (expected) word, (2) a word that was semantically related to the expected word, or (3) a semantically unrelated word. Both (2) and (3) were semantic violations in the sentence context. In literal contexts, we obtained a graded N400, being largest for the semantically unrelated words, intermediate for semantically related words, and smallest for correct words. In contrast, in idiomatic contexts the N400s to semantically related and unrelated words were indistinguishable. These results suggest that expectations that may arise during language comprehension are not always semantically specified, and lend support to models of idiom processing in which literal word meanings are not crucial. Violations also elicited a late positivity (500-1200 ms) in idioms, regardless of semantic relatedness, of which only the later part (800-1200 ms) was also observed in literal contexts. Possible interpretations are discussed.

Keywords: idioms, anticipation, semantic expectancy, N400, sentence comprehension

Corresponding author: Joost Rommers, Max Planck Institute for Psycholinguistics, P.O. Box 310, 6500 AH Nijmegen, the Netherlands, Joost.Rommers@mpi.nl

1. Introduction

Understanding language is about mapping incoming forms such as letters, sounds, and different types of extralinguistic information onto meaning. We are known to perform this task extremely rapidly. In current views of sentence comprehension, the anticipation - or even more strongly, prediction - of upcoming words plays an increasingly important role (for reviews see Federmeier, 2007; Kamide, 2008; Pickering & Garrod, 2007; van Berkum, Brown, Zwitserlood, Kooijman, & Hagoort, 2005). Evidence suggests that sufficiently constraining contexts allow us to predict, on-line, the semantics of words that are likely to come up (Federmeier & Kutas, 1999). In the long run it might turn out that predicting upcoming meaning is our brain's way to process information before it comes in, which might form part of the answer to the broad question many psycholinguistic papers pose in their introduction: how is it possible that we understand language as quickly as we do? In the words of Kutas and Federmeier (2000), "the brain uses sentence context information to predict (i.e. to anticipate and prepare for) the perceptual and semantic features of items likely to appear, in order to comprehend the intended meaning of a sentence at the fast speed with which it usually comes." (p. 466). However, predicting the semantics of upcoming words makes sense only for the case in which the meanings of individual words are relevant for the ultimate interpretation: the case of literal language. We investigated whether semantic expectancy extends to the case of opaque idiomatic expressions, for which word meanings may be irrelevant to the overall interpretation.

1.1 Semantic expectancy

Word meaning expectancy is mainly based on information derived from, or stored knowledge activated by, prior context. In agreement with this, it has been shown that a congruent sentence context facilitates the word recognition process (e.g., Fischler & Bloom, 1979). This happens in a constraint-dependent manner: high constraint sentences engender a more narrow scope of facilitation compared to low constraint sentences (Schwanenflugel & Shoben, 1985)). These findings can also be explained by facilitated integration of a word with its context after word recognition, but they are not inconsistent with the idea that expectancy may play a role during sentence comprehension.

Both semantic processes and linguistic expectations are known to be indexed at the electrophysiological level by the N400, a negative deflection in the event-related potential (ERP) that peaks at around 400 ms after presentation of a content word and is maximal at centroparietal recording sites. This component was first discovered as the response to semantically anomalous words in a sentence context, such as "socks" in "He spread the warm bread with socks" (Kutas & Hillyard, 1980). Later studies established the N400 as part of the brain's normal response to any content word, with its size depending on various factors (for a review, see Kutas & Federmeier, 2000). For instance, the N400 decreases with the build-up of contextual constraint over the course of a sentence. Furthermore, the component's amplitude is smaller to high frequency words compared to low frequency words, although this effect disappears further downstream in longer sentences (van Petten & Kutas, 1990). The N400 is often contrasted with the qualitatively different P600, a positive deflection in the ERP with an onset at around 500 ms, which has been found in response to syntactic (e.g., Hagoort, Brown, & Groothusen, 1993; Osterhout & Holcomb, 1992) and orthographic violations (Münte, Heinze, Matzke, Wieringa, & Johannes, 1998; Vissers, Chwilla, & Kolk, 2006) and seems to have to do with reanalysis processes, although its precise functional significance is under debate.

The N400 has been used to demonstrate that expectancy can be semantic in nature. Federmeier and Kutas (1999) presented participants with contexts consisting of two sentences that led them to expect a specific word, such as They wanted to make the hotel look more like a tropical resort. So along the driveway they planted rows of … . There were three conditions. The context ended with (1) the expected word (e.g., palms), (2) an unexpected and contextually inappropriate word from the same semantic category as the expected word (e.g., pines), or (3) an unexpected and contextually inappropriate word from a different semantic category (e.g., tulips). Both unexpected endings elicited N400 effects relative to the expected word, but the N400 to words from the same semantic category as the expected word was significantly smaller compared to the N400 to words from a different semantic category. The effect further depended upon the degree of constraint of the sentence context. Constraint was operationally defined as cloze probability: the probability that a participant completes a particular sentence fragment with a particular word in an off-line sentence completion task. The amplitude of the N400 to anomalous words from an unexpected

semantic category remained unaffected by the degree of constraint, but the N400 to words from the expected semantic category was smaller in more highly constraining contexts compared to less constraining contexts, despite their lower rated plausibility in those sentences. In other words, the difference between processing words from an expected compared to an unexpected semantic category is larger in highly constraining contexts. From these results Federmeier and Kutas concluded that context can lead to specific semantic expectations.

In the present ERP study in Dutch, we focussed on semantic aspects of anticipation not only in literal contexts, but also in a different context in which individual word semantics are less relevant: contexts containing idiomatic expressions, or idioms. Idioms form a subclass of fixed expressions, and consist of several words that together bear a single figurative meaning. Although such expressions can be very predictable, individual word meanings may be irrelevant for understanding the overall meaning. Especially for opaque (as opposed to transparent) idioms, the figurative meaning does not follow logically from the individual meanings of the expression's component words; rather, it is known through common use. An example of a Dutch opaque idiom is "tegen de lamp lopen" (literal translation to walk against the lamp). This expression's figurative meaning, to get caught, is unrelated to walking or a lamp.

It seems an intuitively reasonable idea that the expectancy for the final noun of a predictable idiom might differ from that for a predictable word in a literal context. Consider, for instance, the word "lamp" in the following Dutch examples: a literal context (1) and an idiomatic context (2) (English literal translations are provided in Italics).

(1) Na de lunch draaide de electricien het nieuwe peertje in de lamp gisteren.

After lunch the electrician screwed the new light bulb into the lamp yesterday.

(2) Na vele transacties liep de onvoorzichtige fraudeur uiteindelijk tegen de lamp gisteren.

After many transactions the uncautious fraud eventually walked against the lamp yesterday.

For native speakers of Dutch, the word "lamp" is highly predictable in both cases, but the predictability is presumably due to different types of knowledge in the different types of context. In (1), the literal context, the predictability likely stems from various types of world and text knowledge, such as the knowledge that in the world that we live in light bulbs are usually screwed into lamps. In (2), the expectation for the same word is based on the reader's knowledge of a specific Dutch idiom. The second type of predictability has been scarcely investigated, and its semantic aspects remain unknown.

Idioms may seem like a peripheral part of our linguistic repertoire, but Jackendoff (1995, 2007) suggests that the number of fixed expressions (including, besides idioms, phenomena such as compounds, clichés, titles, quotes, etc.) might be so large that it equals the number of single words in our vocabulary: that is, some 40.000 expressions in languages like English. Sprenger (2003) observed that 7% of the words in a written corpus of Dutch belonged to the class of fixed expressions. Furthermore, idioms are not treated as a difficult exception by the language system, since they do not lead to additional processing effort: in a lexical decision task, participants are actually faster to decide whether a string of words is meaningful or not when it is an idiom than when it is an otherwise comparable literal phrase (Swinney & Cutler, 1979).

Most importantly, idioms are interesting cases to test general claims about the architecture and behaviour of the language system. Some of the core processes thought to be involved in sentence comprehension are, on the one hand, the retrieval of pieces of lexical information from long-term memory, and, on the other hand, combinatorial operations (unification) that continuously assemble these lexical building blocks into larger structures using at least syntactic, phonological, and semantic information (Hagoort, 2005, 2007). The lexical building blocks referred to in this type of view are usually specified as words. However, in the case of idioms, application of retrieval and semantic unification routines based on individual words would lead to an erroneous interpretation: the literal one. This raises the question whether these processes of semantic retrieval and unification, which are meant as a general framework for understanding all language input, are involved in the comprehension of idioms at all.

In behavioural research on idiom comprehension (discussed below), a main issue that has been adressed is whether literal word meanings become activated during idiom comprehension, leading to several proposals for models of how idioms are represented and processed. This issue is intimately related to semantic expectancy, namely through the notion of relevance to the overall meaning: it is plausible that literal word meanings are activated

or not depending on their relevance to the overall meaning, and the same relevance might also determine whether anticipatory processes include the anticipation of specific semantic properties of words or not. In other words, word meanings that play no role in on-line processing are unlikely to be anticipated, whereas word meanings that are actually used are likely to be anticipated when the context allows for it. Therefore, the present experiment can derive hypotheses from the available evidence on the activation of literal word meanings as well as yield implications for models of idiom processing.

1.2 Processing and representation of idioms

Many idioms, such as to kick the bucket, can be interpreted both literally and figuratively. Even in the case where a literal interpretation of the entire idiom is impossible or implausible, such as to wear one's heart on one's sleeve, the literal meanings of the individual words might become activated, for instance if we cannot help but process the literal meaning of every word that comes in. Models of the representation and processing of idioms must therefore address the question of which meaning(s) become(s) available and, if multiple meanings are activated, whether this happens in a serial or in a parallel fashion. Several models are discussed below, mainly evaluating their predictions regarding the activation of literal word meanings. Note that the predictions of the models may differ depending on various factors; we focus specifically on the case of opaque idioms that are predictable on the basis of prior sentence context such as the idiom in example (2) above.

Several models and hypotheses would predict no literal word meaning involvement in the comprehension of predictable idioms. In some models, idioms are represented as wholistic units with no internal structure (Bobrow & Bell, 1973; Gibbs, 1980), implying that the meanings of the words contained in the idiom are not activated. In a different model, the absence of literal word meaning activation stems from the processes specified in it. This configuration hypothesis (Cacciari & Tabossi, 1988) represents idioms as configurations of words which may activate their own literal meanings, but in a context-dependent manner: incoming words are analyzed literally until at a certain point, called the key of the idiom, sufficient information has accumulated for the reader or listener to recognize the idiom as such. After this point, any remaining lexical items may not be processed literally. Hence, in the case in which the final noun of an idiom is predictable (as in example (2)), literal word meanings should not be activated.

In line with this absence of literal word meaning activation during idiom processing, Peterson, Burgess, Dell and Eberhard (2001) found that concrete target words were not named faster than abstract targets in idioms, whereas a concreteness effect was obtained in literal contexts. Raposo, Moss, Stamatakis and Tyler (2009) observed somatotopically organized premotor cortex activation for arm- and leg-related action verbs in isolation (e.g., grab/kick), in literal sentences (e.g., The fruit cake was the last one so Claire grabbed it), but not in idiomatic sentences (e.g., The job offer was a great chance so Claire grabbed it). Raposo et al.'s findings are in apparent disagreement with those of Boulenger, Hauk and Pulvermüller (2009) who did find somatotopic motor cortex activation in idiomatic sentences (e.g., John grasped the idea), but in their materials the action words occurred before the idiom could be recognized as such. Therefore, their action words were ambiguous between being literal or part of an idiom and could therefore have been analyzed literally. With contexts that bias the comprehender towards an idiomatic interpretation, as in Raposo et al.'s (2009) design, semantic somatotopy does not extend to words in idioms. However, as Raposo et al. indicate themselves, these studies do not have the temporal resolution to address whether literal meanings might be activated very shortly and then quickly suppressed.

In contrast to the above, several models would predict that activation of literal word meanings does occur during the comprehension of idiomatic expressions. For instance, the lexical representation hypothesis (Swinney & Cutler, 1979) employs, in parallel with the idiom retrieval process which retrieves the entire idiom as one lexical unit, a literal analysis. This literal analysis runs along in parallel and retrieves literal word meanings. Because the computations carried out by the literal stream take longer than the retrieval of the idiom as a whole, the idiomatic meaning is accessed before the literal meaning – which explains Swinney and Cutler's (1979) own finding that idioms are processed faster compared to literal language. However, the unitary representation prevents idioms from showing syntactic flexibility, even though there are idioms that allow syntactic modifications (Katz, 1973). In "hybrid" models (Cutting & Bock, 1997; Sprenger, Levelt, & Kempen, 2006), an idiom has a unitary representation connected to separate lexical entries

for the single words composing the idiom, and it is these single words that cause literal word meanings to become activated. Both hybrid models are designed for idiom production rather than comprehension, but they make important claims about how idioms are represented in the mental lexicon, which presumably also pertain to idiom comprehension given that the lexicon is thought to be shared between production and comprehension (e.g., Roelofs, 2003). [1]

In line with models predicting the activation of literal word meanings during idiom comprehension, several studies have found that words in idioms can prime literally related words (e.g., Cacciari & Tabossi, 1988; Colombo, 1993; Hillert & Swinney, 2000; Swinney, 1981). In the case of priming, hybrid models even predict stronger effects in idioms compared to literal language. This is because activation of a word (e.g., "lopen", to walk) will spread to the unitary representation of the full idiom (e.g., "tegen de lamp lopen", to walk against the lamp). Further spreading of activation will cause increased activation for all of the words constituting the idiom, effectively priming them even more. Indeed, Sprenger et al. (2006) found stronger identity priming effects in idioms compared to literal phrases.

It should be noted that two other approaches make different predictions depending on the type of idiom. First, idioms can differ in compositionality, which refers to the fact that parts of an idiom can carry part of the idiomatic meaning. For instance, the idiom to pop the question is decomposable because pop has some relationship with proposing something and marriage is the result of a specific question. In contrast, the idiom to kick the bucket is not decomposable. Gibbs and Nayak (1989; based on Nunberg, 1978) found more syntactic flexibility and facilitated processing of decomposable idioms compared to non-decomposable idioms, leading them to argue that only non-decomposable idioms are recognized as a whole. However, several other studies failed to find effects of compositionality (Cutting & Bock, 1997; Libben & Titone, 2008; Tabossi, Fanari, & Wolf, 2005) or found effects in different directions in different experiments, making interpretation difficult (Sprenger, et al., 2006). In sum, there is little support for compositionality as the crucial factor in idiom processing. Second, idioms can differ in salience. According to the graded salience hypothesis (Giora, 1997), the salience of idioms – described in terms of frequency, conventionality, and familiarity – determines whether the idiomatic or literal meaning is accessed first. In support of this, Laurent, Denhieres, Passerieux, Iakimova, and Hardy-Bayle (2006) observed that N400 amplitudes were smaller to idioms with highly salient compared to less salient idiomatic meanings. Although salience is a difficult property to derive predictions from, we take this hypothesis to predict no literal word meaning activation in the case of predictable opaque idioms such as those in example (2), since at least prior context is highly biased towards the idiomatic meaning. To summarize, both evidence in favour of and against the activation of literal word meanings is present in the literature.

1.3 The present study

In the present study, we investigated semantic expectancy in both literal and idiomatic contexts. The main issue was whether semantic expectancy, known to be driven mainly by semantic and world knowledge that is activated upon reading a predictable context, occurs specifically in literal sentences or extends to the case of opaque idioms. In addition, although somewhat indirectly, the adequacy of existing models of idiom comprehension was assessed.

Regarding these aims, the following issues are at stake. If semantic expectancy does extend to idiomatic expressions, this would have two possible interpretations. On the one hand, it could be seen as showing that the semantics of upcoming words are predicted even if they are irrelevant to the overall interpretation. This would challenge the entire idea of anticipation being central to the comprehension process, since the system generates expectations that are not used in subsequent sense-making processes. On the other hand, one could view such a result as showing that the semantics of individual words in opaque idioms are actually of relevance to the interpretation, given that otherwise they would not be expected by a system as quick and probably economic as the language faculty. Alternatively, the present experiment could lead to the observation that semantic expectancy does not extend to idiomatic expressions. This would highlight the context-dependent nature of expectations in language comprehension. Furthermore, given that the materials in this study are predictable and likely give rise to expectations, it would show that expectations are not always semantic in nature. Such a result would

[1] Although the configuration hypothesis represents idioms in a similar hybrid way, it does not predict literal word meaning activation in the case of the predictable idioms used in the present study due to its processing stages involving the notion of key. Because of this it is not discussed together with the other hybrid models.

also challenge models of idiom processing in which literal word meanings play an important role.

Much like Federmeier and Kutas (1999), in the present study the electro-encephalogram (EEG) was recorded while we presented participants with sentences containing a critical word that was (1) expected on the basis of prior context and consequently also fitted this context, or (2) did not fit the context but was semantically related to the expected word, or (3) did not fit the context and was semantically unrelated to the expected word. However, the prior context and hence the basis for expectancy was either a highly constraining literal context or an equally constraining idiomatic context. The idiomatic context was a sentence containing an idiom, of which the final noun was the critical word.

The hypotheses were as follows. First, for literal sentences, we expected to obtain a "graded" N400 pattern similar to what Federmeier and Kutas (1999) observed: both semantically related and semantically unrelated words were expected to elicit larger N400s compared to the correct (expected) word, but the N400 to semantically related words should be smaller compared to the N400 to semantically unrelated words. This would not only indicate the reliability of the graded effect by replicating it, but also establish that it can be obtained with our specific materials, providing the basis for further inferences regarding idioms. For words in idiomatic contexts, the same graded N400 pattern was predicted to occur only if semantic expectancy extends to this type of context. If semantic expectancy does not extend to idiomatic contexts, the expectancy for a word should not selectively facilitate the processing of semantically related words and therefore N400 responses to words that are semantically related to the expected word should not differ from those to semantically unrelated words.

Two published ERP studies come close to this idea. Both of these show that N400 effects to unexpected words occur not only in literal contexts, but also in idioms. First, Moreno, Federmeier, and Kutas (2002) examined ERPs to words in idioms and literal sentences. The critical words were predictable words, "lexical switches" (literal synonyms of the predictable words) or code switches (Spanish translations of the expected English words). Relative to expected words, lexical switches showed larger N400 amplitudes in both literal and idiomatic contexts. In as far as the lexical switches (synonyms) used by Moreno et al. (2002) resemble semantically related words, it is interesting to note that N400 effects to lexical switches were not different in idioms compared to literal contexts, suggesting at least some resemblance in semantic processes in both types of context. However, the semantic effect (a difference between semantically related and unrelated items) that is of interest to the current study cannot be inferred from these existing data, since there was no semantically unrelated control condition. Furthermore, literal and idiomatic contexts were not matched on cloze probability; rather, idioms were explicitly used as a way to boost the predictability of upcoming words. It is therefore unclear whether any differences between words in literal and idiomatic sentences is attributable to differences between idioms and literal language per se or rather to differences in the level of constraint. In the present study we aimed to examine the effect of "idiomaticity" while keeping cloze probability constant.

Besides the N400, Moreno et al. also observed a late frontal positivity (650-850 ms), which was elicited by both lexical switches and code switches and was larger in idioms compared to literal contexts. Therefore, we also included an analysis of later effects in the present study. Given that anticipations which turn out to be wrong can lead to reanalysis processes, the different kinds of predictability in idioms compared to literal sentences might also lead to differences in the P600 component.

A second ERP study was more directly targeted at processes of expectancy during idiom comprehension. Vespignani, Canal, Molinaro, Fonda and Cacciari (in press) manipulated words in idioms that were either at the key or one position further downstream in the sentence. When the word at the key was replaced with a different word, this led to an N400 effect. After the key, a replacement also led to an N400, but the control condition in which the entire idiom was left intact seemed to show a P300 which the authors relate to the special type of predictability that is present in predictable idioms. Yet, Vespignani et al. (in press) did not address the specific issue of there being a difference between expectations in idioms and literal language at the semantic level.

2. Methods

2.1 Materials and design

The materials consisted of 90 sets of 6 sentences. An example set of sentences is shown in Table 1.

In every set, one type of sentence set up an Idiomatic context for a critical word. This critical

Table 1. Dutch example sentences and their translation equivalents in English (italicized). For the Idiomatic context, an approximate translation of the figurative meaning is provided between brackets. Critical words are underlined, printed in bold and coloured according to the condition for readability. The critical word that appeared in a given sentence depended on the condition. Black = Correct, green = Semantically Related Violation, red = Semantically Unrelated Violation.

Idiomatic context
Na vele transacties liep de onvoorzichtige fraudeur uiteindelijk tegen de **lamp** / kaars / vis gisteren.
After many transactions the uncautious fraud eventually walked against the lamp / candle / fish yesterday.
[After many transactions the uncautious fraud eventually got caught yesterday.]
Literal context
Na de lunch draaide de electricien het nieuwe peertje in de **lamp** / kaars / vis gisteren.
After lunch the electrician screwed the new light bulb into the lamp / candle / fish yesterday.

word was the final noun of an idiom (for instance, "lamp" in the Dutch idiom "tegen de lamp lopen"). For the other sentence type, a Literal context was constructed around the same critical word. Both types of context were highly constraining. There were three possible types of critical word in the Idiomatic and Literal contexts: (1) the Correct word, which was highly expected on the basis of the preceding context, (2) a Semantically Related Violation (abbreviated as the Sem.Rel. condition), consisting of a word that did not fit the sentence context but was semantically related to the correct word, or (3) a Semantically Unrelated Violation (the Sem.Unrel. condition), consisting of a word that did not fit the sentence context but was semantically unrelated to the Correct word (i.e., a standard semantic violation).

The design included two within-subject factors: Idiomaticity, with two levels (Literal, Idiomatic) specifying the type of predictive context, and Condition, with three levels (Correct, Semantically Related Violation, Semantically Unrelated Violation) specifying the type of critical word in the context. Across the item set, the same critical words were used in the Idiomatic sentences and their Literal counterparts. The six possible sentences from each set were divided across three lists using a Latin square design, such that no context or critical word was repeated on a list. In every list, each condition was represented by 30 items.

In order to reduce the proportion of violations in the experiment, the same 60 correct filler items (30 correct idiomatic and 30 correct literal sentences) were added to each list so that each list contained 240 sentences, of which half was idiomatic and half was literal, and half of the items contained one of the two types of violation and half was correct. Every list was used for eight participants in the EEG experiment, who each received a different randomization. In order to minimize the chance that participants would become aware of the different conditions represented by the different sentences in the experiment, items were pseudorandomized under the constraints that (1) the same condition did not occur more than two times in a row, and that (2) items based on the same Correct critical word occurred with at least 10 intervening items. For instance, the items "After lunch the competent electrician put a new light bulb in the candle yesterday" and "After many transactions the uncautious fraud eventually walked against the fish yesterday" do not have a sentence context or critical word in common, but share the expectancy for the Correct word "lamp" at the position of the critical word. To avoid interference from sentence wrap-up effects, critical words were never placed in the final position of a sentence.

2.1.1 Semantic relatedness

Words for the Sem.Rel. condition were obtained in two steps. First, free association norms for Dutch words (A. M. B. de Groot & de Bil, 1987; Lauteslager, Schaap, & Schievels, 1986; van Loon-Vervoorn & van Bekkum, 1991) were consulted in order of recency of publication. These norms were generally collected by having 100 participants respond to a word with their first association and subsequently computing the frequency with which each association occurred. Norms were available for 42 of the 90 Correct words. The word with the highest association frequency in the norms was not always an appropriate substitution for the correct critical word in a sentence due to differences compared to the correct word in grammatical class, gender, number, and concreteness. In other cases the word fitted in the literal sentence context too well (recall that the criterion was not only to use semantically related words, but to create Semantically Related Violations). In these cases, the next best option was examined until a suitable word was found. On average the third most frequent association was

used, with on average approximately 10% of the participants having indicated the word as their first association in response to the correct word.

As a second step, inspiration for semantically related words for the remaining 48 items was obtained using latent semantic analysis (LSA, Landauer & Dumais, 1997; Landauer, Folz, & Laham, 1998, available on the Internet at http://lsa.colorado.edu/). This is a semantic similarity measure that computes how often two words co-occur with the same set of other words. LSA has been used successfully in semantic priming research (Chwilla & Kolk, 2002). Words were translated to English and submitted to the on-line "near neighbors interface" using the General_Reading_up_to_1st_year_college topic space, which yielded a list of candidate words to choose from. Semantically unrelated words were added and LSA values were computed for all of the 90 items by submitting them to the "pairwise (term to term) comparison", once comparing the Sem.Rel. condition to the Correct word and once comparing the Sem.Unrel. condition to the Correct word, again using the General_Reading_up_to_1st_year_college topic space. The average LSA value for all of the 90 Sem.Rel. items was 0.36 (standard deviation (SD) 0.19) whereas for the Sem.Unrel. items it was 0.08 (SD 0.05), a difference that was significant, [$t(89) = 13.68$, $p < .001$].

2.1.2 Word frequency and word length

For the three types of critical word the log-transformed lemma frequency and word length in number of characters were extracted from the Dutch CELEX lexical database (Baayen, Piepenbrock, & Gulikers, 1993). One-way ANOVAs indicated that the three conditions did not differ significantly in word frequency, [$F(2, 267) = 1.42$, $p = 0.244$], which was 1.5 on average (SD 0.5), but that there was a difference in word length, [$F(2, 267) = 5.78$, $p < .01$]. Bonferroni-corrected post-hoc comparisons revealed that words from the Sem.Rel. condition were significantly longer compared to both the Correct words, [$p < .01$] and the words from the Sem.Unrel. condition [$p < .05$]. However, for the goals of the present study it was most important to make sure that words for the Sem.Rel. condition were as highly related as possible to words from the Correct condition; this received priority over controlling for word length. Also, the effect size was only half a character: Sem.Rel. items consisted of 5 characters on average, compared to 4.5 characters for critical words in the Sem.Unrel. condition and in the Correct condition.

2.2 Pretests

Before carrying out the EEG experiment, the items were pretested on several dimensions (see below). We started out with 151 items. In the course of pretesting, items were discarded when they did not meet certain criteria, leaving a final set of 90 items for the EEG experiment.

2.2.1 Idiom selection and ratings

Because idioms are not a homogeneous group (as discussed in the Introduction), they were pretested on two dimensions: familiarity and transparency. It was important to use familiar idioms, because our interest was in idiomatic processing and familiar idioms are more likely to be processed idiomatically, whereas unfamiliar or new idioms might be interpreted literally (and possibly erroneously). Regarding transparency - the degree to which an idiom's figurative meaning can be derived from the literal meanings of its component words -, we chose to use opaque idioms. This was done because in opaque idioms literal word meanings bear no relationship to the idiomatic meaning. As such, these idioms provide the strictest test for semantic expectancy for literal word meanings: if literal word meanings play a role even in the case that they are as irrelevant as possible, this would lend the strongest support to the hypothesis that the language system's basis for expectations is always semantic in nature, even in idioms.

Familiarity and transparency values were obtained using a paper-and-pencil rating task. Although only opaque idioms were relevant for the EEG experiment, more transparent idioms were also included in the rating task in order to present participants with idioms from the full scale from transparent to opaque. Using our own sense of opacity, 151 opaque idiomatic expressions (for instance, "tegen de lamp lopen", to walk against the lamp, [to get caught]) and 151 transparent idioms (for instance, "iemand voor de rechter slepen", to drag someone before the judge, [to sue someone]) were selected from a Dutch idiom dictionary (H. de Groot, 1999). To rule out order effects, four lists containing the same items were created: the items were randomized once for list one, then each half of the items was reversed for list two, list three was the reverse of list one, and for list four each half of the items in list three was reversed. Each list was used for five participants.

The familiarity and transparency ratings were obtained from the same participants in a combined

test. This allowed us to discard transparency ratings from participants who did not know an idiom. Idioms were presented out of context, in infinitival form (e.g., "tegen de lamp lopen", to walk against the lamp), with the critical word underlined for the transparency ratings (see further). Participants were asked to rate both their familiarity with and the transparency of each expression before turning to the next expression.

For the familiarity ratings, participants answered three multiple choice questions by circling the answer that applied to them: (1) "How often do you come across this expression?" (often/sometimes/never), (2) "Do you know its meaning?" (yes/approximately/no), and (3) "Do you use it yourself?" (often/sometimes/never). In the analysis, answers would be coded as 0 (never/no), 1 (sometimes/approximately), or 2 (often/yes), and added up for each idiom for each participant separately. This yielded "idiom familiarity values" ranging from 0 (unfamiliar) to 6 (highly familiar).

For the transparency ratings, participants were asked to rate each expression's transparency by judging "to what extent the underlined word has something to do with the figurative meaning of the expression" on a 7-point scale (1 = not transparent at all, 7 = very transparent). 20 students (mean age 21, range 18-25, 14 women and 6 men) volunteered to do the familiarity and transparency test and were paid for participation. Testing took approximately one hour.

2.2.1.1 Familiarity

For all 151 items that we had selected as being opaque, familiarity values were calculated per item, averaging over participants. The average familiarity value for these items was 3.8 (SD 0.9, range 0.9-5.6). The criterion for including an idiom in the EEG experiment was that at least 90% of the participants had a familiarity value of 2 or higher for that particular idiom, which led to the removal of 35 items from the set. The average familiarity value of the 90 items used in the EEG experiment (i.e., after removal of 61 items based on all pretests including this one and those discussed below) was 4.2 (SD 0.6, range 2.8-5.6).

2.2.1.2 Transparency

Transparency ratings from participants who did not know an idiom (familiarity value below 2) were discarded before computing the average transparency per item, averaging over participants. Over all of the 302 items used in the rating test, the idioms that we had selected as being transparent received an average transparency rating of 4.9 on the 7-point scale (SD 1.1, range 2.4-6.8) compared to 2.0 (SD 0.7, range 1.0-5.7) for opaque idioms. This difference was significant, [$t(150) = 27.858$, $p < .001$], indicating that at least at a general level the participants agreed with our sense of transparency. To make sure that only opaque idioms would be used in the EEG experiment, idioms with an average transparency rating above 3.5 (i.e., idioms close to or on the transparent side of the scale) were excluded from the set. Besides the 35 idioms that had already been excluded due to low familiarity, 4 additional idioms were discarded based on a too high level of transparency. The final set of 90 items used in the EEG experiment, with transparency ratings averaged over participants for each item, had a transparency rating of 2.0 on average (SD 0.5, range 1.1-3.5).

2.2.2 Cloze probability

In previous research, idioms have been used as a way to boost the predictability of words in a sentence context (Moreno, et al., 2002). For the purpose of the present study we wanted to vary the context categorically (literal vs. idiomatic). Keeping the cloze probability constant across contexts was important given that, as mentioned in the introduction, the ERP response to unexpected words that are related to an expected word has been shown to differ depending on contextual constraint: the N400 to unexpected words is smaller in sentences with a high cloze probability compared to sentences with a lower cloze probability for the correct (expected) word (Federmeier & Kutas, 1999). For these reasons, we constructed the literal sentences such that they would be equally constraining as the idiomatic ones. In order to verify the degree of constraint, we performed a paper-and-pencil cloze probability test.

All 302 sentence contexts up to the critical word were included (this was at a stage before removal of items based on familiarity and transparency) and divided into two randomized lists. In doing so, we made sure that idiomatic and literal contexts that were predictive of the same word did not appear on the same list. Of these two lists, two additional versions were created by reversing the order of items of each list. Participants were instructed to complete each sentence fragment with the first word or words that came to mind, keeping it short but grammatical without trying to be original. 30 students participated (mean age 21, range 18-30, 20 women and 10 men; one additional participant

was excluded from analysis for the reason of having grown up outside the Netherlands in a different Dutch-speaking country). 15 participants were randomly assigned to each list (pooling over original and reversed versions). A subset of 8 literal items was rewritten and clozed separately by 15 other students (mean age 22, range 19-24, 8 women and 7 men). Testing took approximately half an hour.

The cloze probability of a word in a sentence context was calculated as the proportion of participants that chose to complete the sentence fragment with that particular word. For the 112 items that had met the familiarity and transparency criteria, the average cloze probability for the Correct words was 0.85 (SD 0.19) in Idiomatic contexts and 0.78 (SD 0.23) in Literal contexts. To decrease this difference, the difference between the cloze probability for the Idiomatic and Literal context was calculated for each item, and the 16 item pairs with the largest difference in favour of the Idiomatic context were discarded, leaving 96 items in the set. For the 90 items used in the EEG experiment, both literal and idiomatic contexts were highly constraining (mean cloze probability: 0.84, SD 0.20). Critical words in literal sentences had a mean cloze probability of 0.82 (SD 0.20) and critical words in idiomatic sentences had a mean cloze probability of 0.85 (SD 0.20), a difference that was not significant, [t (89) = 1.262, p = 0.210]. Cloze probability for the two types of violations was always zero.

2.2.3 Plausibility ratings

The fact that participants never chose to complete a sentence with one of the violations in the cloze probability test shows that the violations were not considered the best ending for the sentence contexts. However, it is possible that one of the two types of violation, most likely the Sem.Rel. condition, was an unlikely but plausible ending and the word could therefore be integrated into its sentence context. To test for this, participants were asked to rate the plausibility of each sentence on a scale from 1 to 7 (1 = highly implausible, 7 = highly plausible). They were told beforehand that the set would contain very normal sentences as well as complete nonsense sentences. Since we were interested in the plausibility at the point of the critical words, sentence fragments after the critical words were deleted as much as possible to avoid contamination of the ratings. Deleting these fragments was not always possible because they were sometimes obligatory constituents in Dutch grammar. All of the 6 conditions were included in the plausibility rating task. These 666 sentences (111 sets of 6 sentences each, including the 96 sets of sentences that had met the familiarity, transparency, and cloze probability criteria and some additional items that had not yet been deleted) were divided across three lists using a Latin square design so that no critical word or sentence context would be repeated within a list. One additional version of each list was created by reversing the order of items. 30 students participated (mean age 22, range 18-32, 20 women and 10 men); each of the three lists (pooling over original and reversed versions) was completed by 10 participants. Testing took approximately one hour.

Mean plausibility ratings and standard errors for the different conditions in the final 90 sets of six items that were used in the EEG experiment are shown in Figure 1.

Plausibility ratings were averaged within each condition for each participant. The criterion for discarding items that were meant to contain a violation was that they received a mean plausibility rating above 4 (i.e., were on the plausible side of the scale). 6 of the 96 items were too plausible, leaving 90 items in the final item set for the EEG experiment. Plausibility ratings for these items were submitted to a 2 × 3 repeated-measures ANOVA with two within-subject factors: Idiomaticity (Literal, Idiomatic) and Condition (Correct, Sem.Rel., Sem.Unrel.). All p- and Mean Squared Error (MSE)-values are Greenhouse-Geisser corrected where necessary, but the original degrees of freedom are reported.

The ANOVA yielded a main effect of Idiomaticity, [F (1,29) = 20.955, MSE = .106, p < .001], which indicated that the plausibility ratings of Literal items (3.51, standard error (SE) 0.10) were higher compared to those of Idiomatic items (3.29, SE 0.09), and a main effect of Condition, [F (2,58) = 799.20, MSE = .747, p < .001]. The interaction between Idiomaticity and Condition was also

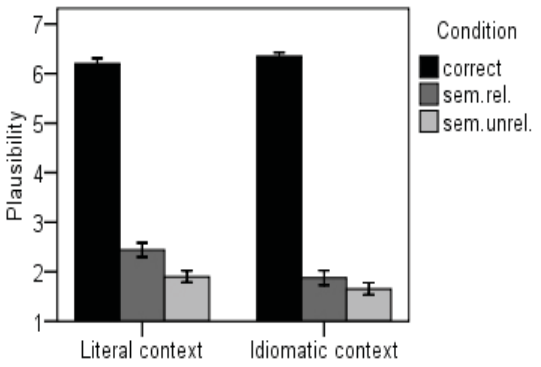

Figure 1. Plausibility ratings (n = 30) on a 7-point scale (1 = highly implausible, 7 = highly plausible) for each type of critical word in each type of context. Error bars denote standard error of the mean.

significant, [F (2,58) = 30.12, MSE = .067, p < .001]. This interaction was further clarified using contrasts, which revealed that all conditions differed from one another in both contexts. In Literal contexts, participants rated both the Sem.Rel. condition (2.44, SD .79) and the Sem.Unrel. condition (1.90, SD .66) as being more implausible compared to Correct words (6.20, SD .60), [F (1,29) = 681.925, MSE = .622, p < .001] and [F (1,29) = 830.741, MSE = .668, p < .001], respectively. The Sem.Unrel. condition was significantly more implausible compared to the Sem. Rel. condition, [F (1,29) = 39.982, MSE = .219, p < .001]. Idiomatic contexts showed the same pattern: both the Sem.Rel. condition (1.87, SD .81) and the Sem.Unrel. condition (1.65, SD .68) were judged to be implausible compared to the Correct condition (6.35, SD .43), [F (1,29) = 68.832, MSE = .872, p < .001] and [F (1,29) = 949.758, MSE = .696, p < .001], respectively. Again, the Sem.Unrel. condition was judged to be more implausible compared to the Sem.Rel. condition, [F (1,29) = 13.815, MSE = .106, p = .001]. The effect of Idiomaticity was also evaluated at each level of Condition using simple effects tests. There was a trend towards Correct words being more plausible in Idiomatic contexts as compared to Literal contexts, [F (1,29) = 3.999, MSE = .162, p = .055], whereas both the Sem.Rel. and the Sem.Unrel. condition were significantly more implausible in Idiomatic contexts compared to Literal contexts, [F (1,29) = 47.980, MSE = .200, p < .001] and [F (1,29) = 17.689, MSE = .103, p < .001], respectively.

2.3 EEG experiment

2.3.1 Participants

Twenty-four student volunteers from the University of Nijmegen and the HAN University of Applied Sciences (mean age 22, range 18-30, 21 women and 3 men) gave informed consent and were paid for their participation in the EEG experiment. All were right-handed, native speakers of Dutch with normal or corrected-to-normal vision and no history of neurological disorders or language disorders. None of them took part in any of the pretests. Data from two additional participants were discarded due to excessive blinking or high amplitude alpha activity and tiredness.

2.3.2 Procedure

Participants were tested individually in a single session in a soundproof, electrically shielded room. They were seated in a comfortable chair at a distance of approximately 60 cm from a computer screen and instructed to relax and read the sentences for comprehension while avoiding blinks and movements. The instructions were given in written form and then repeated orally. The session began with a short practice block consisting of 10 sentences to allow participants to familiarize themselves with the task and the way the sentences were presented. When the instructions were clear, the experiment started. Each trial began with a fixation cross (+) that remained on the screen for a duration of 1000 ms to orient the participant toward the center of the screen. A sentence was then presented one word at a time in the center of the screen, in black letters of the font Tahoma, size 30, on a white background. Each word was presented for 300 ms, with a 300 ms blank screen following each word. After every sentence, three asterisks (* * *) appeared for a duration of 3000 ms. During this period participants were free to blink. The experiment was divided into twelve short blocks of 20 sentences each (each block lasting approximately 4 minutes). After each block, participants were allowed to take a break for as long as they wanted. The session included half an hour of electrode application and instruction and approximately one hour of reading sentences.

2.3.3 EEG recording

EEG was recorded from 61 active Ag/AgCl electrodes, of which 59 were mounted in a cap (actiCap), referenced to the left mastoid. Electrode sites are shown in figure 2.

Two separate electrodes were placed at the left and right mastoids. Blinks were monitored through an electrode on the infraorbital ridge below the left eye. Horizontal eye movements were monitored through two electrodes in the cap (LEOG and REOG), placed approximately at each outer canthus. The ground electrode was placed on the forehead. Electrode impedance was kept below 10 kΩ. EEG and EOG recordings were amplified through BrainAmp DC amplifiers using a bandpass filter of 0.016 - 100 Hz, digitized on-line with a sampling frequency of 500 Hz, and stored for off-line analysis.

2.3.4 Data analysis

2.3.4.1 Preprocessing

Data was rereferenced off-line to the average of the left and right mastoids. Bipolar vertical EOG was computed as the difference between the

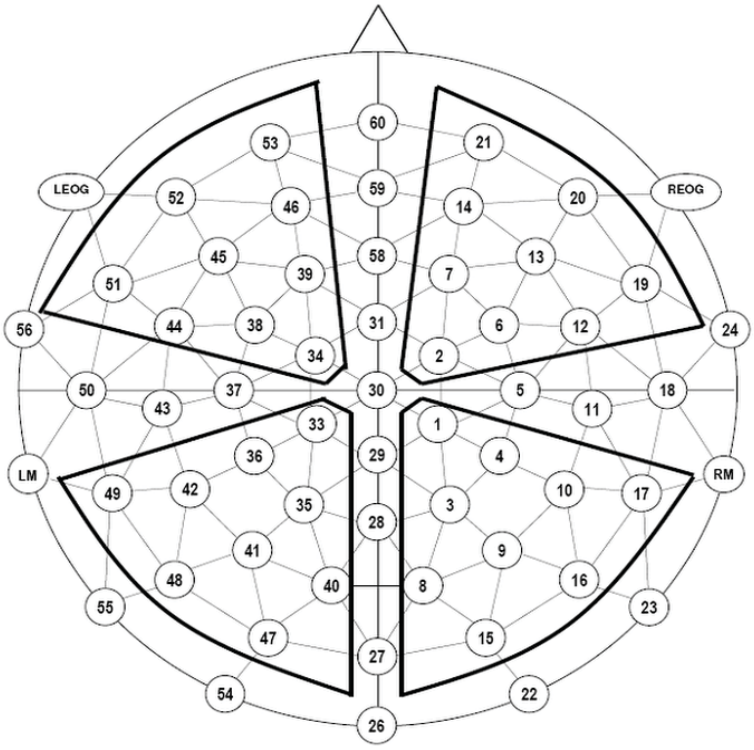

Figure 2. Electrode layout. Thick lines indicate quadrants used for mean amplitude analyses (see Statistical analysis). Left mastoid (LM) and right mastoid (RM) electrodes were placed outside the cap directly onto the mastoids. LEOG = left electrooculogram; REOG = right electrooculogram.

electrode on the infraorbital ridge of the left eye and electrode 53 (see figure 2). Bipolar horizontal EOG was computed as the difference between the LEOG and REOG electrodes. A bandpass filter of 0.1 to 30 Hz was applied. The continuous EEG was then segmented into epochs of 1350 ms, lasting from 150 ms before word onset until 1200 ms after word onset (i.e., including the critical word, a blank screen period, the next word, and another blank screen presentation period). An average baseline of 150 ms before stimulus onset was subtracted. Trials were screened for artifacts semi-automatically, and those contaminated by blinks, eye movements, muscle activity, etc. were removed. Approximately 6% of the trials was lost due to such artifacts. Average ERPs were then computed across trials for each type of critical word (Correct, Sem.Rel., Sem.Unrel.) in each type of context (Idiomatic, Literal).

2.3.4.2 Statistical analyses

To assess the significance of observed N400 effects, mean voltage measures were taken in a time window of 300 to 500 ms. The N400 in the visual modality is known to last from approximately 300 to 500 ms after word presentation, and this time window has been used in many N400 studies. However, due to possible component overlap with a late positivity in our specific data (see Results), the N400 time window was additionally split up into two time windows of 100 ms each: an Early N400 and a Late N400 time window, ranging from 300 to 400 ms and from 400 to 500 ms, respectively. Late positivities were of interest as well. For these, mean voltage measures were examined from 500 to 1200 ms (the end of the segmented epoch). Although this time window was successfully used for late positivities by Hahne (2001) and Hahne and Friederici (2001), upon visual inspection of the data it was decided to split the window up into two smaller time windows – one 500-800 ms time window and one 800-1200 ms time window –, since otherwise a late effect more specifically present from 800-1200 ms would have been overlooked (see Results). For both the N400 and late positivity time windows, mean voltage measures were averaged over quadrants of 9 electrodes each, which divided the data into anterior, posterior, left and right parts of the scalp (see figure 2). The data were then subjected to 2 × 2 × 2 × 3 repeated-measures analyses of variance (ANOVAs) with the factors Hemisphere (Left, Right), Anteriority (Anterior, Posterior), Idiomaticity (Literal, Idiomatic) and Condition (Correct, Sem.Rel., Sem.Unrel.).

3. Results

Grand average ERPs for the three types of critical word (Correct, Sem.Rel., Sem.Unrel.) are shown in Figure 3 for Literal contexts and in Figure 4 for Idiomatic contexts.

Here and in all following analyses, main effects

and interactions are reported only when they involve the factors Idiomaticity and/or Condition. Omnibus ANOVAs are reported in tables and the results of follow-up analyses are referred to in the text. Non-significant effects are reported only in the tables with results from omnibus ANOVAs, and for follow-up analyses only when the lack of significance is relevant for the interpretation. All p- and Mean Squared Error (MSE)-values are Greenhouse-Geisser corrected where necessary, but the original degrees of freedom are reported.

3.1 N400 time windows

As can be seen from Figure 3, critical words of the Sem.Rel. and the Sem.Unrel. condition in Literal contexts elicited negativities relative to words in the Correct condition, lasting from approximately 300 to 500 ms and exhibiting a centroparietal maximum (N400s). In comparison to the data of the Literal contexts, N400s were short-lasting in the Idiomatic contexts (figure 4): the second half of the N400, from 400 to 500 ms, was greatly diminished in amplitude. Although component overlap is difficult to prove, it seems plausible that this N400 reduction was due to component overlap with a late positivity. Looking at the scalp distributions (more specifically the "Sem.Unrel - Correct" and "Sem.Rel. - Correct" scalp topographies in Idiomatic contexts, figure 4), a centroparietal negativity similar to the start of the N400 in Literal contexts can be observed in the 300-400 ms time window, suggesting that regular N400 effects were present in the Idiomatic condition. The voltage maps for the 400-500 ms time window show a rather different pattern: a frontal negativity, and a neutral but somewhat positive-going voltage at central and posterior sites. Given that the late positivity in the 500-800 ms time window also has a central-posterior distribution, it is possible that the late positivity overlapped with the second half of the N400 in Idiomatic contexts.

Given that the N400 was the main test case for our hypotheses, it was important to obtain a decent estimate of its size in the various conditions. Therefore, the N400 time window was split up into a relatively unaffected Early N400 window (300-400 ms), and a Late N400 time window (400-500 ms) in which the N400 in Idiomatic contexts was diminished. These two time windows were analyzed separately. For completeness, results for the standard 300-500 ms time window are reported in short below. Results of the omnibus ANOVA are shown in Table 2.

The average voltage to critical words in Idiomatic contexts (1.30 μV) was more positive compared to that of critical words in Literal contexts (-.85 μV). This difference was larger over the right hemisphere (2.39 μV difference) compared to the left hemisphere (1.90 μV difference). A main effect of Condition indicated that there were differences between the conditions, for which the means were: 1.29 μV for Correct words, .11 μV for the Sem.Rel. condition, and -.73 μV for the Sem.Unrel. condition. The three-way interaction between Anteriority, Idiomaticity,

Table 2. Results of the omnibus ANOVA on the mean amplitude measures in the standard N400 (300-500 ms) time window in the two levels of Idiomaticity (Literal, Idiomatic), three levels of Condition (Correct, Sem.Rel., Sem.Unrel.), two levels of Hemisphere (Left, Right) and two levels of Anteriority (Anterior, Posterior). Mean Squared Error (MSE)- and p-values are Greenhouse-Geisser corrected, but the original degrees of freedom (df) are reported.

Effect	df	F	MSE	p
Idiomaticity	(1,23)	42.336	15.627	< .001 ***
Condition	(2,46)	22.855	9.681	< .001 ***
Hemisphere × Idiomaticity	(1,23)	7.678	1.095	.011 *
Anteriority × Idiomaticity	(1,23)	1.364	2.746	.255
Hemisphere × Anteriority × Idiomaticity	(1,23)	.320	.175	.577
Hemisphere × Condition	(2,46)	.182	1.379	.786
Anteriority × Condition	(2,46)	1.101	3.408	.336
Hemisphere × Anteriority × Condition	(2,46)	.508	.187	.569
Idiomaticity × Condition	(2,46)	3.070	8.448	.058
Hemisphere × Idiomaticity × Condition	(2,46)	.395	.805	.671
Anteriority × Idiomaticity × Condition	(2,46)	3.469	1.375	.043 *
Hemisphere × Anteriority × Idiomaticity × Condition	(2,46)	.767	.151	.460

* $p < .05$
** $p < .01$
*** $p < .001$

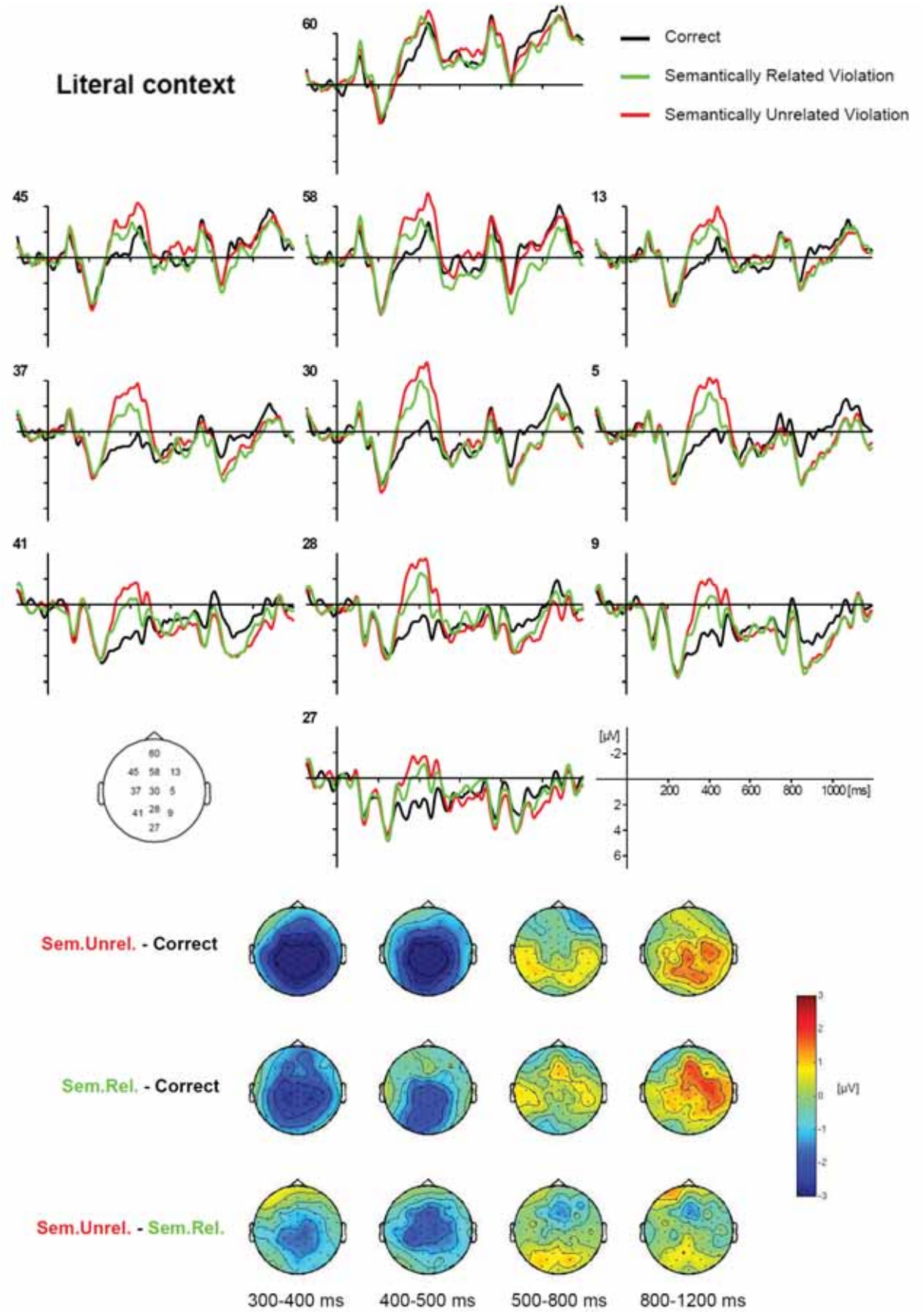

Figure 3. Grand average (n = 24) ERP waveforms and scalp topographies elicited by the three types of critical word in Literal contexts. Each critical word was presented at time = 0 ms. Waveforms are shown (negative voltage plotted up) for 11 representative electrodes, of which the locations are given on a head map (left). Scalp topographies are given for the difference between each of the conditions for the four time intervals used in the statistical analyses. Blue color indicates negative voltage. Sem.Unrel. = Semantically Unrelated Violation; Sem.Rel. = Semantically Related Violation.

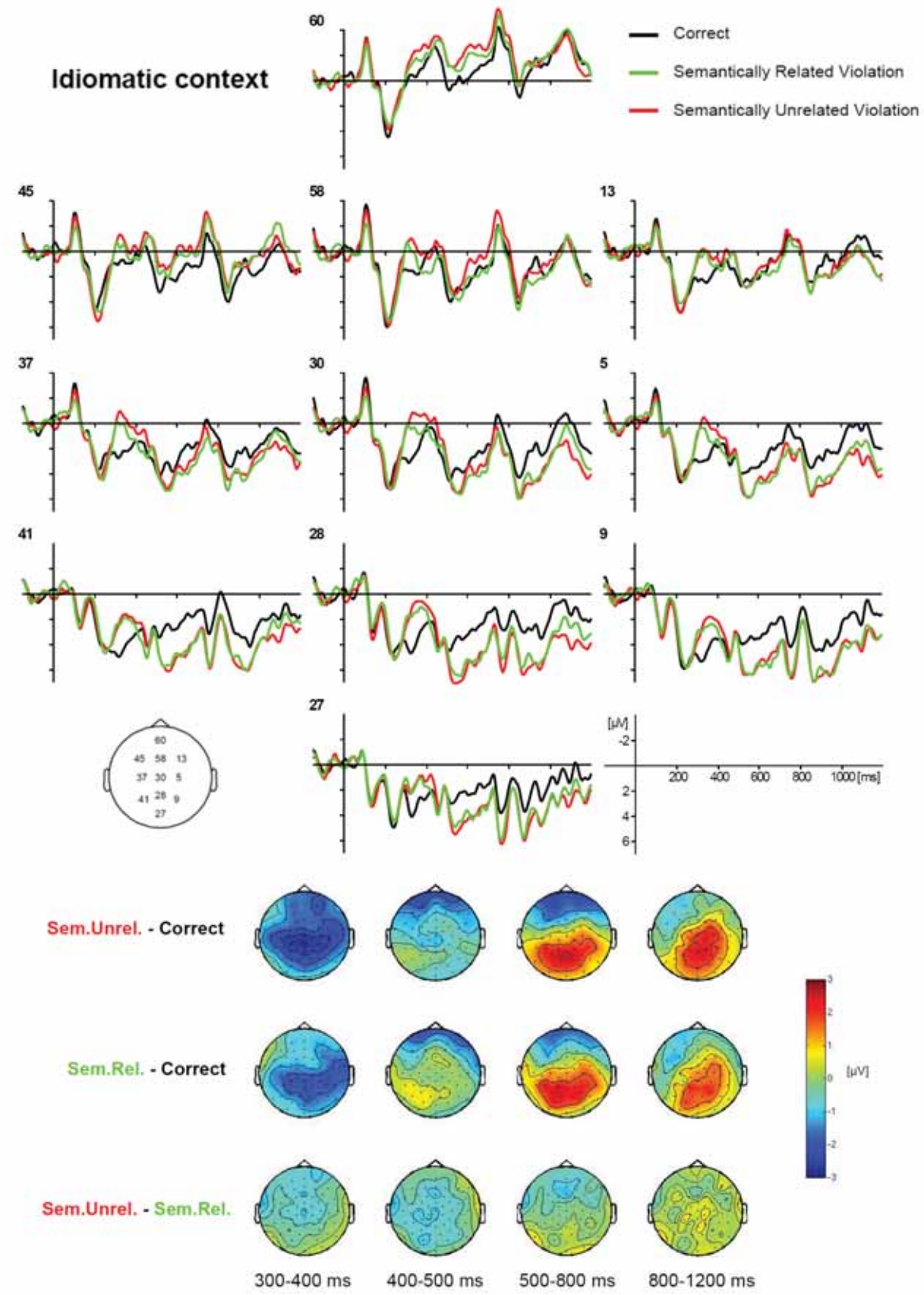

Figure 4. Grand average (n = 24) ERP waveforms and scalp topographies elicited by the three types of critical word in Idiomatic contexts. Each critical word was presented at time = 0 ms. Waveforms are shown (negative voltage plotted up) for 11 representative electrodes, of which the locations are given on a head map (left). Scalp topographies are given for the difference between each of the conditions for the four time intervals used in the statistical analyses. Blue color indicates negative voltage. Sem.Unrel. = Semantically Unrelated Violation; Sem.Rel. = Semantically Related Violation.

and Condition was followed up by evaluating the significance of the interaction between Idiomaticity and Condition at Anterior and Posterior sites with data from left and right quadrants combined. There was a significant interaction between Idiomaticity and Condition at Posterior sites, [F (2,46) = 5.52, MSE = 2.47, p < .01], but not at Anterior sites, [F (2,46) = .87, MSE = 2.48, p = .424]. At posterior sites, contrasts between the different conditions were performed for Literal and Idiomatic contexts separately. These indicated that in Literal contexts, all types of critical word differed significantly from one another. Both the Sem.Unrel. (-1.22 μV) and Sem.Rel. (.07 μV) conditions showed a negativity relative to Correct words (2.08 μV), [F (1,23) = 48.94, MSE = 5.32, p < .001] and [F (1,23) = 24.83, MSE = 3.92, p < .001], respectively. Importantly, the mean voltage of the Sem.Unrel. condition was also significantly more negative compared to the Sem. Rel. condition, [F (1,23) = 8.70, MSE = 4.53, p < .05]. In contrast, in Idiomatic contexts, not every type of critical word differed significantly from the other. The voltage for the Sem.Unrel. condition (2.01 μV) was more negative compared to Correct critical words (3.28 μV), [F (1,23) = 7.00, MSE = 5.53, p < .05]. The difference between the Sem.Rel. condition (2.55 μV) and Correct critical words was marginally significant in this 300-500 ms time window, [F (1,23) = 3.33, MSE = 3.87, p = .081]. Different from Literal contexts, there was no significant difference between the Sem.Unrel. and the Sem.Rel. conditions, [F (1,23) = 1.24, MSE = 5.60, p = .278]. Thus, a "graded N400" was obtained in Literal but not in Idiomatic contexts.

3.1.1 Early N400 (300-400 ms)

Results of the omnibus ANOVA on mean voltage measures in the smaller 300 to 400 ms (Early N400) time window are shown in Table 3.

Critical words in Idiomatic contexts had a more positive voltage (1.10 μV) compared to critical words in Literal contexts (-0.57 μV). This effect was larger over the right hemisphere (1.86 μV difference) compared to the left hemisphere (1.47 μV difference). The response to the different types of critical word also differed, with the Correct condition eliciting the most positive voltage (1.62 μV), the Sem.Unrel. condition eliciting the most negative voltage (-0.77 μV) and the Sem.Rel. condition being intermediate in amplitude (-0.06 μV).

No interactions between Idiomaticity and Condition were found in the Early N400 time window. Nonetheless, to test our specific hypothesis that the Sem.Rel. and the Sem.Unrel. condition differed from one another in the Literal but not in the Idiomatic context, planned comparisons between the conditions in each level of Idiomaticity were carried out. This was done using amplitude averaged over the two posterior quadrants as the dependent variable. In Literal contexts, all conditions differed significantly from one another: the Sem.Unrel. condition (-1.02 μV) was more negative compared to the Correct condition (2.46 μV), [F (1,23) = 56.24,

Table 3. Results of the omnibus ANOVA on the mean amplitude measures in the Early N400 (300-400 ms) time window in the two levels of Idiomaticity (Literal, Idiomatic), three levels of Condition (Correct, Sem.Rel., Sem.Unrel.), two levels of Hemisphere (Left, Right) and two levels of Anteriority (Anterior, Posterior). Mean Squared Error (MSE)- and p-values are Greenhouse-Geisser corrected, but the original degrees of freedom (df) are reported.

Effect	df	F	MSE	p
Idiomaticity	(1,23)	19.942	19.958	< .001 ***
Condition	(2,46)	36.728	9.469	< .001 ***
Hemisphere × Idiomaticity	(1,23)	4.884	1.110	.037 *
Anteriority × Idiomaticity	(1,23)	.009	2.340	.926
Hemisphere × Anteriority × Idiomaticity	(1,23)	.119	.261	.734
Hemisphere × Condition	(2,46)	.377	1.909	.636
Anteriority × Condition	(2,46)	2.24	4.229	.128
Hemisphere × Anteriority × Condition	(2,46)	1.126	.227	.324
Idiomaticity × Condition	(2,46)	1.352	10.247	.268
Hemisphere × Idiomaticity × Condition	(2,46)	.766	.716	.465
Anteriority × Idiomaticity × Condition	(2,46)	1.595	1.678	.216
Hemisphere × Anteriority × Idiomaticity × Condition	(2,46)	.043	.157	.954

* p < .05
** p < .01
*** p < .001

Table 4. Results of the omnibus ANOVA on the mean amplitude measures in the Late N400 (400-500 ms) time window in the two levels of Idiomaticity (Literal, Idiomatic), three levels of Condition (Correct, Sem.Rel., Sem.Unrel.), two levels of Hemisphere (Left, Right) and two levels of Anteriority (Anterior, Posterior). Mean Squared Error (MSE)- and p-values are Greenhouse-Geisser corrected, but the original degrees of freedom (df) are reported.

Effect	df	F	MSE	p
Idiomaticity	(1,23)	69.101	14.354	< .001 ***
Condition	(2,46)	9.502	14.714	< .001 ***
Hemisphere × Idiomaticity	(1,23)	10.073	1.195	.004 **
Anteriority × Idiomaticity	(1,23)	3.664	3.814	.069
Hemisphere × Anteriority × Idiomaticity	(1,23)	.584	.151	.453
Hemisphere × Condition	(2,46)	.057	1.153	.928
Anteriority × Condition	(2,46)	.231	3.333	.784
Hemisphere × Anteriority × Condition	(2,46)	1.020	.215	.358
Idiomaticity × Condition	(2,46)	4.059	10.725	.024 *
Hemisphere × Idiomaticity × Condition	(2,46)	.142	1.129	.868
Anteriority × Idiomaticity × Condition	(2,46)	7.198	1.620	.002 **
Hemisphere × Anteriority × Idiomaticity × Condition	(2,46)	2.255	.201	.121

* p < .05
** p < .01
*** p < .001

MSE = 5.14, p < .001] and the Sem.Rel. condition (0.21 μV) was also more negative compared to the Correct condition, [F (1,23) = 31.97, MSE = 3.78, p < .001]. Importantly, the mean voltage to the Sem. Unrel. condition was also significantly more negative compared to the Sem.Rel. condition in Literal contexts, [F (1,23) = 9.64, MSE = 3.76, p < .01]. In Idiomatic contexts, not all conditions differed significantly from one another: whereas both the Sem.Unrel. condition (1.40 μV) and the Sem.Rel. condition (1.78 μV) elicited a significant negativity relative to Correct critical words (3.50 μV), [F (1,23) = 14.54, MSE = 7.26, p < .01] and [F (1,23) = 17.20, MSE = 4.15, p < .001] respectively, the Sem.Rel. and Sem.Unrel. conditions did not differ significantly from each other, [F (1,23) = .78, MSE = 4.28, p = .387]. [2]

3.1.2 Late N400 (400-500 ms)

Results of the omnibus ANOVA on mean voltage measures in the 400 to 500 ms (Late N400) time window are shown in Table 4.

The mean voltage to critical words in Idiomatic contexts (1.49 μV) was more positive compared to that of critical words in Literal contexts (-1.13 μV). This effect was larger over the right Hemisphere (2.91 μV difference) compared to the left Hemisphere (2.34 μV difference). There were differences between the three conditions, which had the following mean amplitudes: .96 μV for the Correct condition, .27 μV for the Sem.Rel. condition, and -.69 μV for the Sem. Unrel. condition.

The three-way interaction between Anteriority, Idiomaticity and Condition was further clarified with data averaged over left and right quadrants as the dependent variables representing Anterior and Posterior sites. This analysis indicated that the interaction between Idiomaticity and Condition was not significant at Anterior sites, [F (2,46) = 1.10, MSE = 3.37, p = .342], whereas it was significant at Posterior sites, [F (2,46) = 8.39, MSE = 2.82, p < .01]. For these Posterior sites, follow-up analyses for Literal and Idiomatic contexts indicated a significant effect of Condition in Literal contexts, [F (2,46) = 17.58, MSE = 3.37, p < .001], but not in Idiomatic contexts, [F (2,46) = .89, MSE = 3.60, p = .414], unlike in the Early N400 time window. Contrasts between the three conditions in Literal contexts showed, comparable to the Early N400 time window, that all three conditions differed from one another. ERPs to the Sem.Unrel. condition (-1.42 μV) were more negative-going compared to Correct words (1.70 μV), [F (1,23) = 32.02, MSE = 7.27, p < .001], and so were ERPs to the Sem.Rel. condition (-.08 μV), [F (1,23) = 12.56, MSE = 6.07,

[2] When a more liberal analysis was performed, using only the data from the central electrode with the maximum raw effect (electrode 30; 1.01 μV difference) averaged over the 300-400 ms time window in which the effect occurred, a planned comparison again did not indicate a significant difference between the Sem.Rel. and the Sem.Unrel. conditions in Idiomatic contexts, [F (1,23) = 2.04, MSE = 12.15, p = .167], thus confirming the quadrant analysis.

$p < .01$]. ERPs to the Sem.Unrel. condition in this time window were also significantly more negative-going compared to the Sem.Rel. condition, [$F(1,23) = 6.39$, $MSE = 6.67$, $p < .05$]. In sum, whereas for Literal contexts the posterior graded N400 effect from the Early N400 time window continued into the Late N400 time window, ERPs in Idiomatic contexts revealed no effects of condition in the Late N400 time window.

3.2 Late positivities

Mean amplitude measures were taken in two later time windows (500-800 ms and 800-1200 ms) in order to test for late positive effects. The choice of these time windows was based on visual inspection, as data averaged over a somewhat standard 500-1200 ms time window would not be able to distinguish between late and still later effects that were present in the data.

3.2.1 500-800 ms time window

Results of the omnibus ANOVA with mean amplitude in the 500-800 ms time window as the dependent variable are shown in Table 5.

The voltage to critical words in Idiomatic contexts (2.14 μV) was more positive compared to that of critical words in Literal contexts (.56 μV). The difference was larger at Posterior sites (2.18 μV difference) compared to Anterior sites (.98 μV difference). There was also a trend towards an interaction between Hemisphere and Idiomaticity, with mean amplitudes suggesting that the difference in Idiomaticity was larger over the right hemisphere (1.74 μV difference) compared to the left hemisphere (1.41 μV difference).

The four-way interaction between Hemisphere, Anteriority, Idiomaticity and Condition was further clarified by testing for the effects of Hemisphere, Idiomaticity and Condition at the two levels of Anteriority. The analysis at Anterior sites yielded a main effect of Idiomaticity, [$F(1,23) = 7.495$, $MSE = 9.168$, $p < .05$], which arose from critical words in Idioms eliciting a more positive average voltage (.61 μV) compared to critical words in Literal contexts (-.37 μV). No further main effects or interactions were found (all p's > .1). At Posterior sites, there was a main effect of Idiomaticity, [$F(1,23) = 32.969$, $MSE = 10.389$, $p < .001$] reflecting that the average voltage to critical words in Idiomatic contexts (3.67 μV) was more positive compared to Literal contexts (1.49 μV). A strong trend towards an interaction between Idiomaticity and Hemisphere, [$F(1,23) = 4.249$, $MSE = .527$, $p = .051$], arose from the fact that the effect of idiomaticity was larger over the right hemisphere (2.36 μV difference) compared to the left hemisphere (2.00 μV difference). Differences between the conditions led to a main effect of Condition, [$F(2,46) = 6.391$, $MSE = 6.468$, $p < .01$], to which the following means apply: 1.85 μV for the Correct condition, 2.88 μV for the Sem.Rel. condition, and 3.02 μV for the Sem.Unrel. condition. However, these differences depended on the context

Table 5. Results of the omnibus ANOVA on the mean amplitude measures in the P600 (500-800 ms) time window in the two levels of Idiomaticity (Literal, Idiomatic), three levels of Condition (Correct, Sem.Rel., Sem.Unrel.), two levels of Hemisphere (Left, Right) and two levels of Anteriority (Anterior, Posterior). Mean Squared Error (MSE)- and p-values are Greenhouse-Geisser corrected, but the original degrees of freedom (df) are reported.

Effect	df	F	MSE	p
Idiomaticity	(1,23)	20.671	17.369	< .001 ***
Condition	(2,46)	1.149	12.021	.326
Hemisphere × Idiomaticity	(1,23)	3.497	1.134	.074
Anteriority × Idiomaticity	(1,23)	23.851	2.188	< .001 ***
Hemisphere × Anteriority × Idiomaticity	(1,23)	.137	.115	.715
Hemisphere × Condition	(2,46)	.556	1.111	.552
Anteriority × Condition	(2,46)	12.491	2.796	< .001 ***
Hemisphere × Anteriority × Condition	(2,46)	3.147	.294	.069
Idiomaticity × Condition	(2,46)	.704	8.777	.499
Hemisphere × Idiomaticity × Condition	(2,46)	.549	.784	.572
Anteriority × Idiomaticity × Condition	(2,46)	9.222	1.686	.001 **
Hemisphere × Anteriority × Idiomaticity × Condition	(2,46)	3.541	.194	.042 *

* $p < .05$
** $p < .01$
*** $p < .001$

in which the words representing the conditions appeared, as evident from a significant interaction between Idiomaticity and Condition, [F (2,46) = 3.900, MSE = 5.234, p < .05]. This interaction was clarified by testing for the simple effect of Condition at the two levels of Idiomaticity separately. An effect of Condition was not obtained for Literal contexts, [F (2,46) = .559, MSE = 2.235, p = .575], but was present in Idiomatic contexts, [F (2,46) = 8.320, MSE = 3.608, p < .01]. Posterior contrasts between the conditions in Idiomatic contexts indicated that, relative to the Correct condition (2.42 μV), both the Sem.Rel. condition (4.30 μV) and the Sem.Unrel. condition (4.30 μV) had a significantly more positive average voltage, [F (1,23) = 12.649, MSE = 6.691, p < .01] and [F (1,23) = 6.54, MSE = 8.63, p < .05], respectively. The Sem.Unrel. and Sem.Rel. conditions did not differ significantly from each other, [F (1,23) < .001, MSE = 6.691, p = .996]. In sum, there was a significant posterior positivity for violations in idioms, regardless of semantic relatedness.

3.2.2 800-1200 ms time window

Results of the omnibus ANOVA on mean amplitude measures in the 800-1200 ms time window are shown in Table 6.

Critical words in Idiomatic contexts (1.89 μV) elicited a more positive voltage compared to Literal contexts (.14 μV). The three-way interaction between Hemisphere, Anteriority and Condition was followed up by testing for the effects of Hemisphere and Condition at the two levels of Anteriority (Anterior, Posterior). Given the absence of any interactions with Idiomaticity, data from Idiomatic and Literal contexts were combined.

The analysis on Anterior electrode sites yielded an interaction between Hemisphere and Condition, [F (2,46) = 8.743, MSE = .383, p < .01]. The simple effect of Condition was evaluated at both levels of Hemisphere (Left, Right). The effect of Condition was not significant at left anterior electrode sites, [F (2,46) = .008, MSE = 2.517, p = .990], but a trend was observed at right anterior electrode sites, [F (2,46) = 2.750, MSE = 2.529, p = .078], to which the following means apply: -.76 μV for the Correct condition, .24 μV for the Sem.Rel. condition, and .02 μV for the Sem.Unrel. condition. The analysis on Posterior electrode sites yielded a main effect of Condition, [F (2,46) = 6.663, MSE = 4.391, p < .01]. The interaction between Hemisphere and Condition showed a small trend, [F (2,46) = 2.591, MSE = .246, p = .092], which seemed to reflect that the difference between the two types of violation and the Correct condition was somewhat larger over the right hemisphere. Data from both levels of Hemisphere were combined to test for the effect of Condition at Posterior electrode sites. The effect of Condition was significant, [F (2,46) = 6.663, MSE = 2.195, p < .01]. Contrasts indicated that both the Sem.Rel. condition (2.47 μV) and the Sem.Unrel. condition (2.71 μV) had a significantly more positive average voltage compared to the Correct condition (1.38 μV), [F (1,23) = 5.638, MSE = 5.106, p < .05] and [F (1,23) = 18.898, MSE = 2.268, p < .001], respectively. The Sem.Rel. and Sem.Unrel. condition

Table 6. Results of the omnibus ANOVA on the mean amplitude measures in the 800-1200 ms time window in the two levels of Idiomaticity (Literal, Idiomatic), three levels of Condition (Correct, Sem.Rel., Sem.Unrel.), two levels of Hemisphere (Left, Right) and two levels of Anteriority (Anterior, Posterior). Mean Squared Error (MSE)- and p-values are Greenhouse-Geisser corrected, but the original degrees of freedom (df) are reported.

Effect	df	F	MSE	p
Idiomaticity	(1,23)	21.284	20.693	< .001 ***
Condition	(2,46)	3.125	16.083	.060
Hemisphere × Idiomaticity	(1,23)	.365	1.338	.552
Anteriority × Idiomaticity	(1,23)	.078	2.594	.782
Hemisphere × Anteriority × Idiomaticity	(1,23)	1.019	.222	.323
Hemisphere × Condition	(2,46)	6.426	1.058	.004 **
Anteriority × Condition	(2,46)	5.702	1.962	.007 **
Hemisphere × Anteriority × Condition	(2,46)	6.723	.176	.003 **
Idiomaticity × Condition	(2,46)	.093	11.072	.900
Hemisphere × Idiomaticity × Condition	(2,46)	1.200	.650	.309
Anteriority × Idiomaticity × Condition	(2,46)	2.291	1.696	.120
Hemisphere × Anteriority × Idiomaticity × Condition	(2,46)	1.234	.269	.299

* p < .05
** p < .01
*** p < .001

did not differ significantly from each other, [F (1,23) = .389, MSE = 3.590, p = .539]. In sum, a posterior positivity was found for both types of violation relative to the Correct condition, regardless of (Literal, Idiomatic) context.

4. Discussion

In the present study, we investigated whether the expectation for upcoming words' semantics, as it is known to occur in literal contexts in which word meanings are relevant to the overall interpretation of the sentence, extends to idiomatic contexts, in which literal word meanings are unrelated to the figurative and ultimately relevant overall meaning. To this end, we examined the ERP response to visually presented words that were expected on the basis of prior sentence context (Correct condition) and to contextually anomalous words that were either related (Sem.Rel. condition) or unrelated (Sem. Unrel. condition) to the expected word. The context in which these critical words occurred was varied categorically by employing literal and idiomatic contexts, in which the same critical words were predictable on the basis of general world knowledge in the case of literal contexts, or knowledge of an opaque idiom in the case of idiomatic contexts.

These two types of predictability led to distinct ERPs for the two types of context. ERPs to critical words in literal contexts showed a "graded" N400 pattern lasting from approximately 300 to 500 ms, being largest for the semantically unrelated words, intermediate for semantically related words, and smallest for correct words. In idiomatic contexts, the pattern was not graded: both the Sem.Rel. and the Sem.Unrel. condition elicited short-lived N400 effects (300-400 ms approximately) relative to the Correct condition, but their amplitudes were statistically indistinguishable. In addition, a centroparietal late positivity (500-800 ms) was elicited by violations in Idiomatic contexts, regardless of semantic relatedness. A similar positivity was found in the 800-1200 ms time window, in which it occurred for the Sem.Rel. and Sem.Unrel. conditions in both literal and idiomatic contexts.

4.1 Specific semantic expectancy does not extend to idiomatic contexts

Given that word meanings are considered a basic building block in sentence comprehension (e.g., Hagoort, 2005, 2007) and given that in some models they are thought to become activated not only in literal language but also in idioms (e.g., Cutting & Bock, 1997; Sprenger, et al., 2006; Swinney & Cutler, 1979) it is only a small step to assume that when idioms are highly predictable, the semantics of upcoming words are somehow anticipated in the same way they are in literal sentences. The present data however indicate otherwise. Whereas a clear difference between the processing of words that were semantically related to contextually expected words and words that were semantically unrelated to expected words was observed in ERPs for literal contexts, replicating Federmeier and Kutas' (1999) results, no such semantic effect was reliably observed in idiomatic contexts. We take the N400 results to suggest that, although idioms can be very predictable, the semantics of upcoming words are not part of readers' expectations during the comprehension of idioms. The finding is all the more convincing given that both types of context exhibited practically identical degrees of constraint (no significant difference in average cloze probability) and that the exact same critical words (across lists) were used in both contexts, ensuring that the degree of semantic relatedness between the expected word and the word that was actually presented was exactly matched across contexts. Before discussing further implications however, let us first consider alternative interpretations of the data.

One possibility is to relate the ERP findings to the plausibility ratings that were part of the series of pretests conducted prior to the EEG experiment. Indeed, these showed a pattern remarkably similar to that of the ERP data, at least for literal contexts: correct words elicited the smallest N400 and received the highest plausibility ratings, semantically unrelated words elicited the largest N400 and received the lowest plausibility ratings, and semantically related words had intermediate N400s and plausibility ratings. One might want to take this monotonic (inverse) relationship between plausibility and N400 amplitude to suggest that ease of integration rather than semantic expectancy caused the difference between the semantically related and unrelated words in literal contexts. However, when taking data from the idiomatic contexts into account, at least two observations point to the fact that plausibility alone fails to explain the ERP data pattern.

First, whereas the Sem.Rel. and Sem.Unrel. conditions in idioms were significantly different in the plausibility ratings, this difference was not mirrored in N400 amplitudes. Admittedly, the difference in plausibility was smaller in idioms compared to literal contexts, leaving open the possibility that it was too small to modulate the N400. However, plausibility

ratings are an offline task in which participants can take as long as they want to make their judgement, whereas the N400 reflects direct online processing. This means that the discrepancy between the measures may have arisen during offline processes which contributed only to the plausibility ratings.

The second relevant observation is that there is also a discrepancy when comparing the difference between correct words and violations across contexts. In the plausibility ratings, the difference between correct words and violations was larger in idioms compared to literal contexts (Correct - Sem.Rel. condition: 4.48 in idiomatic contexts, 3.76 in literal contexts; Correct - Sem.Unrel. condition: 4.70 in idiomatic contexts, 4.30 in literal contexts). In other words, when a violation occurred in an idiom, this made the item very implausible. Reasoning from an inverse relationship between plausibility and N400 amplitude, it would be predicted that the largest N400 effects would be elicited in idioms. Our ERP data showed the opposite, namely that the violations yielded smaller N400 effects in idiomatic contexts compared to literal contexts (Sem.Rel. - Correct condition: 1.72 μV difference in idiomatic contexts, 2.75 μV difference in literal contexts; Sem.Unrel. - Correct condition: 2.10 μV difference in idiomatic contexts, 3.48 μV difference in literal contexts). Thus, there are discrepancies between the plausibility ratings and N400 amplitudes both in the absence and presence of differences between conditions and in the relative magnitude of differences between conditions compared across contexts. We conclude that, although it cannot be entirely ruled out that plausibility played some role in our data, it is an unlikely candidate for explaining the crucial N400 effects.

A different concern one might want to bring up is the presence of lexical associations between words in the experimental sentences, especially in literal contexts. For instance, in the literal example used throughout this paper, After lunch the electrician put a new light bulb into the lamp yesterday, lexical associations exist between electrician and lamp, and between light bulb and lamp. Indeed, it may well be the case that over the entire set of items lexical associates were more frequently present in literal compared to idiomatic contexts in our materials. Given that the N400 reflects semantic processes which may be facilitated in the presence of lexical associates, it would then be predicted that the N400 to the Sem.Rel. condition would be selectively diminished in literal contexts because of priming by previously encountered words in those contexts. Because it is likely that the lexical associates were not associated with words from the Sem.Unrel. condition, they would leave the N400 to this condition intact, thus explaining the difference between the Sem.Rel. and Sem.Unrel. conditions. A first point to be made against such a position is that effects of lexical associates have been shown to decay very quickly, often vanishing within one intervening word (e.g., Ratcliff & McKoon, 1988). Let us consider, nevertheless, an additional prediction that follows from the lexical association claim: the N400 to words from the semantically related condition should be smaller in literal contexts, being reduced by the presence of lexical or semantic associates, compared to idiomatic contexts, where no or far fewer lexical associates were present. The ERP data show the opposite: the N400 to semantically related words seems generally of lower amplitude in idiomatic compared to literal contexts, and the difference between correct words and semantically related critical words is also smaller in idiomatic contexts compared to literal contexts (see Figure 4). For these reasons we take semantic associations between words to fail as an explanation for the ERP effects.

Another issue is related to component overlap within the dataset. N400 responses to words in idioms were short-lived (300-400 ms), and a late positivity that immediately followed the N400 was observed only in idioms. The notion of component overlap helps to explain this pattern by assuming that from 400-500 ms a positivity overlapped with the N400, leading to a reduction in the N400 amplitude. Although this explanation of the data is tentative, it led us to analyze the relatively unaffected early part (300-400 ms) of the N400 separately, presumably keeping the measurement safe from interference with the late positivity. Still, one might want to explore the possibility that the positivity had an onset even earlier than at around 400 ms. If correct, this might have limited the access to the N400 as the measure of interest for the main hypotheses. However, an evaluation of the predictions of this hypothesis again indicates limited effects at best.

One possibility is that the late positivity simply diminished all effects in the N400 time window. The data readily speak against this, since there were N400 effects in idioms in the early 300-400 ms time window, and the scalp distributions of these effects look typical of an N400.

A more challenging issue is whether the late positivity might have diminished some conditions selectively, essentially causing what we have interpreted as N400 effects. Hypothetically, in a worst case scenario a graded N400 pattern was actually present

in idiomatic contexts just like in literal contexts, but it was washed away by a positivity that selectively decreased the measured N400 amplitude for the Sem.Rel. condition, leaving the N400 in response to the Sem.Unrel. condition intact. However, such a scenario remains unsupported, given that the late positivity was equally large for both types of violation in the late time window (500-800 ms) where we have the best view on it (it does not suffer from N400 interference). In our view this makes it highly unlikely that positivity could have selectively affected the Sem.Unrel. condition in idioms.

Given the weaknesses in the alternative explanations discussed above, we conclude that the lack of a graded N400 effect in idioms is best explained as a lack of semantic expectancy when readers process predictable opaque idioms. Besides revealing a property of idioms, this result also informs us about the nature of semantic expectancy: apparently, this process is not triggered by just any kind of constraining context. The data on idioms show that there are contexts in which, even though they are highly constraining and participants can easily come up with the correct completion in a cloze task, we do not anticipate semantic features of upcoming words. Our findings thus support the idea that expectancy is different in idioms compared to literal language.

This conclusion is very much in line with recent data from Vespignani et al. (in press). At a point in the sentence before the idioms became predictable (i.e., in Cacciari & Tabossi, 1988's terms before and after the key) violations led to an N400 effect and longer self-paced reading times also on following words (a so-called spillover effect), typical of literal language, whereas after the key violations led to N400 effects and longer self-paced reading times without a spillover effect. Strikingly, predictable words in these idioms seemed to elicit a P300, which is not typically observed in literal language. In their explanation of these effects, Vespignani et al. (in press) also assumed different types of predictability in idioms compared to literal language. What the present study adds to the literature regarding this matter is that this difference can be seen specifically at the semantic level, as evidenced by the N400 which remained unaffected by semantic relatedness.

4.2 How do the results relate to the activation of literal word meanings?

Now that implications for the general process of semantic expectancy have been discussed, we can also look at potential consequences for models of idiom comprehension. These models do not make specific predictions about whether expectancies during idiom comprehension are semantically specified or not. However, as also briefly touched upon in the Introduction, there may be quite a direct link between semantic expectancy and the activation of literal word meanings.

A plausible idea to start from is that context can lead to specific expectations. These expectations can, in an active view of language comprehension, lead to on-line predictions (Federmeier, 2007; Pickering & Garrod, 2007; van Berkum, et al., 2005). In our view, there is really only one way in which prediction can work: as a mechanism that preactivates certain information, bringing the activation closer to thresholds or at least making the information more easily accessible. Preactivation is only separated from the notion of activation by time, in the sense that preactivation happens at a point in time before one would expect 'regular' activation to take place. The preactivation of literal word meanings makes sense in the case of literal sentences, since the meanings that are preactivated are necessary for understanding the overall meaning of the sentence. Preactivation makes this relevant semantic information easier to access, which in turn makes it easier to construct meaning at the sentence level. However, preactivating literal word meanings in the case of idioms makes sense only if these literal word meanings are subsequently necessary for the overall interpretation, in other words if literal word meanings need to be activated in order to understand idioms. Given this reasoning, we feel that even though the present experiment may not address the activation of literal word meanings directly, as is done in priming research for instance, we are entitled to evaluate our data in the light of claims about literal word meaning activation advocated by models of idiom comprehension.

For models of idiom comprehension in which literal word meanings become active (e.g., Cacciari & Tabossi, 1988; Cutting & Bock, 1997; Sprenger, et al., 2006; Swinney & Cutler, 1979), just like in literal language, there is no obvious reason to assume that expectations for upcoming words would not be present, allowing the same facilitatory effect as in literal language. However, the results of the present study do not support this; rather, expectations seem to be very context-dependent. When we read idioms, for which the figurative meaning is the relevant meaning, we do not continue to expect and preactivate literal word meanings.

Although this result converges with Peterson et al. (2001) who suggested that literal word meanings

are not processed in the case of predictable idioms, several studies have indicated that words in idioms do prime literally related words (e.g., Cacciari & Tabossi, 1988; Colombo, 1993; Hillert & Swinney, 2000; Sprenger, et al., 2006; Swinney, 1981), although limits to this have been shown in the sense that anaphora in idioms do not activate their referents (Needham, 1992). Indeed, we certainly do not want to claim that literal word meanings are never activated during idiom comprehension. An important difference, however, is that in the priming studies the individual words were actually presented to the participants, whereas in the present study (and in Peterson et al.'s) they were only expected. The results can be reconciled by assuming that literal word meanings are not used for the overall interpretation. Rather, their activation may be an epiphenomenon of the way idioms are stored (connected to the individual words used in literal language, e.g., Cacciari & Tabossi, 1988; Cutting & Bock, 1997; Sprenger, et al., 2006) or processed (with a literal anlysis running in parallel, e.g., Swinney & Cutler, 1979). Hence, the semantics of individual words are not part of the expectations that may arise during idiom comprehension, but when individual words are actually read, heard, or produced, they may be sufficiently deeply processed to prime semantically related words.

4.3 If not semantics, what is expected during idiom comprehension?

One question has been left unanswered in the previous discussion: if expectations in idioms are not specified semantically, but they are likely to occur in the present experiment given the predictability of the idioms in the materials that were used, what exactly is the functional level from which expectations arise? Although the present study was not designed to answer this question, a tentative answer may be present in our data given the late positivities that were elicited by violations.

In the 500-800 ms time window, violations elicited a posterior positivity in idioms but not in literal contexts. The effect resembles the P600, which has been found in the domain of literal language in response to at least syntactic violations (e.g., Hagoort, et al., 1993; Osterhout & Holcomb, 1992), orthographic violations (Münte, et al., 1998; Vissers, et al., 2006), and semantic "reversal anomalies" such as "The fox that hunted the poachers..." (Kolk, Chwilla, van Herten, & Oor, 2003). Several different interpretations exist as to what the P600 reflects (e.g., Bornkessel-Schlesewsky & Schlesewsky, 2008; Hoeks, Stowe, & Doedens, 2004; Kim & Osterhout, 2005; Kolk, et al., 2003; Kuperberg, 2007), but one possibility is that, given the P600 effects to orthographic and syntactic violations, words that were meant to be semantic violations are taken as a form violation in idioms. The notion of form here refers to the form of the idiomatic expression as a whole. This interpretation is in line with models suggesting a unitary representation of idioms at some level (e.g., Cacciari & Tabossi, 1988; Cutting & Bock, 1997; Sprenger, et al., 2006; Swinney & Cutler, 1979). The notion of a unitary representation for idioms is also relevant for more general language comprehension models, including the unification model (Hagoort, 2007), in the sense that the basic building blocks in sentence comprehension are not (always) word meanings, but may be entire phrases that are stored in, and retrieved as such from, long-term memory. Perhaps the form is even part of readers' expectations, and when an unexpected form is detected a kind of reanalysis process is triggered that is reflected by the P600.

In the later 800-1200 ms time window, a similar late positivity was elicited by violations regardless of semantic relatedness or the type of context (literal or idiomatic). On the one hand, this effect could be related to processing of the next word (presented at 600 ms), reflecting further difficulties after the sentence already had stopped making sense due to the earlier semantic violation. On the other hand, this very late positivity could be part of the P600, being a continuation of the positivity in idiomatic contexts, and in the case of literal sentences the start of it, with the component having a much later onset. The present data cannot prove or disprove either of the two, and it does not seem crucial for the main issue of semantic expectancy. For at least two reasons, it must be stressed that more research on late positivities in general is necessary before drawing any final conclusions. First, the P600 in idioms is in need of replication: although a late positivity (650-850 ms) was also observed by Moreno et al. (2002) in response to words that did not fit idiomatic contexts, this effect had an anterior distribution rather than the strikingly posterior distribution of the effect in the present experiment. Second, the interpretation of the P600 reflecting a violation in form does not directly explain why the effect would occur in the processing of semantic reversal anomalies such as "The fox that hunted the poachers..." (Kolk, et al., 2003). At a general level however, we feel that the present study together with Vespignani et al. (in press), Laurent et al. (2006) and Moreno et al. (2002) demonstrates that our understanding of language

comprehension might profit from recording EEG during idiom comprehension.

Acknowledgements

I would like to thank Jos van Berkum, Rob Schreuder and Herbert Schriefers for helpful comments on informal presentations, Suzanne den Engelsman for proofreading parts of this text (remaining errors are entirely my own), Christian Forkstam for help with and use of his stimulus presentation scripts, and Lilla Magyari, Daphne van Moerkerken, Jacqueline de Nooijer, Merel van Rees Vellinga, Britt Oosterlee, Vitória Piai, Matthias Sjerps, Josje Verhagen and Lin Wang for assistance with preparing subjects for the EEG experiment. Special thanks to Vitória for being a great "research buddy". Two anonymous reviewers deserve gratitude for helpful suggestions. I also thank all of the participants. Last but not least, of course my supervisors Marcel Bastiaansen and Ton Dijkstra deserve a big thank you for their support. Marcel, whenever I had another list of questions or ideas, your office door was wide open. One of the scientific things you taught me is to try and use convincing argumentation to motivate whatever step we took in the course of the project. Ton, you were always enthusiastic about the ideas and curious about the results, which strengthened my belief in the research.

References

Baayen, R. H., Piepenbrock, R., & Gulikers, L. (1993). The CELEX lexical database [CD-ROM]. Philadelphia: University of Pennsylvania, Linguistic Data Consortium.

Bobrow, S. A., & Bell, S. M. (1973). On catching on to idiomatic expressions. Memory & Cognition, 1, 343-346.

Bornkessel-Schlesewsky, I., & Schlesewsky, M. (2008). An alternative perspective on "semantic P600" effects in language comprehension. Brain Research Reviews, 59, 55-73.

Boulenger, V., Hauk, O., & Pulvermüller, F. (2009). Grasping ideas with the motor system: semantic somatotopy in idiom comprehension. Cerebral Cortex, 19, 1905-1914.

Cacciari, C., & Tabossi, P. (1988). The comprehension of idioms. Journal of Memory and Language, 27, 668-683.

Chwilla, D. J., & Kolk, H. H. J. (2002). Three-step priming in lexical decision. Memory & Cognition, 30(2), 217-225.

Colombo, L. (1993). The comprehension of ambiguous idioms in context. In C. Cacciari & P. Tabossi (Eds.), Idioms: Processing, Structure and Interpretation (pp. 163-189). Hillsdale, NJ: Lawrence Erlbaum Associates.

Cutting, J. C., & Bock, K. (1997). That's the way the cookie bounces: syntactic and semantic components of experimentally elicited idiom blends. Memory & Cognition, 25, 57-71.

de Groot, A. M. B., & de Bil, J. M. (1987). Nederlandse woordassociatienormen met reactietijden. Lisse: Swets & Zeitlinger.

de Groot, H. (1999). Van Dale Idioomwoordenboek: verklaring en herkomst van uitdrukkingen en gezegden. Amsterdam/ Brussels: The Reader's Digest NV.

Federmeier, K. D. (2007). Thinking ahead: the role and roots of prediction in language comprehension. Psychophysiology, 44, 491-505.

Federmeier, K. D., & Kutas, M. (1999). A rose by any other name: Long-term memory structure and sentence processing. Journal of Memory and Language, 41, 469-495.

Fischler, I., & Bloom, P. A. (1979). Automatic and attentional processes in the effects of sentence contexts on word recognition. Journal of Verbal Learning and Verbal Behavior, 18, 1-20.

Gibbs, R. W., Jr. (1980). Spilling the beans on understanding and memory for idioms in conversation. Mem Cognit, 8(2), 149-156.

Gibbs, R. W., Jr., & Nayak, N. P. (1989). Psycholinguistic studies on the syntactic behavior of idioms. Cognitive Psychology, 21(1), 100-138.

Giora, R. (1997). On the priority of salient meanings: studies of literal and figurative language. Journal of Pragmatics, 31, 919-929.

Hagoort, P. (2005). On Broca, brain, and binding: a new framework. Trends in Cognitive Sciences, 9(9), 416-423.

Hagoort, P. (2007). The memory, unification, and control (MUC) model of language. In A. S. Meyer, L. Wheeldon & A. Krott (Eds.), Automaticity and control in language processing (pp. 243-270). Hove: Psychology Press.

Hagoort, P., Brown, C. M., & Groothusen, J. (1993). The Syntactic Positive Shift (SPS) as an ERP measure of syntactic processing. Language and Cognitive Processes, 8, 439-483.

Hahne, A. (2001). What's different in second-language processing? Evidence from event-related potentials. Journal of Psycholinguistic Research, 30, 251-266.

Hahne, A., & Friederici, A. D. (2001). Processing a second language: Late learners' comprehension mechanisms as revealed by event-related brain potentials. Bilingualism: Language and Cognition, 4, 123-141.

Hillert, D., & Swinney, D. A. (2000). The processing of fixed expressions during sentence comprehension. In A. Cienki (Ed.), Conceptual structure, discourse, and language. Stanford: CSLI.

Hoeks, J. C. J., Stowe, L. A., & Doedens, G. (2004). Seeing words in context: the interaction of lexical and sentence level information during reading. Cognitive Brain Research, 19, 59-73.

Jackendoff, R. (1995). The boundaries of the lexicon. In M. Everaert, E.-J. van der Linden, A. Schenk & R. Schreuder (Eds.), Idioms: structural and psychological perspectives (pp. 133-165). Hillsdale, NJ: Lawrence Erlbaum Associates.

Jackendoff, R. (2007). A Parallel Architecture perspective on language processing. Brain Research, 1146, 2-22.

Kamide, Y. (2008). Anticipatory processes in sentence processing. Language and Linguistics Compass, 2(4), 647-670.

Katz, J. J. (1973). Compositionality, idiomaticity, and lexical substitution. In S. R. Anderson & P. Kiparsky (Eds.), A festschrift for Morris Halle (pp. 357-376). New York: Holt, Rinehart & Winston.

Kim, A., & Osterhout, L. (2005). The independence of combinatory semantic processing: evidence from event-related potentials. Journal of Memory and Language, 52,

205-225.

Kolk, H. H. J., Chwilla, D. J., van Herten, M., & Oor, P. J. (2003). Structure and limited capacity in verbal working memory: a study with event-related potentials. Brain & Language, 85, 1-36.

Kuperberg, G. R. (2007). Neural mechanisms of language comprehension: challenges to syntax. Brain Research, 1146(23-49).

Kutas, M., & Federmeier, K. D. (2000). Electrophysiology reveals semantic memory use in language comprehension. [Journal; Peer Reviewed Journal]. Trends in Cognitive Sciences, 4(12), 463-470.

Kutas, M., & Hillyard, S. A. (1980). Reading senseless sentences: brain potentials reflect semantic incongruity. Science, 207(4427), 203-205.

Landauer, T. K., & Dumais, S. T. (1997). A solution to Plato's problem: The latent semantic analysis theory of acquisition, induction, and representation of knowledge. Psychological Review, 104, 211-240.

Landauer, T. K., Folz, P. W., & Laham, D. (1998). Introduction to latent semantic analysis. Discourse Processes, 25, 259-284.

Laurent, J. P., Denhieres, G., Passerieux, C., Iakimova, G., & Hardy-Bayle, M. C. (2006). On understanding idiomatic language: The salience hypothesis assessed by ERPs. Brain Res, 1068(1), 151-160.

Lauteslager, M., Schaap, T., & Schievels, D. (1986). Schriftelijke woordassociatienormen voor 549 zelfstandige naamwoorden. Lisse: Swets & Zeitlinger.

Libben, M. R., & Titone, D. A. (2008). The multidetermined nature of idiom processing. Memory & Cognition, 36, 1103-1121.

Moreno, E. M., Federmeier, K. D., & Kutas, M. (2002). Switching languages, switching palabras (words): an electrophysiological study of code switching. Brain & Language, 80(2), 188-207.

Münte, T. F., Heinze, H.-J., Matzke, M., Wieringa, B. M., & Johannes, S. (1998). Brain potentials and syntactic violations revisited: no evidence for specificity of the syntactic positive shift. Neuropsychologia, 36, 217-226.

Needham, W. P. (1992). Limits on literal processing during idiom interpretation. J Psycholinguist Res, 21(1), 1-16.

Nunberg, G. (1978). The pragmatics of reference. Bloomington, IN: Indiana University Linguistics.

Osterhout, L., & Holcomb, P. J. (1992). Event-related brain potentials elicited by syntactic anomaly. Journal of Memory and Language, 31, 785-806.

Peterson, R. R., Burgess, C., Dell, G. S., & Eberhard, K. M. (2001). Dissociation between syntactic and semantic processing during idiom comprehension. J Exp Psychol Learn Mem Cogn, 27(5), 1223-1237.

Pickering, M. J., & Garrod, S. (2007). Do people use language production to make predictions during comprehension? Trends in Cognitive Sciences, 11, 105-110.

Raposo, A., Moss, H. E., Stamatakis, E. A., & Tyler, L. K. (2009). Modulation of motor and premotor cortices by actions, action words and action sentences. Neuropsychologia, 47, 388-396.

Ratcliff, R., & McKoon, G. (1988). A retrieval theory of priming in memory. Psychological Review, 95, 385-408.

Roelofs, A. (2003). Modeling the relation between the production and recognition of spoken word forms. In A. S. Meyer & N. O. Schiller (Eds.), Phonetics and phonology in language comprehension and production: Differences and similarities (pp. 115-158). Berlin: Mouton de Gruyter.

Schwanenflugel, P. J., & Shoben, E. J. (1985). The influence of sentence constraint on the scope of facilitation for upcoming words. Journal of Memory and Language, 24, 232-252.

Sprenger, S. A. (2003). Fixed expressions and the production of idioms. PhD thesis, MPI Series in Psycholinguistics, 21, University of Nijmegen.

Sprenger, S. A., Levelt, W. J. M., & Kempen, G. (2006). Lexical access during the production of idiomatic phrases. Journal of Memory and Language, 54, 161-184.

Swinney, D. A. (1981). Lexical processing during sentence comprehension: effect of higher order constraints and implications for representation. In T. Meyers, J. Laver & J. Anderson (Eds.), The cognitive representation of speech. Amsterdam: North-Holland (Advances in Psychology Series).

Swinney, D. A., & Cutler, A. (1979). The access and processing of idiomatic expressions. Journal of Verbal Learning and Verbal Behavior, 18, 523-534.

Tabossi, P., Fanari, R., & Wolf, K. (2005). Spoken idiom recognition: meaning retrieval and word expectancy. J Psycholinguist Res, 34(5), 465-495.

van Berkum, J. J. A., Brown, C. M., Zwitserlood, P., Kooijman, V., & Hagoort, P. (2005). Anticipating upcoming words in discourse: Evidence from ERPs and reading times. Journal of Experimental Psychology: Learning, Memory, and Cognition, 31(3), 443-467.

van Loon-Vervoorn, W. A., & van Bekkum, I. J. (1991). Woordassociatielexicon. Amsterdam/Lisse: Swets & Zeitlinger.

van Petten, C., & Kutas, M. (1990). Interactions between sentence context and word frequency in event-related brain potentials. [Journal; Peer Reviewed Journal]. Memory & Cognition, 18, 380-393.

Vespignani, F., Canal, P., Molinaro, N., Fonda, S., & Cacciari, C. (in press). Predictive mechanisms in idiom comprehension. Journal of Cognitive Neuroscience.

Vissers, C. T. W. M., Chwilla, D. J., & Kolk, H. H. J. (2006). Monitoring in language perception: the effect of misspellings of words in highly constrained sentences. Brain Research, 1106, 150-163.

Hippocampal theta modulation of neocortical spike times and gamma rhythm

Eelke Spaak[1]
Supervisors: Magteld Zeitler[1], Stan Gielen[1]

[1]*Donders Institute for Brain, Cognition and Behaviour, Radboud University Nijmegen, Nijmegen, The Netherlands*

The hippocampal theta and neocortical gamma rhythms are two prominent examples of oscillatory neuronal activity. The hippocampus has often been hypothesized to influence neocortical networks by its theta rhythm, and, recently, evidence for such a direct influence has been found. We examined a possible mechanism for this influence by means of a biophysical model study. We found, in agreement with previous studies, that networks of fast-spiking GABA-ergic interneurons, coupled with shunting inhibition, synchronize their spike activity at a gamma frequency and are able to impose this rhythm on a network of pyramidal cells to which they are coupled. When our model was supplied with hippocampal theta-modulated input fibres, the theta rhythm biased the spike timings of both the fast-spiking and pyramidal cells. Furthermore, both the amplitude and frequency of local field potential gamma oscillations were influenced by the phase of the theta rhythm. We show that the fast-spiking cells are essential for this latter phenomenon, thus highlighting their crucial role in the interplay between hippocampus and neocortex.

Keywords: gamma synchronisation, theta rhythm, fast-spiking cells, hippocampus, phase/amplitude coupling

Corresponding author: Eelke Spaak, Donders Institute for Brain, Cognition, and Behaviour, Centre for Neuroscience, Geert Grooteplein 21, 6525 EZ Nijmegen, The Netherlands; email: eelke.spaak@gmail.com

1. Introduction

The hippocampal theta rhythm (3–8 Hz) and the neocortical gamma rhythm (30–100 Hz) are two prominent examples of oscillatory neuronal activity (Buzsáki, 2002, Buzsáki & Draguhn, 2004). The hippocampal theta rhythm is thought to reflect the "activation state" of the hippocampus (Buzsáki, 2002) and is important for the temporal coordination of a variety of different functions (e.g., O'Keefe & Recce, 1993, O'Keefe & Burgess, 2005, Harris et al., 2002)[1]. In the neocortex, cell assembly formation, a crucial prerequisite for cognitive processing, is strongly associated with gamma oscillations (Fries, 2005, Gray, König, Engel, & Singer, 1989, Gray & Singer, 1989).

Both the hippocampus and the neocortex, in particular the prefrontal cortex, seem to play complementary, yet highly interdependent, roles in the formation and retrieval of memories (Lavenex & Amaral, 2000, O'Reilly & Norman, 2002, Dolan & Fletcher, 1997, Eichenbaum, 2000). When we take this finding into account, along with the functional importance of the theta and gamma rhythms, it is not too far-fetched to hypothesize a direct influence of the hippocampal theta rhythm on neocortical networks.

Indeed, evidence for such a direct influence has recently been found. In both awake and sleeping rats, the hippocampal theta rhythm was found to bias both the spike times of individual prefrontal cortex neurons and the occurrence of localized neocortical gamma oscillations (Sirota et al., 2008, Siapas, Lubenov, and Wilson, 2005, Sirota, Csicsvari, Buhl, and Buzsáki, 2003; see also Jones and Wilson, 2005). Furthermore, in the human neocortex, the power of the "high gamma" rhythm (80–150 Hz) was found to be phase-locked to theta oscillations (Canolty et al., 2006).

1.1 Physiological and anatomical background

The mechanisms by which the hippocampus is able to influence neocortical networks through its theta rhythm are not well-understood. In contrast, quite some physiological and biophysical work is available concerning the neuronal networks responsible for the generation of the gamma rhythm.

Networks of fast-spiking (FS) GABA-ergic interneurons, connected to one another with strong inhibitory chemical synapses as well as electrical synapses (gap junctions) tend to synchronize their spiking activity at a gamma frequency. Hence, they are thought to be responsible for the generation of the gamma rhythm in the neocortex (Tamás, Buhl, Lörincz, & Somogyi, 2000, Galarreta & Hestrin, 1999, Gibson, Beierlein, & Connors, 1999, Wang & Buzsáki, 1996, Sohal & Huguenard, 2005). Most likely, the inhibition involved in the synchronization of such fast-spiking interneurons is of the shunting type, where a GABA-ergic synaptic event can actually be excitatory when the post-synaptic membrane potential is at or only slightly above the resting potential (Vida, Bartos, & Jonas, 2006, Bartos, Vida, & Jonas, 2007).

Hippocampal efferent fibres project directly onto neurons of the prefrontal cortex (Dégenètais, Thierry, Glowinski, & Gioanni, 2003, Rosene & Van Hoesen, 1977). Both pyramidal cells and interneurons are the targets of these projections. The projections to the interneurons, however, are stronger than those to the pyramidal cells (Tierney, Degenetais, Thierry, Glowinski, & Gioanni, 2004, Gabbott, Headlam, & Busby, 2002).

Taken together, (1) the empirically observed interaction between the hippocampal theta and neocortical gamma rhythms, (2) the crucial role played by prefrontal cortex interneurons in the generation of the gamma rhythm, and (3) the preferential projection of hippocampal fibres onto these interneurons, led us to hypothesize that the fast-spiking interneurons of the neocortex are the key players in the mechanism by which the hippocampal theta rhythm influences neocortical networks. In this paper, we present support for this hypothesis in the form of a biophysical model.

Section 2 of the present paper outlines the architecture and dynamics of our model and provides details for the analyses performed to obtain our results. Section 3 contains our results, which can be briefly summarized as follows. First, we replicated earlier findings (Wang & Buzsáki, 1996, Vida et al., 2006, Bartos et al., 2007, Sohal & Huguenard, 2005) by showing that networks of coupled fast-spiking interneurons are robust gamma oscillators (3.2) and that these will impose their rhythm on pyramidal cells synaptically innervated by them (3.3). Second, hippocampal theta input to a coupled pyramidal cell/interneuron network results in theta phase biased spike timings (3.4). Third, and most importantly, the frequency and amplitude of

[1] Oscillations in the hippocampus are not limited to the theta band. See section 4.2.4 for a discussion of how the present model might apply to nested hippocampal theta and gamma oscillations.

neocortical gamma oscillations is modulated by the phase of the hippocampal theta rhythm if and only if the neocortical fast-spiking interneurons receive hippocampal theta input (3.5); no such modulation is observed if only the neocortical pyramidal cells receive hippocampal theta input.

2. Methods

To study the influence of hippocampal theta oscillations on neocortical spike times and gamma oscillations, we modelled a patch of neocortex by two interconnected subnetworks: one comprised of fast-spiking inhibitory interneurons (FS cells), another comprised of pyramidal cells (P cells). Each of these is discussed, in turn, below. See Figure 1 for an overview of the architecture of the model.

All network simulations were conducted using version 7.1 of the NEURON simulation environment (Hines & Carnevale, 1997), released on January 15th, 2009. All data analyses were conducted using custom scripts, written either for NEURON 7.1, or for MATLAB (Mathworks Inc., Natick, MA, USA).

2.1 Interneuron subnetwork

The interneuron subnetwork was modelled after some quite extensive previous neurophysiological and modelling work (Bartos et al., 2002, 2007), and consists of a virtual ring of 200 single-compartmental Hodgkin-Huxley-like model neurons (Hodgkin & Huxley, 1952) with a resting potential of E_{REST} = -65 mV and a membrane surface area of 100 μm^2. Leakage, Na^+, and K^+ conductances were inserted into each neuron according to the model of Wang & Buzsáki (1996; 'WB' conductances). These differ from standard Hodgkin-Huxley ('HH') conductances in two important respects (see appendix for detailed equations): first, the fast Na^+ current activation variable m is substituted by its steady-state value m_∞; second, the remaining gating kinetics for the Na^+ and K^+ current are sped up by a factor $\varphi = 5$:

$$\frac{dh_{WB}}{dt} = \phi \frac{dh_{HH}}{dt} \quad (1)$$

$$\frac{dn_{WB}}{dt} = \phi \frac{dn_{HH}}{dt} \quad (2)$$

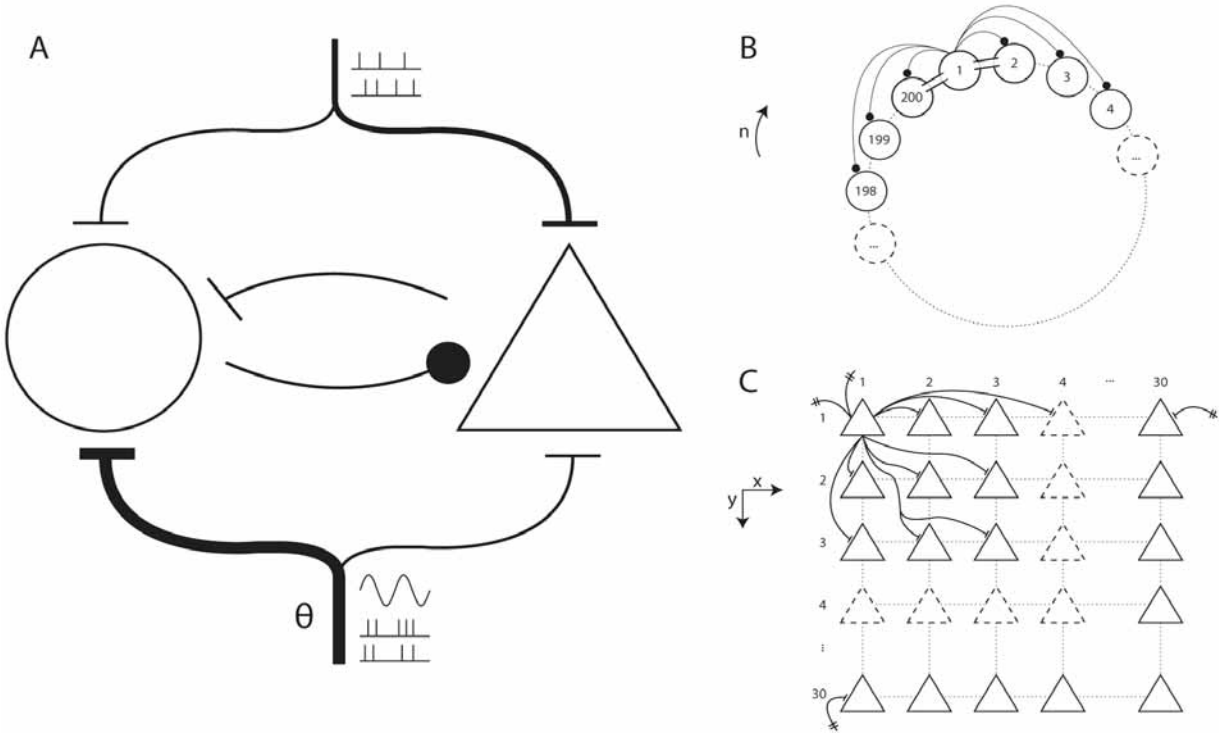

Figure 1. A. patch of neocortex modelled by a network of interneurons coupled with a network of pyramidal cells. A The macroarchitecture of the model. Shown are the fast-spiking inhibitory interneuron network (circle, left), the pyramidal cell network (triangle, right), the cortical long-range afferent spike trains (top), and the theta-modulated subcortical afferent spike trains (bottom). **B.** The ring-like structure of the interneuron model. Shown are some of the inhibitory synaptic connections (solid circles) and gap junctions ('conduits' between adjacent cells) for cell 1. **C** The two-dimensional structure of the pyramidal cell network. Shown are some of the excitatory synaptic projections from cell (1,1) to its neighbours. Note the projections to (30,1) and (1,30) are possible because the effective distance from (1,1) to those cells equals 1 (see section 2.2).

These specifics are computationally efficient, because of the $m = m_\infty$ substitution, and, because of the adjusted time course of the currents, ensure that a firing pattern emerges that is characteristic of fast-spiking inhibitory interneurons (Wang & Buzsáki, 1996).

Each neuron receives incoming GABA-ergic synapses from a subset of its neighbours on the ring with a Gaussian probability dependent upon the distance between two cells, up to a maximum connection distance of 50 cells ($3\sigma = 50$). Synapses were either on or off; the Gaussian probability only governs whether or not there will be a synapse and is not used in determining synapse strength.

Synaptic events were modelled by insertion of a conductance determined by a two-state kinetic scheme of the form:

$$g_{syn}(t) = \bar{g}_{syn} N \left(e^{-\frac{t}{\tau_2}} - e^{-\frac{t}{\tau_1}} \right) \qquad (3)$$

with rise time $\tau_1 = \tau_{rise}$, decay time $\tau_2 = \tau_{decay}$, and resulting current:

$$I_{syn}(t) = g_{syn}(t)(V(t) - E_{syn}) \qquad (4)$$

where syn is the synapse maximum conductance, Esyn is the synapse reversal potential, and N is a normalization factor:

$$N = \frac{1}{\exp\left(-\frac{\tau_1}{\tau_2-\tau_1}\ln\left(\frac{\tau_2}{\tau_1}\right)\right) - \exp\left(-\frac{\tau_2}{\tau_2-\tau_1}\ln\left(\frac{\tau_2}{\tau_1}\right)\right)} \qquad (5)$$

that ensures that the peak conductance is given by the relevant parameter syn.

The GABA-ergic synapses were governed by a rise time constant of $\tau_{GABA,rise} = 0.16$ ms and a decay time constant of $\tau_{GABA,decay} = 1.8$ ms. The unitary post-synaptic peak conductance was $\bar{g}_{GABA} = 0.1$ mS cm^{-2}. These values are consistent with empirical findings (Bartos, Vida, Frotscher, Geiger, & Jonas, 2001, Buhl, Cobb, Halasy, & Somogyi, 1995). The synaptic reversal potential was varied for the study of gamma rhythm generation, while it was set to $E_{GABA} = -57$ mV for all subsequent simulations, in accordance with gamma rhythm results and previous studies (Vida et al., 2006, Chance, Abbott, & Reyes, 2002).

In addition to GABA-receptors, AMPA- and NMDA-receptors were also present at the membrane of the fast-spiking cells, in order to model the connections between the two subnetworks and to model incoming spike trains as input (see section 2.3). These were modelled by conductance insertion according to two separate bi-exponential functions of the type described by equation 3. Separate time constants were used to model the AMPA and NMDA currents: $\tau_{AMPA,rise} = 0.5$ ms, $\tau_{AMPA,decay} = 2.0$ ms, $\tau_{NMDA,rise} = 3$ ms, $\tau_{NMDA,decay} = 40$ ms (Kleppe & Robinson, 1999, Gabbiani, Midtgaard, & Knopfel, 1994). The reversal potential for both receptor types was set to $E_{AMPA} = E_{NMDA} = 0$ mV. The unitary post-synaptic peak conductances for the glutamatergic synapses on the fast-spiking cells were given by $\bar{g}_{AMPA} = 0.5$ μS cm^{-2} and $\bar{g}_{NMDA} = 0.05$ μS cm^{-2}. These conductance values were chosen to ensure that the average net current input to the fast-spiking cells, resulting from synaptic events, was comparable in amplitude to the direct current input used in the model of Vida and colleagues (2006).

Apart from the above-mentioned chemical synapses, electrical synapses, or gap junctions, were also included in the interneuron network. Gap junctions allow small quantities of ions to flow between two coupled cells; a given cell is thereby able to directly influence the membrane potential of another cell. Between each cell and its 8 closest neighbours, a gap junction was inserted with a probability of 0.5, resulting in, on average, 4 gap junctions per cell (Vida et al., 2006).

Gap junctions were modelled by a constant conductance insertion of ggap = 10 pS between two cells (Venance et al., 2000, Traub et al., 2001). The resulting current between two coupled cells i and j is given by

$$I_{gap} = g_{gap}(V_i - V_j) \qquad (6)$$

2.2 Pyramidal cell subnetwork

The pyramidal cell subnetwork consists of a two-dimensional sheet of 30 x 30 = 900 single-compartmental Hodgkin-Huxley model neurons (Hodgkin and Huxley, 1952; standard NEURON implementation, Hines and Carnevale, 1997). This results in an anatomically realistic ratio of 900 = 82% pyramidal cells versus 200 = 18% interneurons (Sirota et al., 2008). The resting potential of the pyramidal cells was equal to that of the interneurons, $E_{rest} = -65$ mV, and standard Hodgkin-Huxley conductances were inserted to model cell membrane channels (Hodgkin & Huxley, 1952). Each neuron received glutamatergic synaptic afferents from a subset of its neighbours according to a two-dimensional Gaussian probability, dependent on cell distance. Maximum connection distance was 8 cells ($3\sigma_x = 3\sigma_y = 8$), ensuring a realistic ratio of synaptic densities within the pyramidal cell subnetwork (see

Table 1). The standard Euclidean measure was used to define the distance between cells:

$$d(a,b) = \sqrt{(x_a - x_b)^2 + (y_a - y_b)^2} \quad (7)$$

To avoid edge effects, opposing edges of the two-dimensional sheet were folded onto each other:

$$\forall y : d((x_{max}, y), (x_{min}, y)) = 1$$
$$\forall x : d((x, y_{max}), (x, y_{min})) = 1$$

Incoming glutamatergic and GABA-ergic synaptic events were modelled by the same bi-exponential functions as described above for the fast-spiking cells (see equation 3), with the only difference lying in the peak conductances: for the pyramidal cells, $\bar{g}_{AMPA}$ = 3 μS cm^{-2}, $\bar{g}_{NMDA}$ = 0.4 μS cm^{-2}, and $\bar{g}_{GABA}$ = 0.05 mS cm^{-2}. These values were chosen to obtain accurate cortical pyramidal cell firing characteristics for the model neurons; most importantly, they ensured an ongoing 'background firing noise' of about 1 - 2 sp/s (Hirase, Leinekugel, Czurkó, Csicsvari, & Buzsáki, 2001, Sirota et al., 2008).

2.3 Subnetwork interconnections and network input

For the investigation of theta–gamma coupling, each pyramidal cell received GABA-ergic afferents from, on average, 14 randomly chosen fast-spiking cells and each fast-spiking cell received glutamatergic afferents from, on average, 45 randomly chosen pyramidal cells. These values were chosen to obtain realistic ratios of synaptic densities between the two subnetworks (see Table 1). For the investigation of the influence of the gamma-synchronized interneuron subnetwork on the synchronization of the pyramidal cells, the average number of incoming P synapses per FS cell was kept constant at 45, while the average number of incoming FS synapses per P cell was varied between 0 and 20.

[2] Wang & Buzsáki (1996) define network coherence K as a function of bin size and, indeed, this measure is quite strongly dependent upon bin size. Network synchrony is most accurately reflected by K, however, when bin size is small. As a statistic, therefore, we report this measure only for a bin size of 1 ms, i.e., our K = K(1). This is in accordance with previous work (Bartos et al., 2002).

[3] All results reported in the present article were robust across simulations; i.e., the network always settled into the same state when initial conditions were identical. Noise due to the random number generator was (evidently) different across simulations.

Table 1. Model connectivity values. Shown is the number of synapses of different types, presented as ratios of the total number of synapses. Model values were either chosen to reflect connectivity known from anatomy (reported anatomical values are from Liley &Wright, 1994), or based on previous modelling work (Vida et al., 2006)

	Model (%)	Anatomy (%)
FS → FS	4.24	1.34
P → FS	4.47	4.97
P → P	28.09	28.17
FS → P	6.30	7.62
ext → FS	7.09	6.66
ext → P	49.80	50.66

For the investigation of gamma rhythm generation by the interneuron subnetwork, a direct current input was supplied to the fast-spiking cells. The amplitude of the current varied for different cells, and as a function of time. This resulted in a variable intrinsic firing frequency for each fast-spiking cell, enabling the study of the amount of network synchronization due to different parameters.

Specifically, drive amplitude was determined by drawing a mean drive μ_i for each cell $i \in \{1,2,\ldots,200\}$ from a normal distribution with mean I_μ and then, for each time window of 1 ms, drawing a specific drive amplitude from a new normal distribution with mean μ_i:

$$\mu_i = \mathcal{N}(I_\mu, \sigma^2) \quad (8)$$
$$I_{ext,i}(t) = \mathcal{N}(\mu_i, \sigma_i^2) \quad (9)$$

The spread of the distributions was defined in terms of coefficients of variation (CV), resulting in standard deviations $\sigma = CV_{cells} I_\mu$ and $\sigma_i = CV_{time} \mu_i$. The variation over time was kept constant, CV_{time} = 10%, while both I_μ and CV_{cells} were varied to assess the network's robustness in generating a gamma rhythm.

To investigate (1) the influence of the gamma-synchronized interneuron subnetwork on the pyramidal cells and (2) the influence of the theta rhythm on the interconnected network of fast-spiking and pyramidal cells, direct current input was replaced by Poisson spike train input acting on glutamatergic synapses, to serve as a more realistic model of actual neuronal input.

Two pools of Poisson process input spike trains were initialized, both consisting of 1 000 fibres. The fibres in the first pool had a constant average spiking rate, r_{const} = 40 sp/s, modelling cortical background noise. The firing patterns of these fibres were mutually uncorrelated. The fibres in the second pool

varied their spiking rate according to a sinusoid, modelling the ascending fibres that carry the theta rhythm. The spiking rate for the 'variable-spiking' fibres is given by:

$$r_{var}(t) = A + y\sin(2\pi f_\theta t) \qquad (10)$$

with average spiking rate A = 40 sp/s, amplitude y = 30 sp/s, and frequency f_θ = 4 Hz. For each fibre in the two pools, the probability of a time window of Δt = 1 ms containing a single spike (≥ 2 spikes per bin are highly unlikely and not modelled) is given by $p_{spike} = r\Delta t$.

Each pyramidal cell received incoming synapses from, on average, 100 randomly selected constant-spiking fibres and 10 randomly selected variable-spiking fibres, while each fast-spiking cell received incoming synapses from, on average, 50 randomly selected constant-spiking fibres and 20 randomly selected variable-spiking fibres. The strong projection from hippocampal afferents to interneurons, relative to pyramidal cells, is in accordance with previous morphological and physiological findings (Gabbott et al., 2002, Tierney et al., 2004).

All of the synaptic densities reported above (i.e., concerning synapses within one of the two subnetworks, synapses between the two subnetworks, and external afferent synapses) were either chosen to reflect anatomically known ratios of different synaptic types (Liley and Wright, 1994; see Table 1), or based on previous modelling work (Vida et al., 2006).

2.4 Network analyses and simulation characteristics

2.4.1 Assessment of network synchrony

Two different measures were used to assess network synchrony. The first is the normalized averaged cross-correlation based 'network coherence' measure K introduced by Wang & Buzsáki (1996). To determine this measure, two binary spike trains with bin size Δt = 1 ms[2] and resulting length K = T/Δt are given by X(l) = 0 or 1, Y(l) = 0 or 1, with 0 – no spikes and 1 – a spike present in time bin with index l = 1,2,…,K. The pairwise coherence between two spike trains X and Y is given by:

$$\kappa_{XY} = \frac{\sum_{l=1}^{K} X(l)Y(l)}{\sqrt{\sum_{l=1}^{K} X(l)\sum_{l=1}^{K} Y(l)}} \qquad (11)$$

The network coherence measure K is then defined as the average pairwise coherence for all neuron pairs in the network.

As a second measure of network synchrony, we introduce the average spike volley peak height λ. To automatically determine the occurrence of a volley peak, all of the network's spikes are first aggregated in Δt = 1 ms bins, such that the number of spikes in the interval [t - Δt, t) is given by A(t) (time in ms). The occurrence of a peak is then defined as:

$$k(t) = \begin{cases} & \text{if } A'(t-\Delta t) > 0, \\ 1 & \text{and } A'(t) < 0, \\ & \text{and } A(t) \geq A_{thr} \\ 0 & \text{otherwise.} \end{cases} \qquad (12)$$

where A_{thr} = 1/10 N_{cells} for the fast-spiking cells and A_{thr} = 1/200 N_{cells} for the pyramidal cells. The discrete derivative A'(t) = A(t+Δt)-A(t)/Δt . The average spike volley peak height is given by:

$$\lambda = \frac{\sum_{t=t_0}^{t_{stop}} k(t)A(t)}{\sum_{t=t_0}^{t_{stop}} k(t)} \qquad (13)$$

with t_0 and t_{stop} being the beginning and end times (in ms) of the simulation period to be analyzed, respectively.

2.4.2 Simulation timings

At the beginning of a network simulation, at t = -400 ms, no synaptic connections are inserted, either within or between the two subnetworks. Because of this, a truly (pseudo-)random firing pattern will emerge in the network, ensuring that no initialization effects will influence the results. At t = -200 ms, synapses and gap junctions are created, and all analyses of network firing characteristics are started at t = t_0 = 0 ms, allowing the network to settle into its new, connected, state and preventing transient network properties due to synapse initialization from influencing the results[3] . For the study of gamma generation, simulations were stopped at t = t_{stop} = 2^{11} - 1 = 2 047 ms; for the study of theta modulation, simulations were stopped at t = t_{stop} = 2^{16} - 1 = 65 535 ms.

2.4.3 Measure of electrical activity

The main phenomena in which gamma oscillations are usually said to occur are the local field

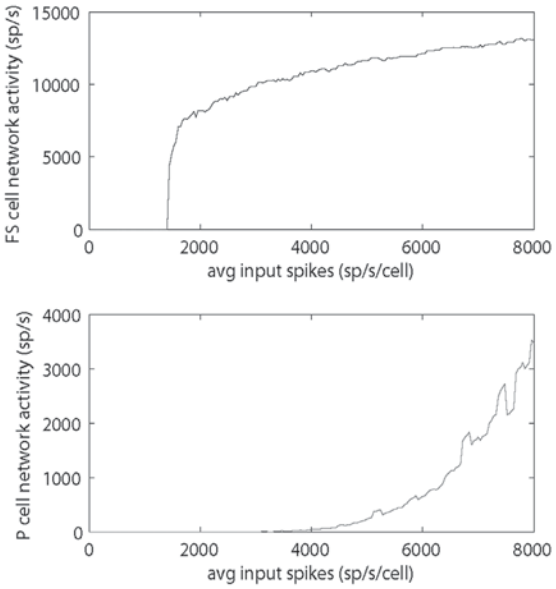

Figure 2. Frequency/input curves for the two model subnetworks: the fast-spiking cells (top) and the pyramidal cells (bottom).

potential (LFP) and electro-encephalogram (EEG). Both these measures of neural activity are thought to reflect the summed total electrical activity in the dendrites of pyramidal cells (see, e.g., Logothetis, 2003). In order to be able to analyse not only the spike times, but also the continuous electrical activity of our network, we generated a simulated LFP by calculating the negative summed total pyramidal cell potential:

$$V_{\text{total}}(t) = -\sum_{j=1}^{N_{\text{pyr}}} V_j(t) \qquad (14)$$

and low-pass filtering this signal up to 300 Hz. The LFP is taken as the negative, rather than the positive, summed total, because the LFP is measured outside the cells in electrophysiological work. The summed total pyramidal cell potential in our model corresponds to the potential inside the cells, so a sign change is needed for our simulated LFP to accurately correspond to its electrophysiological counterpart.

2.4.4 Assessment of theta modulation of spike times

To quantify the amount of theta modulaton of spike times in both the fast-spiking and pyramidal cell populations, we employed two measures. To compute these, all of a subnetwork's spikes are first summed into 1 ms non-overlapping bins, such that the number of spikes in the interval [t-1, t) is given by A(t) (time in ms). The resulting population activity measure is then aggregated over all theta periods:

$$A_{\text{aggr}}(\tau) = \sum_{k=0}^{\frac{t_{\text{stop}}}{T_\theta}-1} A(kT_\theta + \tau) \qquad (15)$$

with theta period $T_\theta = 1/f_\theta$ and $\tau \in \{1,2,\ldots,T_\theta\}$.

The first measure used to quantify spike time theta modulation is the squared Pearson correlation coefficient r^2, computed between this aggregate activity measure and the 'raw' theta signal given by:

$$\theta(t) = \sin(2\pi f_\theta t) \qquad (16)$$

As a second measure of theta modulation of spike times, we introduce a simple modulation score ξ. To compute this measure, the aggregate activity A_{aggr} with bin size 1 ms is re-binned into 25 ms bins, resulting in an activity measure $B(\nu)$ with $\nu \in \{1,2,\ldots, T_\theta/25\}$. This re-binning prevents any high-frequency (>40 Hz) information from influencing the modulation score. The modulation score ξ is then given by:

$$\xi = \frac{\max(B) - \min(B)}{2 \cdot \text{mean}(B)} \qquad (17)$$

and can be interpreted as the relative amplitude of any theta oscillation, if such an oscillation is reflected in the spiking activity of the network. We use this relative amplitude, rather than a measure of absolute amplitude, because we want to be able to compare the variations in activity in the two subpopulations of cells with respect to this measure. Since the average spiking activity differs strongly between both subpopulations, an absolute amplitude measure would give inaccurate results.

Note that, because of the period-wise aggregation described by equation 15, the time indices τ and ν mentioned above correspond to certain phases $\varphi_\theta \in (0,2\pi]$ in the theta cycle:

$$\varphi_\theta = \frac{2\pi\tau}{T_\theta} = 25\frac{2\pi\upsilon}{T_\theta} \qquad (18)$$

This relationship will be used in plotting spike counts versus theta phase.

2.4.5 Measure of cross-frequency phase/ amplitude coupling

One of the questions this study attempts to address is whether gamma oscillations, occurring in the LFP of a theta fibre-innervated patch of simulated neocortex, show a preferred phase in the

theta cycle. In other words, we were interested in whether or not a coupling between gamma amplitude and theta phase could be observed.

To quantify this cross-frequency phase/amplitude coupling, we used a measure very similar to that employed by Canolty et al. (2006).

First, a gamma-only signal is derived from the LFP by band-pass filtering the latter signal between 30 and 150 Hz. We denote this gamma-only signal by $x_\gamma(t)$. We obtain the analytic representation $u_\gamma(t)$ of $x_\gamma(t)$ by using the Hilbert transform:

$$u_\gamma(t) = x_\gamma(t) + i \cdot \hat{x}_\gamma(t) \quad (19)$$

$$= a_\gamma(t) \cdot e^{i\varphi_\gamma(t)} \quad (20)$$

where f denotes the Hilbert transform of a function f, $a_\gamma(t)$ is the analytic amplitude time series, and $\varphi_\gamma(t)$ is the analytic phase time series. We also obtain the analytic representation $u_\theta(t)$ of the 'raw' theta signal (equation 16) used in determining the spike rates of the variable-rate input fibres:

$$u_\theta(t) = \theta(t) + i \cdot \hat{\theta}(t) \quad (21)$$

$$= a_\theta(t) \cdot e^{i\varphi_\theta(t)} \quad (22)$$

These two measures are combined into a single, complex-valued signal z(t):

$$z(t) = a_\gamma(t) \cdot e^{i\varphi_\theta(t)} \quad (23)$$

Theta phase is distributed uniformly, since the theta rhythm is generated according to a simple sine function. Therefore, if gamma amplitude and theta phase are independent, the distribution of z(t) values should be approximately radially symmetric around the origin of the complex plane. If, however, the two are not independent, clustering of z(t) values in the complex plane should occur. We use the distribution of z(t) in the complex plane as a measure of theta phase/gamma amplitude coupling (see Figure 8).

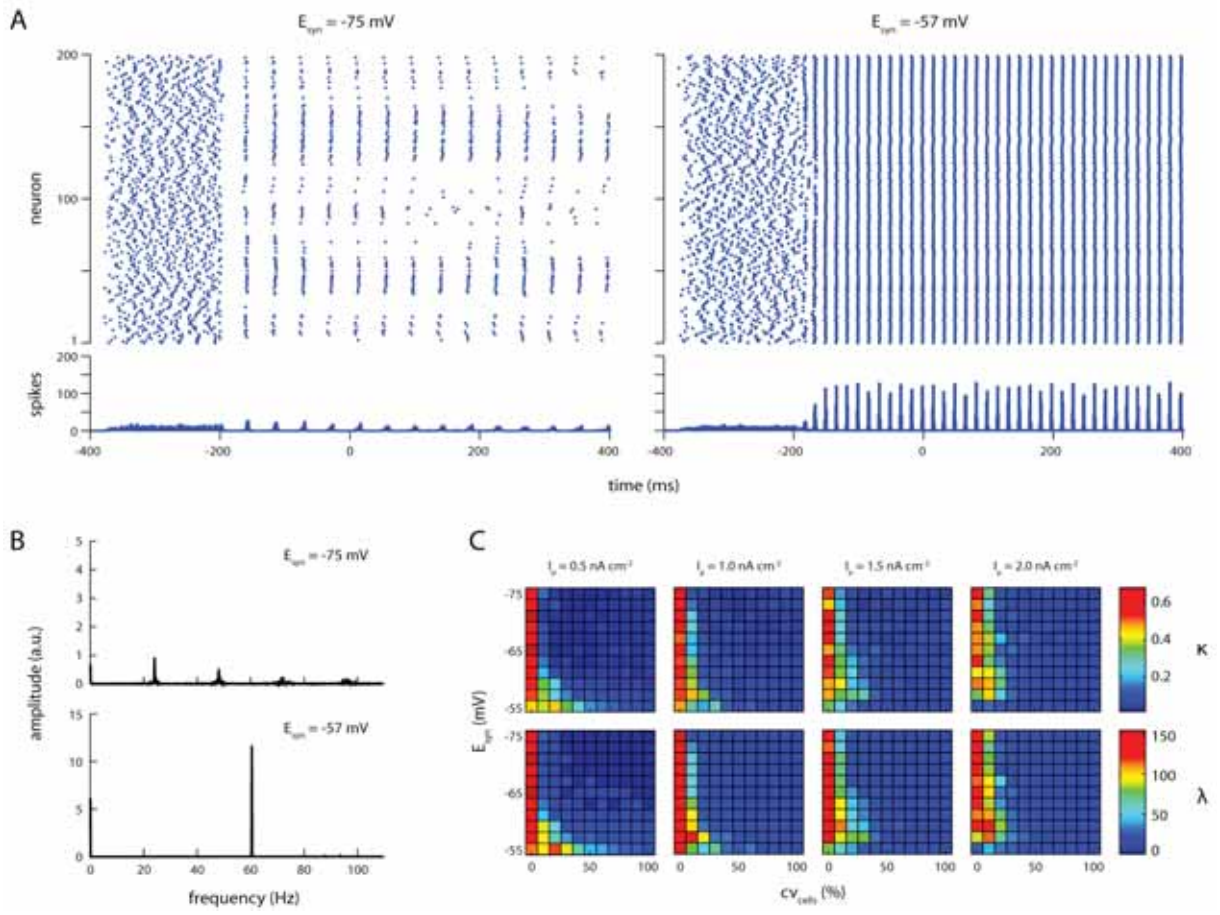

Figure 3. Shunting inhibition increases robustness in a network of fast-spiking inhibitory interneurons. **A.** Rasterplots (top) and spike histograms (bottom) for GABA-synaptic reversal potentials of -75 mV (left) and -57 mV (right). For these plots, mean drive $I\mu$ = 0.5 nA cm^{-2}, drive variation CV_{cells} = 10 %. Synapses were activated at t = -200 ms; plots are truncated at t = 400 ms. **B.** Amplitude spectra for spike histograms. Spectral analyses were performed on complete histograms, ending at t = t_{stop} = 2 047 ms. **C.** Two measures of network synchronization, network coherence κ(top row) and average spike volley peak height (bottom row), as a function of drive variation over cells CV_{cells} (x-axis), synaptic reversal potential E_{syn} (y-axis), and mean drive $I\mu$ (separate columns). Shunting values of E_{syn} result in stronger synchronization with increasing drive heterogeneity.

Finally, note that our measure differs in an important respect from that used by Canolty et al. (2006). Canolty et al.'s measure was computed on two signals that were obtained by band-pass filtering the same signal using two different frequency bands. Our analysis uses a (gamma) band-pass filtered signal for the amplitude time series, but uses a different signal altogether for the phase time series, namely the raw theta signal that governs the variable-rate input spike trains.

3. Results

3.1 Subnetwork firing characteristics

In a first analysis of our model network, we assessed the firing characteristic of both subnetworks in response to different amounts of input. Subnetwork input was of the Poisson spike train type (see section 2.3) and varied in the average frequency with which spike events arrived at a single cell.

As is evident from Figure 2, the fast-spiking cells remain silent for an input spike rate of up to about 1 500 sp/s. When the input is greater than this, spikes in the network of FS cells tend to occur with a frequency around 10 000 sp/s, with little variation. This value corresponds to a single-cell firing frequency of about 50 sp/s, since the network consists of 200 FS cells.

The pyramidal cells remain silent for an input spike rate of up to about 4 000 sp/s, above which they seem to show an exponential increase of population activity with input spikes.

3.2 Gamma generation by a ring of fast-spiking cells

Networks of fast-spiking inhibitory interneurons with fast, strong, and shunting (i.e., with a synaptic reversal potential above the resting potential; as opposed to hyperpolarizing) inhibitory synapses and gap junctions are hypothesized to be the main generators for the cortical gamma rhythm, and there is quite a bit of empirical evidence available that supports this hypothesis (Wang & Buzsáki, 1996, Bartos et al., 2007).

In an attempt to replicate some of this evidence, we simulated the dynamics of a ring-like network of the type just described when provided with a direct current input.

When the amplitude of the direct current input is small, $I_{\mu} = 0.5$ nA cm^{-2}, and there is a moderate amount of variation over cells, coefficient of variation $CV_{cells} = 10$ %, networks in which the GABA-synaptic reversal potential was hyperpolarizing ($E_{syn} = -75$ mV) show only weak synchronization (Figure 3A, left). Shunting GABA-synapses ($E_{syn} = -57$ mV), on the other hand, result in a strongly synchronized network (Figure 3A, right). Additionally, for the shunting inhibition, all cells in the network fire exactly once per gamma cycle, while the strongly hyperpolarizing reversal potential of $E_{syn} = -75$ mV causes the strongly excited cells to silence out the more weakly excited ones (Kopell & Ermentrout, 2004).

Spectral analyses of spike histograms revealed only a moderate peak around 23 Hz (and higher harmonics) for a synaptic reversal potential of $E_{syn} = -75$ mV (Figure 3B, top), while a strong peak at the gamma frequency of 60 Hz can be observed for a synaptic reversal potential of $E_{syn} = -57$ mV (Figure 3B, bottom).

To assess the effect of synaptic reversal potential on network synchronization in a more general sense, we employed two different measures of network synchrony: network coherence K (Wang and Buzsáki, 1996; see equation 11) and average volley peak height λ (see equation 13). As expected, these yield highly similar results, as revealed by correlation analysis ($r = 0.99$; $p<0.0001$). K and were consistently high with homogeneous drive ($CV_{cells} = 0$ %; Figure 3C, first column within each plot), and decreased with increasing heterogeneity (Figure 3C, x-axis of plots).

As reported previously by other authors (Vida et al., 2006), the rate of decrease with heterogeneity was dependent upon the reversal potential of the GABA-ergic synapses. Specifically, with a small drive of $I_{\mu} = 0.5$ nA cm^{-2}, coherent oscillations ($K \geq 0.15$) only occurred at heterogeneity levels of $CV_{cells} \leq 10$ % when synapses were hyperpolarizing ($E_{syn} = -75$ mV), while shunting inhibition ($E_{syn} = -55$ mV) resulted in coherent oscillations up to $CV_{cells} \leq 60$ % of heterogeneity (Figure 3C, left).

Interestingly, and to our knowledge not previously reported, the most robust synaptic reversal potential (i.e., the value of E_{syn} that results in coherent network synchronization up to the highest level of drive heterogeneity) changed when the amplitude of

[4] We will use the term 'theta fibres' to refer to the projections from the theta-modulated Poisson spike trains to the cells of our model network. We do not wish to imply that there are anatomically identifiable fibres running from the hippocampus to the neocortex that are dedicated exclusively to the propagation of the theta rhythm.

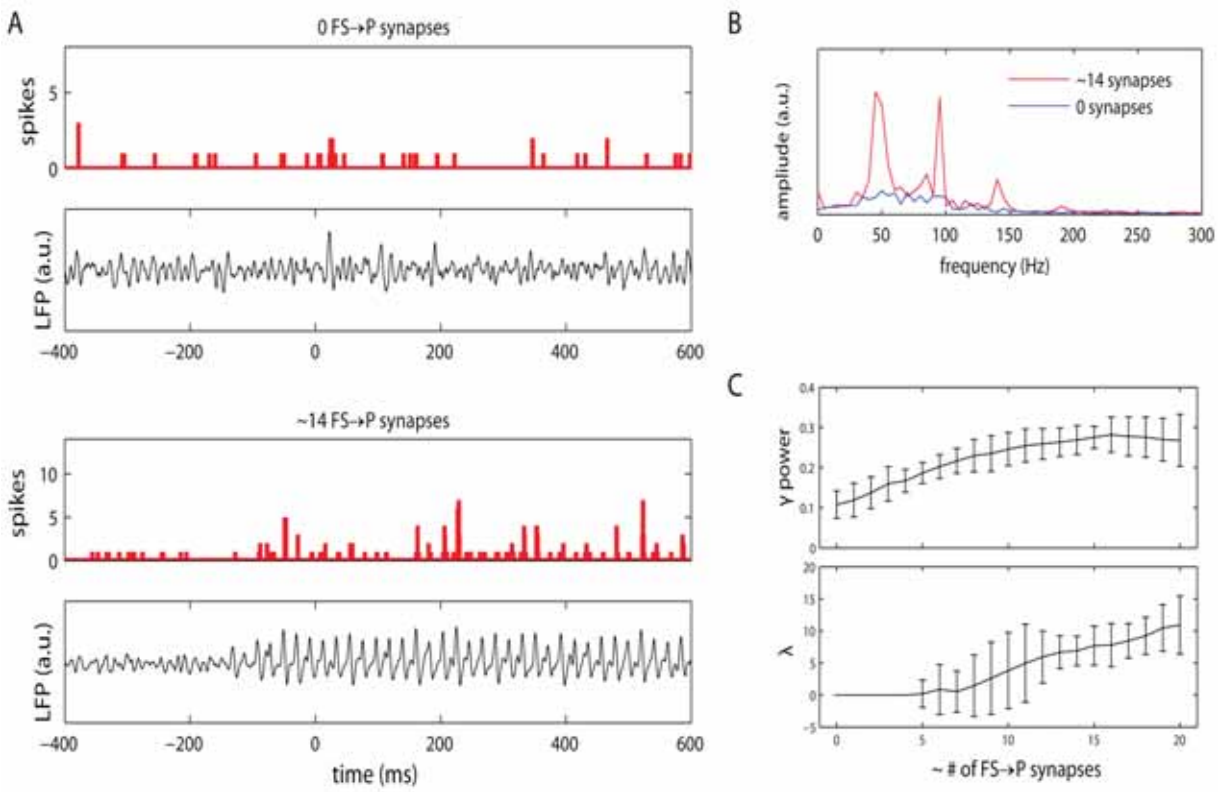

Figure 4. Pyramidal cells show gamma-synchronized activity when cells receive shunting inhibition. **A.** Spike histograms and simulated LFP traces for the unconnected (0 synapses per P-cell) and connected (14 synapses per P-cell) conditions. Input to the P-cells consisted of constant-rate Poisson spike trains. **B.** Amplitude spectra for the simulated LFP in the connected (red) and unconnected (blue) conditions. The LFP spectrum for the connected condition shows a clear increase in power in the gamma band (30–80 Hz). **C.** Relative gamma band power (top) and pyramidal cell network synchronization (bottom) as a function of the average number of GABA-ergic projections from the FS cells to a single P-cell. Relative gamma power increases steadily with number of synapses, reaching a maximum at ≥ 15 synapses per P-cell. Network synchronization starts to occur at ≥ 5 synapses per P-cell. Shown are the mean values for 30 simulation runs; error bars represent 95 % confidence interval.

the input current was varied: for a drive of I_μ = 1.0 nA cm^{-2}, optimally robust oscillations (up to $CV_{cells} \leq 30$ %) still occurred at E_{syn} = -55 mV, but when the drive was further increased to I_μ = 1.5 nA cm^{-2}, network synchronization was most robust at E_{syn} = -57 mV (again, up to $CV_{cells} \leq 30$ %; Figure 3C, third column of plots). At I_μ = 2.0 nA cm^{-2}, the optimum reversal potential for synchronization was E_{syn} = -59 mV (synchronization up to $CV_{cells} \leq 20$ %; Figure 3C, right-most column of plots).

This phenomenon of optimum reversal potential shifting towards more negative values with increasing external input current likely reflects the important role of strong mutual inhibition between the FS cells in the generation of the gamma rhythm. When the input current is strong, the FS cells become strongly excited, and the inhibition balancing this excitation is not strong enough when the synaptic reversal potential is relatively high. This allows some cells to fire out of phase with the gamma rhythm. Lower synaptic reversal potentials, on the other hand, result in sufficiently strong inhibition to silence out any 'rogue' cells during the interval between population spike peaks. Note that the optimum reversal potential, although varying with input current amplitude, was still always within the shunting range ($E_{syn} \geq E_{rest}$).

The optimum reversal potential seemed to continue to shift for even higher values of I_μ>2.0 nA cm^{-2}, but, starting at I_μ = 2.5 nA cm^{-2}, the percentage of active cells in the network and dependence of network coherence on drive variation started to decrease markedly (data not shown).

3.3 Pyramidal cell network gamma oscillations by interneuron shunt

The previous section has shown that gamma synchronization does indeed occur in a ring of fast-spiking inhibitory interneurons. This raises the question whether this mechanism is sufficient to drive gamma oscillations in a network of pyramidal cells.

To address this question, we investigated the behavior of a network of 30 x 30 = 900 pyramidal cells. The P cells were synaptically coupled to a subset of the other pyramidal cells (see section

2.2). Additionally, they received incoming synapses from input fibres, and projected to the fast-spiking cells. Each pyramidal cell received a variable number of incoming GABA-ergic synapses from the fast-spiking cells (see section 2.3).

First, we analyzed the spike timings of the pyramidal cells. When the pyramidal cell subnetwork only received constant-rate Poisson spike train input (see section 2.3) and did not receive shunting inhibition, a non-synchronized activity pattern was observed (Figure 4A, top spike histogram). When the fast-spiking cells projected to the pyramidal cells, however, the latter tended to synchronize in a gamma rhythm (Figure 4A, bottom spike histogram). The gamma synchronization of the pyramidal cells involved a much smaller portion of cells than that of the fast-spiking cells: for the simulation shown, the maximum proportion of cells active in a single 1 ms time window was 1 % for the pyramidal cells and 63 % for the fast-spiking cells (compare Figures 3A, right bottom spike histogram, and 4A, bottom spike histogram).

Apart from the spike timings, as shown by the histograms, we also analyzed the electrical activity of the pyramidal cells, as measured by the simulated local field potential (LFP; see equation 14). The simulated LFP traces are shown in Figure 4A, below the spike histograms. The simulated LFP shows irregular oscillations for the condition in which the pyramidal cells do not receive shunting inhibition from the fast-spiking cells (Figure 4A, top). However, when the GABA-ergic projections from the FS-cells to the P-cells are active, the simulated LFP shows a regular oscillatory pattern (Figure 4A, bottom).

This effect is evident even more clearly from the LFP amplitude spectra (Figure 4B): the spectrum for the connected condition (red) shows a marked increase in gamma-band power over the unconnected condition (blue). In particular, a peak around 49 Hz can be observed. Note that this frequency is somewhat different from that reported in section 3.2. This is because the net total input to the interneuron subnetwork was somewhat different for the present analyses (i.e., Poisson spike train projections) than it was for the analyses presented in section 3.2 (i.e., direct current input; see section 2.3 for details). We used Poisson spike trains because we believe them to be a more realistic model of actual neuronal input than a direct current. The results presented in the previous section were based on a direct current input because this allows a better comparison with the work of Vida et al. (2006).

To determine the amount of GABA-ergic shunting needed for the pyramidal cells to synchronize in a gamma rhythm, we systematically varied the average number of projections from the fast-spiking interneuron subnetwork to each pyramidal cell. The relative power in the gamma band (30–80Hz) of the simulated LFP steadily increased with the number of synapses, and reached a plateau at around $\geq$15 synapses per cell (Figure 4C, top). The network remained in an unsynchronized state for up to $\leq$ 7 synapses per cell, and network synchronization increased steadily above this threshold (Figure 4C, bottom).

The continuity in rise of the relative gamma power with respect to number of synapses, when contrasted with the initial zero-valued plateau that was observed for the synchronization, is explained by the fact that the LFP is primarily a measure of post-synaptic potentials (PSPs): for a small, but non-zero connection strength between a network synchronized at a gamma frequency (i.e., the FS cells) and the network of interest (i.e., the P-cells), the PSPs will also oscillate, albeit with a small amplitude, at gamma frequency. This will not be reflected in the spiking activity and, consequently, not be observed as network synchronization, unless the synchronized PSPs are sufficiently strong to have an effect that is comparable to the cells' spike threshold.

3.4 Theta modulation of spike times

To investigate the influence of ascending hippocampal fibres, carrying a theta rhythm, on the spike times of neocortical fast-spiking and pyramidal cells, we supplied our model network with variable-rate Poisson spike trains, in addition to the constant-rate background input already present. These 'theta fibres'[4] varied their firing frequency according to a sinusoid oscillating at a theta frequency of $f_\theta = 4$ Hz (see equation 10; this particular frequency was chosen to correspond to observed theta frequencies in anaesthetized rats (Sirota et al., 2008)). Each fast-spiking cell received, on average, 20 incoming

[5] Note that the data histograms in Figure 8B do not directly correspond to a single 'arm' of the polar phase/amplitude histograms shown in Figure 8A. To obtain the distributions most accurately corresponding to the two theta extremes, bins for 8B were centered at either the theta peak or trough, while the theta peak and trough correspond to a bin edge for 8A.

[6] We used gamma distribution fits for our amplitude data because we wanted to be able to compare our results with Canolty et al. (2006). The distribution we observed, however, seems to correspond more to a bimodal distribution (also visible as two concentric rings of higher distribution density in all four plots of Figure 8A).

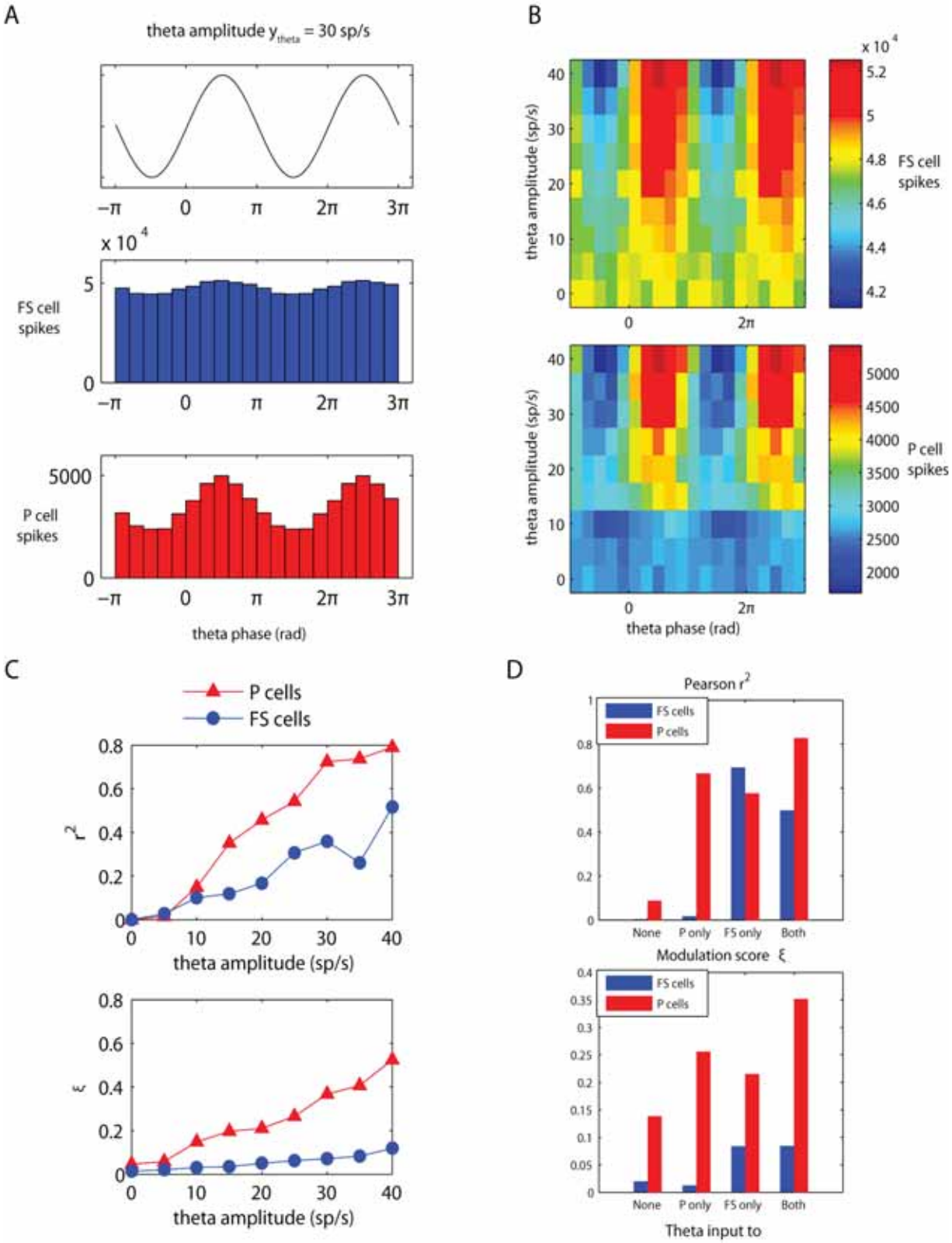

Figure 5. Theta modulation of fast-spiking and pyramidal cell spike times. Fast-spiking cells received, on average, twice as many theta-modulated input synapses as the pyramidal cells, which, relative to the total input, is even four times as many (see main text for details). **A.** Spike histograms for the fast-spiking (blue, middle) and pyramidal (red, bottom) cells relative to theta phase. The amplitude of the incoming theta rhythm was set to y_0 = 30 sp/s (see equation 10). Histogram bin size is 25 ms. Above the spike histograms, a 'cartoon plot' of the theta rhythm is shown. **B.** Spike counts (color code) relative to theta phase (x-axis) for the fast-spiking (top) and pyramidal (bottom) cells as a function of theta amplitude y_0 (y-axis). Again, spike count bin size is 25 ms and bins were non-overlapping. **C.** Two different measures of theta modulation of spike times: Pearson's r^2 (top) and relative modulation amplitude ξ (bottom; see equation 17) as a function of incoming theta amplitude y_0. **D.** The same two measures as a function of theta input distribution.

synapses from these variable-rate fibres, while each pyramidal cell received, on average, 10 (see section 2.3 for details).

An analysis of the spike times of the fast-spiking and pyramidal cells revealed that the number of spikes (in 25 ms bins) occurring at the peak of the theta rhythm is larger than the number of spikes occurring at the theta trough (Figure 5A). This finding holds for both cell populations, and is presumably due to the modulation of net excitation experienced during the theta cycle (the role of 'coincidence detection'-like phenomena in the increased number of spikes during theta peaks is probably negligible; P cell time constant is around 6 - 7 ms). Furthermore, theta modulation of spike times increases with increasing theta input amplitudes (Figure 5B).

3.4.1 Differential modulation of pyramidal and fast-spiking cells

The theta modulation of pyramidal cells was much stronger than that of the fast-spiking cells (Figure 5A and B). This finding is remarkable, since the fast-spiking cells receive, on average, twice as many incoming theta-modulated synapses as the pyramidal cells (20 vs. 10), and even four times as many when the ratio of theta-modulated to constant-rate fibres is taken into account (FS: 20/50; P: 10/100; see section 2.3 for details). The resulting differential theta-modulation is in accordance with physiological findings (Sirota et al., 2008).

In order to quantify this difference, we computed two measures of theta modulation: Pearson's r^2, computed between the raw theta signal and the aggregated spike histograms; and our modulation score ξ, as described by equation 17. Indeed, plots of these measures confirm that the theta modulation of the pyramidal cells is consistently higher than that of the fast-spiking cells (Figure 5C). For a theta modulation amplitude of $y_\theta = 30$ sp/s, the parameter setting used for Figure 5A, the relevant values were $r^2_{FS} = 0.358$; $r^2_P = 0.724$; $\xi_{FS} = 0.072$; $\xi_P = 0.367$.

An explanation for the much stronger theta-modulation of spike activity of the P cells, when compared to the FS cells, can be found in the different response of both subpopulations to differing levels of input (Figure 6; see also section 3.1 and Figure 2). The FS cells show a reasonably flat response to increasing input after an initial strong rise, whereas the P cells show a very steep, exponential response. For a theta input amplitude of $y_\theta = 30$ sp/s, the spike rate of the theta-modulated input fibres varies between $A_{\theta,trough} = 10$ sp/s and $A_{\theta,peak} = 70$ sp/s. Consequently, the average total input (the sum of the constant-rate input and the theta-modulated input) experienced by a single FS cell varies between 50 * 40 + 20 * 10 = 2200 and 50 * 40+20 * 70 = 3400 sp/s. The average total input experienced by a single P cell varies between 100 * 40+10 * 10 = 4100 and 100 * 40+10 * 70 = 4700 sp/s. These values correspond to the vertical lines in Figure 6. Evident from this figure is the relatively much larger y-axis range corresponding to these input values for the P cells, when compared to the FS cells. This explains why the theta-modulation of P cell activity is so strong, even though the FS cells receive a much more strongly theta-modulated input.

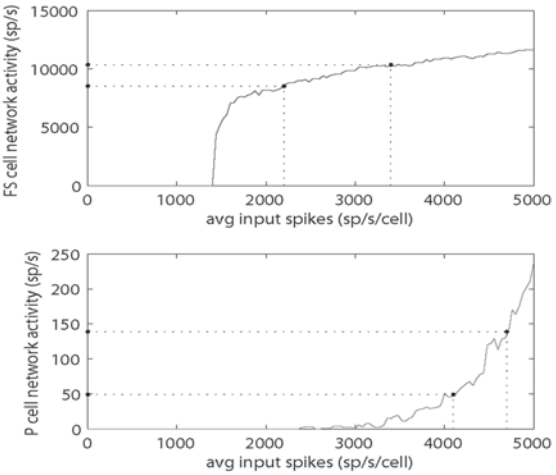

Figure 6. Differential effect of theta-modulated input on both cell subpopulations. Shown are the frequency/input curves also presented in Figure 2. Dotted lines perpendicular to the x-axis represent the total range of spike train input experienced by the subnetworks due to the theta-modulated input fibres. Dotted lines perpendicular to the y-axis represent the resulting subnetwork spike activity. While the theta-modulation of input spikes is stronger for the FS cells than for the P cells, the resulting difference in subnetwork spike activity is greater for the P cells, a can clearly be observed from the intersection of the horizontal lines with the y-axis.

3.4.2 Effect of theta input to different subnetworks

In the above-mentioned simulations and analyses, theta-modulated input, when present, was always presented to both subnetworks of our model network. We also investigated the effect of theta-modulated input to each of the subnetworks separately.

In Figure 5D, results for these simulations are shown. As is clear from these graphs, the spiking activity of the pyramidal cells is theta-modulated when either (or both) of the two subnetworks receives theta-modulated input. The spiking activity of the

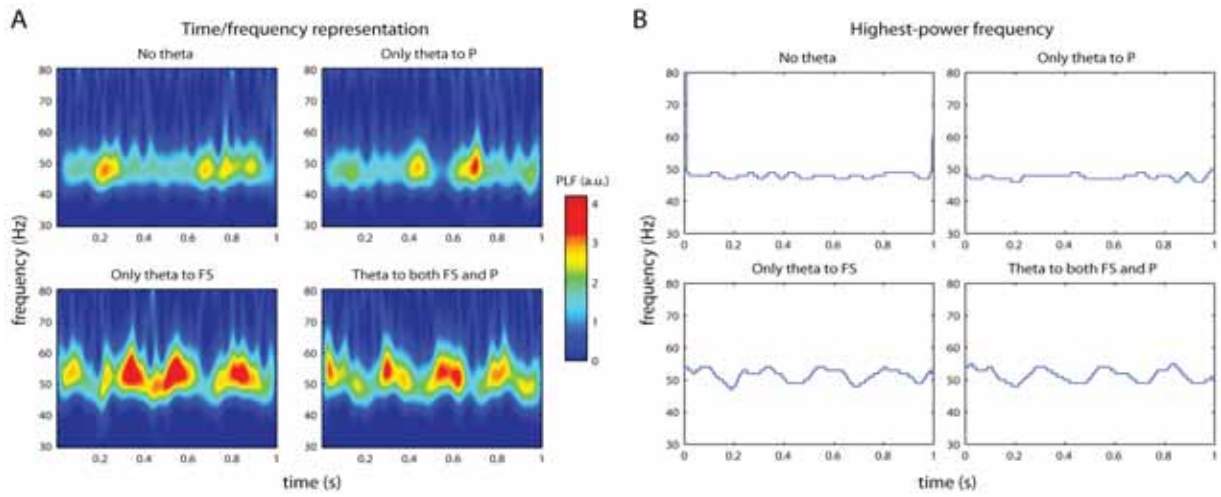

Figure 7. Effect of theta-modulated input on LFP gamma frequency. **A.** Time-frequency representations of one second of pyramidal cell LFP activity. Different plots correspond to theta-modulated input fibres projecting to different parts of the model network. **B.** Highest-power frequencies for the time-frequency representations shown in A. Theta phase/gamma frequency coupling can be observed when the FS cells receive theta-modulated input.

fast-spiking cells, however, is only theta-modulated when they directly receive theta-modulated input, irrespective of whether the pyramidal cells receive theta-modulated input or not.

This finding is easily explained by noting that (1) the FS cells show a flat input response curve (as mentioned previously), thereby requiring a large change in input for a small change in activity, and (2) the overall spiking activity of the P cells is very low, when compared to the FS cells or the input spike trains. When only the P cell subnetwork receives theta-modulated input, this will be reflected in the spiking activity of this subnetwork (as evident from Figure 5D). The P cell subnetwork activity is still very low, however, when compared to the total input to a single FS cell, coming from other FS cells and input spike trains. Therefore, the theta-modulated P cell activity will not have a large enough impact on the FS cells to be noticeable in their spiking activity.

3.5 Theta modulation of LFP gamma activity

The previous section has shown that the spiking activity of the pyramidal and fast-spiking cells is theta-modulated when these subnetworks are presented with theta-modulated input spike trains. Additionally, it was shown that pyramidal cell activity is theta-modulated if either the pyramidal cells themselves or the fast-spiking cells receive theta-modulated input, while fast-spiking cell activity is only theta-modulated when they directly receive theta-modulated input.

This raises the following two interrelated questions. First, is the LFP gamma activity, caused by the FS cell shunting inhibitory synapses on the P cells (see section 3.3), also theta-modulated? And second, if a theta/gamma coupling can be observed, which theta-modulated input fibre projections are necessary and, therefore, presumably responsible, for this coupling?

3.5.1 Gamma frequency modulation by theta phase

To answer these questions, we recorded simulated LFP from our model network in four different conditions: no theta input, theta input only to the P cells, theta input only to the FS cells, or theta input to both subnetworks. Time-frequency representations for 1 s of these recordings are shown in Figure 7A. Clearly visible in all four conditions are bands of spectral power in the gamma range, mostly around 50 Hz.

To determine whether a phase/frequency coupling between the incoming theta signal and the gamma LFP occurred in our network, we plotted the highest-power frequency from the above-mentioned time-frequency representations as a function of time (Figure 7B). As evident from these plots, the highest-power gamma frequency varied with the theta rhythm only when the FS cells received theta-modulated input.

3.5.2 Gamma amplitude modulation by theta phase

To determine whether gamma amplitude is modulated by theta phase, we computed a composite theta phase/gamma amplitude signal

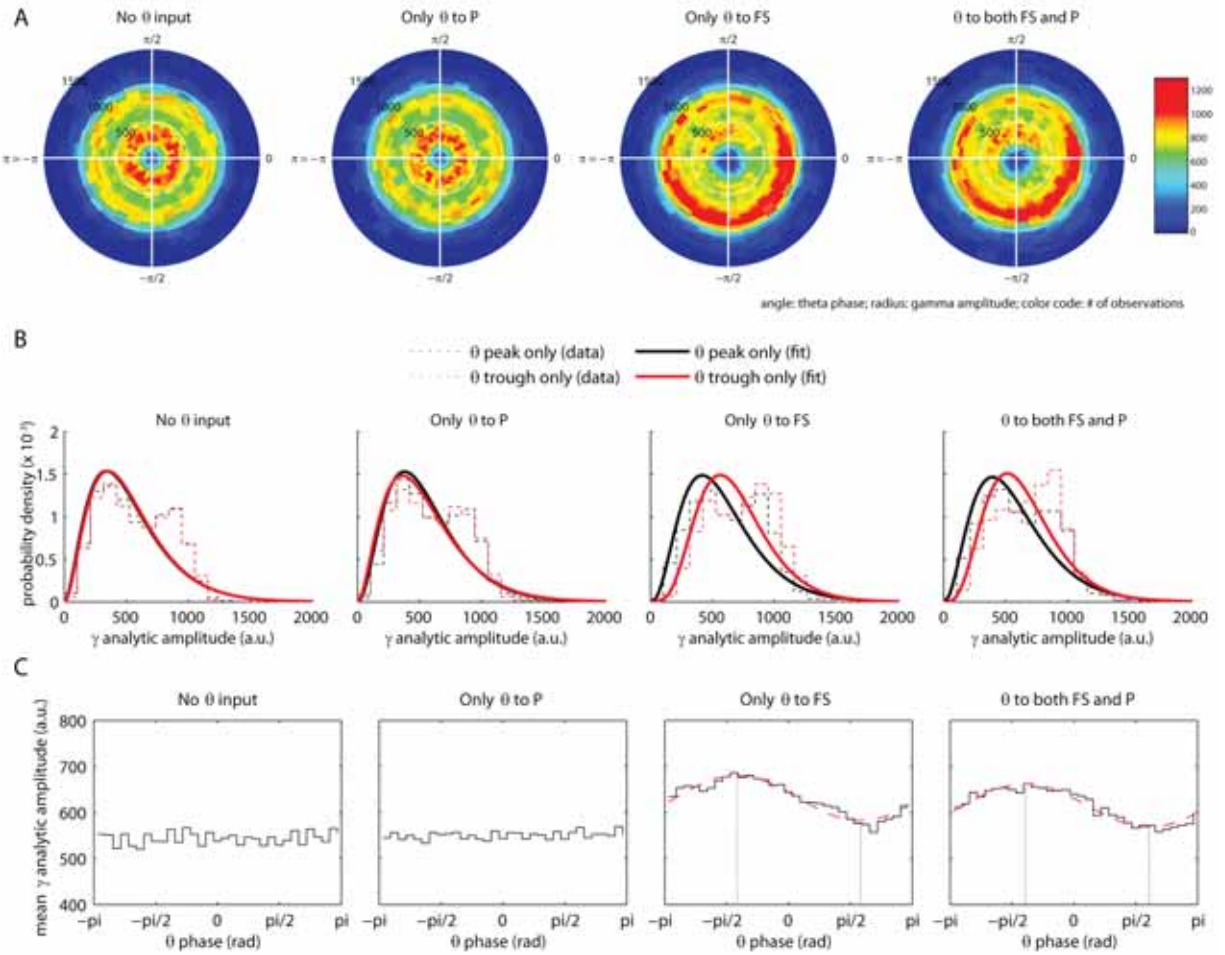

Figure 8. Effect of theta-modulated input on LFP gamma amplitude. **A.** The distribution of a composite theta phase/gamma amplitude signal z(t) (see section 2.4.5) in the complex plane. Color code represents the number of observations; angle corresponds to theta phase (divided into 32 equal-sized bins); radius corresponds to gamma amplitude (divided into 32 equal-sized bins). **B.** Histograms of gamma amplitudes occurring in $2\pi/32$ wide phase bins centered at the peak of the theta rhythm ($\varphi\theta = \pi/2$; black) and at the trough ($\varphi\theta = -\pi/2$; red). Dashed lines correspond to the observed data histograms; solid lines represent the best-fit gamma distribution for this data. When FS cells receive theta-modulated input, the best-fit distribution for the theta trough is shifted to the right, compared to the distribution for the theta peak (parameter differences are significant, $p < 0.0001$). **C.** Mean gamma amplitudes as a function of theta phase. For the two rightmost plots, the best-fit sine functions are shown with a dashed red line. Gamma amplitudes are higher at the trough than at the peak of the theta rhythm, and the lowest and highest gamma amplitudes (indicated with dotted vertical lines) occur somewhat after the theta peak and trough, respectively.

z(t). Theta phase is distributed uniformly, since the theta rhythm is generated according to a simple sine function. Therefore, clustering of z(t) in the complex plane (resulting in a radially asymmetric distribution around the origin) is an indication of phase/amplitude coupling (see section 2.4.5 for details). Distributions of z(t), for each of the four theta input conditions, are shown in Figure 8A. z(t) is distributed uniformly with respect to theta phase when only the P cells receive theta-modulated input. However, when the FS cells receive theta-modulated input, the distribution is clearly non-uniform.

To get a more detailed view of the nature of theta phase/gamma amplitude coupling, we investigated the distribution of gamma amplitudes a_γ at just the peaks and troughs of the theta rhythm (the phase used is sine phase, so a peak is at $\varphi_\theta = \pi/2$ and a trough is at $\varphi_\theta = -\pi/2$). Shown in Figure 8B are these distributions for each of the four theta input conditions[5]. The solid lines in this figure correspond to the best-fit gamma distributions[6] of gamma amplitudes for the theta trough (red) and the theta peak (black). The best-fit distribution is shifted to the right, compared to the distribution for the theta peak, when the FS cells receive theta-modulated input. The differences between the distribution parameters are significant ($p<0.0001$). This indicates that gamma amplitude is higher at the theta trough than at the theta peak; a finding that is in accordance with physiological findings in humans (Canolty et al., 2006).

Finally, to get a quick 'bird's eye' view of the

coupling between theta phase and gamma amplitude, we divided theta phase into 32 bins and computed the mean gamma amplitude for each of these bins. Plots of these data (Figure 8C) clearly show that, when the FS cells receive theta-modulated input, gamma amplitudes are higher at the trough than at the peak of the theta rhythm. The lowest and highest gamma amplitudes occur somewhat after the theta peak and trough, respectively. More specifically, the extremes in gamma amplitudes lag behind the (opposite) theta extremes by 0.26 rad (for the FS only condition) or 0.34 rad (for the FS+P condition). These values correspond to delays of 10.36 and 13.54 ms.

4. Discussion

We have put forward a biophysical neural network model, composed of fast-spiking (FS) and pyramidal (P) cells, that displays robust gamma oscillations. When supplied with hippocampal theta-modulated input fibres, the model network shows spike activity that is biased by the theta rhythm. Furthermore, local field potential (LFP) gamma oscillations are modulated by the phase of the theta rhythm, both concerning frequency and amplitude. However, this latter phenomenon only occurs when the FS cells directly receive hippocampal theta-modulated input, highlighting the crucial role these cells play in the interplay between neocortex and hippocampus.

4.1 Gamma synchronization and oscillations

When studied in isolation, our subnetwork of FS cells, coupled with fast inhibitory synapses and gap junctions, shows synchronized activity at a gamma frequency. For GABA-ergic synapses with a hyperpolarizing reversal potential, this synchronization quickly dissipates with increasing heterogeneity of the input drive. For shunting reversal potentials, however, the network remains robustly synchronized for relatively high levels of drive variation. This finding is a replication of earlier work (Vida et al., 2006, Bartos et al., 2007).

The optimally robust synaptic reversal potential for the gamma synchronization of the FS cells was dependent upon mean input drive. For relatively weak input currents, the optimal reversal potential lay at relatively high levels. With stronger input currents, the optimal reversal potential shifted towards more negative values. This phenomenon likely reflects the important role of strong mutual inhibition between the FS cells in the generation of the gamma rhythm (Wang & Buzsáki, 1996). When the input current is strong, the FS cells become strongly excited, and the inhibition balancing this excitation is not strong enough when the synaptic reversal potential is relatively high. This allows some cells to fire out of phase with the gamma rhythm. Lower synaptic reversal potentials, on the other hand, result in sufficiently strong inhibition to silence out any 'rogue' cells during the interval between population spike peaks.

The FS cells proved effective in imposing their synchronized rhythm on a population of P cells. When the FS cell subnetwork was coupled to the P cell subnetwork, the LFP quickly became dominated by the GABA-ergic post-synaptic potentials caused by the FS cells' spiking activity. This resulted in an increase in LFP power in the gamma band and in an increased synchronization of the P cells' spike timings.

Both LFP gamma band power and P cell gamma synchronization steadily increased as a function of connection strength between the two subnetworks. However, P cell gamma synchronization only occurred above a certain connection strength threshold; below this value, no synchronization was observed. This can be explained by noting that the LFP is primarily a measure of post-synaptic potentials (PSPs): for a small, but non-zero connection strength between a network synchronized at a gamma frequency (i.e., the FS cells) and the network of interest (i.e., the P-cells), the PSPs will also oscillate, albeit with a small amplitude, at gamma frequency. This will not be reflected in the spiking activity and, consequently, not be observed as network synchronization, unless the synchronized PSPs are sufficiently strong to have an effect that is comparable to the cells' spike threshold.

4.2 Effect of theta-modulated input

4.2.1 Modulation of spike times

When our model network received not only constant-rate input, but also input from theta-modulated hippocampal afferent fibres, its spiking activity reflected the theta rhythm. Both the FS cells and the P cells fired more often during the peak of the theta rhythm than during its trough. The amount of theta modulation of spike activity was strongly related to the amplitude of the incoming theta oscillations: stronger modulation occurred for higher theta amplitudes.

The P cells were consistently more strongly theta-modulated than the FS cells, a finding that

is in accordance with physiological studies in animals (Sirota et al., 2008). An explanation for this difference in modulation strength can be found in the different response of both subpopulations to differing levels of input, as seen in Figure 6. Evident from this figure is the relatively much larger y-axis range corresponding to the input amplitude for the P cells, when compared to the FS cells. This explains why the theta-modulation of P cell activity is so strong, even though the FS cells receive a much more strongly theta-modulated input.

The spiking activity of the P cells was theta-modulated when either, or both, of the two subpopulations received theta-modulated input; the spiking activity of the FS cells was theta-modulated only when they directly received theta-modulated input. A theta-modulated input only to the P cells did not affect the FS cell spiking activity. This finding is easily explained by noting that (1) the FS cells show a flat input response curve (see Figures 2 and 6, upper panels), thereby requiring a large change in input for a small change in activity, and (2) the overall spiking activity of the P cells is very low, when compared to the FS cells or the input spike trains. When only the P cell subnetwork receives theta-modulated input, this will be reflected in the spiking activity of this subnetwork (as evident from Figure 5D). The P cell subnetwork activity is still very low, when compared to the total input to a single FS cell, coming from other FS cells and input spike trains. Therefore, the theta-modulated P cell activity will not have a large enough impact on the FS cells to be noticeable in their spiking activity.

4.2.2 Modulation of gamma oscillations

Theta-modulated input to our model network also had an effect on the gamma oscillations visible in the LFP. Both the frequency and the amplitude of the gamma oscillations were modulated by the phase of the theta rhythm, but only when the FS cells directly received a theta-modulated input. Theta/gamma coupling was completely absent, both concerning frequency and amplitude, when only the P cells received theta-modulated input, even though the P cells' spiking activity was theta-modulated in this condition (see section 3.4.2). This can be explained by noting the fact that the gamma rhythm is generated by the FS cells and imposed upon the P cell subnetwork by these cells. It follows easily that, when the activity of the FS cells is not theta-modulated (as it is not, when these cells do not directly receive theta-modulated input), the gamma rhythm, as observed in the LFP, is not theta-modulated.

The frequency of the gamma rhythm was higher during the peak of the theta rhythm than during the trough. The gamma rhythm is generated by the FS cells; during the theta peaks these experience a stronger net total input, therefore increase their firing rate while remaining synchronized, hence resulting in a higher frequency of the corresponding gamma oscillations.

The analytic amplitude of the LFP gamma oscillations was also influenced by the phase of the incoming theta rhythm. Gamma amplitude was higher during the trough than during the peak of the theta rhythm, a phenomenon that has also been found in humans (Canolty et al., 2006). The highest gamma amplitude occurred somewhat after the theta trough and the lowest gamma amplitude occurred somewhat after the theta peak.

The mechanisms by which the amplitude of gamma oscillations is actually highest during the periods of least net total input to the network are not entirely clear to us. Canolty et al. (2006) found a similar phase/amplitude coupling between the theta and gamma rhythms, both measured in the human neocortex. As to the mechanism of this coupling, they hypothesize that "basal forebrain cortical-projecting GABAergic neurons (…) preferentially synapse onto intracortical GABAergic neurons (…), with disinhibitory spike bursts causing a brief increase in gamma power at the theta trough" (Canolty et al., 2006, p. 1628).

While the basal forebrain (BF) GABA-ergic neurons probably indeed play a role in the modulation of neocortical networks (Lin, Gervasoni, & Nicolelis, 2006), our present results suggest that they are not responsible for the coupling between theta phase and gamma amplitude. We were able to reproduce such a coupling using only excitatory (glutamatergic) fibres to carry the theta rhythm. Of course, this does not directly preclude the alternative hypothesis (i.e., the BF GABA-ergic neurons playing the crucial role), but we believe this alternative to be unlikely for the following reason. The gamma oscillations visible in the EEG and LFP are mainly due to post-synaptic potentials in the pyramidal cells resulting from spike events in intracortical GABA-ergic fast-spiking cells. If the latter cells receive inhibition (e.g., from BF GABA-ergic neurons), the result would be a weakening of the gamma oscillations, and not an increase in amplitude. Therefore, we believe that excitatory, rather than inhibitory, projections to the FS cells are responsible for the modulation of gamma amplitude by theta phase.

4.2.3 Dependence of the results on FS/P-differential theta input strengths

Physiological data suggests that the projections from the hippocampus to neocortical networks are stronger to interneurons than to pyramidal cells (Tierney et al., 2004, Gabbott et al., 2002). We incorporated this difference into our model by supplying the FS cells with a more strongly theta-modulated input than the P cells, yielding the results described above. We highlighted the crucial role the FS cells play in the coupling between the theta and gamma rhythms. An additional simulation, in which we switched the two theta-modulated input strengths (i.e., in which the input to the P cells was more strongly theta-modulated than the input to the FS cells), resulted in the same outcome: a coupling between the theta and gamma rhythms only occurred in the two conditions in which the FS cells received theta-modulated input (results not shown). Therefore, the crucial role played by the FS cells is not dependent on them receiving more strongly theta-modulated input than the P cells.

4.2.4 Application of our model to other theta/gamma coupling phenomena

Oscillations in the hippocampus are by no means limited to the theta band. Hippocampal gamma oscillations are prominently observable as well, and they show clear interactions with the hippocampal theta rhythm (Bragin et al., 1995, Buzsáki & Draguhn, 2004). Furthermore, it is known that the theta-modulated input to the hippocampus from the medial septum-diagonal band of Broca (MS-DBB) is crucial for the hippocampal theta rhythm (Stewart & Fox, 1990), even though its contribution is less direct than has traditionally been assumed (Buzsáki, 2002). Therefore, it seems possible that our model of hippocampal theta/neocortical gamma coupling could be adapted to describe the hippocampal theta/gamma-nesting, observed as a result of theta-modulated MS-DBB-input fibres to the hippocampus, as well.

However, at present, our model is not applicable to this phenomenon. The 'theta-carrying' fibres from the MS-DBB to the hippocampus most likely project with hyperpolarizing inhibitory synapses (Buzsáki, 2002). If we change our model to employ inhibitory, rather than excitatory, theta-carrying fibres, the result would either be a negative correlation between the theta and gamma rhythm, or a disruption of the gamma rhythm altogether. Empirical studies show that, in the hippocampus, theta activity is positively correlated with gamma activity (Bragin et al., 1995). Therefore, our model does not seem to apply.

The model could, presumably, be changed more substantially in order to account for this phenomenon; for instance by employing a different model of gamma rhythm generation (e.g., Whittington, Traub, Kopell, Ermentrout, & Buhl, 2000). Note, however, that such a change would mean that our model is no longer applicable to the coupling of hippocampal theta and neocortical gamma that the present article is concerned with; the model would be an altogether different one. This is no surprise, of course, since the mechanisms of theta-projection from the MS-DBB to the hippocampus are different from the mechanisms by which the hippocampus relays its theta rhythm to the neocortex. It would, nevertheless, be highly interesting to see if such a project (i.e., the adaptation of our model to nested hippocampal theta and gamma) can successfully be attempted.

References

Bartos, M., Vida, I., Frotscher, M., Geiger, J. R. P., & Jonas, P. (2001). Rapid signaling at inhibitory synapses in a dentate gyrus interneuron network. Journal of Neuroscience, 21(8), 2687.

Bartos, M., Vida, I., Frotscher, M., Meyer, A., Monyer, H., Geiger, J. R. P., . (2002). Fast synaptic inhibition promotes synchronized gamma oscillations in hippocampal interneuron networks. Proceedings of the National Academy of Sciences, 99(20), 13222–13227.

Bartos, M., Vida, I., & Jonas, P. (2007). Synaptic mechanisms of synchronized gamma oscillations in inhibitory interneuron networks. Nature Reviews Neuroscience, 8(1), 45–56.

Bragin, A., Jando, G., Nadasdy, Z., Hetke, J., Wise, K., & Buzsaki, G. (1995). Gamma (40-100 hz) oscillation in the hippocampus of the behaving rat. Journal of Neuroscience, 15, 47–60.

Buhl, E. H., Cobb, S. R., Halasy, K., & Somogyi, P. (1995). Properties of unitary IPSPs evoked by anatomically identified basket cells in the rat hippocampus. European Journal of Neuroscience, 7(9), 1989–2004.

Buzsáki, G. (2002). Theta oscillations in the hippocampus. Neuron, 33(3), 325–340.

Buzsáki, G., & Draguhn, A. (2004). Neuronal oscillations in cortical networks. Science, 304(5679), 1926–1929.

Canolty, R. T., Edwards, E., Dalal, S. S., Soltani, M., Nagarajan, S. S., Kirsch, H. E., . (2006). High gamma power is phase-locked to theta oscillations in human neocortex. Science, 313(5793), 1626–1628.

Chance, F. S., Abbott, L. F., & Reyes, A. D. (2002). Gain modulation from background synaptic input. Neuron, 35(4), 773–782.

Dégenètais, E., Thierry, A. M., Glowinski, J., & Gioanni, Y. (2003). Synaptic influence of hippocampus on pyramidal cells of the rat prefrontal cortex: an in vivo intracellular recording study. Cerebral Cortex, 13(7), 782–792.

Dolan, R. J., & Fletcher, P. C. (1997). Dissociating prefrontal and hippocampal function in episodic memory encoding. Nature, 388, 582–585.

Eichenbaum, H. (2000). A cortical–hippocampal system for declarative memory. Nature Reviews Neuroscience, 1, 41–50.

Fries, P. (2005). A mechanism for cognitive dynamics: neuronal communication through neuronal coherence. Trends in Cognitive Sciences, 9(10), 474–480.

Gabbiani, F., Midtgaard, J., & Knopfel, T. (1994). Synaptic integration in a model of cerebellar granule cells. Journal of Neurophysiology, 72(2), 999–1009.

Gabbott, P., Headlam, A., & Busby, S. (2002). Morphological evidence that CA1 hippocampal afferents monosynaptically innervate PV-containing neurons and NADPH-diaphorase reactive cells in the medial prefrontal cortex (areas 25/32) of the rat. Brain Research, 946(2), 314–322.

Galarreta, M., & Hestrin, S. (1999). A network of fast-spiking cells in the neocortex connected by electrical synapses. Nature, 402, 72–75.

Gibson, J. R., Beierlein, M., & Connors, B. W. (1999). Two networks of electrically coupled inhibitory neurons in neocortex. Nature, 402, 75–79.

Gray, C. M., König, P., Engel, A. K., & Singer, W. (1989). Oscillatory responses in cat visual cortex exhibit inter-columnar synchronization which reflects global stimulus properties. Nature, 338(6213), 334–337.

Gray, C. M., & Singer, W. (1989). Stimulus-specific neuronal oscillations in orientation columns of cat visual cortex. Proceedings of the National Academy of Sciences, 86(5), 1698–1702.

Harris, K. D., Henze, D. A., Hirase, H., Leinekugel, X., Dragoi, G., Czurkó, A., . (2002). Spike train dynamics predicts theta-related phase precession in hippocampal pyramidal cells. Nature, 417, 738–741.

Hines, M. L., & Carnevale, N. T. (1997). The NEURON simulation environment. Neural Computation, 9(6), 1179–1209.

Hirase, H., Leinekugel, X., Czurkó, A., Csicsvari, J., & Buzsáki, G. (2001). Firing rates of hippocampal neurons are preserved during subsequent sleep episodes and modified by novel awake experience. Proceedings of the National Academy of Sciences, 98(16), 9386.

Hodgkin, A. L., & Huxley, A. F. (1952). A quantitative description of membrane current and its applications to conduction and excitation in nerve. The Journal of Physiology, 117, 500–544.

Jones, M. W., & Wilson, M. A. (2005). Phase precession of medial prefrontal cortical activity relative to the hippocampal theta rhythm. Hippocampus, 15(7), 867–873.

Kleppe, I. C., & Robinson, H. P. C. (1999). Determining the activation time course of synaptic AMPA receptors from openings of colocalized NMDA receptors. Biophysical Journal, 77(3), 1418–1427.

Kopell, N., & Ermentrout, B. (2004). Chemical and electrical synapses perform complementary roles in the synchronization of interneuronal networks. Proceedings of the National Academy of Sciences, 101(43), 15482–15487.

Lavenex, P., & Amaral, D. G. (2000). Hippocampal-neocortical interaction: a hierarchy of associativity. Hippocampus, 10(4).

Liley, D. T. J., & Wright, J. J. (1994). Intracortical connectivity of pyramidal and stellate cells: estimates of synaptic densities and coupling symmetry. Network: Computation in Neural Systems, 5(2), 175–189.

Lin, S., Gervasoni, D., & Nicolelis, M. (2006). Fast modulation of prefrontal cortex activity by basal forebrain noncholinergic neuronal ensembles. Journal of Neurophysiology, 96(6), 3209.

Logothetis, N. K. (2003). The underpinnings of the BOLD functional magnetic resonance imaging signal. The Journal of Neuroscience, 23(10), 3963–3971.

O'Keefe, J., & Burgess, N. (2005). Dual phase and rate coding in hippocampal place cells: theoretical significance and relationship to entorhinal grid cells. Hippocampus, 15(7), 853–866.

O'Keefe, J., & Recce, M. L. (1993). Phase relationship between hippocampal place units and the eeg theta rhythm. Hippocampus, 3(3), 317–330.

O'Reilly, R. C., & Norman, K. A. (2002). Hippocampal and neocortical contributions to memory: Advances in the complementary learning systems framework. Trends in Cognitive Sciences, 6(12), 505–510.

Rosene, D. L., & Van Hoesen, G. W. (1977). Hippocampal efferents reach widespread areas of cerebral cortex and amygdala in the rhesus monkey. Science, 198(4314), 315–317.

Siapas, A. G., Lubenov, E. V., & Wilson, M. A. (2005). Prefrontal phase locking to hippocampal theta oscillations. Neuron, 46(1), 141–151.

Sirota, A., Csicsvari, J., Buhl, D., & Buzsáki, G. (2003). Communication between neocortex and hippocampus during sleep in rodents. Proceedings of the National Academy of Sciences, 100(4), 2065–2069.

Sirota, A., Montgomery, S., Fujisawa, S., Isomura, Y., Zugaro, M., & Buzsáki, G. (2008). Entrainment of neocortical neurons and gamma oscillations by the hippocampal theta rhythm. Neuron, 60(4), 683–697.

Sohal, V. S., & Huguenard, J. R. (2005). Inhibitory coupling specifically generates emergent gamma oscillations in diverse cell types. Proceedings of the National Academy of Sciences, 102(51), 18638–18643.

Stewart, M., & Fox, S. (1990). Do septal neurons pace the hippocampal theta rhythm? Trends in Neurosciences, 13(5), 163–169.

Tamás, G., Buhl, E. H., Lörincz, A., & Somogyi, P. (2000). Proximally targeted GABAergic synapses and gap junctions synchronize cortical interneurons. Nature Neuroscience, 3(4), 366–371.

Tierney, P. L., Degenetais, E., Thierry, A. M., Glowinski, J., & Gioanni, Y. (2004). Influence of the hippocampus on interneurons of the rat prefrontal cortex. European Journal of Neuroscience, 20(2), 514.

Traub, R. D., Kopell, N., Bibbig, A., Buhl, E. H., LeBeau, F. E. N., & Whittington, M. A. (2001). Gap junctions between interneuron dendrites can enhance synchrony of gamma oscillations in distributed networks. Journal of Neuroscience, 21(23), 9478.

Venance, L., Rozov, A., Blatow, M., Burnashev, N., Feldmeyer, D., & Monyer, H. (2000). Connexin expression in electrically coupled postnatal rat brain neurons. Proceedings of the National Academy of Sciences, 97(18), 10260–10265.

Vida, I., Bartos, M., & Jonas, P. (2006). Shunting inhibition improves robustness of gamma oscillations in hippocampal interneuron networks by homogenizing firing rates. Neuron, 49(1), 107–117.

Wang, X. J., & Buzsáki, G. (1996). Gamma oscillation by synaptic inhibition in a hippocampal interneuronal network model. Journal of Neuroscience, 16(20), 6402–6413.

Whittington, M. A., Traub, R. D., Kopell, N., Ermentrout, B., & Buhl, E. H. (2000). Inhibition-based rhythms: experimental and mathematical observations on network dynamics. International Journal of Psychophysiology, 38(3), 315–336.

Genetic variation of the alpha2b-adrenoceptor affects neural correlates of successful emotional memory formation

Maren Urner[1]
Supervisors: Guido van Wingen[1,2], Barbara Franke[1,3,4], Mark Rijpkema[1], Guillén Fernández[1,2], Indira Tendolkar[1,4]

[1] *Donders Institute for Brain, Cognition and Behaviour, Radboud University Nijmegen, Nijmegen, The Netherlands*
[2] *Department of Neurology, Radboud University Nijmegen Medical Centre, Nijmegen, The Netherlands*
[3] *Institute for Genetic and Metabolic Diseases, Department of Human Genetics, Radboud University Nijmegen Medical Centre, Nijmegen, The Netherlands*
[4] *Department of Psychiatry, Radboud University Nijmegen Medical Centre, Nijmegen, The Netherlands*

Enhanced memory for emotionally charged events helps us to remember potentially vital information. Although large interindividual differences in emotional memory enhancement exist, which might explain variance in vulnerability for mood disorders, little is known about their neurobiological basis. Here we show that a common deletion variant of ADRA2B, the gene coding the alpha2b-adrenergic receptor, is related to enhanced activity in the amygdala and inferior frontal gyrus during emotional memory formation, but not retrieval. Deletion carriers showed a larger differential response in these brain regions between later remembered and later forgotten stimuli than non-deletion carriers did. These results demonstrate that the ADRA2B polymorphism specifically influences mnemonic operations underlying emotional memory formation, which might contribute to the vulnerability for mood disorders.

Keywords: amygdala, emotional memory, functional MRI, mood disorders, noradrenaline, prefrontal cortex

Corresponding author: Maren Urner, University College London, Gower Street WC1E 6BT, London;
e-mail: maren.urner.09@ucl.ac.uk

1. Introduction

Enhanced memory for emotional events is a well-recognized phenomenon that has an obvious adaptive value in evolutionary terms, because it is vital to remember both dangerous and favorable situations (McGaugh, 2004). Across individuals, differences in the strength of emotional memories are associated with vulnerability to and maintenance of mood disorders (Haas & Canli, 2008). However, little is known about the neurobiological mechanisms underlying these individual differences. Recently, a functional deletion variant of three glutamic acids (residues 301–303) in the third intracellular loop of the ADRA2B gene that codes for the alpha2b-adrenoceptor (Small, Brown, Forbes, & Ligget, 2001) has been shown to affect memory for emotional experiences (De Quervain et al., 2007). Carriers of the deletion variant showed enhanced memory for emotional pictures compared to non-deletion carriers, and civil war survivors with the deletion variant re-experienced traumatic events more than non-carriers did. Taken together, these findings suggest that the deletion variant of the ADRA2B gene may affect emotional memory processing, leading to enhanced memory for emotional events.

At present, the mechanism by which the deletion variant in the ADRA2B gene influences emotional memory remains unclear; it is not known whether it leads to increases or decreases in noradrenergic signaling, and whether it affects memory formation, retrieval or both. The key brain region associated with the enhancement of memory for emotional events is the amygdala. It stimulates memory processes in other brain regions such as the hippocampus, inferior temporal cortex and prefrontal cortex (McGaugh, 2004; Cahill, Babinsky, Markowitsch, & McGaugh, 1995; Kilpatrick & Cahill, 2003; Richardson, Strange, & Dolan, 2004; Morris et al., 1998). Besides its central role for memory formation and consolidation, it is also involved in memory retrieval (Dolcos, LaBar, & Cabeza, 2005). The amygdala contributes via noradrenergic activation to emotional memory formation, but less to retrieval (Cahill, Prins, Weber, & McGaugh, 1994; Strange & Dolan, 2004; McGaugh & Roozendaal, 2002). The presynaptically located alpha2b-adrenoceptor plays an important role in the negative feedback loop of noradrenergic signaling (Eason & Liggett, 1992). In vitro studies have shown agonistic and antagonist effects of the deletion variant (Small et al., 2001), making it impossible to formulate directed predictions about the effect on noradrenergic signaling. Conversely, behavioral findings suggest that the deletion leads to increased noradrenergic signaling (De Quervain et al., 2007). Indeed, recently Rasch and colleagues (2009) showed that deletion carriers have increased amygdala responses compared to non-deletion carriers when processing emotionally negative photographs. However, they did not observe any interaction between this genetic effect on amygdala activity and memory. Therefore, we set out to investigate the influence of the variation in the ADRA2B gene on the activity in brain structures associated with both emotional memory formation and retrieval by means of functional MRI (fMRI); we focused on brain activity associated with processes underlying successful memory formation and retrieval.

Both, the behavioral data as well as the recent fMRI data of de Quervain and colleagues (2007; Rasch et al., 2009) suggest that the behavioral effects of the deletion are independent of emotional valence of the stimuli. However, other studies indicate that valence-specific effects may be larger for mood-congruent stimuli (Bower, Gilligan, & Monteiro, 1981). Moreover, Rasch and colleagues (2009) provide evidence for a neural processing bias of in particular negative stimuli in dependence of the genotype. Therefore, we used a negative mood induction procedure in combination with emotional negative and positive stimuli to explore further valence-specific memory effects. During scanning, negative mood was induced by showing negative movie clips, which was interleaved with a memory task that included pictures with either positive or negative emotional valence. The participants initially memorized those pictures while making an emotional valence decision, and subsequently performed a recognition memory test. Based on the aforementioned background, we hypothesized that deletion carriers would show higher activity in the amygdala and possibly also in connected hippocampal, inferior temporal and prefrontal regions, compared to non-deletion carriers during successful memory formation, but not retrieval, of emotional stimuli.

2. Methods

2.1 Participants

Forty-two right-handed healthy volunteers (21 male) with a mean age of 23 years (range 19 – 34) participated in the study. They were physically and mentally healthy as determined by a self-report

questionnaire, and reported no history of psychiatric or somatic diseases potentially affecting the brain. To avoid any confound due to threshold depressive symptoms, subjects were screened using the Dutch version of the standard Beck Depression Inventory (BDI-II; (Beck, Steer, & Brown, 1996)), and all had a score below 10. Data of two participants were lost because of technical failure. Moreover, data of five participants were excluded because their memory performance was at ceiling, resulting in too few miss trails for the fMRI analysis (< 10). Therefore, the reported results are based on the data of 35 participants, including 18 non-carriers (10 male) and 17 deletion carriers (8 male). In line with previous studies, heterozygous and homozygous (2 male and 2 female) deletion carriers were treated as one group (De Quervain et al., 2007). The groups did not reveal significant differences with respect to age ($t(33) = 0.2$, $P > 0.8$), gender ($X2(1)= 0.0$, $P > 0.8$), and level of education ($X2(3) = 2.1$, $P > 0.5$). To assess whether the genotype groups differed on personality traits and the experience of life events, the short version of the Dutch Temperament and Character Inventory (VTCI; (Duijsens, Spinhoven, Verschuur, & Eurelings-Bontekoe, 1999)) and the Dutch version of the List of Threatening Experiences (Brugha, Bebington, Tennant, & Hurry, 1985) were administered. No significant group differences in temperament and character as assessed by the VTCI consisting of the 7 scales novelty seeking, harm avoidance, reward dependence, persistence, self-directedness, cooperativeness and self-transcendence, were observed ($P > 0.1$). Moreover, no group differences in the number of life events ($P > 0.1$) were observed. Possible changes in mood in response to the experiment were examined by the Dutch shortened five scale version of the Profile and Mood States Questionnaire (POMS; (McNair, Lorr, & Droppleman, 1971)). Finally, to control for diurnal variation of mood, participants were scheduled between 11 a.m. and 1 p.m. (e.g. (Schmidt, Collette, Cajochen, & Peigneux, 2007)). The study was approved by the local ethics committee (CMO region Arnhem-Nijmegen, The Netherlands) and all volunteers gave written informed consent prior to participating in the study.

2.2 Negative mood induction procedure

Based on a previous study (Kernis, Greenier, Herlocker, Whisenhunt, & Abend, 1997), negative mood induction consisted of participants watching and listening to six movie clips interspersed throughout the scanning session. Clips were taken from the movie "Sophie's Choice" (1982) about the holocaust and lasted between 3:00 min and 7:30 min. Before and after each clip participants rated their current mood on a visual analogous scale (ranging from -10 to 10).

2.3 Memory paradigm

During scanning participants completed a memory task using positive and negative pictures. During study participants were asked to memorize 240 pictures in total while making a valence decision. Thereafter, subjects were required to recognize the old and reject the same amount of randomly intermixed new pictures during recognition (480 pictures in total). Participants were encouraged to make a decision between old and new, but also had the option to make an unsure decision. The pictures showed emotional scenes displaying one or more humans. 480 pictures were taken from a pool of positive and negative pictures which had been rated during a behavioral pilot study (five-point scale ranging from 'emotionally positive' to 'emotionally negative'; mean valence rating of negative pictures was ≤ 2 and mean valence rating of positive pictures was ≥ 4). Half of the pictures were taken as study items (including 120 positive and 120 negative pictures) and the other half as lures during test. This assignment was counterbalanced across the factors test phase (i.e. which half was taken as study items and which half as test items) and gender. The content of positive and negative pictures (i.e. individual or group, child or adult, male or female person(s)) was equally distributed across stimulus sets. The order of picture presentation was randomized. Pictures were presented for 0.5 s with a jittered interstimulus interval of 3.7 – 4.7 s.

2.4 Image acquisition

Data were acquired with a 1.5 T Siemens Sonata MR scanner (Siemens, Erlangen, Germany), equipped with a CP head array coil. T2*-weighted blood oxygenation level-dependent (BOLD) images were acquired using echo-planar imaging (EPI), with each volume consisting of 32 slices (voxel size: 3.3 * 3.3 * 3.5 mm3; TR = 2340 ms, TE = 35 ms, 64*64 matrix, FOV = 212 mm, FA = 90°). High resolution T1-weighted structural MR images were acquired for spatial normalization procedures (MPRAGE, TR = 2250 ms, TE = 2.95 ms, TI = 850 ms, 176 1 mm slices, 256 * 256 matrix, FOV = 256 mm).

2.5 Image analysis

Image analysis was performed with SPM5 (Wellcome Department of Imaging Neuroscience, London, UK). The first five EPI-volumes were discarded to allow for T1 equilibration, and the remaining images were realigned to the first volume. Images were then corrected for slice acquisition time, coregistered to the anatomical scan, spatially normalized to the Montreal Neurological Institute (MNI) T1 template, resampled into 2*2*2 mm3 voxels, and spatially smoothed with a Gaussian kernel of 8 mm FWHM.

Statistical analysis was performed within the framework of the general linear model. Later remembered and later forgotten stimuli were separately modeled for the study phase, while hits, misses, correct rejections and false alarms were separately modeled for the recognition phase. Furthermore, all stimuli were differentially modeled according to their valence. Stimuli with an incorrect valence decision or omission during study or with an unsure response or omission during the recognition test were included in a condition of no interest. The explanatory variables (0.5 s) were temporally convolved with the hemodynamic response function of SPM5. In addition, the realignment parameters were included to model potential movement artifacts, as was a high-pass filter (cut-off at 1/128 Hz). The data were proportionally scaled to account for various global effects, and temporal autocorrelation was modeled with an AR(1) process. The relevant parameter images contrasting each condition were entered in a random-effects mixed-model ANOVA with a nonsphericity correction. Statistical tests were family-wise error rate corrected for multiple comparisons across the entire brain ($p < 0.05$) or the search volume for regions of interests using a small volume correction (Worsley, Marrett, Neelin, Vandal, Friston, & Evans, 1996). The search volumes for amygdala, hippocampus, and left inferior frontal gyrus were anatomically defined, based on macroscopic anatomical parcellation of a canonical T1-weighted MRI scan in MNI space (Tzourio-Mazoyer et al., 2002; Maldjian, Laurienti, Kraft, & Burdettea, 2003). Peak voxels of activated clusters are reported in MNI coordinates.

2.6 Behavioral performance analysis

The discrimination index d' was used as a measure of recognition accuracy (Snodgrass & Corwin, 1988). These measures are based on the hit and false alarm rates, which were defined as the number of hits or false alarms divided by the number of old or new trials for which an old or new decision was made. Behavioral data was analyzed with SPSS 16 (SPSS, Inc., Chicago IL) and Greenhouse-Geisser corrections were used when appropriate.

2.7 Genotyping

For the analysis of the deletion polymorphism in ADRA2B we used fragment length analysis on a genetic analyzer. In short, amplification of a fragment containing the variant was performed in a total volume of 10 µl containing 50 ng of DNA and 1 x PCR buffer II (Applied Biosystems, Nieuwerkerk aan de IJssel, The Netherlands), 2,5 mM MgCl2 (Applied Biosystems), 0,25 mM dNTPs (GE Healthcare, Zeist, The Netherlands), 0,5 µl (10 pmol/µl) of each primer (Applied Biosystems), i.e. a NED-labeled forward primer (NED-AGA AGG AGG GTG TTT GTG GGG) and a reverse primer carrying a 'PIG tail' (ACC TAT AGC ACC CAC GCC CCT-GTTTCTT), 0,5 M betaine (Sigma, Zwijndrecht, The Netherlands), 0,04 units AmpliTaq Gold (Applied Biosystems). The amplification protocol consisted of an initial 12 minutes at 95°C, followed by 32 cycles of 1 minute at 94°C, 1 minute at 66°C and 1 minute at 72°C, and finishing with a step of 7 minutes at 72°C. For the fragment length analysis on an ABI Prism 3730 Genetic Analyser, 1 µl of diluted PCR product was added to 8.7 µl formamide (Applied Biosystems) and 0.3 µl Liz600 standard (Applied Biosystems). The results were analyzed using GeneMapper® Software, version 4.0 (Applied Biosystems). Testing for Hardy-Weinberg equilibrium did not show deviations from the expected distribution ($X2(1)= 0.24$, $P = 0.62$).

3. Results

3.1 Questionnaires and behavioral performance

The entire procedure including the negative mood induction decreased vigor ($F(1, 32) = 127.4$, $P < 0.001$) and tension ($F(1, 32) = 5.6$, $P = 0.02$), and increased anger ($F(1, 32) = 4.8$, $P = 0.04$) and fatigue ($F(1, 32) = 24.4$, $P < 0.001$), as measured by the POMS. No significant genotype effects were observed ($F(1, 32) < 2.1$, $P > 0.2$). The mood ratings during the experiment show that the negative mood induction was successful in both groups, leading to significantly lower mood ratings throughout

the experiment than before the mood induction procedure ($F(12, 21) = 21.3$, $P < 0.001$). Again, no significant effect of genotype was observed ($F < 1$).

As expected on the basis of the current sample size and the effect size observed in a previous study (De Quervain et al., 2007), no significant difference in recognition memory accuracy between deletion carriers and non-deletion carriers was observed (d' (means ± SEM); deletion carriers: 1.82 ± 0.10; non-deletion carriers: 1.85 ± 0.12; $t(31) = 0.2$, $P = 0.85$). Reaction times during the recognition memory test were significantly shorter for hits than correct rejections than misses and false alarms ($F (3, 96) = 32.8$, $P < 0.001$; paired t-tests, $P < 0.001$), but did not significantly differ between genotypes ($F < 1$). We did not find evidence for an interaction between stimulus valence and recognition memory accuracy (memory x valence interaction: $F(1, 31) = 1.2$, $P = 0.27$; gene x memory x valence interaction: $F < 1$). Also, orientation task performance during the study phase did not differ significantly between genotypes (i.e. decision accuracy and reaction times (means ± SEM); deletion carriers: 0.95 ± 0.01 %, 2199 ± 113 ms; non-deletion carriers: 0.96 ± 0.01 %, 2277 ± 153 ms, both $P > 0.4$).

3.2 Imaging results

3.2.1 Memory formation

Brain regions involved in the successful formation of emotional memories were identified by comparing responses to subsequently remembered and subsequently forgotten items across genotype groups. This analysis revealed significant bilateral activations in the amygdala, hippocampus, left inferior frontal gyrus, fusiform gyrus, and middle temporal gyrus (see Table 1). The results showed no significant main effect of genotype, suggesting that ADRA2B variation did not influence neural responses irrespective of memory ($P > 0.6$, corrected).

The effect of the ADRA2B deletion polymorphism on emotional memory formation was investigated using a genotype x memory interaction. The difference between later remembered and later forgotten pictures was larger in deletion than non-deletion carriers in the left amygdala ((x = -24, y = -2, z = -24), $Z = 3.0$, $P = 0.038$, SVC) and the left inferior frontal gyrus ((x = -40, y = 40, z = -2), $Z = 4.1$, $P = 0.024$, SVC; see Fig. 1). However, no significant interaction with emotional valence within these regions was observed ($P > 0.3$, corrected), suggesting that the emotional processing enhancement in deletion carriers was independent of mood congruency.

Table 1. Brain regions showing a main effect of successful memory encoding. Data are reported for peak voxels of activated clusters ($P < 0.05$, corrected).

Region	MNI coordinates			Z-value	P-value
	x	y	z		
R fusiform gyrus	40	-48	-20	7.4	< 0.001
L fusiform gyrus	-32	-40	-20	> 8	< 0.001
R hippocampus	22	-12	-16	6.4	< 0.001
L hippocampus	-22	-12	-18	5.7	0.001
R amygdala[a]	24	-8	-14	5.1	0.013
L amygdala[a]	-28	-8	-16	5.3	0.005
R middle temporal gyrus	52	-68	18	6.9	< 0.001
L middle temporal gyrus	-40	-80	26	5.7	0.001
L inferior frontal gyrus	-42	32	-12	6.0	0.001

R = right, L = left; a. Coordinates for the amygdala region of interest

3.2.2 Memory retrieval

The brain regions involved in the successful recognition of emotional pictures were identified by comparing responses for hits and misses. This analysis revealed a bilateral activation of the amygdala ((x = 20, y = -2, z = -14), $Z = 4.6$, $P < 0.001$, SVC; (x = -20, y = -4, z = -14), $Z = 4.7$, $P < 0.001$), in line with earlier studies investigating emotional memory retrieval (e.g. (Dolcos et al., 2005)). In addition, the right angular gyrus and the posterior cingulate gyrus were activated at a cluster level ($P < 0.05$, corrected, maxima at (x = 40, y = -72, z = 38) and (x = -2, y = -44, z = 48) respectively). The effect of the ADRA2B deletion polymorphism on memory retrieval was investigated using a genotype x memory interaction. No significant effects were found ($P > 0.2$, corrected). Moreover, no significant interactions with emotional valence were observed ($P > 0.7$, corrected).

4. Discussion

Our results demonstrate that the common ADRA2B deletion affects the neural correlates underlying memory formation of emotional stimuli in the amygdala and inferior frontal gyrus: Deletion carriers showed increased neural activity related to

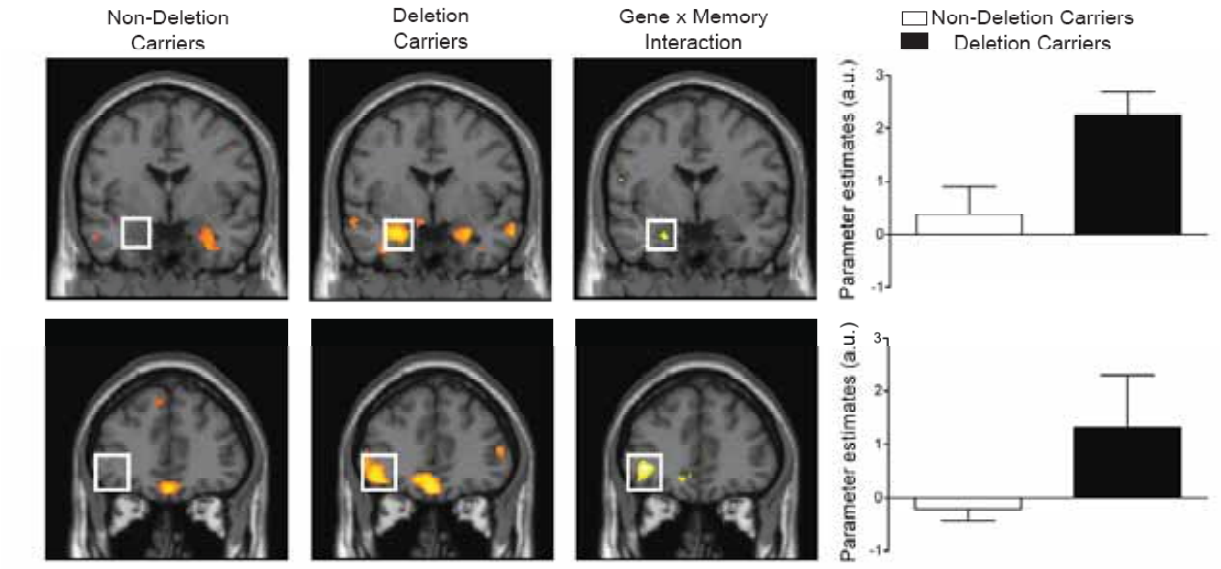

Figure 1. The ADRA2B genotype affects memory formation in the amygdala and inferior frontal gyrus. Coronal slices showing amygdala (upper row) and inferior frontal gyrus (lower row) effects (i.e. subsequent hits – subsequent misses) at the peak of the interaction. Columns show activations for non-deletion carriers, deletion carriers, the interaction between genotype and memory, as well as the cluster averages for non-deletion and deletion carrier, i.e. parameter estimates, mean ± SEM (figures at $P < 0.005$, uncorrected for display purposes; statistics at $P < 0.05$, small volume corrected). In all images, the left side corresponds to the left hemisphere.

successful memory formation compared to non-deletion carriers. In contrast, no effect of genotype was observed during successful memory retrieval. This pattern of results suggests that the variation in the human ADRA2B gene modulates emotional memory formation presumably via increased noradrenergic availability (Small et al., 2001).

Earlier studies have suggested that noradrenergic neurotransmission is more important for memory formation than retrieval. Blockade of noradrenergic signaling during memory formation reduces the memory enhancement for emotional events (Cahill et al., 1994), and is mediated by a reduction of amygdala activity (Strange & Dolan, 2004). However, blocking noradrenergic signaling during memory retrieval does not appear to influence memory performance (De Quervain, 2007). Our results support these findings and show that also genetic variation in noradrenaline signaling mainly affects memory formation rather than retrieval.

Besides the increased amygdala activation during successful memory formation of emotional stimuli, deletion carriers also showed a larger contribution of the inferior frontal gyrus. This brain region is involved in emotional memory formation (Smith, Henson, Dolan, & Rugg, 2004; Erk, Kiefer, Grothe, Wunderlich, Spitzer, & Walter, 2003) and is thought to be related to semantic elaboration (Demb, Desmond, Wagner, Vaidya, Glover, & Gabrieli, 1995; Kapur, Craik, Tulving, Wilson, Houle, & Brown, 1994), indicating that its heightened activity might reflect increased semantic elaboration of emotional content. Given that the amygdala modulates emotional memory processing in other brain regions (Kilpatrick & Cahill, 2003), the prefrontal effect could be a consequence of increased amygdala activity. However, the α2b-adrenoceptor is also expressed in the frontal cortex (Wang, Chang, Wu, & Chang, 2002), suggesting that the larger contribution of the inferior frontal gyrus is potentially mediated by locally increased noradrenergic signaling as well.

Our patterns of results confirm and extend the findings reported by Rasch and colleagues (2009) by showing that deletion carriers have stronger amygdala responses than non-deletion carriers. We were able to add cognitive specificity to this effect by showing an interaction with subsequent memory and extended this finding to the prefrontal cortex. Most likely Rasch and colleagues failed to find a gene x memory interaction due to the small number of used trials. On average, they used less than nine or eight trials for several critical cells of their analysis (e.g. negative misses for deletion carriers, and neutral hits for non-deletion carriers).

Furthermore, the differences in the study designs might have contributed to the fact that we found a gene x memory interaction: The specificity of the induced mood state and the intentional learning instruction combined with a subsequent recognition memory test used in our study are quite different

from the procedures used by Rasch and colleagues. Most likely, these differences contribute differentially to mnemonic processes.

We used a negative mood induction procedure, because valence-specific memory appears strongest for mood-congruent information (Bower et al., 1981). However, in line with the behavioral results from the initial study by de Quervain and colleagues (2007) and the fMRI study by Rasch and colleagues (2009), we did not find any evidence for valence-specific effects of the deletion. Thus, the changed noradrenergic signaling due to the deletion seems to result in a general increase of emotional memory processing without any valence-specificity. This pattern of results is in line with the modulation hypothesis, stating that the amygdala modulates the formation and consolidation of memories of emotionally arousing experiences independently of the valence (McGaugh, 2004; Sergerie, Lepage, & Armony, 2008; Kensinger & Schacter, 2006;, Erk et al., 2003). This is in line with the finding of increased neural activity during the processing of emotionally negative stimuli in deletion compared to non-deletion carriers, as observed by Rasch and colleges (2009); according to the authors those stimuli were more arousing.

Previous in vitro studies have reported both agonistic and antagonistic effects of the deletion variant (Small et al., 2001), making it difficult to discern whether the deletion leads to increased or decreased noradrenergic signaling. Given that propranolol reaches the brain and blocks the subsequent memory effect for emotional stimuli in the amygdala, presumably via a reduction of noradrenergic signaling (Liang, Juler, & McGaugh, 1986), our results are in line with the idea that deletion carriers have higher noradrenaline availability compared to non-deletion carriers (De Quervain, 2007). In the present study, we observed a larger contribution of the amygdala to successful memory formation in deletion carriers. Because this appears to be dependent on noradrenergic signaling (Strange & Dolan, 2004), our results provide additional evidence for the idea that the ADRA2B deletion variant potentiates noradrenergic activity.

In sum, our results show that a common deletion variant in the ADRA2B gene coding for a noradrenergic receptor leads to larger contributions of the amygdala and inferior frontal gyrus druing successful formation of emotional memories. Interestingly, the amygdala and the prefrontal cortex are key brain structures implicated in mood disorders (Drevets, 2003; Philipps, Drevets, Rauch & Lane, 2003). For example, depressed patients show increased amygdala activity during successful memory formation for faces and negative pictures (Robertson-Nay et al., 2006; Hamilton & Gotlib, 2008). Furthermore, increased prefrontal activity during verbal emotional memory formation has been observed in individuals at risk for mood disorders, such as anxiety and depression (Wolfensberger, Veltman, Hoogendijk, De Ruiter, Boomsma & De Geus, 2008). This suggests that the larger contribution of these brain regions during emotional memory formation in deletion carriers might indicate a marker of vulnerability in the development of mood disorders.

Acknowledgements

This work was supported by a grant (918.66.613) from the Netherlands Organization for Scientific Research (NWO). We thank Sabine Kooijman for general assistance, Marlies Naber and Jesse Eernstman for genotyping, Paul Gaalman for technical support and Tari Awipi for comments on the manuscript. In particular, we also thank Dominique de Quervain for constructive suggestions concerning the project and interpretation of the results. The authors have no potential conflict of interest.

References

Beck A.T., Steer R.A., & Brown G.K. (1996). Manual for the Beck Depression Inventory-II. Psychological Corporation: TX.

Bower G.H., Gilligan S.G., & Monteiro K.P. (1981). Selectivity of Learning Caused by Affective States. J Exp Psychol Gen, 110(4), 451-473.

Brugha T., Bebington P., Tennant C., & Hurry J. (1985). The list of threatening experiences: A subset of 12 life events categories with considerable long-term contextual threat. Psychol Med, 15, 189-194.

Cahill L., Babinsky R., Markowitsch H.J., & McGaugh J.L. (1995). The amygdala and emotional memory. Nature, 377(6547), 295-296.

Cahill L., Prins B., Weber M., & McGaugh J.L. (1994). Beta-adrenergic activation and memory for emotional events. Nature, 371(6499), 702-704.

Demb J.B., Desmond J.E., Wagner A.D., Vaidya C.J., Glover G.H., & Gabrieli J.D.E. (1995). Semantic encoding and retrieval in the left inferior prefrontal cortex: a functional MRI study of task-difficulty and process specificity. J Neurosci, 15, 5870-78.

De Quervain D.J. (2007). Preventive effect of beta-adrenoceptor blockade on glucocorticoid induced memory retrieval deficits. Am J Psychiatry, 164(6), 967-969.

De Quervain D.J., Kolassa I.T., Ertl V., Onyut P.L., Neuner F., Elbert T. et al. (2007). A deletion variant of the alpha2b-adrenoceptor is related to emotional memory in Europeans and Africans. Nat Neurosci, 10(9), 1137-1139.

Dolcos F., LaBar K.S., & Cabeza R. (2005). Remembering one year later: role of the amygdala and the medial temporal

lobe memory system in retrieving emotional memories. Proc Natl Acad Sci USA, 102, 2626-2631.

Drevets W.C. (2003). Neuroimaging abnormalities in the amygdala in mood disorders. Ann N Y Acad Sci, 985, 420-444.

Duijsens I.J., Spinhoven P., Verschuur M., & Eurelings-Bontekoe H.M. (1999). De ontwikkeling van de Nederlandse verkorte temperament en karakter vragenlijst (TCI-105). Nederlands Tijdschrift voor de Psychologie, 54, 276-283.

Eason M.G., & Liggett S.B. (1992). Subtype-selective desensitization of alpha 2-adrenergic receptors. Different mechanisms control short and long term agonist-promoted desensitization of alpha 2C10, alpha 2C4, and alpha 2C2. J Biol Chem, 267(35), 25473-25479.

Erk S., Kiefer M., Grothe J., Wunderlich A.P., Spitzer M., & Walter H. (2003). Emotional context modulates subsequent memory effect. NeuroImage, 18(2), 439-447.

Haas B.W., & Canli T. Emotional memory function, personality structure and psychopathology: a neural system approach to the identification of vulnerability markers. Brain Res Rev, 58(1), 71-84.

Hamilton J.P., & Gotlib I.H. (2008). Neural substrates of increased memory sensitivity for negative stimuli in major depression. Biol Psychiatry, 63(12), 1155-1162.

Kapur S., Craik F.I., Tulving E., Wilson A.A., Houle S., & Brown G.M. (1994). Neuroanatomical correlates of encoding in episodic memory: levels of processing effect. Proc Natl Acad Sci USA, 91, 2008-11.

Kensinger E.A., & Schacter D.L. (2006). Amygdala activity is associated with the successful encoding of item, but not source, information for positive and negative stimuli. J Neurosci, 26(9), 2564-2570.

Kernis M.H., Greenier K.D., Herlocker C.E., Whisenhunt C.R., & Abend T.R. (1997). Self-perceptions of reactions to doing well or poorly: The roles of stability and level of self-esteem. Person individ Diff, 22(6), 845-854.

Kilpatrick L., & Cahill L. (2003). Amygdala modulation of parahippocampal and frontal regions during emotionally influenced memory storage. Neuroimage, 20(4), 2091-2099.

Liang K.C., Juler R.G., & McGaugh J.L. (1986). Modulating effects of post-training epinephrine on memory involvement of the amygdala noradrenergic system. Brain Res, 368, 125-133.

Maldjian J.A., Laurienti P.J., Kraft R.A., & Burdettea J.H. (2003). An automated method for neuroanatomic and cytoarchitectonic atlas-based interrogation of fMRI data sets. Neuroimage, 19, 1233-1239.

McGaugh J.L. (2004)The amygdala modulates the consolidation of memories of emotionally arousing experiences. Annu Rev Neurosci, 27, 1-28.

McGaugh J.L., & Roozendaal B. (2002). Role of adrenal stress hormones in forming lasting memories in the brain. Curr Opin Neurobiol, 12(205-210).

McNair D.M., Lorr M., & Droppleman L.F. (1971). Manual: Profile of Mood States. Educational and Industrial Testing Service: San Diego, CA.

Morris J.S., Friston K.J., C. B., Frith C.D., Young A.W., Calder A.J. et al. (1998). A neuromodulatory role for the human amygdala in processing emotional facial expressions. Brain, 121(47-57).

Philipps M.L., Drevets W.C., Rauch S.L., & Lane R. (2003). Neurobiology of emotion perception II: Implications for major psychiatric disorders. Biol Psychiatry, 54(5), 515-528.

Rasch B., Spalek K., Buholzer S., Luechinger R., Boesiger P., Papassotiropoulos A. et al. (2009). A genetic variation of the noradrenergic system is related to differential amygdala activation during encoding of emotional memories. Proc Natl Acad Sci USA, 13 Oct 2009; Epub ahead of print.

Richardson M.P., Strange B.A., & Dolan R.J. (2004). Encoding of emotional memories depends on amygdala and hippocampus and their interaction. Nat Neurosci, 7(3), 278-285.

Roberson-Nay R., McClure E.B., Monk C.S., Nelson E.E., Guyer A.E., Fromm S.J. et al. (2006). Increased amygdala activity during successful memory encoding in adolescent major depressive disorder: An fMRI study. Biol Psychiatry,, 60(9), 966-973.

Schmidt C., Collette F., Cajochen C., & Peigneux P. (2007). A time to think: circadian rhythms in human cognition. Cogn Neuropsychol, 24(7), 755-789.

Sergerie K., Lepage M., & Armony J.L. (2008). A face to remember: emotional expression modulates prefrontal activity during memory formation. Neuroimage, 24(2), 580-585.

Small K.M., Brown K.M., Forbes S.L., & Liggett S.B. (2001). Polymorphic deletion of three intracellular acidic residues of the alpha 2B-adrenergic receptor decreases G protein-coupled receptor kinase-mediated phosphorylation and desensitization. J Biol Chem, 276(7), 4917-4922.

Smith A.P.R., Henson R.N.A., Dolan R.J., & Rugg M.D. (2004). fMRI correlates of the episodic retrieval of emotional contexts. NeuroImage, 22(1), 868-878.

Snodgrass J.G., & Corwin J. (1988). Pragmatics of measuring recognition memory: Applications to dementia and amnesia. J Exp Psychol Gen, 117, 34-50.

Strange B.A., & Dolan R.J. (2004). Beta-adrenergic modulation of emotional memory-evoked human amygdala and hippocampal responses. Proc Natl Acad Sci USA, 101(31), 11454-11458.

Tzourio-Mazoyer N., Landeau B., Papathanassiou D., Crivello F., Etard O., Delcroix N., et al. (2002). Automated Anatomical Labeling of Activations in SPM using a Macroscopic Anatomical Parcellation of the MNI MRI Single-Subject Brain. Neuroimage, 15, 273-289.

Wang G.S., Chang N.C., Wu S.C., Chang A.C. (2002). Regulated expression of alpha2B adrenoceptor during development. Developmental Dynamics, 225(2), 142-152.

Wolfensberger S.P., Veltman D.J., Hoogendijk W.J., De Ruiter M.B., Boomsma D.I., & de Geus E.J. (2008). The neural correlates of verbal encoding and retrieval in monozygotic twins at low or high risk for depression and anxiety. Biological Psychology, 79(1), 80-90.

Worsley K.J., Marrett S., Neelin P., Vandal A.C., Friston K.J., & Evans A.C. (1996). A unified statistical approach for determining significant signals in images of cerebral activation. Hum Brain Mapp, 4, 58-73.

Abstracts web articles

Nijmegen CNS is committed to publishing all submitted theses. However, due to the number of submissions, we make a selection based on the recommendation made by the editors. As a special service to interested readers, we provide the abstracts of the remaining articles on the following pages. The full versions of these articles are available at our website: www.ru.nl/master/cns/journal.

Acute stress modulates genotype effects on amygdala processing in humans

Heleen Cousijn, Supervisors: Mark Rijpkema, Guillén Fernández

Investigating interactions between genetic and environmental factors is crucial for understanding the mechanisms leading to interindividual differences. Here, we investigated whether the current environmental context, by affecting the state of the brain, modulates genotype effects on brain function in humans. We manipulated the context by inducing acute stress which increases noradrenergic activity, and probed its effect on tonic activity and phasic responses in the amygdala. Results show that carriers of a deletion in ADRA2B, the gene coding for the α2b-adrenoceptor, display increased phasic amygdala responses under stress. In contrast, stress increased tonic activity in the amygdala for both genotypes. Thus, stress specifically increases phasic responses in deletion carriers. Our results demonstrate that genetic effects on brain operations can be dependent on the current environmental context.

Recurrent Connectivity and Development of Layer II Stellate Cells of Medial Entorhinal Cortex

Julia Dawitz, Supervisors: Jonathan J. Couey, Menno P. Witter

Grid cells, found mainly in layer II of the medial entorhinal cortex, play a major role in spatial representation and navigation. Network models for grid cell firing predict a recurrent network between groups of synchronous firing grid cells. Connectivity data on their presumed neuronal correlates, the layer II stellate cells of the medial entorhinal cortex, is inconsistent. Here we test direct interconnectivity of stellate cells using multicell patch clamp. We also study the development of grid cell properties using slices taken from a range of postnatal ages. The Ih current, typical for grid cells, was found to become adult like rather abrupt at postnatal day 16 (P16). Stellate cells of layer II showed a sparse recurrent connectivity of about 1%, independent of age. The amplitude however showed a non-significant decreasing trend with age. Until P16 spontaneous high conductance states were observed in all synchronously recorded stellate cells whose appearance was not influenced by age until P16. The detected recurrent connectivity is too sparse to bind simultaneous firing grid cells together, thus we propose that this coupling is realized with the aid of subtreshold oscillations synchronized by a common inhibitory input instead. Since the Ih-current is required for those oscillations, grid cells are not expected to be present before P16. We propose that the high conductance states are EPSPs evoked by up-states in layer V. They however remain poorly understood and have to be further investigated in future.

Processing FM-sweeps: psychophysical sensitivity to acoustic spectrotemporal modulations of tone complexes in macaques and humans

Anne M. M. Fransen, Supervisors: Robert F. Van der Willigen, John Van Opstal, Huib Versnel, Pascal Fries

Frequency-modulated (FM) sweeps are important components of natural sounds. However, to analyse these, the auditory system must perform combined spectral-temporal analysis. Two models on spectral-temporal analysis in the auditory system exist, one of

which is based on combined spectrotemporal feature detectors, whereas the other model assumes separate spectral and temporal filter banks. To discriminate between these models we determined the psychometrical response curves to a large set of broadband spectral-temporal rippled noise stimuli (N=968). From the perceptual thresholds we derived the spectral-temporal transfer characteristic for each subject (5 rhesus monkeys, 5 humans). Our results confirmed all predictions that follow from separate spectral and temporal processing: i) Temporal modulation and spectral spacing do not interact (i.e. the transfer characteristic is separable) ii) The auditory system is equally sensitive to upward and downward moving ripples. iii) The transfer functions are comparable between humans and monkeys. We propose a model to unite separable processing with the ability of the auditory system to encode inseparable FM-sweeps.

Effects of specific DHA- and cholesterol-containing diets on cognition, cerebral hemodynamics and synaptic density in APPswe/PS1ΔE9 Alzheimer mice

Anne Hafkemeijer, Supervisors: Diane Jansen, Valerio Zerbi, Anna-Lena Janssen, Jos Dederen, Ineke van der Zee, Laus Broersen, Arend Heerschap, Amanda Kiliaan

Results from trials and epidemiological studies indicate that docosahexaenoic acid (DHA) may affect the development of Alzheimer's Disease (AD). Furthermore, the addition of uridine-monophosphate (UMP) and other nutrients that are precursors and cofactors for membrane synthesis in the brain may potentiate the effects of DHA. We previously showed that cholesterol and DHA may affect degenerative processes in AD by influencing β amyloid production indirectly via vasculature and via changing neuronal membrane composition. We now investigated the influence of diets containing precursors and cofactors for membrane synthesis in the brain (cholesterol, DHA, UMP, choline, phosphatidylcholine, vitamins B and antioxidants) on cognition, cerebral hemodynamics and synaptic density in APPswe/PS1ΔE9 Alzheimer mice. From two months of age, male wild-type and double-transgenic mice were fed either a standard control diet, a traditional cholesterol or DHA diet, a DHA diet enriched with UMP or a DHA diet enriched with UMP and a multi-nutrient combination of membrane precursors and cofactors (FortasynTM Connect). Cognition was investigated in a (reverse) Morris Water Maze; in which 6-month-old mice (n=60, group 1) were trained to find the location of an escape platform. Mice of 8 months of age were used for relative cerebral blood volume measurements using susceptibility-induced contrast MRI techniques. Synaptic density was measured in another group of 8-month-old wild-type and transgenic-mice (n=40, group 2) using synaptophysin antibody. Results showed an impairment in spatial learning and memory in Alzheimer mice, while intake of the FortasynTM Connect diet increased both learning and memory. No significant differences in cerebral blood volume or synaptic density in AD mice were found. A high cholesterol diet increased the percentage and number of synaptophysin-immunoreactive presynaptic boutons in the stratum radium, indicating a compensatory mechanism. Further research with our mouse model is needed to test long-term effects of DHA/UMP diets on vascular parameters and synaptic density.

Action categories in the human premotor cortex

Florian Krause, Supervisors: Oliver Lindemann, Harold Bekkering

Traditionally, the ability to perform complex actions has been thought to rely on assembling sequences of simpler motor plans, a process supported by computational resources in premotor areas. According to this view, those complex motor plans are capable of combining the movements evoked by individual muscle groups across noncontiguous joints. This combinatorial ability would rely on accessing control neurons distributed over the primary motor cortex, and spatially distributed according to the topographic arrangement and degree of innervation of the controlled muscles (somatotopy principle). Recent studies on the monkey motor cortex suggest an alternative organizational principle. Complex actions are topographically represented on their own, clustered into ethologically relevant action

categories, with a correspondingly spatial organization over the cortical motor system. Preliminary electrophysiological evidence for this hypothesis has been gathered in the cortex of the macaque, along the post-arcuate cortex. This study aimed to test this novel hypothesis in the human motor system. Using high-resolution functional Magnetic Resonance Imaging (fMRI) and a motor imagery task our aim was to identify cortical representations of two complex actions: (1) reaching out to grasp an object (RG) and (2) bringing the hand holding an object to the mouth (HM). In multiple blocks subjects were presented pictures of objects and asked to imagine RG and HM actions. Engagement in imagery was controlled through a manipulation of task di_culty, a_ecting imagery durations. In accordance with the hypothesis described above, we expected to see a dorso-ventral shift of activity along the rostral premotor cortex when subjects imagine an RG or an HM action, respectively. No such shift became evident. Moreover, we could not _nd any consistent topographical mapping of the complex actions we investigated. While this study cannot exclude the existence of action categories in the human motor system, it introduces a feasible new methodology for future experiments.

What did you say just now, bitterness or wife?: An ERP study on the interaction between tone, intonation and context in Cantonese Chinese

Carmen Kung, Supervisors: Dorothee Chwilla, Carlos Gussenhoven, Sara Bögels

In this paper, two ERP experiments were conducted to investigate the online interplay between tone, intonation and context in speech comprehension in Cantonese Chinese. In the two experiments, we compared the processing and identification of critical words at the end of questions to that of statements using a tone identification task and ERPs as an online measure of speech comprehension. In Experiment 1, when the critical words were presented in the sentence-final position, critical words with a low tone at the end of questions yielded very high error rates compared to all other conditions. These words also elicited a biphasic N400-P600 pattern. The results indicated that speech processing is affected by the interaction between tone and intonation. This effect was particularly strong when question intonation was added to the low tones and yielded conflicting F0 information for identifying these low tones. In Experiment 2, critical words were embedded in compounds, which were presented in the sentence-final position. The goal of this manipulation was to test if a highly constraining context would have an effect on the interaction between tone and intonation during speech comprehension. The results showed a significant reduction in error rate for low tones with a question intonation and an absence of a concomitant P600 for these tones. Overall, the results in Experiment 1 and 2 had three implications. First, they provided evidence for an immediate interaction between tone, intonation and context during speech comprehension in real time. Second, the ERP findings highlight the significance of context in speech processing, and particularly, in Cantonese-Chinese, which is characterised by a strong context dependency in speech comprehension. Third, this is the first ERP study that provides evidence for a monitoring process in the auditory domain. The generalization of a monitoring response in the auditory domain further supports that monitoring process plays a vital role in language comprehension.

The development of temporal coordination in joint and single actions during early childhood

Marlene Meyer, Supervisors: Sabine Hunnius, Shirley-Ann Rueschemeyer

For adults, successful joint actions with others are part of their everyday life. Their performance during joint temporal coordination can thereby be as accurate as during individual action performance. The ability to interact successfully, however, is not present from birth on. To date, it is unclear how young children develop joint action capabilities and in which way this development relates to the emergence of intrapersonal coordination. The aim of the current study was thus to investigate how young children coordinate and time their actions when acting alone or together with

a joint action partner and how this develops during early childhood. Elements of joint temporal coordination and the ability to distinguish between joint and parallel actions were found previously in young children around the age of 2½- to 3-years. Therefore, we expected a strong improvement in children's temporal coordination in joint action performance within this age range. For individual coordination our assumption was to find only marginal changes because development of intrapersonal coordination is observed already in younger children. By means of a computer game, playable alone as well as jointly, we tested 2½- and 3-year-old children's temporal coordination performance with respect to variability and error. As expected, behavioural results indicate a clear improvement of temporal coordination in joint action for 3-year-olds compared to 2½-year-old children whereas their individual performance did not differ. In contrast to the younger age group, the joint performance of 3-year-olds approximated their performance level during individual actions. These findings suggest that joint coordination abilities emerge later in development than temporal coordination in individual actions. We can further conclude that joint coordination abilities for the given task approached the level of intrapersonal coordination abilities around the age of 3 years.

On the specificity of auditory and motor simulation. An fMRI study with expert pianists

Giacomo Novembre, Supervisor: Shirley-Ann Rueschemeyer

The present study investigates the neural correlates of visual-driven auditory and motor representations in expert musicians. Expert pianists were presented with videos showing one hand playing chord sequences on a mute keyboard. The last chord of the sequence was either congruent or incongruent to the musical context with regard to (1) auditory expectation (the harmony of the anticipated chord progression) or (2) visual-motor expectation (the set of fingers normally used to play harmonic chords). Both the incongruent conditions were not wrong chords per se, but they were incompatible with the context on the basis of their position along the chord progression. In a behavioural study, we showed that expert pianists were able to significantly discriminate these incongruent conditions, while non-musicians performed at chance-level. This suggests that, although the videos were silent, experts were able to extract very specific auditory and motor information from the visual presentation of the melodies. In order to understand how expert musicians performed this task in the absence of auditory input, we measured the neurophysiological correlates of this ability using fMRI. We hypothesized that auditory and motor simulation of musical actions drove performance in this task. As we expected, acoustically violated trials activated secondary auditory cortex (Middle Temporal Gyrus), suggesting that auditory simulation underlies the establishment of auditory expectancy. Likewise, action-violated trials activated the cerebral motor system (Middle Frontal Gyrus and Inferior Parietal Lobe), suggesting that motor simulation underlies the establishment of visual-motor expectancy. In conclusion, this study provides evidence in favour of specific auditory and motor simulation mechanisms. Additionally, it provides new insights into how musical expectations are derived in expert musicians by showing that expert musicians rely on simulation while observing musical performance. These simulation mechanisms have been speculated to serve action prediction, a crucial component of joint musical actions.

Valt het dan nog steeds wel op? Comprehending Dutch particle verbs

Vitória Magalhães Piai, Supervisors: Marcel Bastiaansen, Rob Schreuder

Dutch particle verbs are formed by a main verb and a particle (e.g., afstuderen 'to graduate'; af 'finished', studeren 'to study') and are separable in that the particle may be realized separated from the main verb in certain contexts (e.g., ik studeer af 'I graduate'). When presented separately, the processor must store the main verb and integrate it with the particle further downstream. Little is known about when and how this integration is realized and which factors may influence this process. We report an EEG study on the comprehension of Dutch

separable particle verbs. We manipulated a) the "family size" of the main verb and b) the actual realization of the particle, which could be (1) a rammatically and semantically correct particle, (2) a particle forming an existing particle verb yet yielding a semantic violation or (3) a particle forming a non-existing particle verb. For a), we found an anterior negativity which seems to be indicative of increased working memory load. Concerning b), both violations yielded an N400 effect relative to the expected particle. The results suggest that the language system is sensitive to particle completions in order to be able to build an appropriate syntactic structure and to retrieve the meaning of the particle verb. Additionally, the results also suggest that the integration of the particle with the main verb is a semantic process, similar to the integration of words in the sentence.

β-Adrenergic blockade reduces cerebral blood flow in stress-related brain regions during acute stress

Vincent C. Schoots, Supervisors: Erno J. Hermans, Guillén Fernández

The stress response is one of the most important mechanisms governed by the neuroendocrine system. Nonetheless, the effect that stress hormones have on the brain remains understudied in humans. We investigated state changes in neuronal activity in a young, healthy male population, during a situation of stress. We measured cerebral blood flow (CBF) with a specialised neuroimaging technique, arterial spin labelling. Using a double-blind, placebo-controlled paradigm, we tested the effects of β-adrenergic receptor blockade and cortisol synthesis inhibition. Salivary cortisol and α-amylase measures confirmed the effectiveness of our pharmacological manipulation. We found specific CBF reductions in response to β-blockade in the right amygdala, and in a cluster spanning the superior medial frontal gyrus/anterior cingulate cortex (sMPF/ACC). In addition, we found a whole brain reduction in CBF in response to β-blockade. We did not find a CBF effect of cortisol inhibition. Our study provides evidence for involvement of the β-adrenergic system in neuronal modulation of the entire brain, with a focus on the amygdala and sMPF/ACC during stress.

Morphological and molecular dissection of the APO-SUS/-UNSUS rat model for neurodevelopmental disorders

Ioannis Zalachoras, Supervisors: Michel M.M. Verheij, Vivian D. Eijsink, Josephus A. van Hulten, Martine van Zweeden, Bruce G. Jenks, Gerard J.M. Martens

Schizophrenia is a chronic neurodevelopmental disorder of unknown aetiology that may include a combination of genetic variations, epimutations and environmental factors. Two different lines of Wistar rats, with either high or low susceptibility to the dopamine agonist apomorphine (APO-SUS and APO-UNSUS rats, respectively), represent an animal model for neurodevelopmental disorders. The two lines are known to differ in a number of behavioural, physiological, endocrinological and pharmacological parameters. APO-SUS rats display various schizophrenia-related features, including distorted information processing, altered stress responses, a high vulnerability to drugs of abuse and a hyperactive dopaminergic system. In the present study, we first assessed differences in the brain morphology between the APO-SUS and APO-UNSUS rats using sectioning and (immuno)staining methods, such as cresyl violet staining and tyrosine hydroxylase immunostaining. The results revealed that the APO-SUS rats have a larger striatum and a smaller prefrontal cortex compared to those in the APO-UNSUS rats. Interestingly, schizophrenia patients present the same morphological features. In addition, the dorsal part of the third ventricle was smaller in the APO-SUS than in the –UNSUS rats. Secondly, after an injection with either apomorphine or saline and a 45-min-long session in a gnawing box, we studied with qRT-PCR the induced differences in the mRNA expression levels of several immediate-early genes (IEGs; arc, c-fos, Ngf1-A, nurr1) and nptx2 in various brain areas (prefrontal cortex, nucleus accumbens, caudate putamen, cingulate cortex and pituitary), either immediately after the gnawing box session or 4 h later. At 0 h our results showed between the two lines differential

expression of Ngf1-A in the caudate putamen, of Nurr1 in the nucleus accumbens and of arc and Nurr1 in the pituitary. Moreover, following apomorphine in general in both lines IEG expression was higher in the striatum and the nucleus accumbens compared to their respective saline control groups. On the other hand, in the cingulate cortex and the pituitary gene expression was lower after apomorphine. The effects of apomorphine were still apparent on the expression of these genes after 4 h, although no individual differences were present. In conclusion, we found morphological differences between the two lines that resemble those observed between schizophrenic patients and control subjects and that apomorphine has a differential effect on IEG expression between the two lines.

Institutes associated with the Master's Programme in Cognitive Neuroscience

Donders Institute for Brain, Cognition and Behaviour: Centre for Cognitive Neuroimaging
Kapittelweg 29
6525 EN Nijmegen

P.O. Box 9101
6500 HB Nijmegen
http://www.ru.nl/neuroimaging/

Donders Institute for Brain, Cognition and Behaviour: Centre for Cognition
Montessorilaan 3
6525 HR Nijmegen

P.O. Box 9101
6500 HB Nijmegen
http://www.ru.nl/cognition/

Donders Institute for Brain, Cognition and Behaviour: Centre for Neuroscience
Geert Grooteplein Noord 21, hp 126
6525 EZ Nijmegen

P.O. Box 9101
6500 HB Nijmegen
http://www.ru.nl/neuroscience/

Max Planck Institute for Psycholinguistics
Wundtlaan 1
6525 XD Nijmegen

P.O. Box 310
6500 AH Nijmegen
http://www.mpi.nl/

Universitair Medisch Centrum St Radboud
Geert Grooteplein-Zuid 10
6525 GA Nijmegen

P.O. Box 9101
6500 HB Nijmegen
http://www.umcn.nl/

Baby Research Center
Montessorilaan 10
6525 HD Nijmegen

P.O. Box 9101
6500 HB Nijmegen
http://babyresearchcenter.nl

Nijmegen Centre for Molecular Life Sciences
Geert Grooteplein 28
6525 GA Nijmegen

P.O. Box 9101
6500 HB Nijmegen
http://www.ncmls.nl